School of Molecular and Life Sciences

Platinum(II) Complexes for Biological Applications

Thomas James Grady

This thesis is presented for the Degree of

Master of Research (Chemistry)

of

Curtin University

February 2021

Declaration

To the best of my knowledge and belief this thesis contains no material previously published by any other person except where due acknowledgment has been made.

This thesis contains no material which has been accepted for the award of any other degree or diploma in any university.

Signature:

Date: 16/02/2021

Abstract

The aim of this research was to investigate the potential biological applications of a series of platinum(II) complexes. These biological applications were to include use as biological imaging agents, and as antimicrobials.

First, a series of platinum(II) complexes bearing cyclometallated N-heterocyclic carbene ligands alongside substituted pyridyl tetrazole ligands was investigated. They were synthesised by the adaptation of existing literature procedures, and their photophysical properties were investigated in room temperature solutions of both DCM and DMSO, as well as in the solid state. Though these complexes displayed promising photophysical properties in the context of developing biological imaging agents, their lack of water solubility prevents their application in that field.

Secondly, palladium(II) analogues of two known platinum(II) complexes bearing ortho-cyclophane ligands were tested for biological activity against a number of pathogenic microbes. One such compound showed good selectivity towards *Cryptococcus Neoformans*, a pathogenic fungus responsible for meningitis in immunocompromised patients. Further biological testing is required to determine if platinum(II) analogue of this complex displays similar activity.

Finally, the development of a general protocol for the synthesis of C^C^N coordinated platinum(II) complexes was attempted. While two dimeric platinum(II) intermediates were reported, the synthesis of a final C^C^N complex is ongoing. The challenges in the development of this family of compounds were the result of issues with the orientation and position of the ligands in the synthetic intermediates.

Acknowledgments

I would like to say thank you to A/Professor Max Massi for the guidance and support you have provided me over the course of this project. In particular I can't thank you enough for your patience and understanding during the somewhat tumultuous transition from honours to masters, I wouldn't have made it even half this far without it.

Thank you to Dr Emma Pearson, for being the door that was always open when I needed someone to talk to, and for all the help you've given me throughout these two years.

Thank you to A/Professor Stephen Moggach at UWA and Professor Mark Ogden for performing the crystallographic analysis on the lone crystal sample I was able to obtain over the course of these two years.

Thank you to Dr Angelo Frei at UQ for performing the testing the activity of the compounds reported in Chapter 4 against a range of pathogenic microbes, and for determining their cytotoxicity and haemolysis values.

Thank you to Dr Frankie Busetti at ECU for performing the HRMS analysis of the compounds reported in Chapter 2.

Thank you to Dr Mark Hackett for organising and running the honours course for 2019, and for continuing to guide me on my transition from honours to masters. I have enjoyed your enthusiasm, and it has helped inspire me to make the most of the setbacks I have encountered in this journey.

Thank you to Professor Mark Ogden for all your insightful feedback during group meetings, your willingness to answer any and all questions I have had over the course of this degree, and in particular for all the help you provided regarding the crystallography data. I would also like to thank you for taking me on as a primary supervisor starting next year, I look forward to working with you.

Thank you to all the technical staff, Dr Chiara Caporale, Dr Ching Goh, Edi Twiss, Joyce Wong, and Peter Chapman for all your assistance with regards to instrumentation, lab practices, and just helping me find whatever I happened to be looking for.

Thank you to Odin Bottrill, for being there every step of the way on this two year journey, and it's been an honour.

Thank you to Bradley Schwehr, for graciously allowing me to borrow your space in the fume hood, and for teaching me your tricks of the trade in the lab.

Thank you to Lee Cameron, for your endless patience with me in the lab, for all your help teaching me to use the fluorimeter, and for all the good vibes you bring to the lab. Most of all, thank you for the enormous effort that you and Caitlin have made in these last two years in keeping lab 2219 running. We all owe you a debt of gratitude.

Thank you to Caitlin Duncan, for the volumes of knowledge that you've provided me with, your advice and guidance in the lab has led to more than one breakthrough in my research. But thank you in particular for the immense amount of work that you and Lee have done to keep 2219 running these past two years. We all owe you a debt of gratitude.

Thank you to Ashlee Gallagher, your endless optimism and support has been one of the few constants though all the ups and downs of the last two years. You've never failed to provide an encouraging word and a smile when I needed it, and that means more to me than I know how to express.

Thank you to everyone in the 2219 family. Seeing you guys in the lab everyday has been the highlight of my time at Curtin.

Thank you to everyone in the Massi-Ogden research group, your input has been invaluable to my growth as a chemist.

Thank you to Braden Grant, for your wise words on the nature of friendship, and for the incredible company you provided during our honours year.

Thank you to the honours cohort of 2019, for being so supportive of not just me, but of each other, it was a phenomenal team effort.

And finally, thank you to my family, for everything. You made me the person I am today, and I couldn't have made it through this degree without you.

Commonly Used Abbreviations and Symbols

τ	Excited state lifetime
Φ	Quantum yield
Φ_r	Quantum yield of reference
λ_{abs}	Absorption wavelength
λ_{em}	Emission wavelength
λ_{ex}	Excitation wavelength
δ	Nuclear magnetic resonance chemical shift
br	Broad (NMR)
CC_{50}	Concentration at 50% cytotoxicity
d	Doublet (NMR)
DCM	Dichloromethane
DETA	Diethylenetriamine
DMF	Dimethylformamide
DMSO	Dimethylsulfoxide
HC_{10}	Concentration at 10% haemolytic activity
HOMO	Highest occupied molecular orbital
HRMS	High resolution mass spectrometry
IC	Internal conversion
IR	Infrared
ISC	Intersystem crossing
J	Coupling constant (NMR)
LC	Ligand centred
LUMO	Lowest unoccupied molecular orbital

m	Multiplet (NMR)
MC	Metal centred
MIC	Minimum inhibitory concentration
MLCT	Metal-to-ligand charge transfer
MMLCT	Metal-to-metal-to-ligand charge transfer
NMR	Nuclear magnetic resonance
NHC	N-heterocyclic carbene
OLEDs	Organic light-emitting devices
s	Singlet (NMR)
t	Triplet (NMR)
TEA	Triethylamine
THF	Tetrahydrofuran
UV	Ultraviolet
Vis	Visible

Commonly Used Abbreviations of Compounds

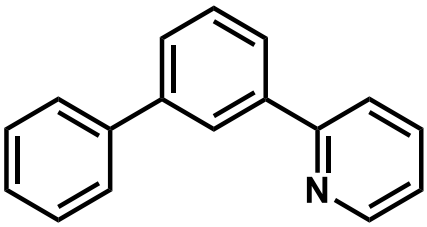

H_2bppy

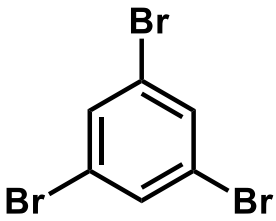

$PhBr_3$

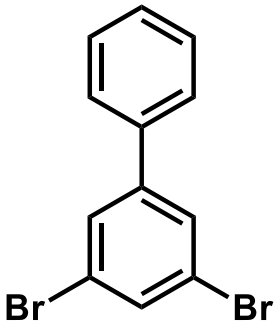

$PhBr_2Ph$

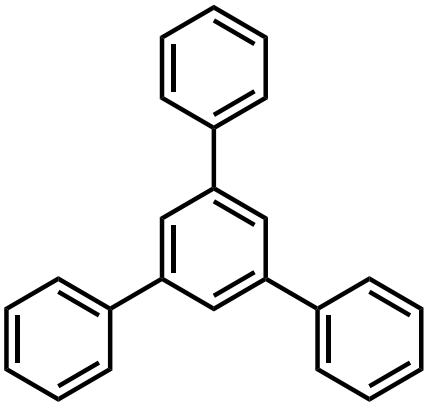

$PhPh_3$

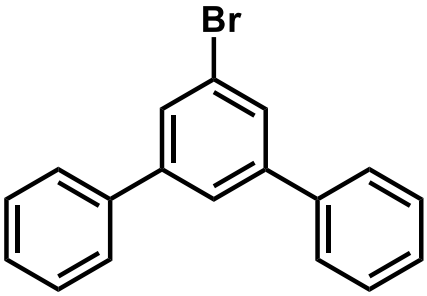

$PhBrPh_2$

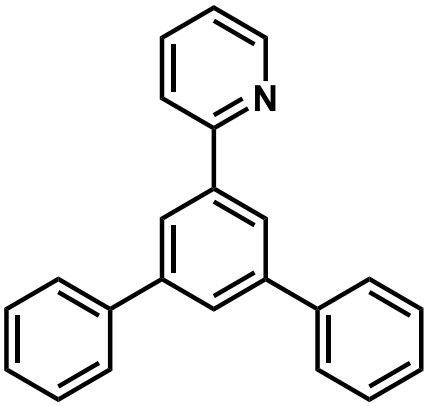

H_2tppy

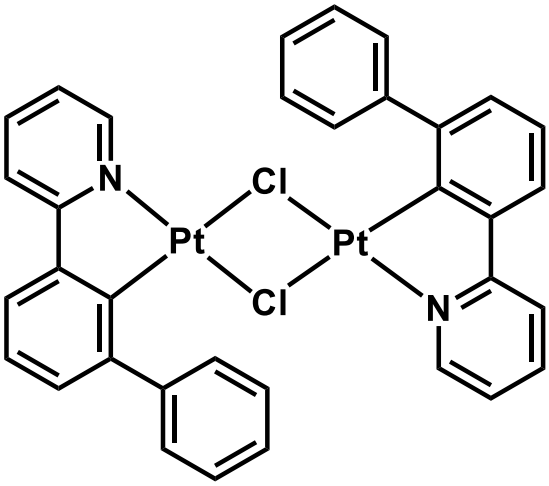

$(Pt(Hbppy)Cl)_2$.a

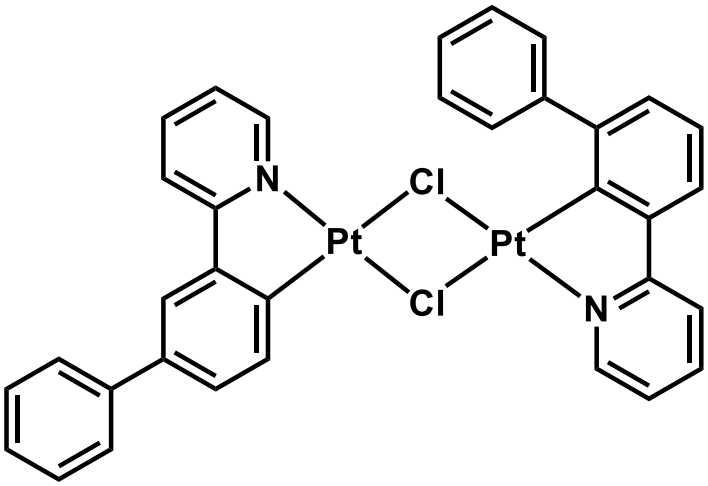

$(Pt(Hbppy)Cl)_2$.b

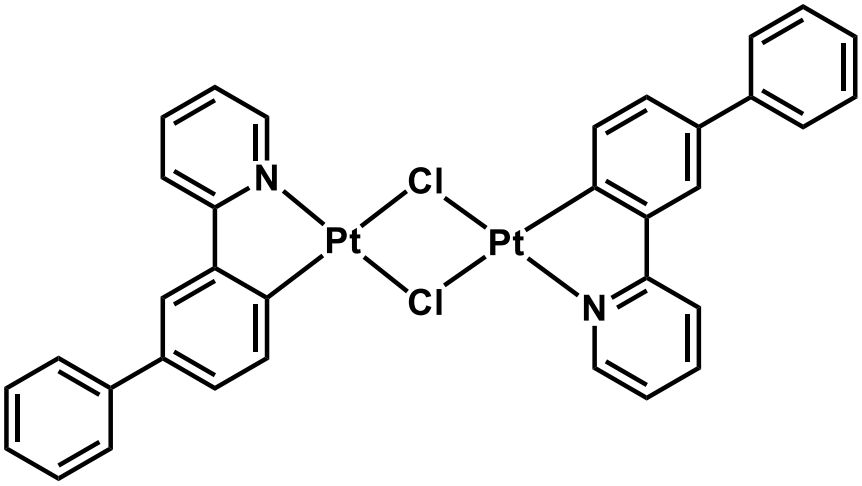

$(Pt(Hbppy)Cl)_2$.c

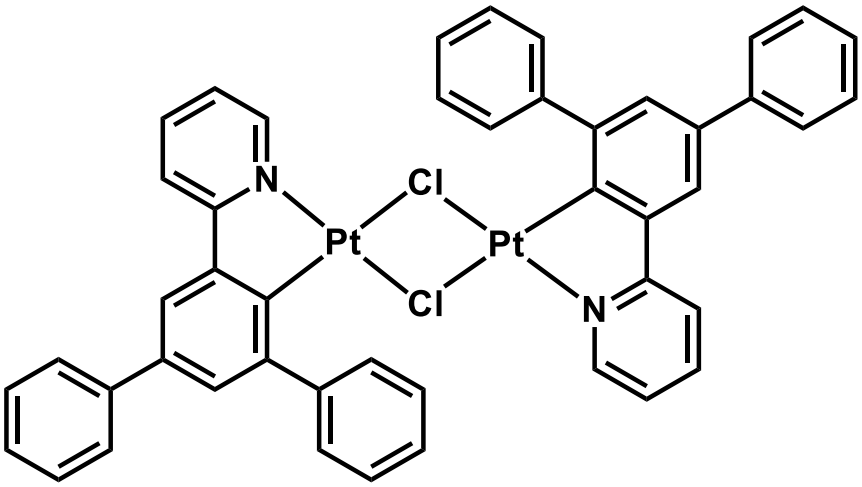

$(Pt(Htppy)Cl)_2$

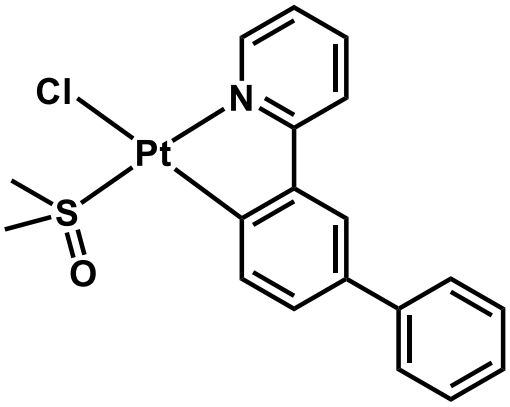

Pt(Hbppy)(DMSO)Cl

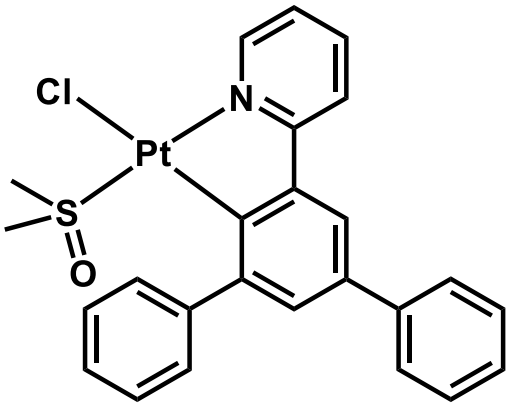

Pt(Htppy)(DMSO)Cl

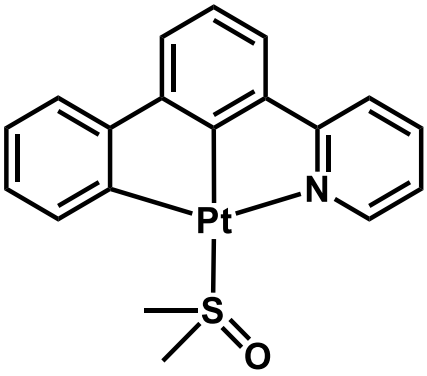

Pt(bppy)DMSO

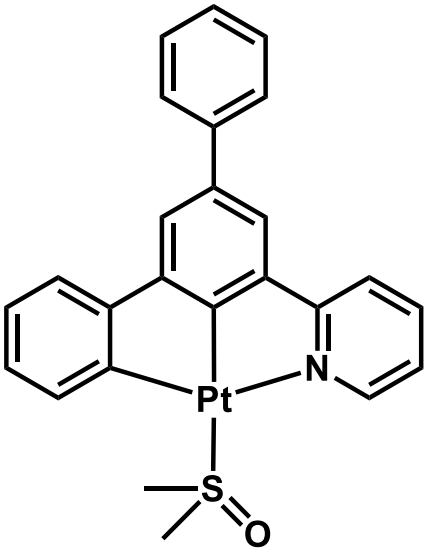

Pt(tppy)DMSO

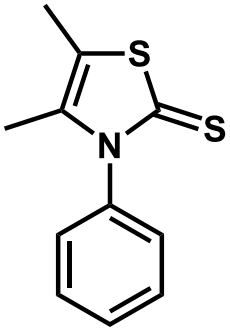

Ph(ThMe$_2$S)

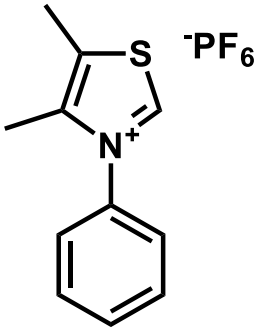

Ph(ThMe$_2$H).PF$_6$

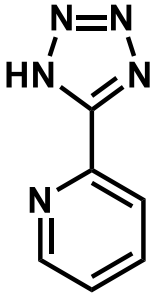

HL1

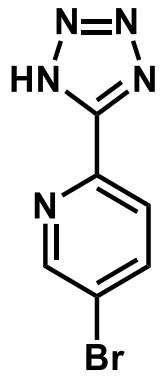

HL2

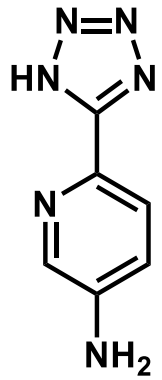

HL3

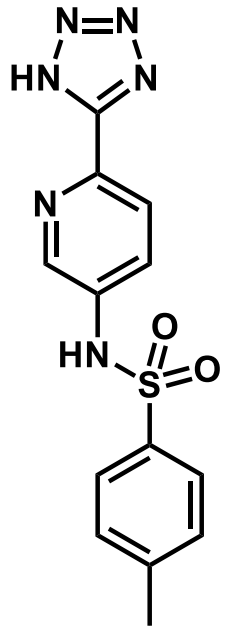

HL4

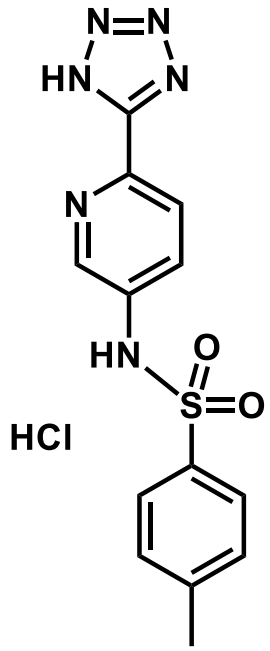

$[H_2L4]Cl$

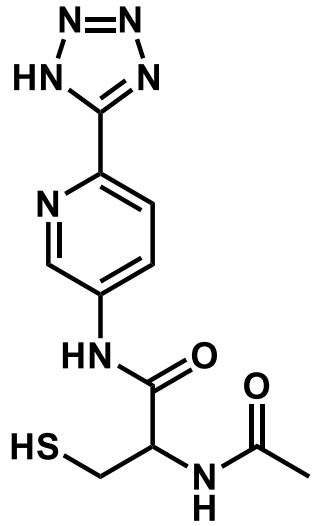

HL5

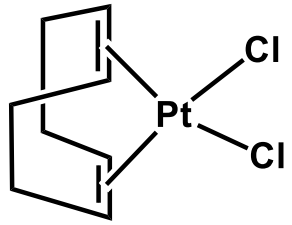

$Pt(COD)Cl_2$

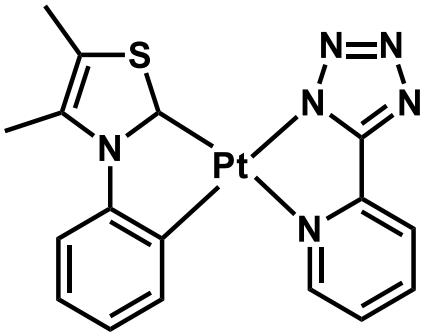

Pt[Ph(ThMe$_2$)]L1

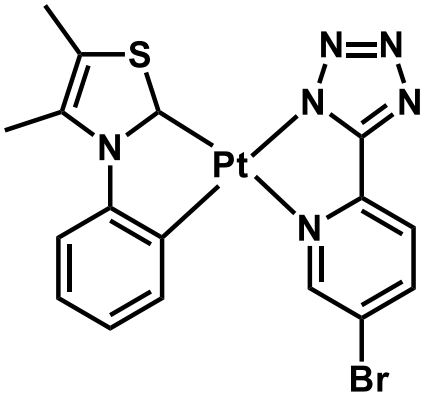

Pt[Ph(ThMe$_2$)]L2

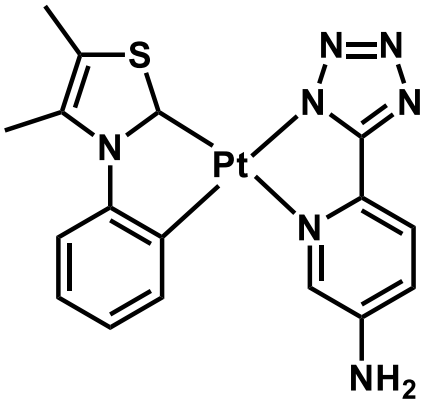

Pt[Ph(ThMe$_2$)]L3

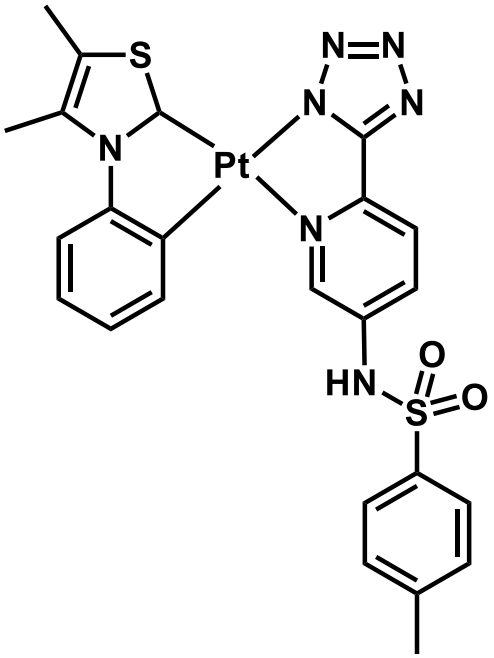

Pt[Ph(ThMe$_2$)]L4

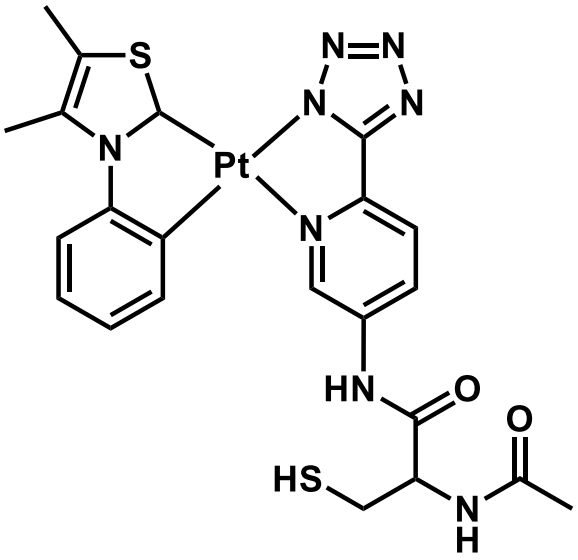

Pt[Ph(ThMe$_2$)]L5

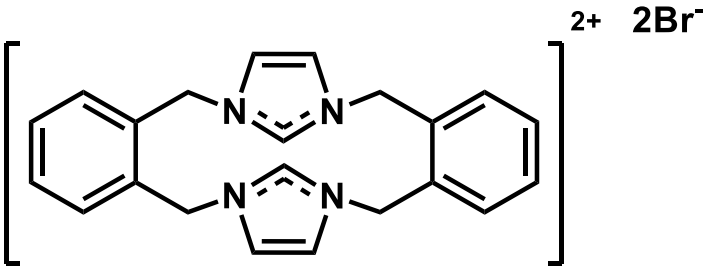

[H$_2$(o-cyc)]Br$_2$

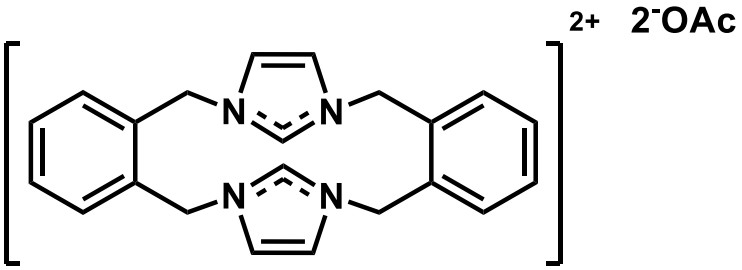

$[H_2(o\text{-}cyc)](OAc)_2$

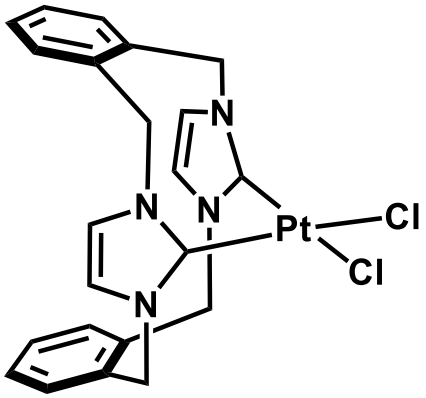

$Pt(o\text{-}cyc)Cl_2$

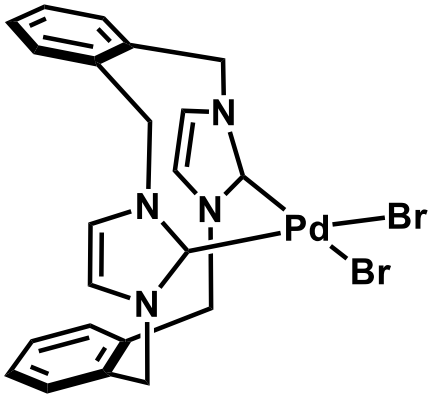

$Pd(o\text{-}cyc)Br_2$

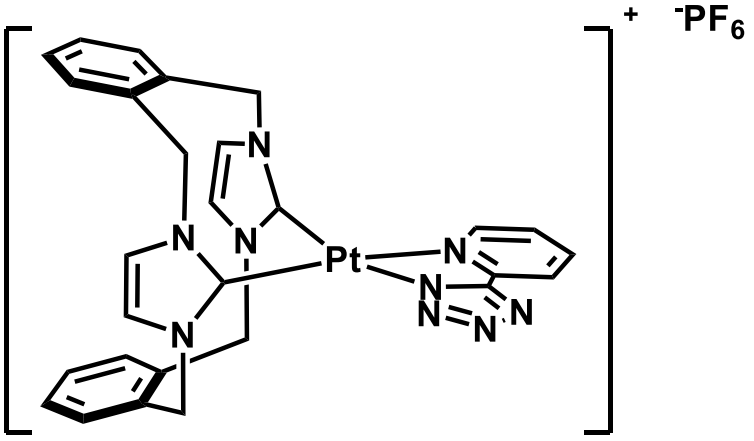

$[Pt(o\text{-}cyc)L1]PF_6$

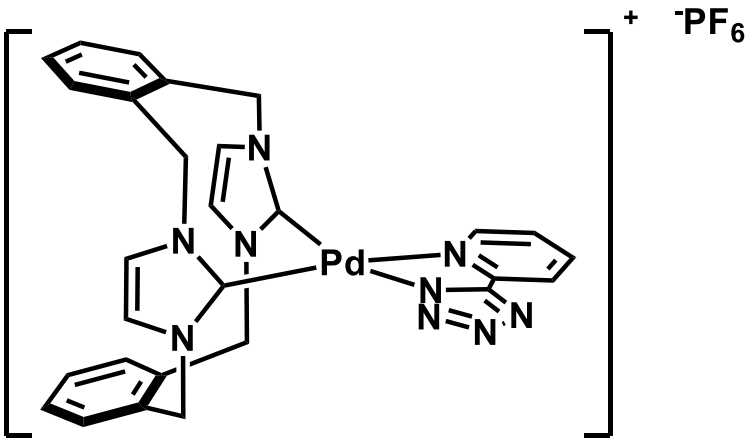

[Pd(o-cyc)L1]PF_6

Table of Contents

Chapter 1: Introduction

1.1 Transition Metals in Biology

Transition metal complexes play a wide range of important roles in biology. Many of these complexes occur naturally in the human body. Haemoglobin is an Fe(II) complex responsible for the transportation of oxygen around the body in red blood cells.[1, 2] Cobalamin, otherwise known as vitamin B_{12}, is a Co(III) complex that functions in a range of roles in the human body including the production of red blood cells, as well as the synthesis of myelin sheaths in the nervous system.[3, 4] Zinc finger proteins contain coordinated Zn(II) atoms that are responsible for binding biologically important molecules such as nucleic acids and other proteins.[5, 6]

There has been an increasing interest in synthetic transition metal complexes for use in biological applications. In 1969, Rosenberg and co-workers[7] reported the platinum(II) based antitumor agent cisplatin, which is used in chemotherapy even to this day.[8] Since then, many biologically active transition metal complexes have been reported.[9, 10] These include a wide range of antimicrobial silver compounds, and gold(III) complexes that provide relief from rheumatoid arthritis.[11, 12] There has also been significant interest in the development of rhenium complexes capable of releasing carbon monoxide under biological conditions to provide anti-inflammatory and anti-apoptotic effects.[13, 14]

Our interest in this field also extends to the application of transition metal complexes as biological probes, often in combination with their use as theraputics.[10] A wide range of such complexes have been reported over the last few decades, incorporating metals including platinum,[15] iridium,[16] rhenium,[17] rhodium,[18] gold,[19] and ruthenium.[20] These complexes have been used to elucidate the localisation and other structural features of a wide range of biologically important species, such as DNA and specific proteins, as well as organelles such as nuclei or lysosomes.[21-26]

1.2 Biological Probes

In the field of biology, the exploration of biochemical processes at the cellular and sub-cellular level contributes to our understanding of not only the human body, but also bacteria and other potential pathogens.[27-29] Therefore, there is demand for the development of biological probes for the imaging of these systems in order to provide important information as to the mechanisms of their function. In the past, the majority of these probes have utilised organic fluorophore groups.[30, 31]

In recent years however, there has been a shift towards the use of transition metal complexes as probes for biological imaging. These complexes display several marked advantages over purely organic fluorophore systems. Transition metal complexes generally display larger Stokes shifts.[9, 10] This results in less overlap between the emission and excitation spectra of these species. This in turn allows for detection of the emission of the probe at wavelengths significantly different from the excitation source, reducing interference effects from scattered incident light. Furthermore, as the emissive state of these complexes is of triplet character, the rate constant of radiative decay is lower due to the spin-forbidden nature of the transition.[9, 16, 20] This in turn leads to longer emission lifetimes, which can allow for easier discrimination between luminescence originating from the probe, and autofluorescence originating from the sample itself through the use of time-gated techniques.[9, 16, 20] Finally, these complexes are generally more stable with respect to photobleaching, allowing them to be used for longer periods of time before degrading.[9]

Transition metal based systems do encounter some challenges with respect to their application as biological probes. Both their excitation and emission wavelengths are generally situated in the deep blue to green region of the electromagnetic spectrum.[32-37] This leads to two issues, the first of which being that shorter wavelength, higher energy photons display poorer penetration into biological samples. The second is that the higher energy incident photons are often damaging to the sample, which limits their usability in live samples.[32-37] Furthermore, due to their long lifetimes and triplet emissive states, these complexes are often highly susceptible to quenching effects, especially due to dissolved dioxygen.[38] Therefore, two significant challenges in the design of transition metal complexes are the red shifting of their excitation and emission profiles, and the minimisation of quenching effects, which platinum(II) complexes are uniquely positioned to overcome.

1.3 Photophysics of Platinum(II) Complexes

1.3.1 Basic Principles

Photophysical processes are changes to a system that occur due to the interaction of a molecule with one or more photons. These processes are illustrated in Figure 1. The absorption of a photon by a molecule may occur if there exists an excited state within that molecule with a difference in energy from the ground state equal to the energy of the incident photon. The energy of the photon is used to promote an electron from an occupied frontier orbital into an unoccupied frontier orbital, resulting in an excited state of singlet character. From this excited state, the electron will non-radiatively decay into the lowest unoccupied molecular orbital (LUMO) through a number of pathways. In most organic fluorophores, the molecule will undergo rapid internal conversion (IC) to vibrationally relax to the lowest energy excited state.[39] From this excited state, the electron can radiatively decay to the ground state, releasing a photon with energy equal to that lost by the molecule during the transition.

In the case of transition metal complexes, the spin-orbit coupling of the heavy metal atom results in the mixing of singlet and triplet characters of the excited states, allowing for intersystem crossing (ISC) into lower energy triplet states.[40] The rate constant of radiative decay from a triplet state to the ground state is reduced due to the formally spin-forbidden nature of the transition.[40]

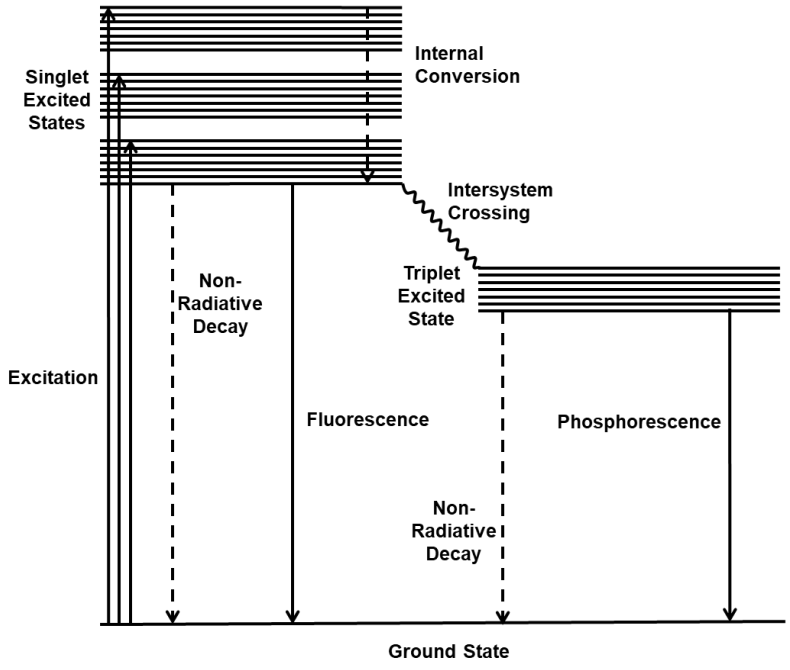

Figure 1: A Jablonski diagram showing the electronic transitions related to luminescence.

1.3.2 Types of Excited States

There are a range of possible excited states attainable by transition metal complexes, not all of which are suitable for emission.

1.3.2.1 Ligand Centred States

Several platinum(II) complexes studied in the past have demonstrated emission from excited states of ligand-centred (LC) character.[41, 42] These excited states arise in complexes containing ligands with conjugated π systems, and involve the promotion of an electron from a bonding π orbital to an antibonding π* orbital.[40] As these transitions are localised within a single ligand, they generally display structured emission spectra due to vibronic coupling with vibrational modes within the ligand.

1.3.2.2 Charge Transfer States

A significant number of highly emissive platinum(II) complexes that have been investigated emit from excited states with significant charge transfer character.[43, 44] Charge transfer states involve the promotion of an electron from one region of the complex to another. This results in the excited state possessing a significantly different dipole moment than the ground state. This change in dipole moment can be used to identify charge transfer bands in a spectrum. By increasing the polarity of the solvent, the more polar of the two states will be reduced in energy relative to the less polar state.[40] Therefore, in cases where the excited state possesses a greater dipole moment than the ground state, increasing the polarity of the solvent will result in a bathochromic shift in emission. Conversely, in cases where the ground state possesses a greater dipole moment than the excited state, increasing the polarity of the solvent will result in a hypsochromic shift in emission. This effect is known as solvatochromism, and can be used to infer charge transfer character in an emission band.[40]

Metal-to-ligand charge transfer (MLCT) states are the result of an electron being promoted from a *d* orbital of the metal centre of the complex to an unoccupied orbital in the ligand, usually a π* orbital.[40] These transitions are most common when the metal is easily oxidised, and the ligand easily reduced. This generally occurs when the metal centre has a low oxidation state, and when the ligands contain conjugated systems with low energy π* orbitals.[40] Therefore, most charge transfer states observed in monomeric platinum(II) complexes are MLCT in nature.

Ligand-to-metal charge transfer (LMCT) states, conversely, are the result of an electron being promoted from an occupied orbital in the ligand, usually a non-bonding (n) orbital, to an unoccupied *d* orbital in the metal centre.[40] These transitions are therefore most common when the metal is easily reduced, and the ligand easily oxidised. This generally occurs when the metal centre has a high oxidation state, and the ligand contains non-bonding electrons, such as those generally occupied by lone pairs.[40] Therefore, these transitions are generally not observed in platinum(II) complexes due to their low oxidation state.

Metal-metal-to-ligand charge transfer (MMLCT) states may occur in planar platinum(II) complexes due to their planar molecular geometry.[45] The planar nature of these complexes allows two or more molecules to 'stack' together with intermolecular separations reaching as low as 3 Å. Due to the fact that the d_z^2 orbitals of the platinum centre are oriented orthogonal to the plane of the complex, they are capable of interacting with the d_z^2 orbitals of the complexes 'stacked' above and below themselves. This interaction results in the formation of bonding (dσ) and antibonding (dσ*) molecular orbitals.[45] The antibonding nature of this dσ* orbital raises its energy considerably, causing it to become the HOMO of the newly formed dimeric species.[45] Furthermore, π*- π* interactions between the aromatic ligands of each molecule can result in the lowering of the energy of the LUMO.[45] These effects result in MMLCT states of displaying a significant bathochromic shift compared to the LC or MLCT emissive states of the monomeric species. The need for intermolecular interaction for the formation of the MMLCT excited states means that such emission is generally only observed in samples at high concentrations or low temperatures, or in the solid state.

1.3.2.3 Metal Centred States

Metal centred (MC) excited states are the result of the promotion of an electron from either the d_z^2 or d_{xy} orbitals to the unoccupied $d_{x^2-y^2}$ orbital. However, due to the strongly antibonding nature of the $d_{x^2-y^2}$ orbital, this transition results in a significant distortion of the molecule. This distortion often results in the formation of an isoenergetic point with the ground state, allowing for rapid vibrational, non-radiative decay.[45] Therefore, MC states are generally non-emissive in platinum(II) complexes. While such states are rarely the lowest energy excited state, they often lie at a low enough energy to be thermally accessible from the lowest energy excited state, especially in complexes utilising simple organic ligands such as diethylenetriamine (DETA). This can result in thermal population at room temperature, allowing the MC state to act as an alternative, nonradiative, decay pathway from the emissive state.[45] Due to the fact that

this nonradiative decay is generally considerably faster than radiative decay from the emissive state, the presence of a low lying MC state often results in simple platinum(II) complexes being non-emissive in room temperature solutions.[45] Therefore, a significant portion of research in the luminescence of platinum(II) complexes has focused on structural motifs designed to raise the energy of MC states, rendering them thermally inaccessible from the emissive state, cutting off the 'drainpipe' of energy.[45]

1.4 Past Work

There has been significant interest in cyclometallated platinum(II) complexes for applications in light emitting materials due to their promising photophysical properties. While these studies have explored a massive range of cyclometallated complexes,[42-44, 46-48] this summary will focus on the two major classes of these compounds that have to date demonstrated the best performance in terms of quantum yield.[42, 49] The first of these classes incorporate N-heterocyclic carbene ligands, which exploit the strong σ donating capacity of the carbene ligand to raise the energy of the MC state. The second class incorporates terdentate ligands, which rigidify the complex, reducing the capacity for non-radiative vibrational relaxation, improving quantum yields.

1.4.1 N-Heterocyclic Carbenes

The first N-heterocyclic carbenes (NHCs) were synthesised as ligands on metal complexes due to their increased stability in this state when compared to the free carbene. Wanzlick and co-workers[50] reported a bis-imidazole mercury(II) complex in 1968. Following this, the first free N-heterocyclic carbene was reported by Arduengo and co-workers[51] in 1991, using bulky adamantyl groups to hinder the formation of dimeric alkene species. This report in turn lead to a wide range of new NHCs being developed and investigated for applications in the areas of molecular photophysics and catalysis, both as ligands for *d*- and *p*- block elements, and as organocatalysts in their own right.[52, 53]

1.4.2 Platinum(II) NHC Complexes

In the last decade, there has been an emerging interest in the application of cyclometallated NHCs as ligands for platinum compounds in the development of phosphorescent organic light emitting diodes (PhOLEDs).[33]

In 2010, Strassner and co-workers[32] reported a range of platinum(II) compounds bound to substituted 1-phenyimidazole ligands with β-diketonate ancillary ligands. The general structure of these complexes is illustrated in Figure 2. These complexes showed highly promising photophysical properties, achieving quantum yields between 0.05 and 0.9, with lifetimes in the tens of microseconds. Furthermore, all but one of these complexes displayed highly structured emission spectra, suggesting significant ligand charge transfer character in the emissive state.

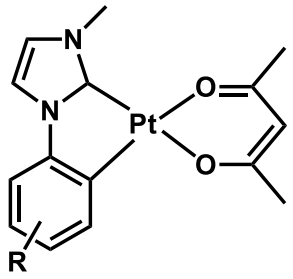

Figure 2: The general structure of the 1-phenylimidazole platinum(II) complexes reported by Strassner and co-workers.[32]

The photophysical properties of these complexes were dependent on the nature of the substituent present on the cyclometallated phenyl ring, as illustrated in Figure 3. The inclusion of a highly electron withdrawing nitro group resulted in an unstructured emission band, alongside a significant bathochromic shift and increase in the lifetime of the emissive state. This was conjectured to be the result of aggregate effects resulting in the formation of an MMLCT state, but this hypothesis was not conclusively proven. Furthermore, extension of cyclometallated aromatic system, by replacing the phenyl ring with dibenzofuran, resulted in a significantly improved quantum yield.

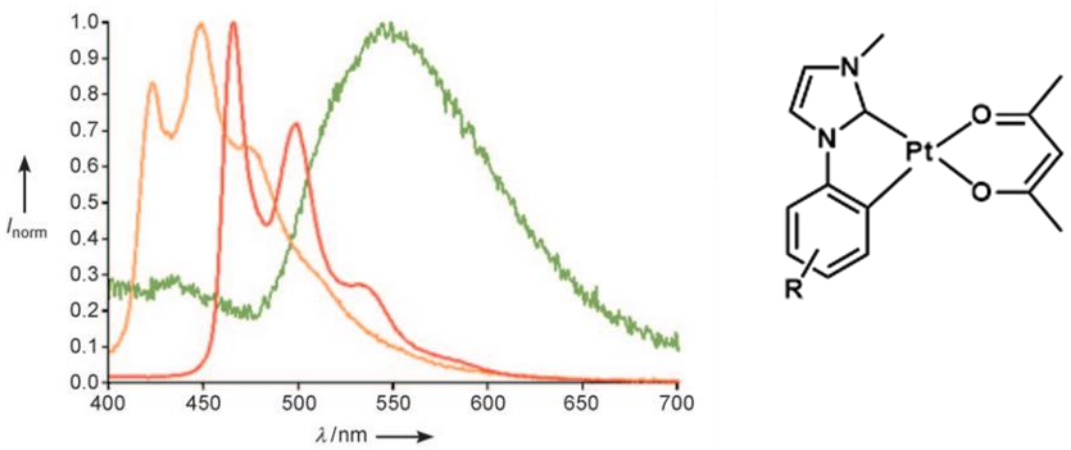

Figure 3: Emission spectra of a number of 3 1-phenylimidazole platinum(II) complexes (2% in PMMA, room temperature).[32] R = 4-NO_2 (green trace), R = 4-Me (orange trace), R = 2,3-OC_6H_4.

In 2013, Strassner and co-workers[54] reported the first incidence of a triazolin-5-ylidene bound to a platinum centre. This work reported a range of platinum(II) complexes bound to both 1-aryl and 4-aryl triazoles. The general structure of these complexes is illustrated in Figure 4. Almost all complexes displayed strong emission at room temperature. The emission profiles for these complexes were highly structured, suggesting a strong ligand centred (LC) or intra-ligand (IL) character to the emission, similar to those reported in the previously reported imidazole complexes.

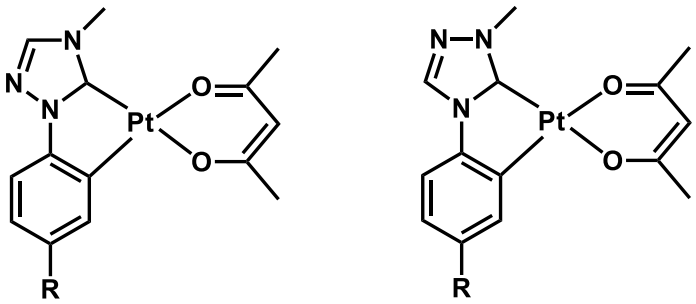

Figure 4: The general structures of the 1-aryl-1,2,4-triazol-5-ylidene (left) and 4-aryl-1,2,4- triazol-5-ylidene (right) platinum(II) complexes reported by Strassner and co-workers.[54]

Following the trend of the previously reported imidazole complexes,[32] the structure of the cyclometallated NHC ligand had a significant influence on the photophysical properties of these complexes, as shown in Figure 5.[54] Those complexes bearing 4-aryl triazole derived ligands showed significantly lower quantum yields, between 0.11 and 0.14, than those bearing 1-aryl triazole derived ligands. The presence of a strongly electron withdrawing nitro group on the phenyl ring of the 4-aryl triazole was found to negate emission almost completely, while the presence of weak electron withdrawing or electron donating groups were not found to have

any appreciable effect on the emission. Those complexes bearing 1-aryl triazole complexes however, were found to have much higher quantum yields, up to 0.41, and displayed slightly redshifted emission compared to the 4-aryl triazole complexes, as illustrated in Figure 5. Additionally, the substituents on the phenyl ring of these complexes were found to have a more significant effect on their emission, allowing for the optimisation of both quantum yield and the wavelength of maximum emission.

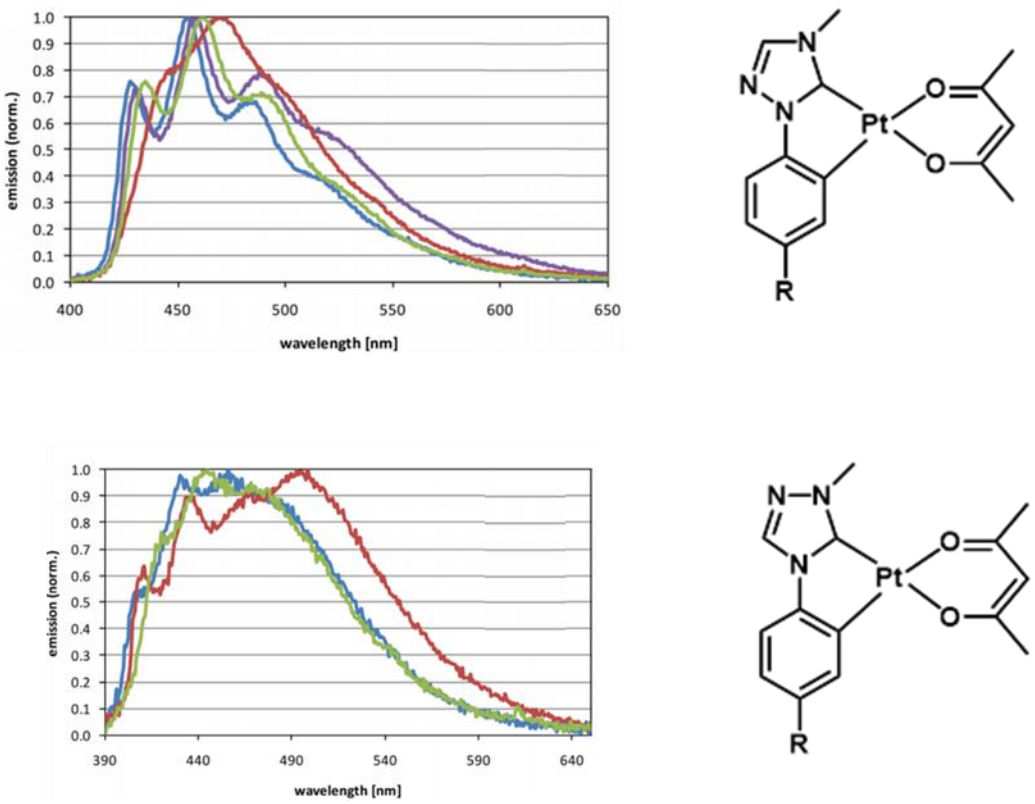

Figure 5: Emission spectra of a number of 1-aryl-1,2,4-triazol-5-ylidene (top) and 4-aryl-1,2,4- triazol-5-ylidene (bottom) platinum(II) complexes (2% in PMMA).[54] Top: R = H (blue trace), R = Cl (purple trace), R = OCH_3 (red trace), R = CH_3 (green trace). Bottom: R = H (blue trace), R = Cl (red trace), R = OCH_3 (green trace).

Two studies by Strassner and co-workers[43, 49] in 2016 and 2017 investigated a range of platinum(II) complexes bound to N-arylthiazole-2-ylidenes, with a variety of substituents on both the phenyl and thiazole rings. The general structure of these complexes is illustrated in Figure 6. Unlike previously reported NHC platinum(II) complexes,[32, 54] these compounds displayed largely unstructured emission bands due to significant MLCT character in the excited state, as illustrated in Figure 7.[43, 49] They also showed promising quantum yields, which ranged from 0.33 to 0.79, and emission lifetimes, which ranged from microseconds to tens of microseconds.

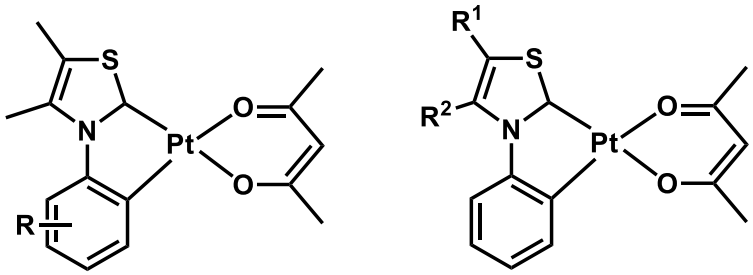

Figure 6: The general structures of the N-phenylthiazole platinum(II) complexes reported by Strassner and co-workers.[43, 49]

Substituents on both the thiazole and phenyl rings were found to have significant effects on the photophysical properties of the resulting complexes. In the case of the thiazole ring, methyl and ester groups were found to have the strongest positive effect on quantum yield. On the phenyl ring, electron withdrawing groups such as esters and nitriles were found to have the strongest positive effect on quantum yield. Interestingly, the wavelength of the emission was largely unaffected by the substitution of the N-arylthiazole-2-ylidene ligand, with only a 29 nm difference between the highest and lowest reported emission maxima.

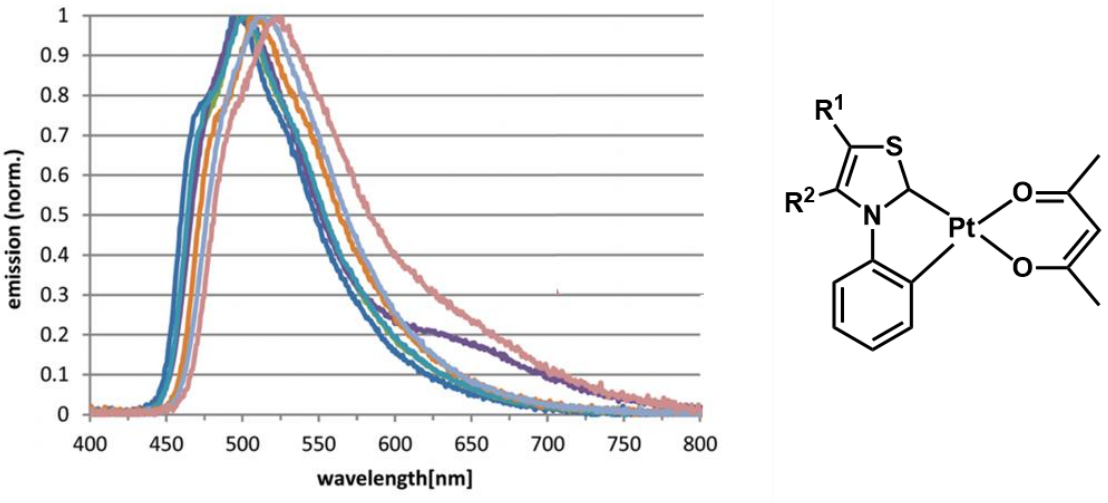

Figure 7: Emission spectra of a number of N-phenylthiazole platinum(II) complexes (2% in PMMA).[43] R^1 = H, R^2 = H (blue trace), R^1 = H, R^2 = Me (green trace), R^1 = CO_2Me, R^2 = Me (purple trace), R^1 = H, R^2 = Ph (teal trace), R^1 = Me, R^2 = Ph (orange trace), R^1 = Ph, R^2 = Ph (grey trace), R^1 = R^2 = (C_4H_4) (salmon trace).

Notably, all photophysical investigations of cyclometallated NHC based platinum(II) complexes have been explored within the context of application of organic light emission devices (OLEDs).[32, 43, 44, 49, 54] In this context, the design goals for these complexes vary slightly from the design goals of complexes intended to act as biological probes. While both

applications benefit from increased quantum yields and longer emission lifetimes, they diverge in their requirements for absorption and emission maxima. Research into OLEDs aims to develop a range of compounds that can emit at any given wavelength, with most platinum(II) complexes developed in this context emitting in the deep blue to green-range regions of the electromagnetic spectrum.[32, 43, 44, 49, 54, 55] For biological applications however, redshifted absorption and emission bands provide significant advantages, namely that lower energy red light is both better able to penetrate soft tissue,[10, 56] and is less damaging to cells.[57, 58]

1.4.3 Terdentate Platinum(II) Complexes

In 1934, Morgan and Francis were the first researchers to report a terpyridyl platinum(II) complex in the form of the 2:2':2"-tripyridylchloroplatinous platinochloride salt, as shown in Figure 8, along with a number of related compounds.[59]

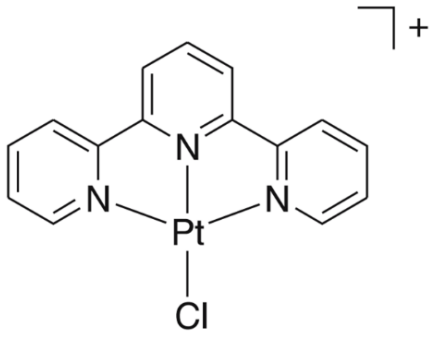

Figure 8: 2:2':2"-tripyridylchloroplatinous ion.[59]

However, following this study, terdentate platinum(II) complexes were not studied in any great detail until the 1970s. In 1977 to 1978 Mureinik and Bidani investigated the reaction kinetics of ligand substitution of the ancillary ligand in terpyridyl platinum(II) complexes.[60, 61] This investigation found that the terpyridyl complexes are significantly more labile than complexes coordinated to bipyridyl ligands and terdentate ligands that involve bases that are not part of a conjugated system. This is likely due the delocalisation of electron density from the d_{xz} and d_{yz} orbitals of the platinum centre into the coplanar π system of the terpyridyl ligand.[60, 61] This idea is supported by similar findings by Conrad and Rund[62] in platinum(II) complexes bearing phenanthroline ligands.

In 1994 McMillin and co-workers[63] led an investigation into the photophysical properties of tripyridyl platinum(II) complexes in fluid solution. They found that the basic chloride terpyridyl complex was not emissive in fluid solution. However, complexes with hydroxide, methoxide, and thiocyanate ancillary ligands gave broad unstructured emission spectra in room temperature solutions of acetonitrile, as illustrated in Figure 9. Based on this lack of a vibronic structure, the emission was assigned to an MLCT excited state.

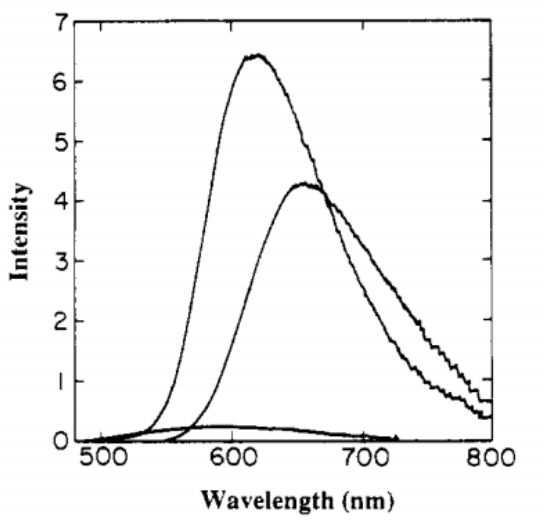

Figure 9: Emission spectra of $[Pt(trpy)OH]^+$, $[Pt(trpy)OMe]^+$, and $[Pt\text{-}(trpy)NCS]^+$ in room temperature MeCN.[63]

It was found that the lifetime of the emissive state was higher in those complexes with lower energy emissive states. This supports the idea that a *d-d* excited state can be thermally populated from the emissive MLCT state, allowing for non-radiative thermal decay, as this *d-d* state would be less accessible to systems with lower energy emissive states.[64] Consequently, even the most emissive of these complexes displayed a quantum yield of just 0.0021.

In 1995 Bailey and co-workers[65] investigated the photophysical properties of tripyridyl complex ions in the solid state. They found that the luminescence of these compounds is strongly influenced by Pt-Pt and π-π ligand interactions between the monomer units due to their planar geometry. Therefore, the identity of the counterion and the solvent from which the solid was crystallised both play a significant role in determining the photophysical properties of the crystal. As different counterions have different sizes and geometries, the crystals they form with the complex ion have varying structures, which influences the strength of these planar interactions, as illustrated in Figure 10. The lowest energy emission in this case was attributed to MMLCT excited states arising from metal-metal interactions, though emission from ligand

centred π-π* transitions was also observed.[41] However, in fluid solution, only the MMLCT emission was observed, and only at temperatures below 150K.

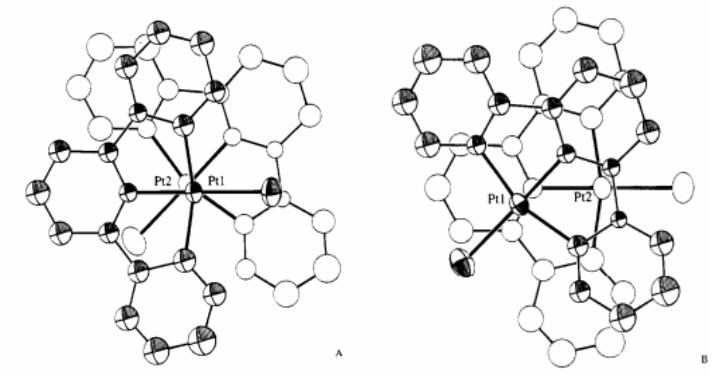

Figure 10: Diagrams showing the two different orientations that occur in the planar stacking of terpyridyl platinum(II) complexes.[65] Both orientations were present in a single stack of complexes in an alternating manner.[65]

A C^N^N coordinated terdentate platinum(II) complex was first reported by Constable and co-workers[66] in 1990, by simply refluxing a mixture of 6-phenyl-2,2'-bipyridine and potassium tetrachloroplatinate in water and acetonitrile. The structure of the complex is shown in Figure 11. This complex was then found to display much the same Pt-Pt interactions forming dimeric units in the solid state as tripyridyl platinum(II) complexes.[67] The photophysical properties of these complexes was then investigated by Che and co-workers[46] in 1996. The emission of Pt(C^N^N)(Cl) in the solid state was found to be fairly similar to that of the analogous tripyridyl complex, owing to their similar crystal structures, and was assigned to a MMLCT excited state.

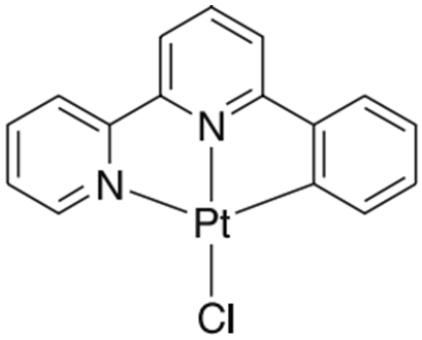

Figure 11: C^N^N platinum(II) chloro complex.

The simple Pt(C^N^N)(Cl) complex showed relatively intense emission in room temperature fluid solutions, with quantum yields up to 0.025, an order of magnitude greater than the most emissive analogous terpyridyl complexes.[63, 65] The emissive state in these complexes was

determined to be MLCT in nature, due to the broad, unstructured nature of the emission profile, as illustrated in Figure 12.[67] The increased intensity can therefore be attributed to the fact that, as a much stronger σ donator than nitrogen, the coordinated carbon atom exerts a much stronger ligand field on the platinum centre, raising the energy of $d_{x^2-y^2}$ orbital and therefore the *d-d* metal centred excited state. This reduces the accessibility of the metal centred state, reducing the amount of non-radiative decay that occurs through that pathway.[45]

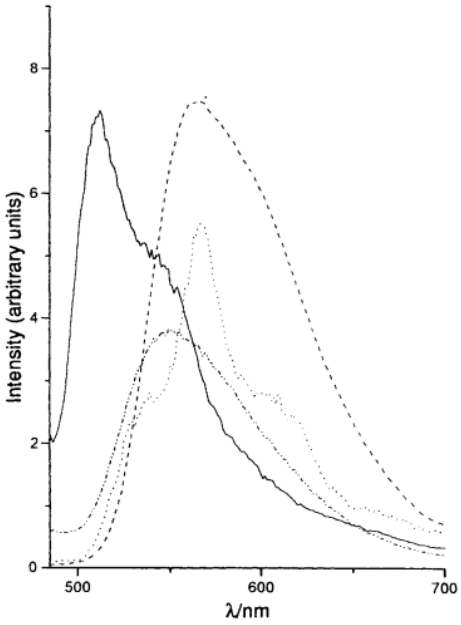

Figure 12: Emission spectra of [PtL(Cl)] in MeCN (298 K) (- . . -), CH_2Cl_2 (298 K) (- - -), MeCN (77 K) (—) and CH_2Cl_2 (77 K) (. . . .).[46]

The first N^C^N coordinated platinum(II) complex was reported by Cardenas and co-workers[68] in 1999. The 1,3-di(2-pyridyl)benzene ligand was produced by a Stille coupling between 1,3-dibromopyridine and (2-pyridyl)tri-n-butylstannane before being cyclometallated with potassium tetrachloroplatinate by refluxing in glacial acetic acid. The structure of the complex is shown in Figure 13.

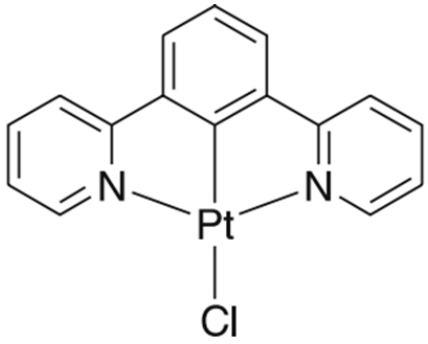

Figure 13: N^C^N platinum(II) chloro complex.

Williams and co-workers[42] subsequently carried out a detailed investigation of the photophysical properties of these complexes in 2003. They were found to be extremely emissive in room temperature fluid solution, with quantum yields of up to 0.68, an order of magnitude greater than those observed in analogous C^N^N coordinated complexes. This increase was attributed to the fact that cyclometallated C-Pt bond length is much shorter in the central position, resulting in a much stronger ligand field. This in turn raises the energy of the *d-d* transition so far as to make it thermally inaccessible, preventing any non-radiative decay from occurring through that pathway. Furthermore, the highly structured nature of the observed emission spectra, as illustrated in Figure 14, led to the emission being assigned to a ligand centred π- π* excited state, as opposed to the MLCT states responsible for the emission of N^N^N and C^N^N coordinated platinum(II) complexes.

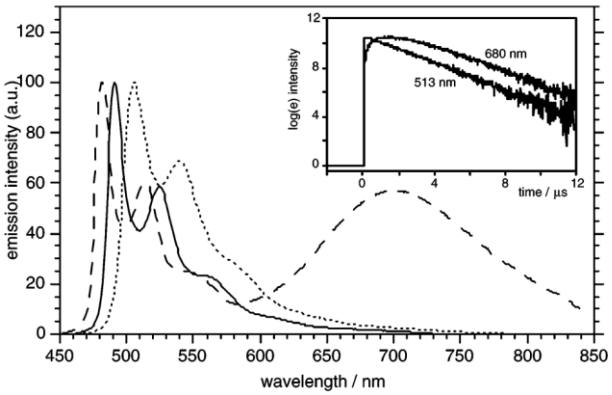

Figure 14: Emission spectra of [PtLCl] (—) and [PtL(Me)Cl] (…) in dilute solution in CH_2Cl_2, and [PtL(OMe)Cl] (- - -) at higher concentration.[42]

The first C^N^C coordinated platinum(II) complex was produced in 1988 by Cornioley-Dueschel and co-workers.[69] The structure of the complex is illustrated in Figure 15. They found that these complexes were emissive in glassy solutions, and that this emission was due to a MLCT excited state, similar to those in analogous N^N^N and C^N^N complexes. However, work by Yam and co-workers[47] found that these species are generally non-emissive in room temperature fluid solution, with a few exceptions due to the influence of crown ether ancillary ligands. This is due to the fact that these complexes become distorted upon being promoted to an excited state, which facilitates non-radiative decay.[70] Therefore, modification of these ligands with substituents or heterocyclic analogues that improve rigidity results in a corresponding improvement in desirable emissive properties due to reduced capacity for distortion.[71]

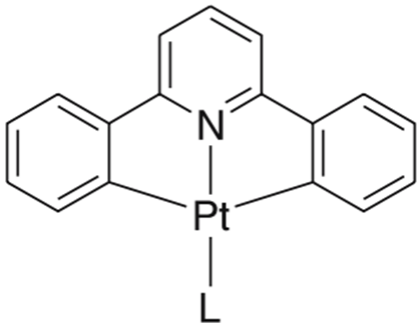

Figure 15: C^N^C platinum(II) complex where L is a neutral ligand.

While C^C^N coordinated platinum(II) complexes are yet to be investigated, Kumar and co-workers[72] led a study into the luminescent properties of C^C^N coordinated gold(III) complexes in 2015. The general structure of these complexes is illustrated in Figure 16.

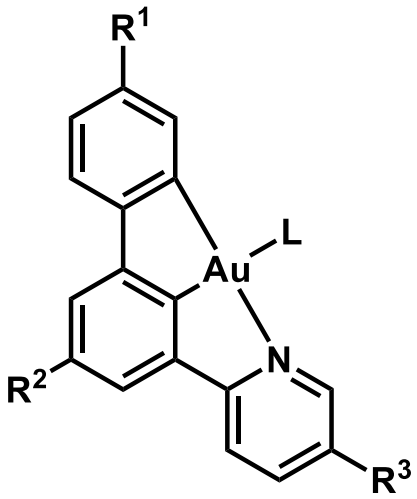

Figure 16: Basic structure of C^C^N gold(III) complexes investigated by Kumar and co-workers.[72]

These complexes were found to be highly emissive in room temperature fluid solutions, with quantum yields of up to 0.28.[72] This was a massive improvement upon the performance of analogous C^N^C coordinated gold(III) complexes, which display quantum yields of around 0.006 to 0.0002.[73] This emission was assigned to π- π* excited states, similar to those observed in N^C^N coordinated platinum(II) complexes, due to the structured nature of the emission profiles, as illustrated in Figure 17.[72] Interestingly, no Au-Au interactions were observed in either the solid state or in solution, despite the planar geometry of the complexes.[72] This suggests that gold(III) complexes are unlikely to demonstrate the same aggregation induced emission from MMLCT states as analogous platinum(II) complexes.[45] This further reinforces the unique advantage of platinum(II) complexes in their ability to redshift their excitation and emission spectra through planar stacking.[45]

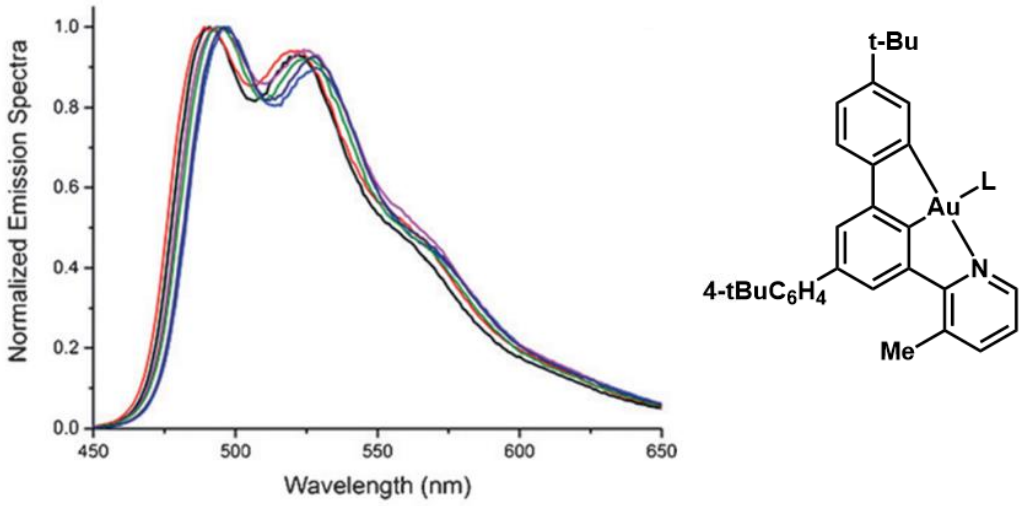

Figure 17: Emission spectra of a number of derivatised C^C^N gold(III) complexes.[72] L = F (black trace), L = Cl (red trace), L = C_2CO_2Me (blue trace), L = C_2Ph (pink trace), L = C_2-4-$tBuC_6H_4$ (green trace), L = C_2-3,5-$(CF_3)_2$-C_6H_3 (purple trace).

1.5 Aim and Scope

The primary aim of the work undertaken in this project was to develop a range of cyclometallated platinum(II) complexes and investigate their photophysical properties to determine if they are suitable compounds for applications in biological imaging. The target complexes were broadly grouped into two families.

The first of these families aimed to incorporate N-arylthiazol-2-ylidene ligands, while replacing the ancillary β-diketonate ligands that characterised the complexes developed by Strassner[43, 49] with various substituted pyridyl tetrazole ligands. The general structure of these target complexes is illustrated in Figure 18. Pyridyl tetrazole was chosen for the purpose due to its ease of synthesis, and the commercial availability and low cost of a wide range of starting materials. By investigating the effects of varying substituents on the 5 position of the pyridine ring on the photophysical properties of the resulting complexes, structural motifs resulting in redshifted emission profiles and improved quantum yields could be identified. Furthermore, the incorporation of highly modifiable groups such as bromo and amino groups allows for the introduction of more complex structural features, including groups that are known to bind specifically to certain biological structures. These include triphenylphosphonium groups for targeting mitochondria and organic azides for binding to lipids.[74, 75]

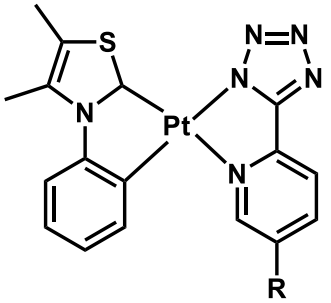

Figure 18: The general structure of the target N-phenylthiazole platinum(II) complexes.

The second of these families aimed to incorporate a terdentate, dicyclometallated ligand motif with a C^C^N coordination pattern, as illustrated in Figure 19. The rationale for this structural motif was the inclusion of a second cyclometallated position on a terdentate complex, increasing its donor strength, and therefore raising the energy of the MC states responsible for non-radiative decay. By having these cyclometallated positions in a cis conformation, it was hoped that the distortion of the excited state could be reduced compared to that of C^N^C coordinated complexes, and therefore improve photophysical properties.

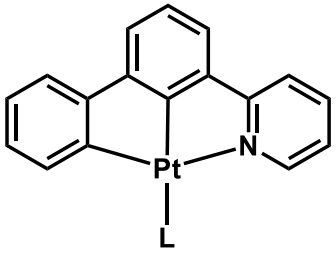

Figure 19: The general structure of the target C^C^N coordinated platinum(II) complexes, where L is a neutral ligand.

Chapter 2: Synthesis and Characterisation of Thiazol-2-ylidene Platinum(II) Complexes and their Precursors

2.1 Overview

This chapter will discuss the synthesis and characterisation of all N-heterocyclic carbene platinum(II) complexes produced in this work, as well as that of their ligand precursors. First the thiazolium salt and pyridyl tetrazole ligands were synthesised from aniline and a range of 5-substituted cyanopyridines respectively. These ligands were then coordinated to platinum in a three stage one pot synthesis as shown in Figure 20.

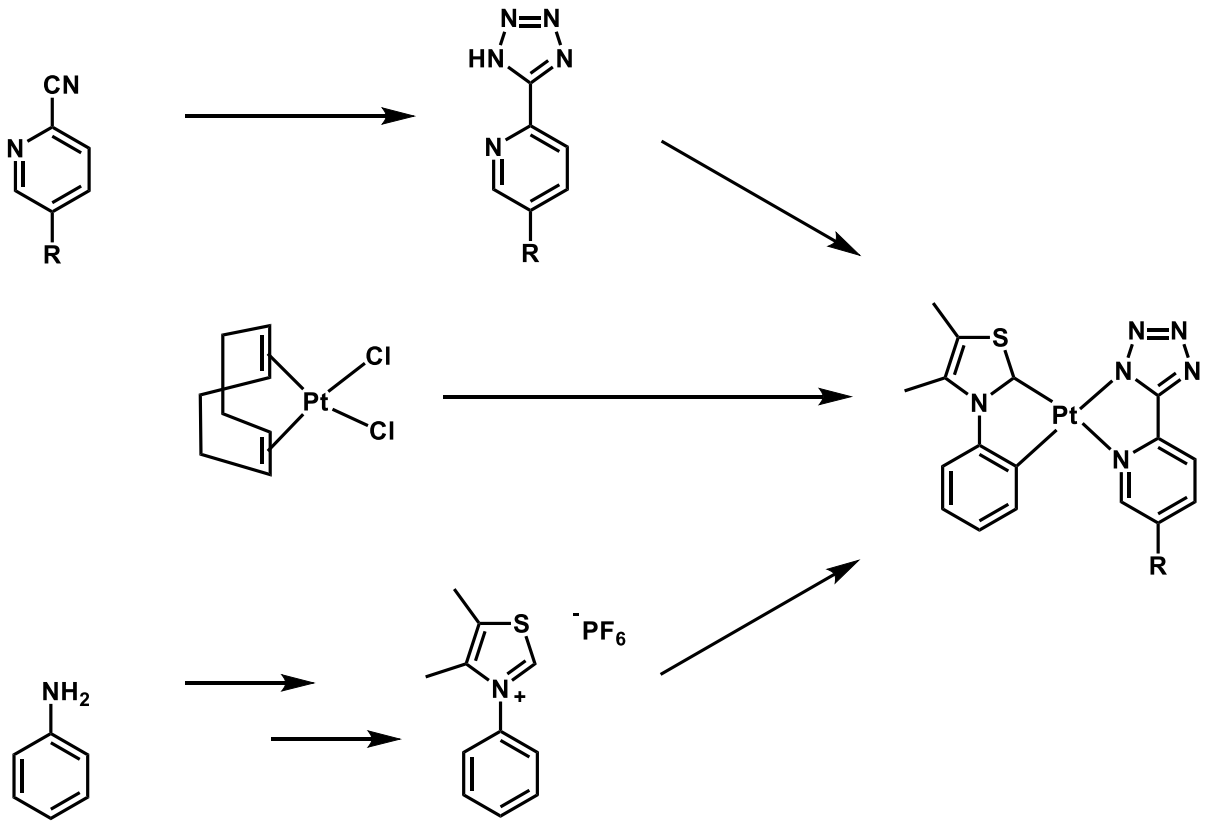

Figure 20: Overview of the general synthetic scheme for the synthesis of NHC platinum(II) complexes.

The focus of this research was on the modification of the 5 position of the pyridine ring, in order to investigate the effect of substituents on ligands other than the NHC on the photophysical and biological properties of these complexes. Five novel complexes were reported with varying functional groups in the 5 position, as shown in Figure 21.

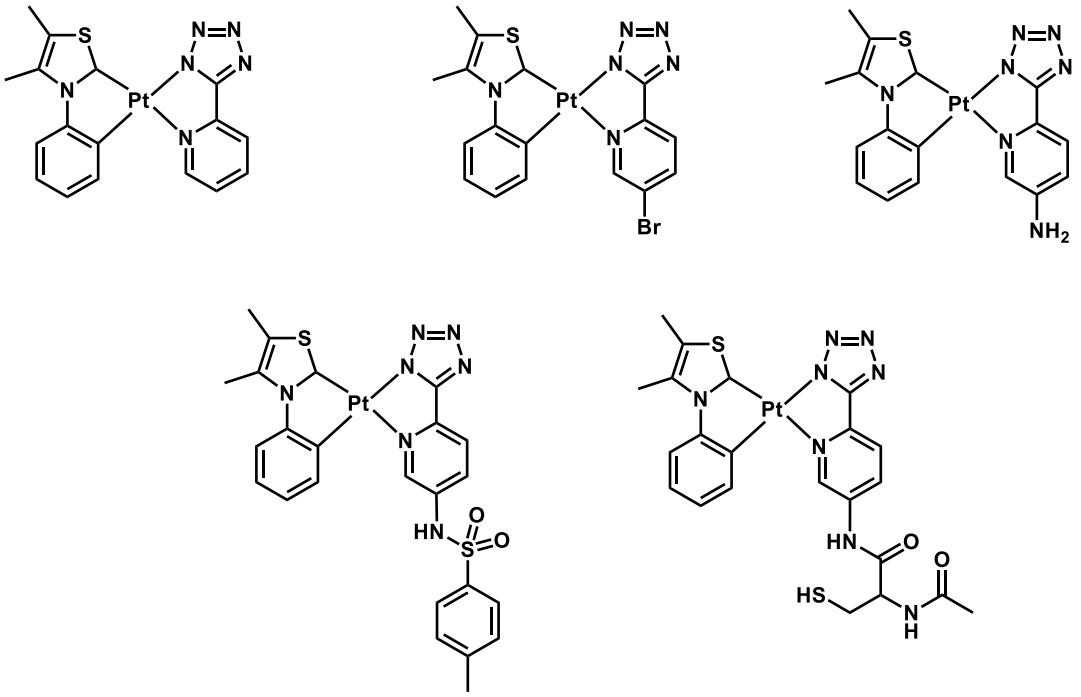

Figure 21: The structures of the five complexes obtained using this synthetic pathway.

2.2 Rationale

Platinum(II) complexes bearing thiazole ligands are known in the literature for their high quantum yields, and for the ease of synthesis of their ligand precursors.[43, 49] Therefore, the thiazole moiety was chosen as the NHC carbene ligand for the compounds synthesised in this chapter. The pyridyl tetrazole ligands were selected for two reasons, the first of which was their widespread use in emissive transition metal complexes in the literature whilst not having been explored in cyclometallated NHC platinum(II) complexes.[76-78] The second being the ease of synthesis of a wide range of substituted ligands from commercially available pyridine carbonitrile starting materials.

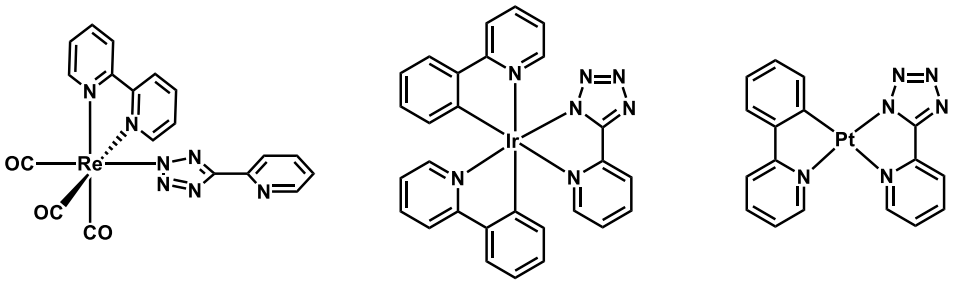

Figure 22: Examples of a number of emissive transition complexes bearing pyridyl tetrazole ligands.[76-78]

The bromo and amino substituted ligands were selected as both are viable handles in a range of coupling reactions. This allowed for further modification of these ligands to incorporate a wide range of functional groups. In the case of the bromo substituent these included palladium catalysed cross coupling reactions such as Suzuki or Stille reactions. In the case of the amino substituent these included amide coupling reactions using a range of coupling reagents such as thionyl chloride or TBTU, or S-N coupling reactions to form sulfonamides. The p-toluenesulfonamide and N-acetylcysteine substituted ligands were selected due to the presence of highly polar functional groups in an attempt to improve the water solubility of their respective complexes, hence improving their viability in biological applications.

2.3 Synthesis of Ph(ThMe$_2$S)

Thiazol-ylidene ligands are generally generated in situ by the deprotonation of thiazolium salt precursors.[43, 49] Therefore, it was necessary to synthesise such a thiazolium salt. This synthesis was achieved in a two step process, through a stable thiazole thione intermediate.

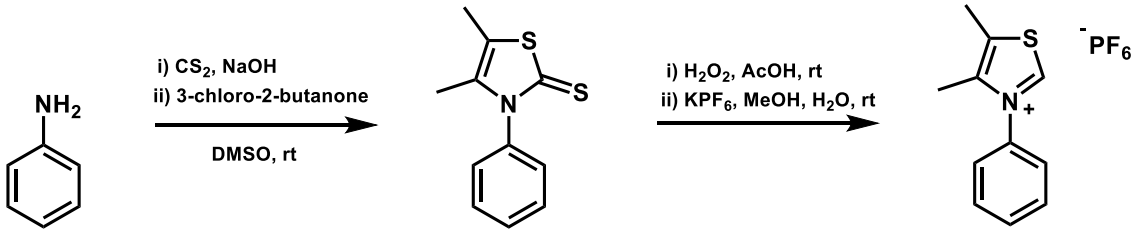

Figure 23: Synthetic pathway for the synthesis of the Ph(ThMe$_2$S) precursor.

Ph(ThMe$_2$S) was synthesised via a method reported by Bach and co-workers[79] using aniline as a starting material. The mechanism for this reaction is illustrated in Figure 24. The first step was a nucleophilic attack by the nitrogen of the aniline on carbon disulfide under basic conditions to generate a dithiocarbamate salt. The subsequent addition of 3-chloro-butanone then resulted in the nucleophilic substitution of the chlorine atom by the sulfur of the dithiocarbamate. Ring closure was then achieved by the nucleophilic addition of the nitrogen atom to the carbonyl. Finally the product was generated by the acid catalysed dehydration of the crude hydroxy-thiazole, and collected via crystallisation from the reaction mixture. No further purification was necessary, and so the product was used as obtained.

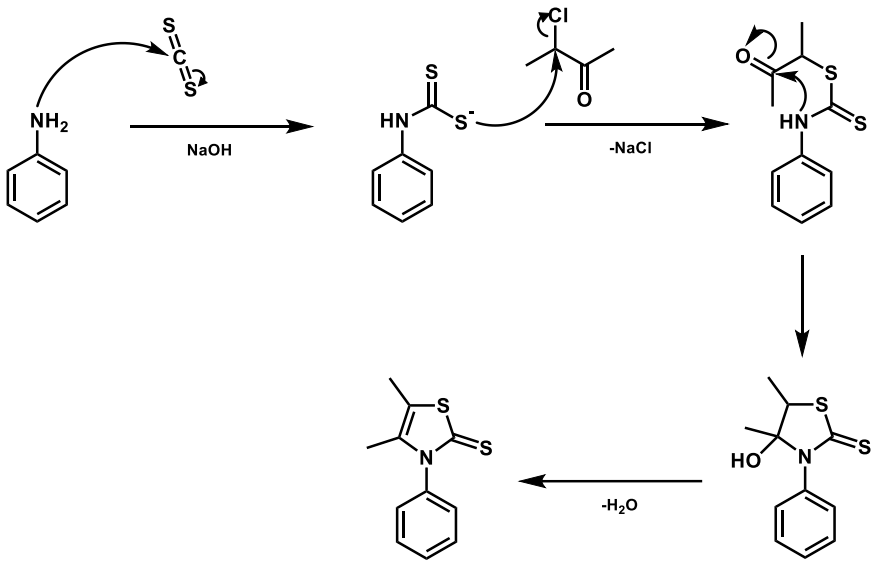

Figure 24: Mechanism for the formation of the Ph(ThMe$_2$S) as proposed by Strassner and co-workers.[49]

Ph(ThMe$_2$S) was confirmed using NMR and IR spectroscopy. The ^{1}H NMR spectrum showed 3 peaks in the aromatic region, representing a total of 5 protons, and showing splitting characteristic of a singly substituted phenyl ring. The two singlets at 2.19 and 1.81 ppm, each integrating for 3 protons, were characteristic of the methyl groups on the thiazole ring. The obtained spectrum was in good agreement with that reported by Strassner and co-workers[49] in 2016. The quintet at 2.50 ppm was assigned as the residual solvent peak of DMSO while the singlet at 3.33 ppm was ascribed to water present as an impurity in the d_6-DMSO.

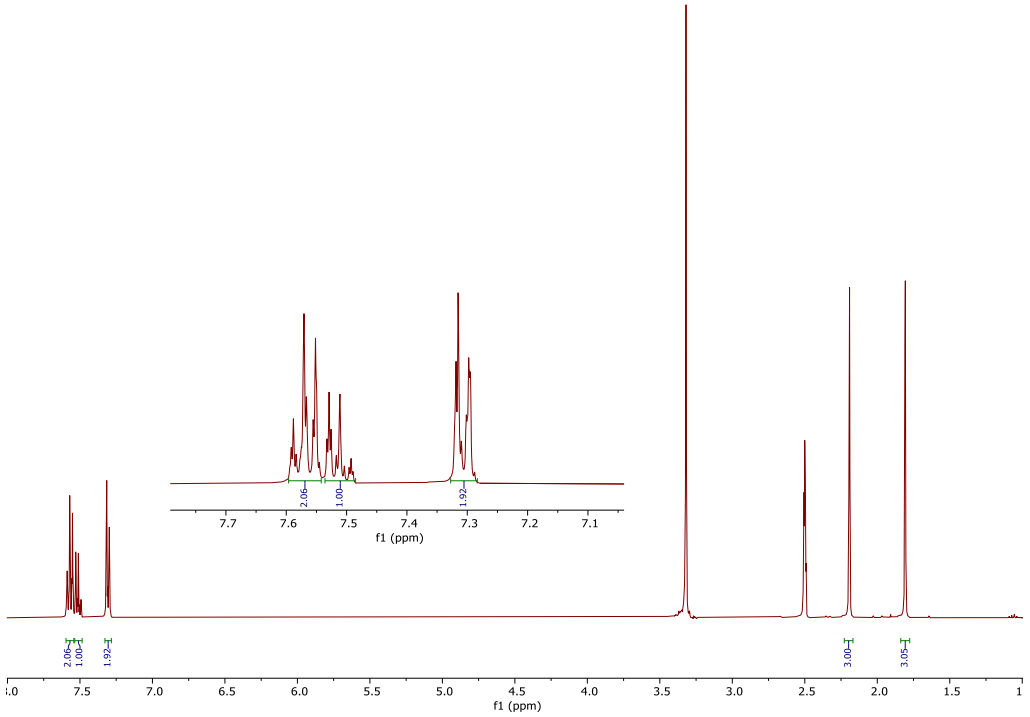

Figure 25: ^{1}H NMR spectrum of the Ph(ThMe$_2$S) in d_6-DMSO.

The infrared spectrum displayed a strong, sharp peak at 1238 cm^{-1}, characteristic of a C=S bond. In addition, the peak at 2916 cm^{-1} was indicative of an aliphatic C-H stretch, while the peaks at 1490 and 1591 cm^{-1} were characteristic of aromatic C=C bonds.

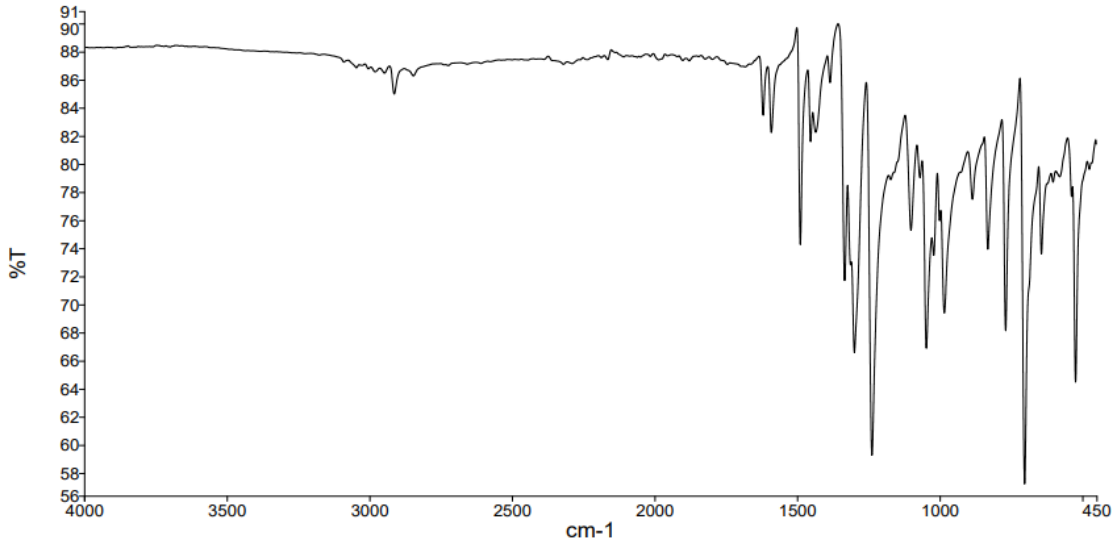

Figure 26: Infrared spectrum of the Ph($ThMe_2S$).

2.4 Synthesis of Ph($ThMe_2H$).PF_6

Ph($ThMe_2H$).PF_6 was then synthesised according to the continuation of the procedure developed by Bach and co-workers.[79] The mechanism for this reaction is illustrated in Figure 27. The addition of 3 equivalents of hydrogen peroxide to the Ph($ThMe_2S$) resulted in the stepwise oxidation of the thione to a sulfonic acid, accompanied by the generation of 3 equivalents of H_2O. This sulfonic acid was then electrophilically substituted by a proton from acetic acid, which also functioned as the solvent for this reaction, generating an acetate salt. However, due to the nature of the acetate counter-ion as a potential ligand, it was necessary to replace it with a non-coordinating anion. Therefore, the final step of this synthesis was an anion exchange with potassium hexafluorophosphate to yield the product as a hexafluorophosphate salt. The hexafluorophosphate counter ion was chosen due to Strassner and co-workers[49] reporting lower hygroscopicity in salts using this ion than in those using a perchlorate counter ion.

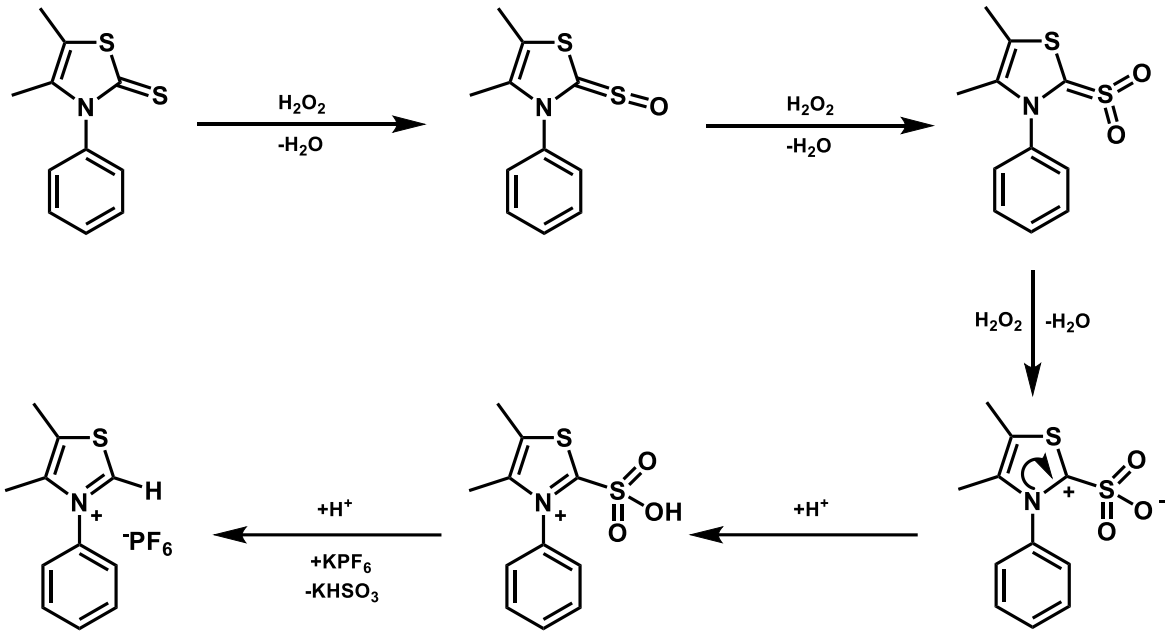

Figure 27: Mechanism for the formation of $Ph(ThMe_2H).PF_6$ as proposed by Strassner and co-workers.[49]

Finally, the product was precipitated by the slow addition of diethyl ether to a stirring solution of dichloromethane (DCM) until turbidity was observed upon addition. The solution was then cooled to 4°C overnight to allow for slow crystallisation. Attempts to precipitate the product more rapidly through the addition of further diethyl ether resulted in the formation a fine powder that proved difficult to collect via vacuum filtration.

The product was confirmed via NMR and IR spectroscopy. The ^1H NMR showed a multiplet from 7.69 to 7.73 ppm, integrating for 5 protons, that represented all 5 hydrogens of the phenyl ring, which could not be resolved from one another. The singlet containing 1 proton at 10.26 ppm was characteristic of the hydrogen at the 2 position of the thiazolium ring. Finally, the two singlets at 2.59 and 2.21 ppm, each containing 3 hydrogens, were assigned to the two methyl groups at the 4 and 5 positions of the thiazolium ring. The downfield shift of these methyl peaks relative to the thiazole thione was due to deshielding caused by the lower electron density of the cationic thiazolium ring. The obtained spectrum was in good agreement with that reported by Strassner and co-workers[49] in 2016. The quintet at 2.50 ppm was assigned as the residual solvent peak of DMSO while the singlet at 3.33 ppm was ascribed to water present as an impurity in the d_6-DMSO.

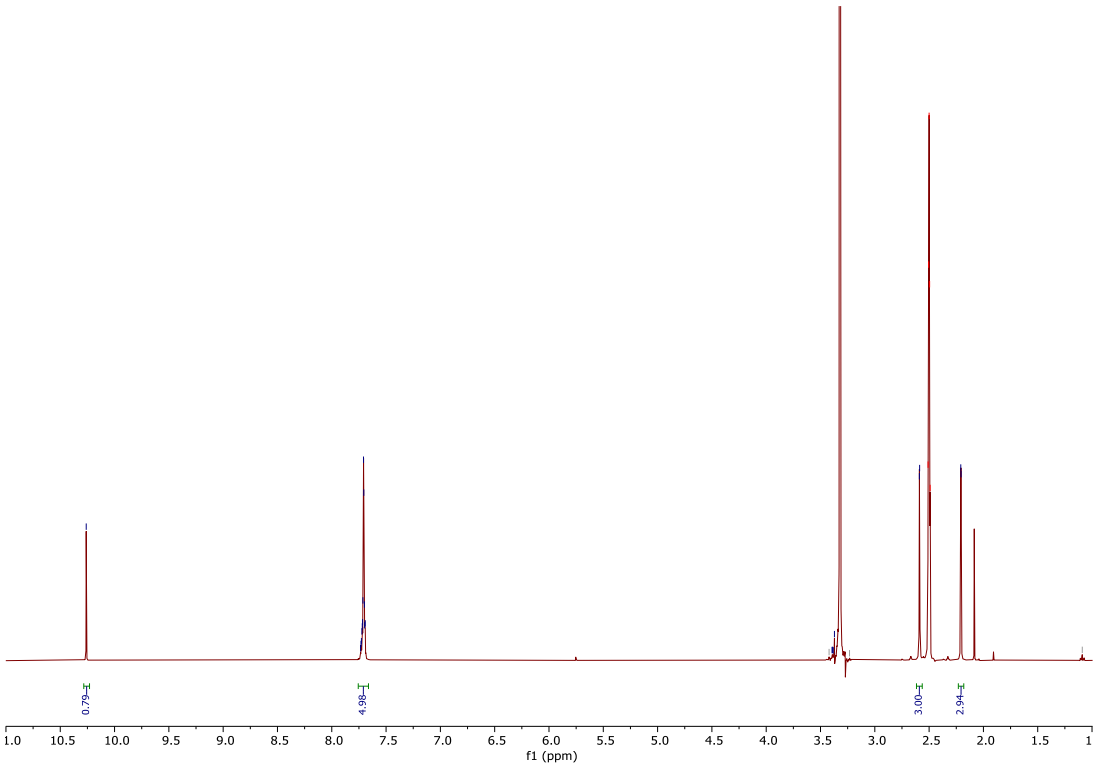

Figure 28: ^{1}H NMR spectrum of the $Ph(ThMe_2H).PF_6$ in d_6-DMSO.

The only diagnostic peaks of the thiazolium ion present in the infrared spectrum occurred at 3124 cm^{-1}, indicating the presence of aromatic C-H bonds, and 1493 and 1594 cm^{-1}, indicating the presence of aromatic C=C bonds. However, the lack of the characteristic thione peak at 1200 cm^{-1} was indicative of the success of the reaction. Additionally, the highly intense absorption band at 826 cm^{-1} was characteristic of a P-F stretching mode in the hexafluorophosphate counter ion.

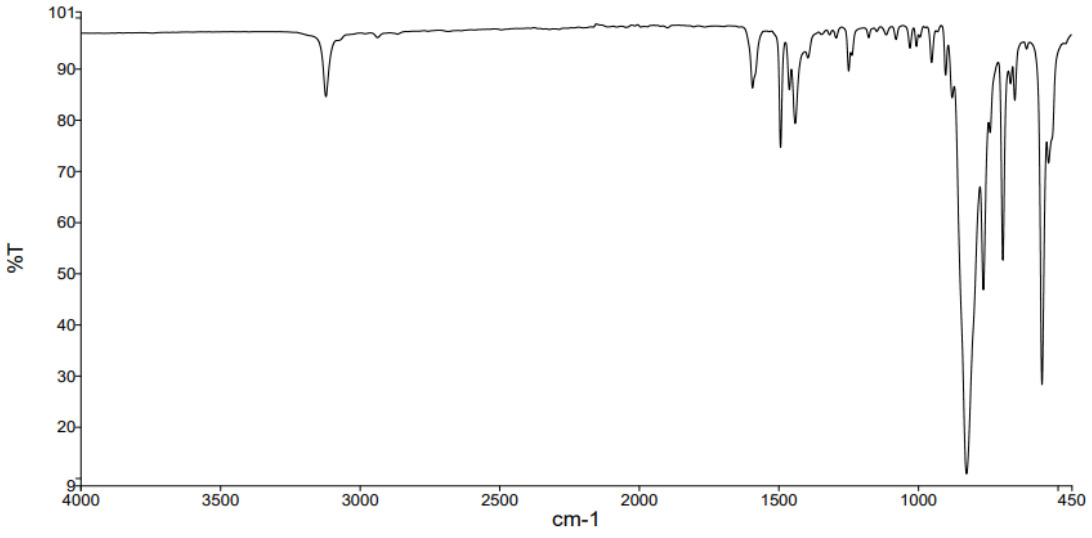

Figure 29: Infrared spectrum of the thiazolium salt.

2.5 Tetrazolation of Cyanopyridines

The various tetrazole ligands required for the formation of the final complexes were obtained using an established in-house method.[80]

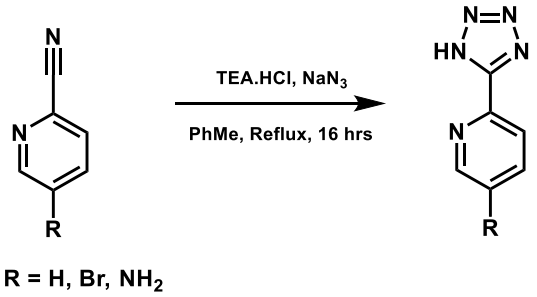

Figure 30: Reaction scheme for the synthesis of tetrazole ligands HL1-3. R = H (HL1), Br (HL2), NH_2 (HL3).

While the mechanism of formation of tetrazoles through the [2+3] cycloaddition of organic azides to nitriles compounds is well established, the mechanism of tetrazole formation using inorganic azides is still subject to debate.[81] However, the two most likely cases are that the reaction proceeds either through a similar concerted [2+3] cycloaddition as organic azides, or through a two step mechanism involving a nucleophilic attack on the nitrile by the azide, followed by a ring closure.[81] These mechanisms are illustrated in Figure 31.

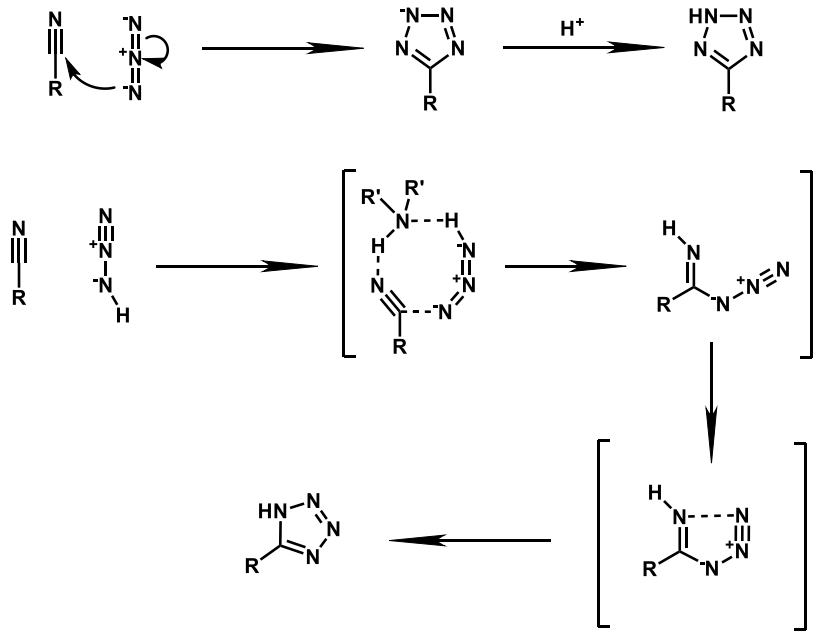

Figure 31: Possible mechanisms for the formation of a tetrazole from an inorganic azide as proposed by Sharpless and co-workers.[81] The concerted [2+3] cycloaddition (top) and nucleophilic attack followed by ring closure (bottom).

The success of the synthesis of these compounds was ascertained through the interpretation of their NMR and IR spectra. In all cases, there was no sharp peak observed in the 2200 cm^{-1} to 2300 cm^{-1} region of the IR spectrum, indicating the absence of a nitrile group. As this nitrile functionality is lost in the formation of a tetrazole, its absence suggested that the reaction had proceeded. This was further supported by the presence of a weak peak at approximately 155 ppm in the ^{13}C NMR spectra of each compound, characteristic of the carbon in a tetrazole ring. The remaining peaks in both the ^{13}C and ^{1}H spectra for these compounds were consistent with the integration and splitting patterns that would be expected of 1 substituted and 1,5 disubstituted pyridine rings. In all ^{1}H spectra, the quintet at 2.50 ppm was assigned as the residual solvent peak of DMSO while the singlet at 3.33 ppm was ascribed to water present as an impurity in the d_6-DMSO. In all ^{13}C spectra, the peak at 39 ppm as assigned as the residual solvent signal of DMSO. The IR, ^{13}C NMR, and ^{1}H NMR spectra of HL1 are shown in Figure 32, Figure 33, and Figure 34 respectively. The IR, ^{13}C, and ^{1}H NMR spectra of HL2-3 are similar to those of HL1, and can be found in Appendix B.

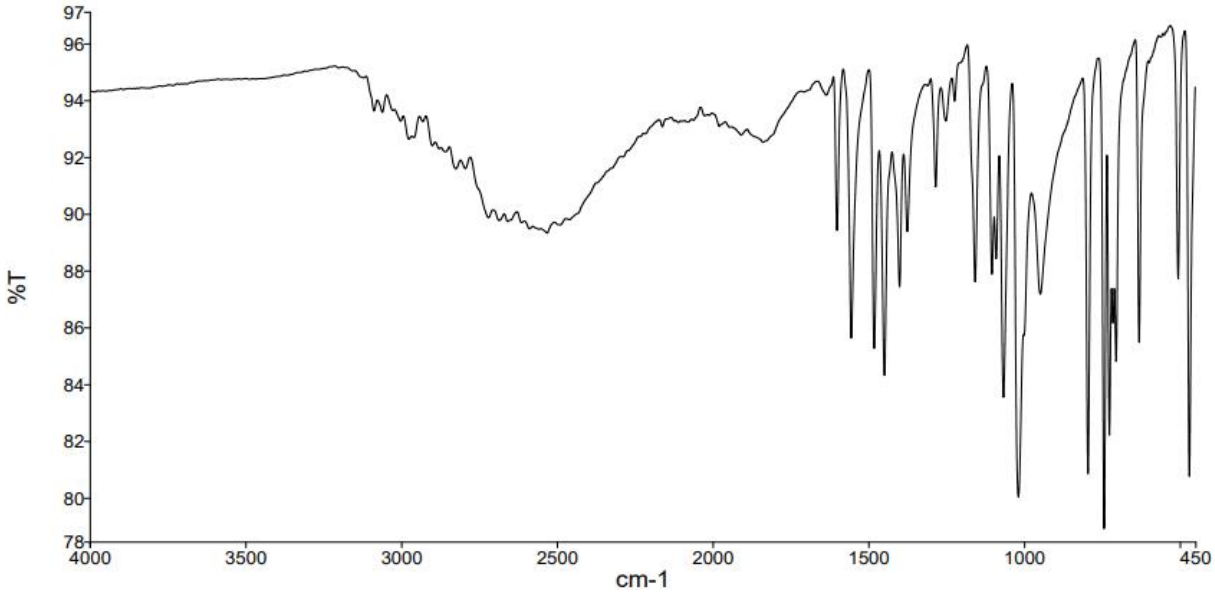

Figure 34: Infrared spectrum of HL1.

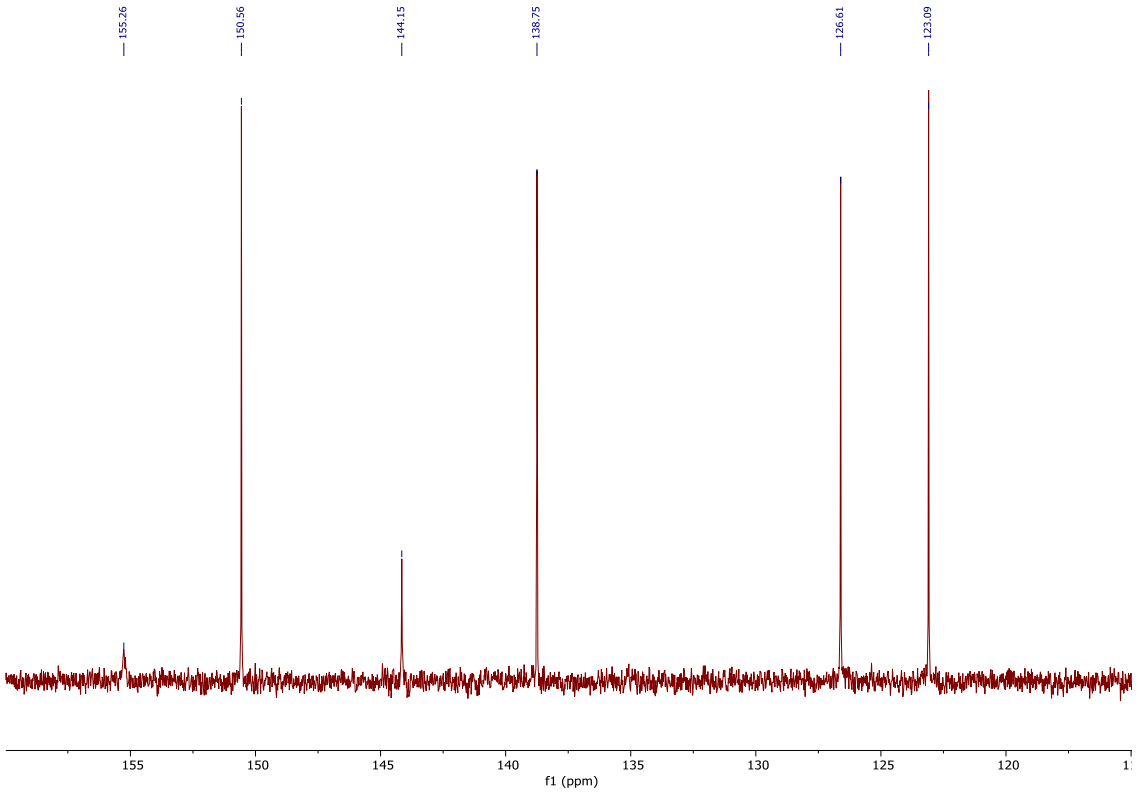

Figure 32: ^{13}C NMR spectrum of HL1 in d_6-DMSO.

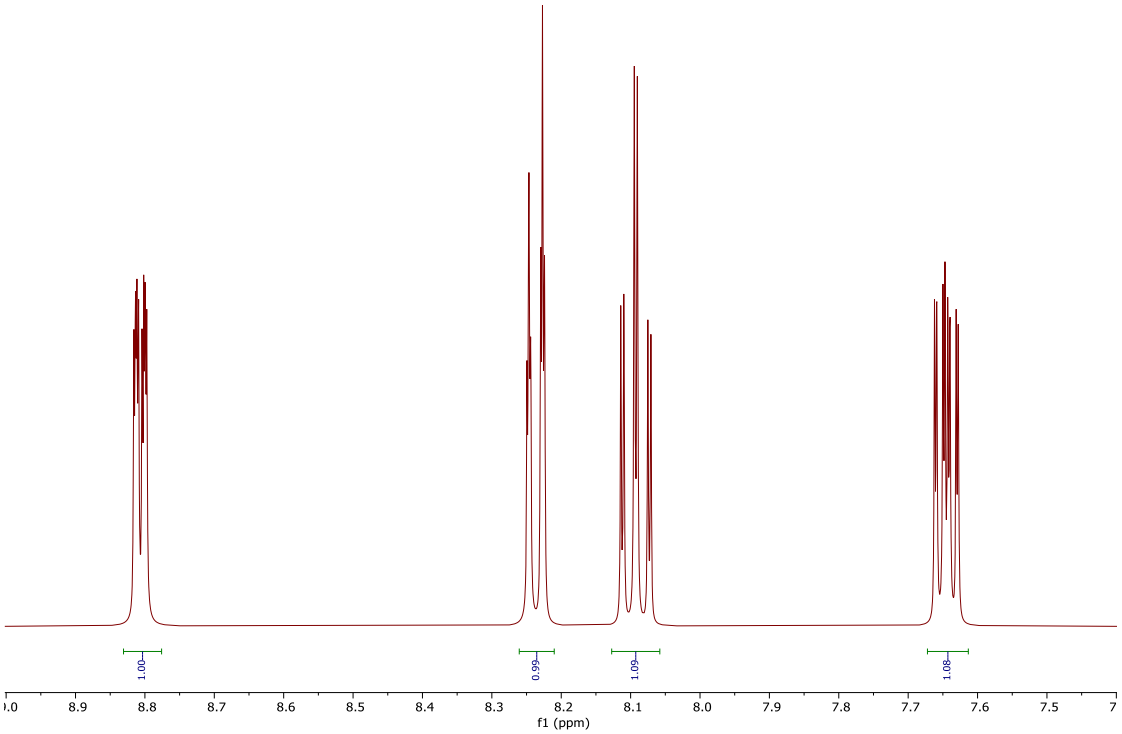

Figure 33: ^{1}H NMR spectrum of HL1 in d_6-DMSO.

2.6 Coupling Reaction with Sulfonyl Chloride

The synthesis of $[H_2L4]Cl$, as shown in Figure 35, was achieved by the reaction of HL3 with p-toluenesulfonyl chloride. The amine group of the starting material served as a nucleophile to attack the electrophilic sulfur of the sulfonyl chloride. This reaction was first attempted using anhydrous DCM as the solvent, with TEA serving as a base to neutralise the hydrochloric acid formed during the reaction. However, the reaction was found not to proceed under these conditions, even when heated at reflux over several days. The same issue was encountered when the solvent was changed to anhydrous tetrahydrofuran (THF). However, when the base was switched to potassium carbonate and the solvent changed to water, the reaction proceeded to completion simply by heating at 80 °C overnight. The addition of hydrochloric acid to the reaction mixture resulted in the precipitation of the product as a HCl salt, which was collected via vacuum filtration and washed with dilute hydrochloric acid and ether. No further purification was necessary.

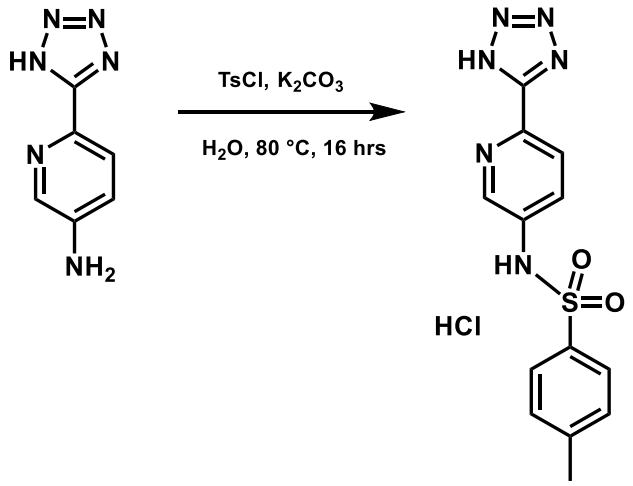

Figure 35: Reaction scheme for the formation of $[H_2L4]Cl$.

$[H_2L4]Cl$ was characterised via NMR and IR spectroscopy, as well as high resolution mass spectrometry. The ^1H NMR spectrum contained a singlet at 2.34 ppm that was assigned to the methyl group present on the phenyl ring. The doublet at 7.39 ppm containing two hydrogens was assigned to the hydrogens meta to the methyl group on the phenyl ring. The multiplet from 7.72 to 7.76 ppm containing three hydrogens was due to the overlapping signals of the hydrogens ortho to the methyl group on the phenyl ring, and the hydrogen in the 4 position of the pyridine ring. The doublets at 8.11 ppm and 8.47 ppm were assigned to the hydrogens in the 3 and 6 positions of the pyridine ring respectively. These assignments were based on the fact that both the peaks at 8.11 ppm and 8.47 ppm showed coupling to the peak at 7.74 ppm in

the COSY spectrum, but did not show coupling to one another. Furthermore, the small *J* value of the doublet at 8.47 ppm was characteristic of coupling to a hydrogen in a meta position, while the large *J* value of the doublet at 8.11 was indicative of coupling to a proton in an ortho position. The broad singlet at 10.98 pm was characteristic of a hydrochloride salt, suggesting that the product was present as such a salt rather than as a free base. The quintet at 2.50 ppm was assigned as the residual solvent peak of DMSO while the singlet at 3.33 ppm was ascribed to water present as an impurity in the d_6-DMSO.

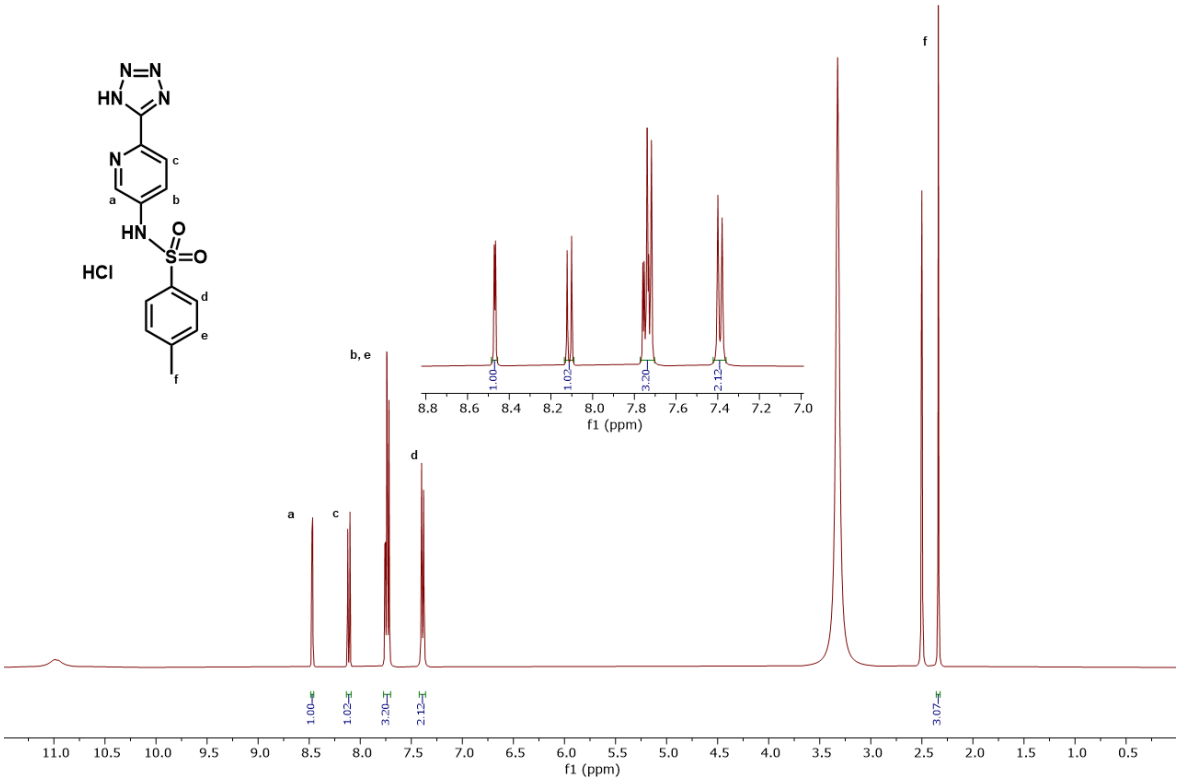

Figure 36: ^{1}H NMR spectrum of [H_2L4]Cl in d_6-DMSO, including peak assignments.

The ^{13}C NMR spectrum of [H_2L4]Cl displayed 9 peaks, where 11 would be expected from its structure. The tetrazolic carbon would be expected to display a weak peak at approximately 155 ppm. However, no such peak was observed. This was likely due to the quaternary nature of the tetrazolic carbon, resulting in a signal too weak to distinguish from the baseline. The other missing peak was also likely due to a quaternary carbon and may also have suffered from insufficient intensity to be distinguished from the baseline.

The two intense peaks at 131 ppm and 127 ppm were assigned to the carbon atoms of the phenyl ring in the meta and ortho positions to the methyl group respectively. These assignments were based on the fact that they showed correlation in the HSQC spectrum to the ^{1}H peaks at

7.39 ppm and 7.74 ppm respectively. The peak at 127 ppm also displayed three bond correlation to the methyl hydrogen peak at 2.34 ppm in the HMBC spectrum. Furthermore, these peaks both displayed a negative phase in the DEPTQ spectrum, indicating that they were coupled to one or three hydrogen nuclei.

The peaks at 124 ppm, 128 ppm, and 141 ppm were assigned to the carbon atoms in the 3, 4, and 6 positions of the pyridine ring respectively. These assignments were based on the fact that they were correlated in the HSQC spectrum to the ^{1}H peaks at 8.11 ppm, 7.74 ppm, and 8.47 ppm respectively. Additionally, these peaks all displayed a negative phase in the DEPTQ spectrum, indicating that they were coupled to one or three hydrogen nuclei.

The peak at 136 ppm was assigned to the carbon in the para position to the methyl group on the phenyl ring. This assignment was based on the three bond correlation between this peak and the ^{1}H peak at 7.39 ppm in the HMBC spectrum. Additionally, this peak displayed a positive phase in the DEPTQ spectrum, indicating that it was due to a quaternary carbon.

The peak at 145 ppm was assigned to the carbon bonded to the methyl group on the phenyl ring. This assignment was based on the three bond correlations between this peak and the ^{1}H peaks at 7.74 ppm and 2.34 ppm. Additionally, this peak displayed a positive phase in the DEPTQ spectrum, indicating that it was due to a quaternary carbon.

Finally, the peak at 21 ppm was assigned to the carbon of the methyl group. This assignment was based on its low chemical shift and correlation to the ^{1}H peak at 2.34 ppm in the HSQC spectrum. Furthermore, this peak displays a negative phase in the DEPTQ spectrum, indicating that it was coupled to either three or one hydrogen nuclei.

The peak at 39 ppm was assigned as the residual solvent peak of DMSO.

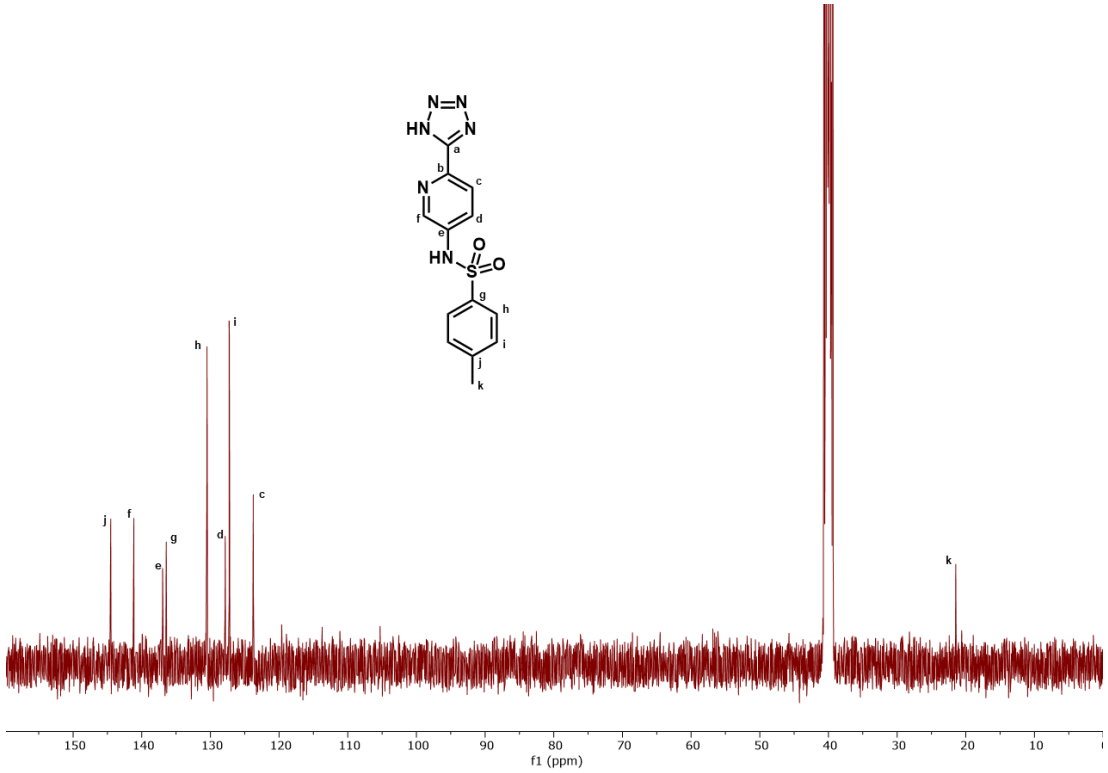

Figure 37: ^{13}C NMR spectrum of $[H_2L4]Cl$ in d_6-DMSO, including peak assignments.

The infrared spectrum of $[H_2L4]Cl$ displayed two intense bands at 1447 cm^{-1} and 1160 cm^{-1} that were characteristic of the S=O bonds in the sulfonamide moiety. Additionally, the band at 3185 cm^{-1} was characteristic of an N-H stretch from the same sulfonamide. The lack of a second absorbance band in the 3100 cm^{-1} region suggested that no primary amine was present, indicating the success of the coupling reaction.

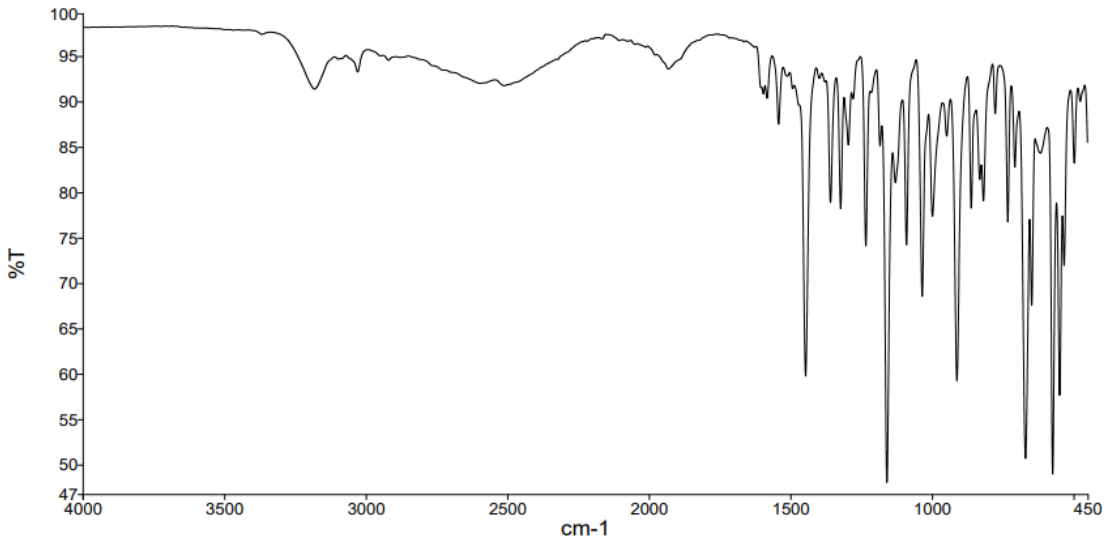

Figure 38: Infrared spectrum of $[H_2L4]Cl$.

The exact mass to charge ratio of the compound as determined by high resolution mass spectroscopy was found to be 316.0863. This was in good agreement with the calculated theoretical exact mass of 316.0742 g mol^{-1}.

2.7 Synthesis of NHC Platinum(II) Complexes

The synthesis of the NHC coordinated platinum(II) complexes was achieved using a three step method adapted from the procedure developed by Strassner and co-workers.[32, 43, 49] This method involves three reactions performed sequentially in a one pot synthetic scheme. While Strassner and co-workers[32, 49] did not provide a rationale for this scheme, it was likely that the silver(I) reaction intermediates were light sensitive,[82] and therefore difficult to isolate and store.

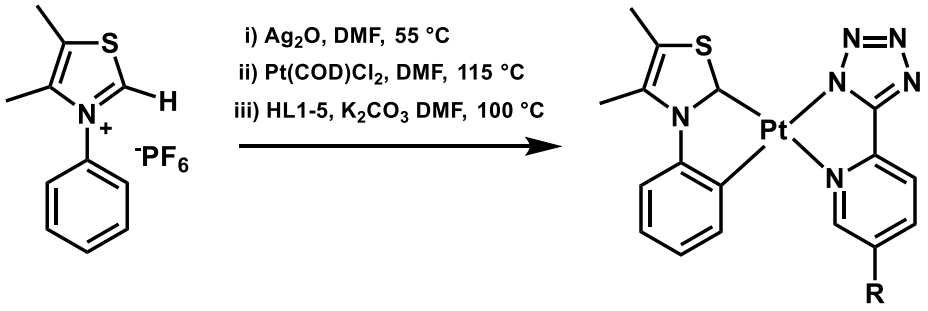

Figure 39: Reaction scheme for the synthesis of the NHC platinum(II) complexes.

The mechanism for this reaction scheme is illustrated in Figure 40. HL1-4 were obtained from the synthesis discussed earlier in this chapter, while HL5 had been previously synthesised in house. First, the thiazolium salt was reacted with silver oxide to form a thiazole silver complex. The thiazole ligand was then transmetallated with dichloro(1,5-cyclooctadiene)platinum(II) to form an NHC platinum complex. The cyclometallated platinum-carbon bond to the phenyl ring was then formed through the application of heat to the reaction mixture. Finally, the pyridyl tetrazole was coordinated to the complex in a ligand exchange reaction. Potassium carbonate was added alongside the pyridyl tetrazole to deprotonate the tetrazole ring, generating an anionic binding site for the platinum.

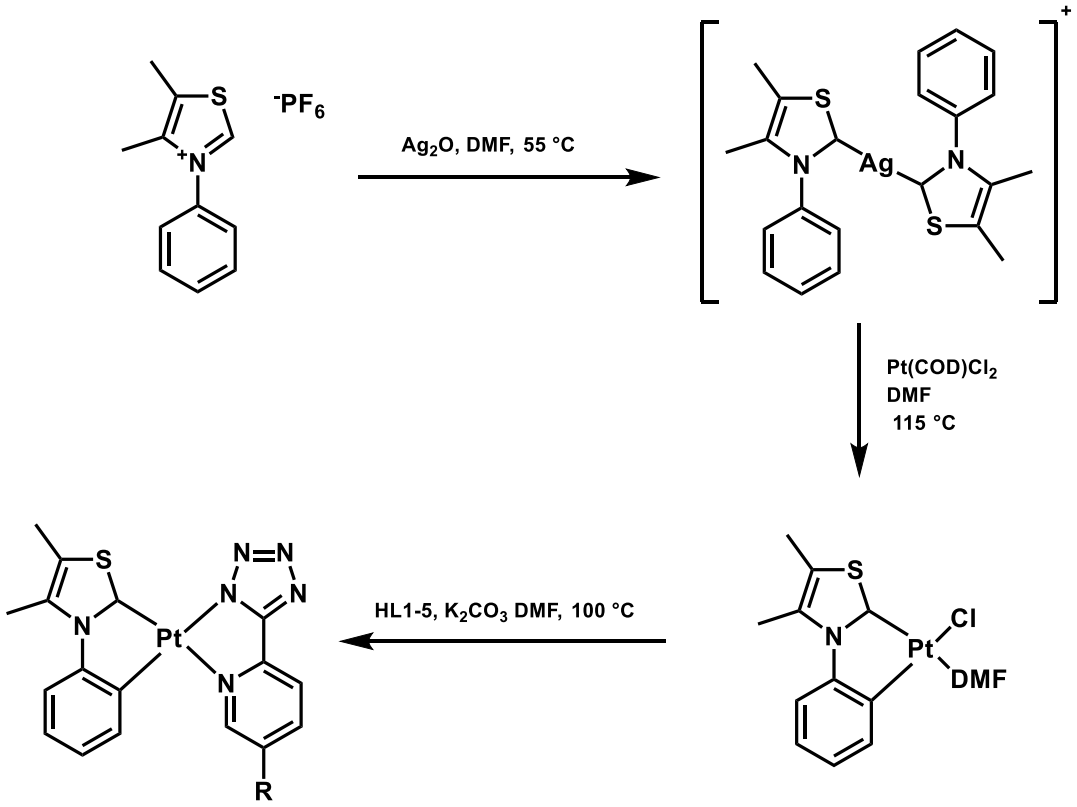

Figure 40: Mechanism for the formation of the thiazol-1yl platinum(II) complexes, including the conjectured structure of the silver(I) intermediate.[43, 49]

The complexes were purified by column chromatography. When Brockmann Grade I alumina was used as the stationary phase, significant coelution of the complex with various impurities was observed. However, these impurities, in all cases, were found to be highly soluble in DCM, while the desired product was only marginally soluble in DCM. Therefore, the impure fractions containing the desired complex were triturated with DCM to obtain the pure compound. When the stationary phase was adjusted to higher grade alumina (Brockmann Grade II or IV), this coelution was reduced, though not entirely eliminated. The fractions containing the compound were combined, evaporated, and the remaining impurities removed by washing with DCM and methanol. The yields of these reactions were extremely low (0.4 – 4.9%). This was likely due to the very low solubility of the complexes preventing them from completely dissolving in the DCM mobile phase of the column. Attempts to recover more product from the column were limited by the unrealistic amount of solvent required (> 10 litres).

Due to the frustratingly low solubility of these complexes in available deuterated solvents (chloroform, DMSO, acetone, methanol, water, and toluene), NMR spectra could not be obtained. Therefore, the complexes were confirmed by high resolution mass spectrometry (HRMS). The HRMS results for complexes Pt[Ph(ThMe$_2$)]L1 to Pt[Ph(ThMe$_2$)]L5 are

summarised in Table 1 (Ph($ThMe_2$) = N-aryl-4,5-methyl-1,3-thiazole-2-ylidene). All five complexes were found to have experimental molecular masses in good agreement with their theoretical values.

Table 1: High resolution mass spectrometry data for complexes Pt[Ph($ThMe_2$)]L1-5.

Compound	Theoretical Molar Mass ($g\ mol^{-1}$)	Experimental Mass to Charge Ratio (m/z^+)
Pt[Ph($ThMe_2$)]L1	529.0700	529.0708
Pt[Ph($ThMe_2$)]L2	606.9805	606.9804
Pt[Ph($ThMe_2$)]L3	544.0809	544.0813
Pt[Ph($ThMe_2$)]L4	698.0898	698.0898
Pt[Ph($ThMe_2$)]L5	689.0955	689.1007

2.8 Conclusions and Further Work

In conclusion, by adapting synthetic procedures developed by Strassner and co-workers[43, 49] for the synthesis of N-phenylthiazole complexes bearing β-diketonate ancillary ligands for use with pyridyl tetrazole ligands, a family of five novel NHC platinum(II) complexes was developed. While full spectroscopic characterisation data for these complexes could not be obtained due to poor solubility, they were confirmed by HRMS analysis.

In addition, a novel ligand containing a p-toluene sulfonamide moiety coupled to a pyridyl tetrazole was synthesised and full characterisation data reported.

The primary issue in the isolation and characterisation of these complexes was their poor solubility in both aqueous and organic media. Therefore, future work should focus on the incorporation of functional groups to improve solubility. It has been established in this research that sulfonamide and protected amino acid groups do not have a significant effect on the solubility of the complex. Therefore, it may be necessary to include charged functional groups such as triphenylphosphonium, or deprotected amino acids that can be solubilised through acid-base chemistry. Alternatively, the incorporation of neutral functional groups that are known to improve solubility of organic compounds such as trimethylsilyl[83] or glutaryl[84] groups may achieve the same result.

Chapter 3: Photophysical Investigation of Thiazol-2-ylidene Platinum(II) Complexes

3.1 Overview

The photophysical properties of thiazole-2-ylidene platinum(II) complexes bearing β-diketonate ligands have been thoroughly explored by Strassner and co-workers.[32, 43, 44, 49, 54] However, to date, no such compounds bearing pyridyl tetrazole ligands have been investigated. Chapter 3 explores the photophysical properties of these compounds, and the effect of substitution in the 5 position of pyridine ligand on these properties.

3.2 Rationale

One of the aims of developing complexes for use as biological probes is to provide redshifted emission maxima to improve cell penetration and reduce damage to the sample. The phenylthiazole complexes developed by Strassner and co-workers[43, 49] were reported to show little variation in their emission maxima with respect to substitution of either the phenyl or thiazole rings. Therefore, this study focused on modifying the pyridine ring in order to determine if this modification would result in redshifted emission. The choice of substituents was governed by considerations regarding the ease of synthesis and solubility issues, and was discussed in Chapter 2.

The majority of photophysical measurements in this chapter are reported in solutions of DCM. DCM was chosen as due to its ubiquity as a solvent for photophysical measurements of platinum(II) complexes in existing literature.[42, 46-48] DMSO was selected in order to explore any potential solvatochromic effect on the photophysical properties by providing a highly polar environment. As biological imaging is performed in an aqueous environment, it would be expected that these measurements also be reported using water as a solvent. Unfortunately, none of the developed complexes demonstrated sufficient solubility in water for photophysical analysis.

3.3 Photophysical Properties in DCM

The absorption properties of the NHC platinum(II) complexes in room temperature solutions of air equilibrated DCM are shown in Table 2. The absorption profiles of the complexes are shown in Figure 41. Due to the marginal solubility of these complexes, it was not possible to determine the exact concentration of the solutions used to obtain these measurements, and therefore molar absorptivity values could not be reported.

Table 2: Absorption data for solutions of complexes Pt[Ph(ThMe$_2$)]L1-5 in room temperature DCM

Compound	λ_{abs} [nm]
Pt[Ph(ThMe$_2$)]L1	263, 295, 370
Pt[Ph(ThMe$_2$)]L2	249, 304, 373
Pt[Ph(ThMe$_2$)]L3	264, 345, 370
Pt[Ph(ThMe$_2$)]L4	262, 318, 372, 544
Pt[Ph(ThMe$_2$)]L5	263, 347, 369, 544

The absorption spectra of all five complexes showed two strong bands at around 260 nm and 370 nm respectively. The position and relative intensity of these bands, when compared to the absorption profiles of known platinum complexes, were characteristic of LC ($\pi \rightarrow \pi^*$) transitions, and MLCT (d $\rightarrow$ π^*) transitions respectively.[36, 37, 43, 85, 86] Complexes Pt[Ph(ThMe$_2$)]L3 and Pt[Ph(ThMe$_2$)]L5 showed an additional band at approximately 345 nm, which were also assigned to MLCT transitions, while complexes Pt[Ph(ThMe$_2$)]L1, Pt[Ph(ThMe$_2$)]L2, and Pt[Ph(ThMe$_2$)]L4 displayed an additional band at 295 to 318 nm. The variance in these additional bands suggested each complex displays slightly different electron densities in the phenylthiazole moiety, with Pt[Ph(ThMe$_2$)]L3 and Pt[Ph(ThMe$_2$)]L5 in particular displaying significantly different profiles from the other complexes. Complexes Pt[Ph(ThMe$_2$)]L4 and Pt[Ph(ThMe$_2$)]L5 additionally showed much weaker absorption bands at approximately 540 nm, which were assigned to spin forbidden (d $\rightarrow$ d) transitions in accordance with the assignments of similar absorption bands in related platinum complexes in the literature.[37]

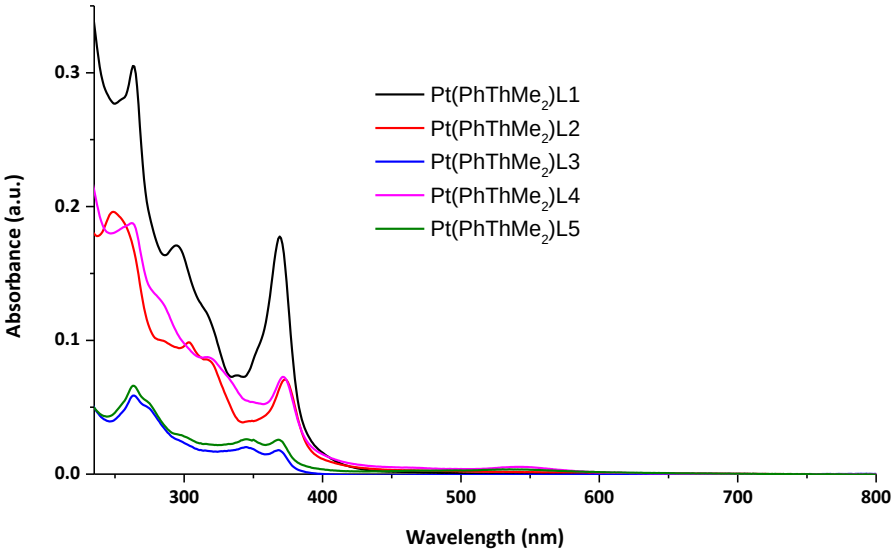

Figure 41: Absorption spectra of NHC platinum(II) complexes Pt[Ph(ThMe$_2$)]L1-5 in DCM.

The emission maxima, excited state lifetimes, and quantum yields of complexes Pt[Ph(ThMe$_2$)]L1-5 in DCM solutions are summarised in Table 3. The emission and excitation profiles for these complexes in DCM solutions are shown in Figure 42. All the complexes displayed emission maxima around 545 nm, and showed vibronic progression with an estimated spacing of approximately 950 cm^{-1}. This emission was assigned to an LC excited state. This assignment was based on the lack of a solvatochromic effect displayed by this emission. See the discussion of the emission profiles in DMSO (Section 3.4) for more details.

All complexes displayed excited state lifetimes between 250 and 300 ns in aerated solutions of DCM and between 850 and 2200 ns in degassed solutions of DCM. This oxygen sensitivity of the emission was indicative of a triplet emissive state. This is due to the triplet ground state of molecular oxygen, which allows for the quenching of triplet excited states through a double electron transfer mechanism.[38] Therefore, in solutions containing no molecular oxygen, this quenching pathway is eliminated, increasing the lifetime of the triplet excited state.

These lifetimes were significantly shorter than those of equivalent thiazol-2-ylidene platinum(II) complexes bearing β-diketonate ancillary ligands, as reported by Strassner and co-workers.[43, 49] This was likely due to the smaller bite angle of the pyridyl tetrazole ligand compared to that of the diketonate ligand. This smaller bite angle may have resulted in a smaller destabilisation of the $d_{x^2-y^2}$ orbital, resulting in the MC state lying at lower energies, resulting in more efficient non-radiative decay, reducing the lifetime of the excited state.

The reported complexes were highly emissive at room temperature, displaying quantum yields ranging from 10 to 18% in degassed solutions, reduced to 0.88 to 2.0% in aerated solutions. This reduction in quantum yield was due to the same oxygen quenching effect responsible for the reduced excited state lifetime of aerated solutions. These quantum yields were significantly lower than those of the aforementioned β-diketonate bearing complexes reported by Strassner and co-workers.[43, 49] This was likely due to the lower bite angle of the pyridyl tetrazole ligands, as discussed previously with regards to the excited state lifetime.

The emission profiles of these complexes showed very little variance, displaying the same vibronic structure and emission maxima that vary by less than 10 nm. This suggested that the pyridyl tetrazole ligand did not contribute significantly to the frontier orbitals involved in the composition of the ground or emissive excited state.

Table 3: Photophysical properties of complexes Pt[Ph(ThMe$_2$)]L1-5 in room temperature solutions of air equilibrated DCM. Measurements obtained from aerated solutions are denoted by [a] while measurements obtained from degassed solutions are denoted by [b].

Compound	λ_{em} [nm]	τ^a [ns]	τ^b [ns]	Φ^a %	Φ^b %
Pt[Ph(ThMe$_2$)]L1	542	259	2186	1.7	15
Pt[Ph(ThMe$_2$)]L2	549	278	2078	2.0	18
Pt[Ph(ThMe$_2$)]L3	540	251	853	0.88	9.8
Pt[Ph(ThMe$_2$)]L4	546	296	2121	2.0	16
Pt[Ph(ThMe$_2$)]L5	539	262	1879	1.0	11

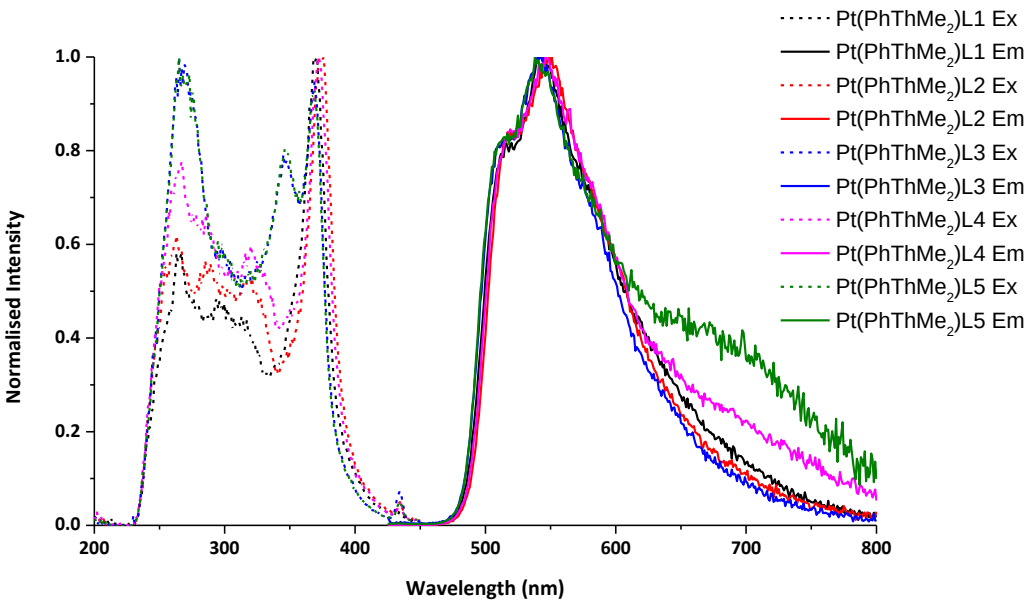

Figure 42: Normalised excitation (....) and emission (----) spectra of complexes Pt[Ph(ThMe$_2$)]L1-5 in room temperature solutions of air equilibrated DCM.

3.4 Photophysical Properties in DMSO

The absorption properties of the NHC platinum(II) complexes in room temperature solutions of air equilibrated DMSO are shown in Table 4. The absorption profiles of the complexes are shown in Figure 43. Similar to the solutions in DCM, it was not possible to determine the exact concentration of the solutions used to obtain these measurements, and therefore molar absorptivity values were not reported.

Table 4: Absorption data for solutions of complexes Pt[Ph(ThMe$_2$)]L1-5 in room temperature DMSO.

Compound	λ_{abs} [nm]
Pt[Ph(ThMe$_2$)]L1	263, 295, 369
Pt[Ph(ThMe$_2$)]L2	302, 371
Pt[Ph(ThMe$_2$)]L3	280, 301, 348, 361
Pt[Ph(ThMe$_2$)]L4	292, 303, 347, 363
Pt[Ph(ThMe$_2$)]L5	280, 301, 348, 361

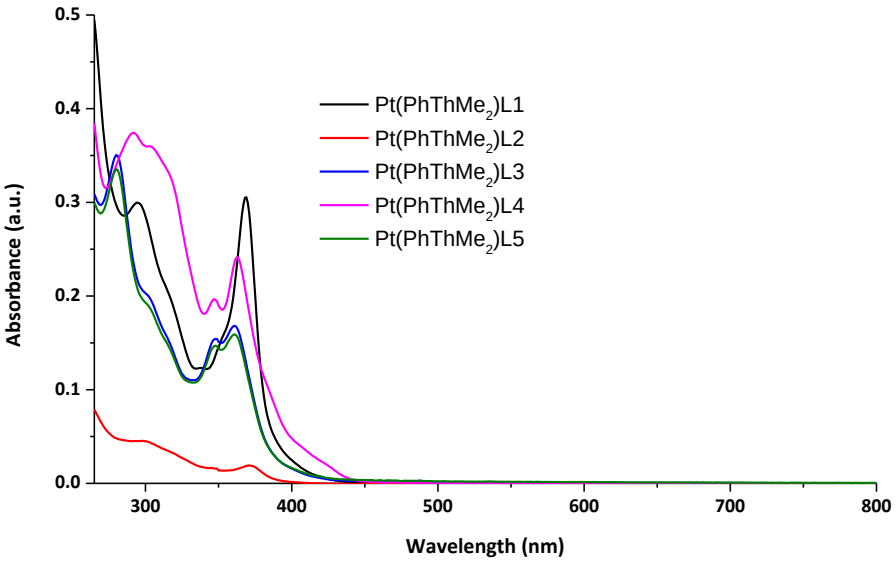

Figure 43: Absorption spectra of complexes Pt[Ph(ThMe$_2$)]L1-5 in DMSO.

All complexes showed two strong absorption bands at 360 to 370 nm and approximately 300 nm, similar to those observed in solutions of DCM. Due to this similarity, these bands were likewise assigned to LC ($\pi \rightarrow \pi^*$) transitions and MLCT ($d \rightarrow \pi^*$) transitions respectively. In complexes Pt[Ph(ThMe$_2$)]L3, Pt[Ph(ThMe$_2$)]L4, and Pt[Ph(ThMe$_2$)]L5, the lower energy band was blue-shifted by approximately 10 nm, and displayed a second peak at around 350 nm. This suggested that these complexes display slightly different electron densities in the phenylthiazole moiety than those in Pt[Ph(ThMe$_2$)]L1 and Pt[Ph(ThMe$_2$)]L2. This differed from what was observed in DCM, in which complex Pt[Ph(ThMe$_2$)]L4 showed similar behaviour to complexes Pt[Ph(ThMe$_2$)]L1 and Pt[Ph(ThMe$_2$)]L2.

The emission and excitation profiles for these complexes in DMSO solutions are shown in Figure 44. Complexes Pt[Ph(ThMe$_2$)]L1, Pt[Ph(ThMe$_2$)]L2, and Pt[Ph(ThMe$_2$)]L4 showed similar emission in DMSO as in DCM, displaying the same emission maxima and vibronic progression. This supported the assignment of this emission as originating from an LC state. As the wavelength of emission was independent of the polarity of the solvent, the polarity of the ground and excited states must be equal, meaning that the excited state is unlikely to have arisen from a charge transfer transition.

Complexes Pt[Ph(ThMe$_2$)]L3 and Pt[Ph(ThMe$_2$)]L5 however, displayed broad, featureless emission bands centred at 565 nm. This emission was assigned to an MLCT excited state, due to the lack of a vibronic structure. This switch from LC to MLCT emission upon increasing the

polarity of the solvent was likely due to the stabilisation of the more polar MLCT excited state by the more polar solvent, lowering its energy to below that of the LC state. This was further supported by the redshift in emission wavelength accompanied by this switch.

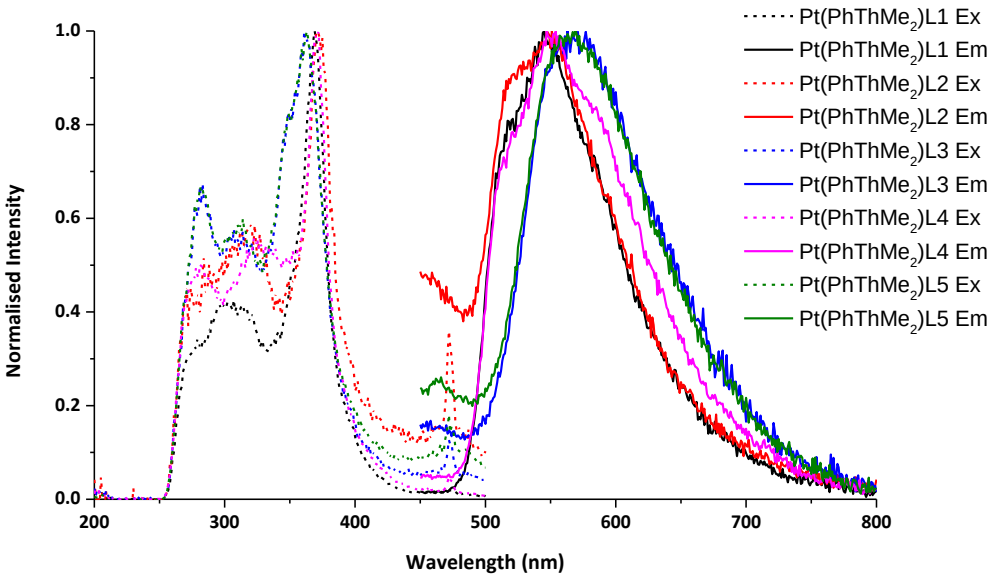

Figure 44: Normalised excitation (....) and emission (----) spectra of complexes Pt[Ph(ThMe$_2$)]L1-5 in room temperature solutions of air equilibrated DMSO.

3.5 Photophysical Properties in the Solid State

The emission profiles of the synthesised complexes in the solid state are shown in Figure 45. The emission maxima and excited state lifetimes of complexes Pt[Ph(ThMe$_2$)]L1-5 in the solid state are summarised in Table 5. All of these complexes displayed broad, featureless emission bands with maxima ranging from 600 to 750 nm. The lack of vibronic progression, as well as the fact that these spectra were obtained in the solid state, suggested that this emission arose from aggregation induced MMLCT states.

The presence of a bromo or sulfonamide group in the 5 position of the pyridine ring was found to result in a significant bathochromic shift in both the excitation and emission spectra in the solid state, accompanied by a significant reduction in the excited state lifetime. The presence of the amino or N-acetylcysteine group also resulted in a less significant redshift, as well as a similar reduction in the excited state lifetime to that caused by the bromo and sulfonamide groups. Due to the fact that these functional groups had no effect on the emission maxima in

solution, this effect was ascribed to changes in crystal packing of the solid state. The varying steric bulk of the different substituents was likely a significant contributing factor in these changes in crystal packing. In addition, the introduction of highly polar groups may have introduced new intermolecular interactions such as hydrogen bonding, which in would in turn have a significant effect on the crystal packing of these complexes in the solid state.

Furthermore, the unsubstituted complex Pt[Ph(ThMe$_2$)]L1 displayed a significantly longer excited state lifetime (380 and 1061 ns) than those of the substituted complexes (76 – 122 and 271 – 342 ns). This effect has been tentatively ascribed to differences in the crystal structure of the solid states of these complexes, resulting in differing intermolecular interactions, and therefore different rates of quenching. However, due to the fact that no data regarding the actual solid state structures of these complexes was obtained, the exact nature of this effect could not be definitively determined.

Table 5: Photophysical properties of complexes Pt[Ph(ThMe$_2$)]L1-5 in the solid state.

Compound	λ_{ex} [nm]	λ_{em} [nm]	τ [ns] (%)
Pt[Ph(ThMe$_2$)]L1	521	690	380 (21), 1061 (79)
Pt[Ph(ThMe$_2$)]L2	618	750	79 (11), 332 (89)
Pt[Ph(ThMe$_2$)]L3	560	701	122 (19), 342 (81)
Pt[Ph(ThMe$_2$)]L4	582	742	76 (15), 271 (85)
Pt[Ph(ThMe$_2$)]L5	557	703	90 (17), 302 (83)

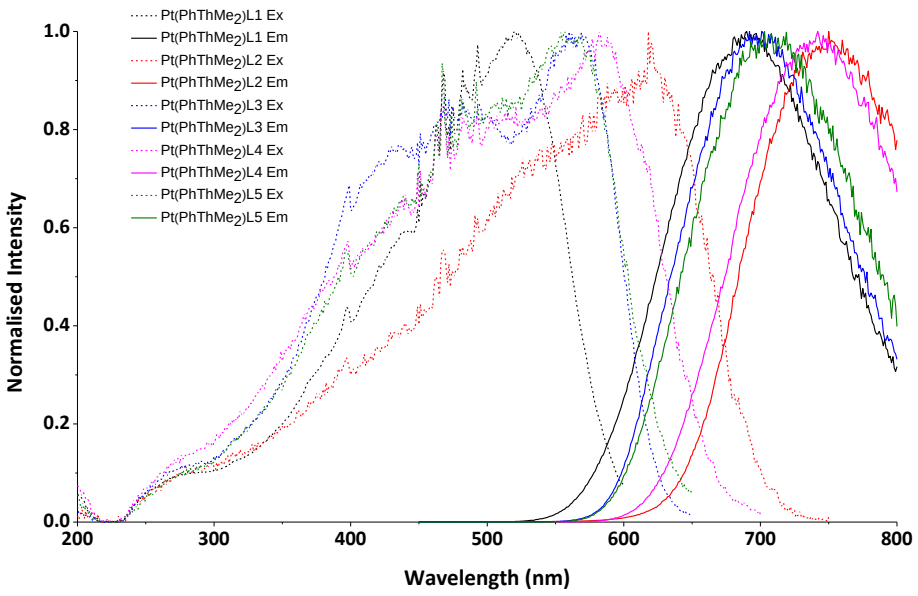

Figure 45: Normalised excitation (....) and emission (—) spectra of complexes Pt[Ph(ThMe$_2$)]L1-5 in the solid state.

3.6 Conclusions and Further Work

The photophysical properties of the five platinum(II) complexes synthesised in Chapter 2 were investigated, in both solution phase and solid state. The complexes displayed promising photophysical properties, with lifetimes in the microsecond range and quantum yields above 10%. The substitution of the 5 position of the pyridine ring was found to have no effect on the wavelength of emission, suggesting that the pyridyl tetrazole was not involved in the emission process. The redshift of the solid state emission upon substitution at the 5 position was attributed to changes in the crystal structure of the complex.

However, the complexes reported in this study were not suitable for use as biological probes due to their insolubility in aqueous media. Therefore, further work should focus on improving the water solubility of these complexes. This could be achieved by the incorporation of any of a range of solubilising groups, as discussed in Chapter 2.

Chapter 4: Synthesis, Characterisation, and Biological Investigation of Cyclophane Complexes

4.1 Overview

This chapter will discuss the synthesis and characterisation a range of platinum(II) cyclophane complexes and their ligand precursors, as well as the results of their biological testing for activity against a range of pathogenic fungi and bacteria. $[Pd(o\text{-}cyc)L1]PF_6$ was synthesised using $Pd(o\text{-}cyc)Br_2$ that had been previously synthesised in house (o-cyc = bis(o-phenylene)-bis(N,N-imidizol-2-ylidene)). The two remaining compounds, $[Pt(o\text{-}cyc)L1]PF_6$ and $Pt(o\text{-}cyc)Cl_2$, identified to be sent for testing had also been previously synthesised in house.[35] The structures of the four complexes identified for synthesis and biological testing are shown in Figure 46.

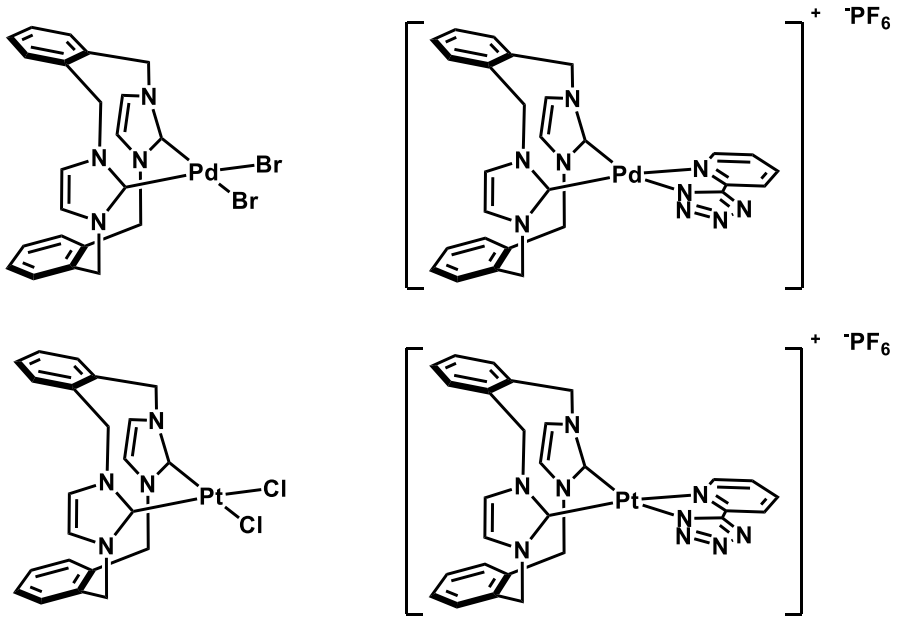

Figure 46: The four cyclophane complexes of Group 10 metals targeted for synthesis and biological testing as part of this study.

Attempts to repeat the synthesis of $[Pt(o\text{-}cyc)L1]PF_6$ and $Pt(o\text{-}cyc)Cl_2$ were unsuccessful, and therefore biological testing of the platinum(II) complexes was not possible within the timeframe of this research.

4.2 Rationale

The majority of platinum(II) complexes reported for medicinal use are antitumor agents.[87-89] However, there has recently been significant interest in the application of platinum compounds, especially those containing heterocyclic ligands, as antimicrobial agents.[87, 90-92] Therefore, this study aimed to investigate the antimicrobial activity of a range of platinum(II) complexes bearing ortho-cyclophane ligands.

4.3 Synthesis of [Pd(o-cyc)L1]PF_6

[Pd(o-cyc)L1]PF_6 was synthesised according to a literature method reported by MaGee and co-workers[35] for the formation of analogous platinum(II) complexes.

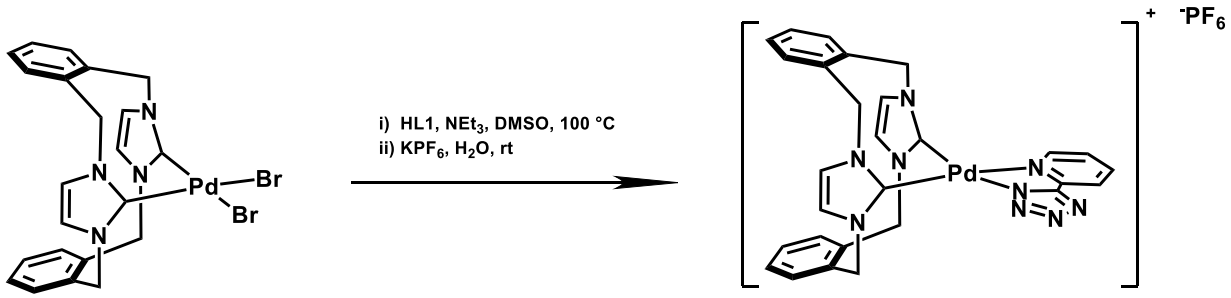

Figure 47: Reaction scheme for the synthesis of [Pd(o-cyc)L1]PF_6.

Pd(o-cyc)Br_2 was heated in DMSO alongside HL1. TEA was added to deprotonate the tetrazole, resulting in the two bromo ligands being exchanged with the pyridyl tetrazole. A saturated solution of potassium hexafluorophosphate was added to generate the hexafluorophosphate salt. The product was then collected by vacuum filtration and purified by recrystallisation from chloroform and acetone.

The product was characterised by ^{1}H NMR spectroscopy. The four doublets, each containing 2 protons, found at 5.39, 5,42, 6.90, and 7.05 ppm were assigned to the methylene bridges between the imidazole and phenyl rings on the cyclophane ligand. The rigid nature of the macrocyclic structure prevented conformational changes, resulting in the two hydrogens on each methyl being inequivalent to one another. This resulted in the splitting of each methylene signal into two doublets. The further resolution into four distinct peaks was due to the loss of symmetry associated with the coordination of the pyridyl tetrazole ligand.

The two multiplets, each containing four protons, found at 7.45 to 7.50 and 7.89 to 7.94 ppm were assigned to the phenyl rings on the cyclophane ligand. Due to the loss of symmetry caused by the presence of the pyridyl tetrazole ligand, all 4 hydrogens on each phenyl ring were inequivalent. However, as the electronic environment of the two sides of the phenyl rings was highly similar due to their significant separation from the pyridyl tetrazole ligand, there was significant overlap between their signals, resulting in the observed multiplets.

The singlet containing 2 protons found at 7.74 ppm, and the multiplet containing 3 protons found at 7.67 to 7.71 ppm were assigned to the two imidazole rings on the cyclophane ligand, with the multiplet also containing one hydrogen from the pyridine ring.

The remaining hydrogens on the pyridine were assigned to the doublet of doublets of doublets containing one proton found at 8.21 ppm, and the multiplet containing 2 protons found at 8.36 to 8.43 ppm.

The quintet at 2.05 ppm was assigned as the residual solvent peak of acetone while the singlets at 2.81 and 7.78 ppm was ascribed to water present as an impurity in the actone-d_6.

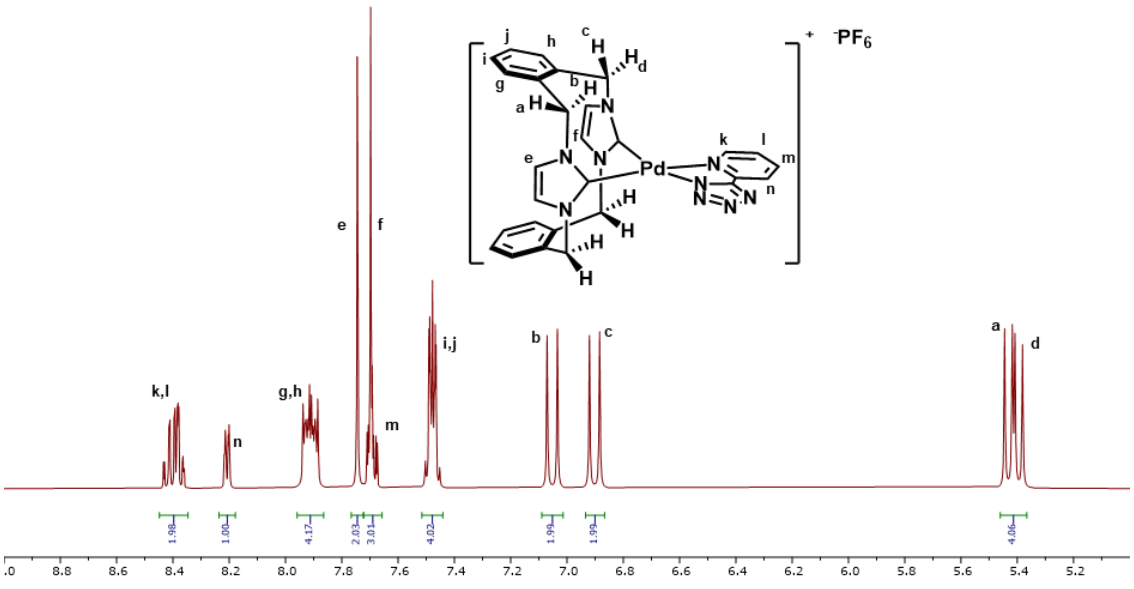

Figure 48: ^{1}H NMR spectrum of [Pd(o-cyc)L1]PF_6 in acetone-d_6. Explicit hydrogens are shown on the methylene bridges for clarity.

4.4 Synthesis of $[H_2(o\text{-}cyc)]Br_2$

The $[H_2(o\text{-}cyc)]Br_2$ was synthesised according to a literature method reported by Baker and co-workers.[93, 94]

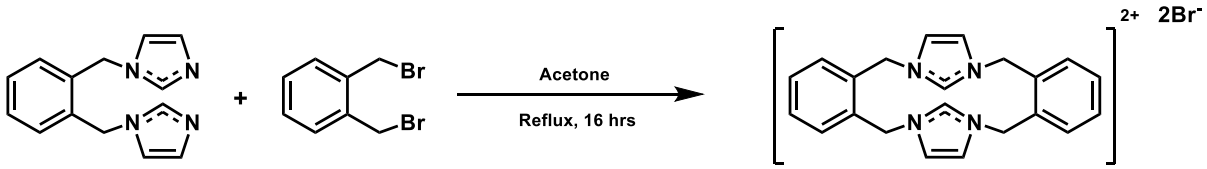

Figure 49: Reaction scheme for the attempted synthesis of $[H_2(o\text{-}cyc)]Br_2$.

Solutions of bis-(bromomethyl)benzene and bis-(imidazole-1-ylmethyl)benzene in acetone were concurrently added dropwise to refluxing acetone. The product precipitated from the reaction mixture and was collected via vacuum filtration. Attempts to purify the product by recrystallisation from methanol, as reported by Baker and co-workers[95] for similar bromide salts, were unsuccessful. The product was therefore used without further purification.

The success of the reaction was determined by ^1H NMR spectroscopy. While the obtained product was highly impure, the ^1H NMR spectrum showed two broad peaks at approximately 7.1 ppm and 5.5 ppm that were characteristic of the methylene hydrogens in cyclophane compounds, in agreement with the literature spectrum obtained by Baker and co-workers.[93]

4.5 Attempted Synthesis of $Pt(o\text{-}cyc)Cl_2$

The synthesis of $Pt(o\text{-}cyc)Cl_2$ was attempted using the literature method reported by Baker and co-workers, [93, 94] utilising $[H_2(o\text{-}cyc)]Br_2$ rather than the analogous acetate salt.

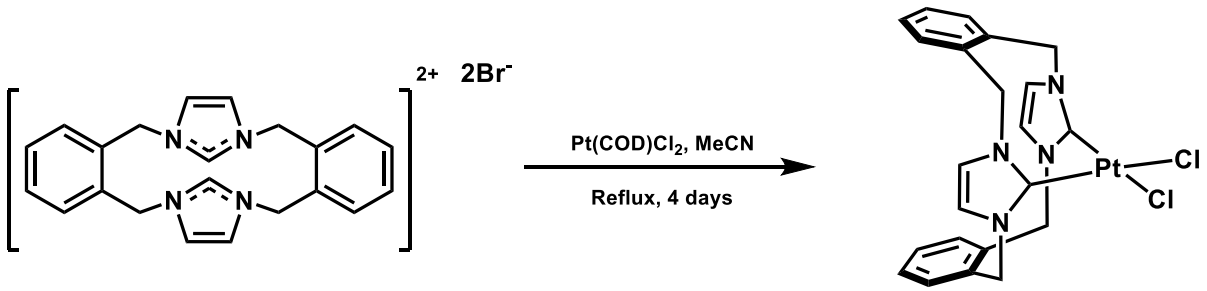

Figure 50: Reaction scheme for the attempted synthesis of $Pt(o\text{-}cyc)Cl_2$.

The cyclophane $[H_2(o\text{-}cyc)]Br_2$ was refluxed in acetonitrile with platinum cyclooctadiene dichloride for four days.

The reaction did not proceed, and only starting material was collected from the reaction mixture. This was conjectured to be the result of using $[H_2(o\text{-}cyc)]Br_2$ where the literature reported that an anion exchange was performed to generate an acetate salt before attempting to complex the cyclophane to platinum. This may have been due to the formation of hydrobromic acid in situ upon deprotonation of the imidazolium salt. Hydrobromic acid is much stronger than acetic acid, and therefore may have deprotonated the imidazole-1-yl, shifting the equilibrium back to $[H_2(o\text{-}cyc)]Br_2$, preventing coordination to the platinum.

4.6 Attempted Synthesis of $[H_2(o\text{-}cyc)](OAc)_2$

Due to the failure of the synthesis of $Pt(o\text{-}cyc)Cl_2$ using the $[H_2(o\text{-}cyc)]Br_2$, it was determined that it was necessary to generate the acetate salt before attempting to coordinate the ligand to platinum.

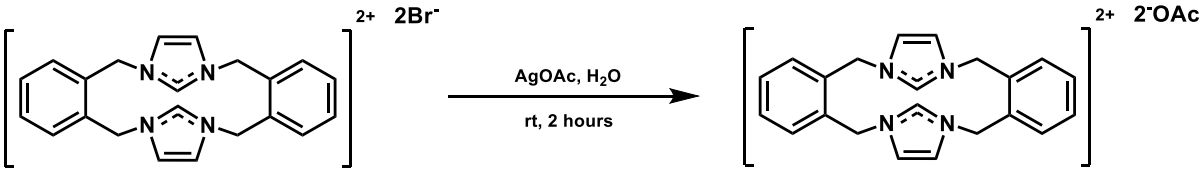

Figure 51: Reaction scheme for the attempted synthesis of $[H_2(o\text{-}cyc)](OAc)_2$.

This was attempted by stirring $[H_2(o\text{-}cyc)]Br_2$ in an aqueous solution of silver acetate at room temperature overnight. The insoluble silver bromide was then removed via filtration and the solvent removed.

The results of this reaction were inconclusive, as ^1H NMR analysis showed a complex mixture. Attempts to isolate a product through recrystallisation were unsuccessful. The observed complex mixture may have been due to the formation of dimeric cyclophane silver(I) complexes, similar to those reported by Baker and co-workers in 2004.[94]

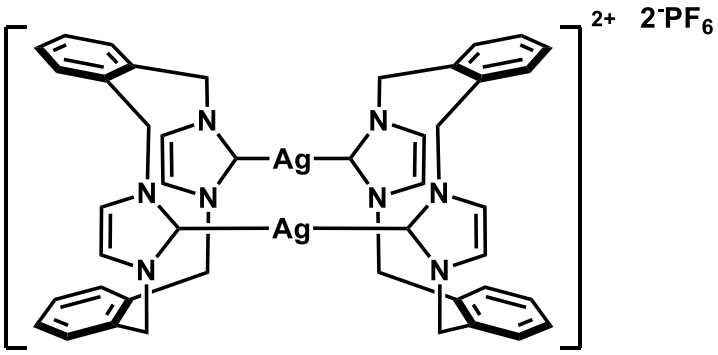

Figure 52: A dimeric silver(I) cyclophane reported by Baker and co-workers.[94]

4.7 Second Attempted Synthesis of $Pt(o\text{-}cyc)Cl_2$

Despite the fact that no single product could be isolated from the attempted synthesis of $[H_2(o\text{-}cyc)](OAc)_2$, the synthesis of the platinum complex was attempted using the crude material obtained.

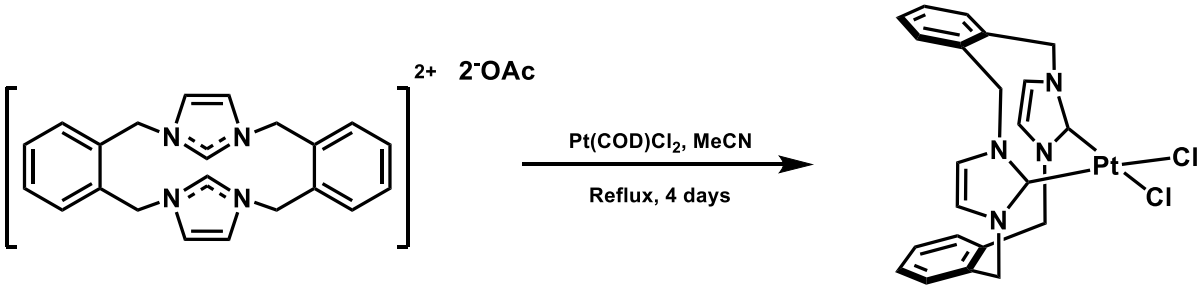

Figure 53: Reaction scheme for the attempted synthesis of $Pt(o\text{-}cyc)Cl_2$.

The cyclophane $[H_2(o\text{-}cyc)](OAc)_2$, was refluxed in acetonitrile with platinum cyclooctadiene dichloride for four days.

This procedure resulted in the formation of a complex mixture. However, the reaction appeared to have proceeded as evidenced by the resolution of clear doublets of doublets around 7.2 ppm and 5.5 ppm. Unfortunately, attempts to purify the product from this complex mixture were unsuccessful, and therefore the product could not be isolated.

4.8 Antimicrobial Investigation

While the synthesis of [Pt(o-cyc)L1]PF_6 and Pt(o-cyc)Cl_2 was unsuccessful in this study, small samples (>5 mg) of both compounds had previously been prepared in house. Consequently, these complexes, along with [Pd(o-cyc)L1]PF_6 and Pd(o-cyc)Br_2 were tested for activity against a range of pathogenic microbes, as well for cytotoxicity towards human cells. At the time of writing, only the results for [Pd(o-cyc)L1]PF_6 and Pd(o-cyc)Cl_2 had been received. The results of this testing are summarised in Table 6. While both compounds were tested for activity against 10 different microorganisms, the only pathogen that either compound showed any activity against was *Cryptococcus neoformans*.

Table 6: Biological testing results of [Pd(o-cyc)L1]PF_6 and Pd(o-cyc)Br_2 against *Cryptococcus neoformans* and human cells.

Compound	MIC (µg/mL)	CC_{50} (µg/mL)	HC_{10} (µg/mL)
Pd(o-cyc)Br_2	0.25 - 0.5	>32	>32
[Pd(o-cyc)L1]PF_6	>32	>32	>32

In these results, the minimum inhibitory concentration (MIC) refers to the minimum concentration of the sample at which greater than 80% inhibition of the growth of the bacteria or fungi was observed. The CC_{50} value refers to the concentration of the sample at which the viability of human cells is reduced by 50%.[96] The HC_{10} value refers to the concentration at which the compound kills 10% of human red blood cells in a sample.[97]

Cryptococcus neoformans is a pathogenic fungi that is responsible for the disease Cryptococcosis.[98-100] Humans with fully functional immune systems are generally able to fight off *Cryptococcus neoformans* infections. Therefore, this disease is generally encountered in immunocompromised or immunosuppressed individuals, such as those with HIV/AIDS and organ transplant recipients.[98-100] Cryptococcosis is responsible for approximately 200,000 deaths annually, mostly in sub-Saharan Africa, and has a 100% mortality rate if left untreated.[101]

There are very few widely available treatments for Cryptococcosis.[101-107] Additionally, many of these treatments have begun to display increased failure rates due to the emergence of drug resistance in *Cryptococcus neoformans*.[101, 107] The current frontline treatment as recommended by the Infectious Diseases Society of America involves a combination therapy of Amphotericin B and Flucytosine.[101] These drugs display MICs of 0.0625 to 0.5 µg/mL and 0.5 to 128 µg/mL respectively, dependent on the level of drug resistance of the strain.[102, 104-106] This is followed by treatment with Fluconazole, which displays an MIC of 1 to 128 µg/mL.[101-103, 105, 106] However, in developing countries, which account for the majority of Cryptococcosis cases, Amphotericin and Flucytosine are not readily available, resulting in monotherapy with Fluconazole representing the majority of treatment regimes.[101, 104] Unfortunately, Fluconazole resistance is widespread in *Cryptococcus neoformans*.[103] It is therefore imperative that new antifungal drugs are developed to increase the variety of available treatments.

Pd(o-cyc)Br_2 was found to have a minimal inhibitory concentration against *Cryptococcus neoformans* from below 0.25 to 0.5 µg/mL. This was considerably lower than that of Fluconazole and Flucytosine, and comparable to that of Amphotericin B. It was also found to show no significant cytotoxicity towards human cells, and not to result in any significant haemolysis. These results were promising for the potential application of o-cyclophane palladium compounds in the treatment of *Cryptococcus neoformans*. However, there did not appear to be any indication of broader range antimicrobial, or even antifungal activity, as Pd(o-cyc)Br_2 was not found to display activity towards any of the other nine pathogenic microbes it was tested against.

[Pd(o-cyc)L1]PF_6, however, while displaying the same lack of toxicity as Pd(o-cyc)Br_2, was not found to exhibit any activity towards *Cryptococcus neoformans*. This suggests that either the bromido ligands are important for the activity of the complex, or that the loss of activity can be directly attributed to the pyridyl tetrazole moiety itself.

Once obtained, the results from testing the biological activity of [Pt(o-cyc)L1]PF_6 and Pt(o-cyc)Cl_2 will provide more information regarding the structure activity relationship of these cyclophane complexes. The comparison between those complexes containing platinum centres as opposed to palladium centres may provide insight as to the importance of the identity of the central metal atom.

4.9 Conclusions and Further Work

One novel palladium complex was synthesised and tested for activity against a range of pathogenic fungi, along with a previously reported palladium complex and two previously reported platinum complexes. Attempts to utilise literature methods to synthesise the previously reported platinum complexes were unsuccessful. One compound, Pd(o-cyc)Br_2, was found to exhibit promising activity towards *Cryptococcus neoformans*, as well as low toxicity towards human cells.

Further work should focus on increasing the understanding of the structure activity relationship in these group 10 cyclophane complexes. This work should target three regions for modification. The first is the metal centre itself, to determine whether the nature of the metal is important to the activity of the compound. This requires that the synthesis of the targeted platinum(II) complexes [Pt(o-cyc)L1]PF_6 and Pt(o-cyc)Cl_2 be achieved. Therefore, future work should focus on optimising the synthetic pathway towards [Pt(o-cyc)L1]PF_6.

The second region for modification is the ancillary ligands, to determine whether the halogen ligands are necessary for the activity of the compound. The final region for modification is the cyclophane ligand, to determine if structure of the macrocycle plays a significant role in the optimisation of the activity of these complexes.

Once a structure activity relationship has been established and optimised drug candidates developed, these complexes should be entered into pre-clinical animal trials to determine their efficacy in vivo.

Finally, these complexes and any new complexes developed should be tested against a wider range of pathogenic fungi to establish if they have the potential to be applied in a broader scope than simply as a treatment for *Cryptococcus neoformans*.

Chapter 5: Towards the Synthesis of a C^C^N Coordinated Platinum(II) Complex

5.1 Overview

This chapter will discuss the attempts to develop a synthetic procedure for the formation of a terdentate platinum(II) complex bearing a C^C^N coordination pattern. First, ligands bearing biphenyl pyridine functionality were synthesised using palladium catalysed cross coupling reactions. These ligands were then coordinated to platinum to form dimeric species that serve as intermediates. The final proposed step was then to lyse these dimers to form a second cyclometallated bond. This procedure was adapted from the synthesis of similar C^N^C complexes reported by Cave and co-workers in 2000.[108]

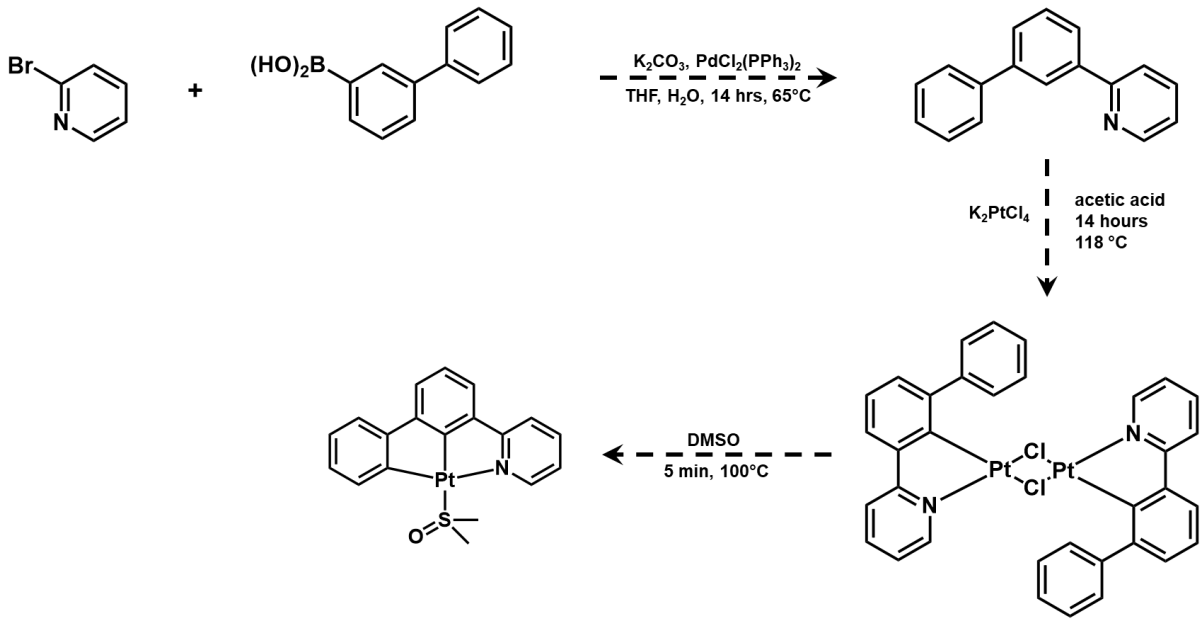

Figure 54: The initial proposed synthetic pathway for the formation of a C^C^N coordinated platinum(II) complex.

Unfortunately, this final step was unsuccessful due to a number of challenges that arose during the synthetic process. This chapter will discuss these challenges, as well as the insight that these challenges provided into potential fundamental issues with the synthetic pathway, and how they might be able to be overcome in future work.

5.2 Rationale

The C^C^N coordination pattern was selected due to the strong sigma donating effect of cyclometallated carbon compared to that of neutrally bound nitrogen. The inclusion of two such cyclometallated carbon atoms should help to raise the energy of the $d_{x^2-y^2}$ orbital, which should in turn raise the energy of the non-emissive MC state. This in turn should prevent the thermal population of the MC state from the emissive triplet state, preventing it from providing a pathway for rapid non-radiative relaxation to the ground state. This should then result in a significant improvement in the photophysical properties of these complexes when compared to analogous terpyridine platinum(II) complexes.

Furthermore, the cis conformation of the cyclometallated positions served a twofold purpose in attempting to improve the photophysical properties when compared to C^N^C coordinated platinum(II) complexes. The first was that, due to the imperfect bite angle of the ligand, the central coordination site has a larger overlap with the $d_{x^2-y^2}$ orbital than the coordination sites on the side positions. This results in a stronger sigma donating effect, which results in a stronger effect on the energy of the MC state. The second was that, as found by Yam and co-workers,[47] the trans positions of the cyclometallated positions in the C^N^C complexes results in a distortion of the triplet excited state, resulting in direct non-radiative decay.[70, 71, 109] It was hoped that by positioning the cyclometallated positions in cis to one another this issue can be avoided, resulting in an improvement of the photophysical properties of the complex.

5.3 Synthesis of H_2bppy

The synthesis of 2-(biphenyl-3-yl)pyridine (H_2bppy) was achieved through the application of a Suzuki coupling reaction. This reaction involves the use of a palladium catalyst to form a carbon-carbon bond between an aryl- or vinyl-boronic acid and an aryl-, vinyl-, or even alkyl halide or pseudohalide.[110, 111] The Suzuki coupling was chosen over other similar coupling reactions due to the advantages it offers with regards to mild reaction conditions and the wide commercial availability of both the desired boronic acid and halide species.[112]

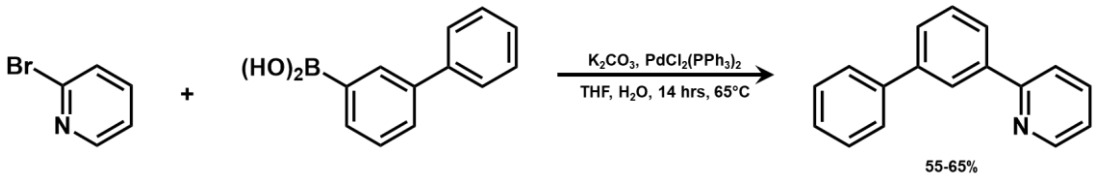

Figure 55: Synthesis of H_2bppy.

The mechanism of Suzuki couplings has been well established, and consists of three major steps, as illustrated in Figure 56.[113-115] The first involves the oxidative addition of the halide species to the palladium centre.[113-115] This is followed by the activation of the palladium complex by a base, usually a carbonate, and the subsequent transmetallation in which the organic group of the boronic acid displaces the hydroxide.[114] The final step involves the reductive elimination of the product, regenerating the catalyst.[113-115]

The rate determining step in this catalytic cycle is usually the oxidative addition[116]. The rate of this oxidative addition is dependent on the reactivity of the halide species, with iodides being the most reactive, followed by bromides, while chlorides are generally unreactive[117]. This reactivity can be increased by the presence of an electron withdrawing group in conjugation with the halide.[110]

The base has several roles in the mechanism of the Suzuki reaction.[114, 118] The primary role of the base is the activation of the palladium complex towards transmetallation following the oxidative addition of the halide species. The [$ArPdXL_2$] species reacts with the base to form [$ArPd(OH)L_2$], which is the active species that undergoes transmetallation with the boronic acid.[114, 118] The choice of base is important for this role, as the hydroxide ion must be produced via reaction of the base with water if hydroxide is not added directly.[118] Therefore, as weaker bases such as carbonates result in an equilibrium in which less hydroxide is present, they result in slower rates of transmetallation. However, the use of strong bases such as hydroxide introduce the potential for side reaction to occur, such as dehalogenation reactions of the halide species.

A less essential, though not insignificant role of the base is the acceleration of the final reductive elimination step. The exact mechanism for this effect is unknown, though it is speculated to involve the formation of a pentacoordinate anionic palladium intermediate.[114] The base, however, also reacts with the boronic acid species to produce a borate, which is unreactive towards transmetallation, slowing the rate of this step.[114, 118] Therefore, high concentrations of base should be avoided, as they result in the deceleration of the reaction.

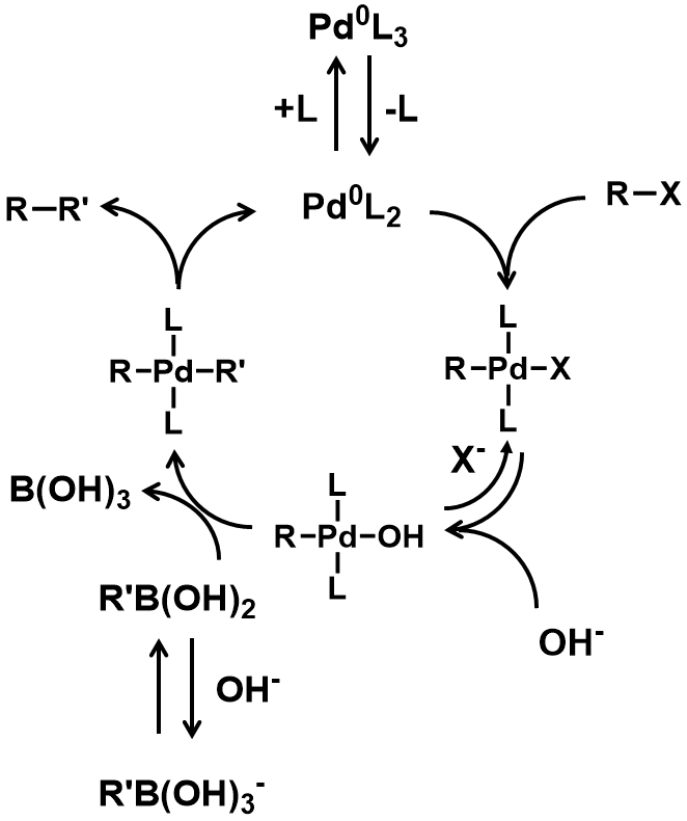

Figure 56: The catalytic cycle of the Suzuki reaction, as proposed by Amatore and co-workers.[114]

The synthesis of H_2bppy was initially successful using sparged water (~30 minute sparge times, N_2) and THF, with bis(triphenylphosphine)palladium chloride as the pre-catalyst, with yields of approximately 55%. These reactions went red within 5 minutes of the application of heat, and black within 1 hour, indicating the oxidation of the active catalyst. However, TLC analysis showed the absence of starting materials, indicating that the reaction had proceeded to completion, which suggested that only some of the catalyst had been oxidised.

The yields were increased to approximately 65% when the solvents were degassed in an ultrasonic bath under reduced pressure. When this procedure was followed, no red or black colouration was observed, suggesting that no significant amount of catalyst was oxidised.

The product was confirmed by ^{1}H NMR analysis through comparison to existing spectra in the literature. The spectrum obtained from the product contained the same peaks as those in the spectrum obtained by Bomben and co-workers.[119] The residual solvent peak could not be resolved due to overlap with the peak assigned as hydrogen b in Figure 57.

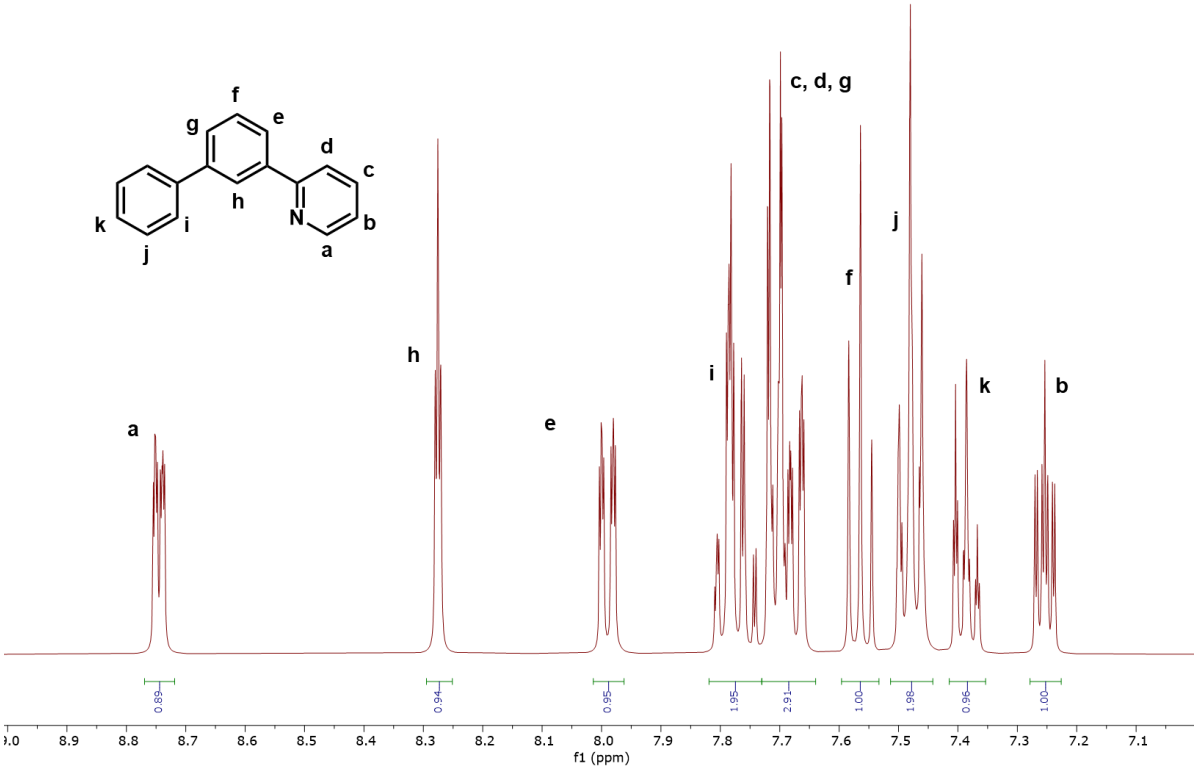

Figure 57: ^{1}H NMR spectrum of H_2bppy in $CDCl_3$.

5.4 Synthesis of Platinum Dimers

The synthesis of C^N^C dicyclometallated platinum compounds by Cave and co-workers [108, 120] involved the formation of monocyclometallated dimers as intermediate species. Due to the fact that the coordination pattern of these dimers was the same in the synthesis of both C^N^C and C^C^N species, the procedure for their formation was adapted from existing literature. Theoretically, there exist six possible isomers of this dimeric intermediate, varying in the cis/trans coordination of the pyridine group, and in the position of the non-cyclometallated phenyl ring. The structures of these dimers are illustrated in Figure 58. The target of this synthesis was either the cis or trans isomer of $(Pt(Hbppy)Cl)_2$.a, as it contains both non-cyclometallated phenyl rings in the ortho position to the existing cyclometallated carbon, facilitating a cyclometallation reaction between that ring and the platinum centre. However, it was postulated that steric effects arising from the interaction of the two non-cyclometallated phenyl rings in the cis isomer could act as a barrier to its formation.

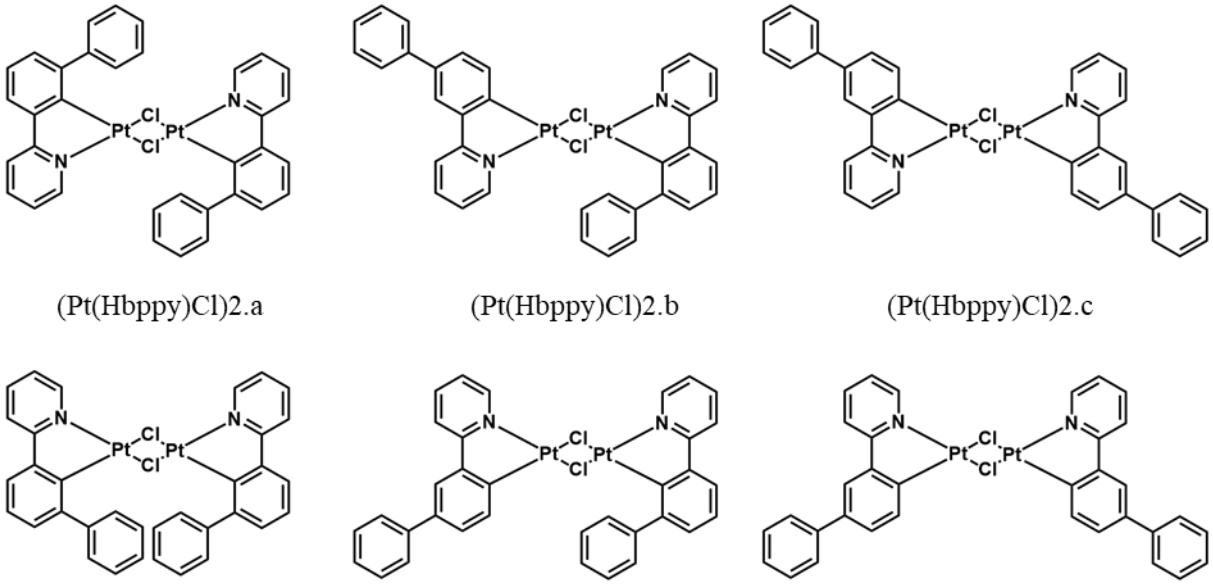

Figure 58: The six possible isomers of $(Pt(Hbppy)Cl)_2$.

H_2bppy was refluxed in glacial acetic acid in the presence of potassium tetrachloroplatinate for 14 hours before being added to water, filtered, and washed with petroleum spirits, as shown in Figure 59. The resulting product showed multiple spots by TLC analysis, and was impure by NMR spectroscopy. However, attempts to purify the product via column chromatography (both neutral alumina and silica) resulted in its degradation into a complex mixture. Recrystallisation was attempted from systems of diethyl ether into chloroform, and petroleum spirits into DCM. However, neither system resulted in any significant purification of the product.

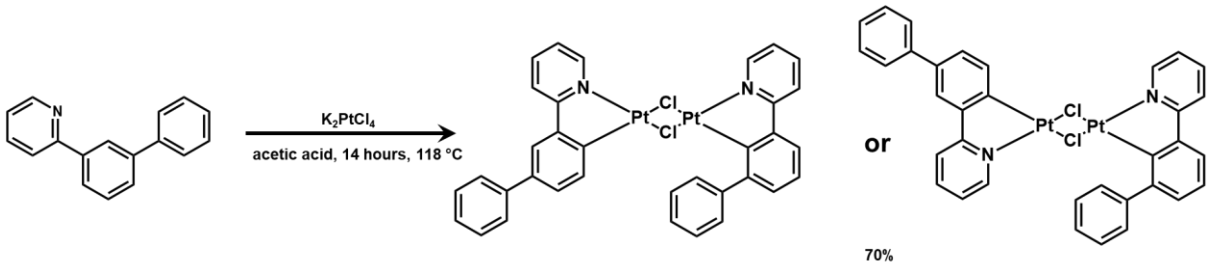

Figure 59: Synthesis of $(Pt(Hbppy)Cl)_2$.b.

The ^{1}H NMR spectrum of the product, as shown in Figure 60, suggested the formation $(Pt(Hbppy)Cl)_2$.b. The aromatic region of the spectrum integrated to 25 hydrogen atoms, though it was determined that this over-integration was due to the low purity of the product, resulting in peaks originating from impurities being superimposed on those originating from the product. The two peaks at 9.71 and 9.23 ppm were both characteristic of protons at the 2 position of a pyridine ring. Therefore, the presence of two such inequivalent pyridine rings suggested the formation of an asymmetric dimer, in which the two aromatic ligands were

inequivalent to one another. The quintet at 2.50 ppm was assigned as the residual solvent peak of DMSO while the singlet at 3.33 ppm was ascribed to water present as an impurity in the d_6-DMSO.

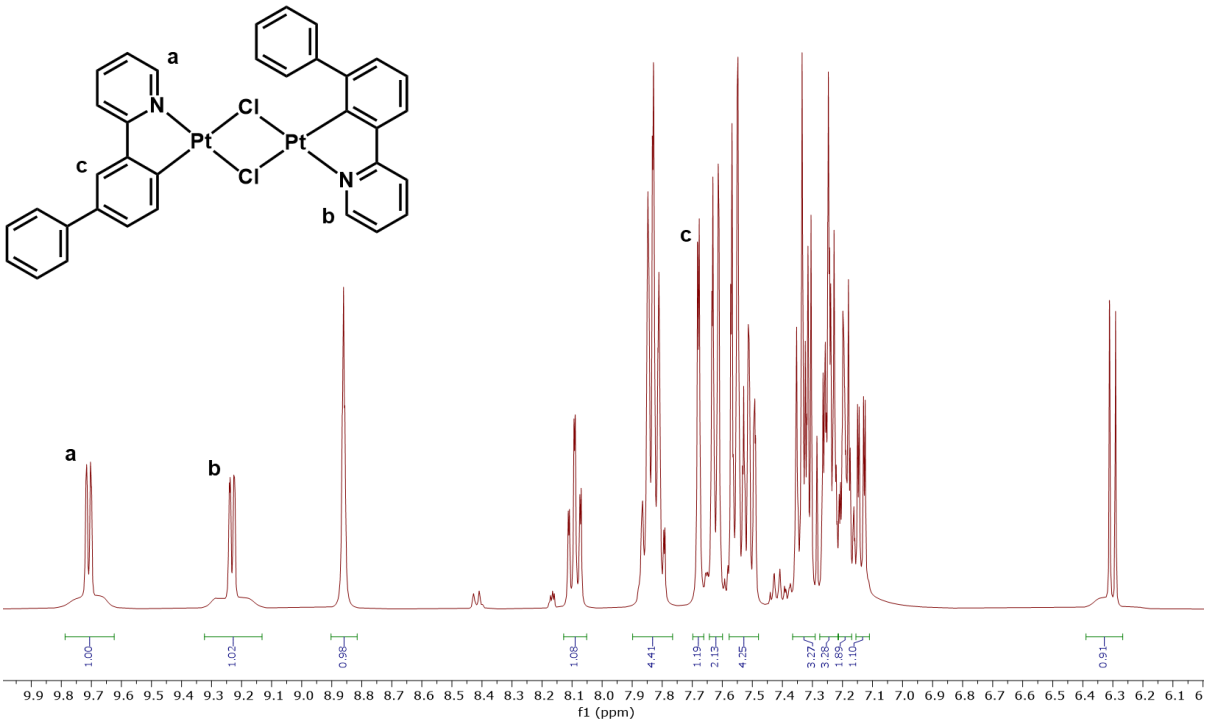

Figure 60: ^{1}H NMR spectrum of $(Pt(Hbppy)Cl)_2$.b in d_6-DMSO.

When this reaction was allowed to reflux for 2 days and subjected to the same workup procedure, a symmetric dimer was obtained, as shown in Figure 61.

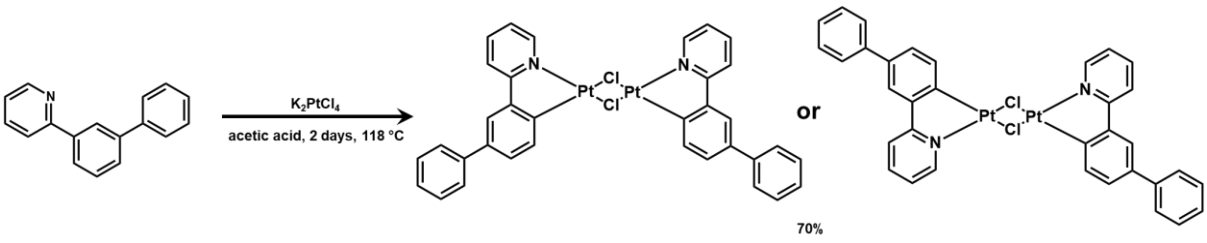

Figure 61: Synthesis of $(Pt(Hbppy)Cl)_2$.c.

The ^{1}H NMR spectrum of the product, as shown in Figure 62, suggested the formation of $(Pt(Hbppy)Cl)_2$.c. The peak at 9.51 ppm was characteristic of a proton at the 2 position of a pyridine ring and contained 2 protons. Furthermore, all other peaks in the aromatic region integrated to 2, 4, or 6 protons, with a total integration of 24. This suggested the presence of

two equivalent aromatic ligands. The peak at 8.09 ppm presented as a doublet with a J value of 2 Hz, which was consistent with coupling to a proton at the meta position. $(Pt(Hbppy)Cl)_2$.a does not contain any protons that would display only meta coupling, while $(Pt(Hbppy)Cl)_2$.c contains two equivalent protons that would display this coupling. The quintet at 2.50 ppm was assigned as the residual solvent peak of DMSO while the singlet at 3.33 ppm was ascribed to water present as an impurity in the d_6-DMSO.

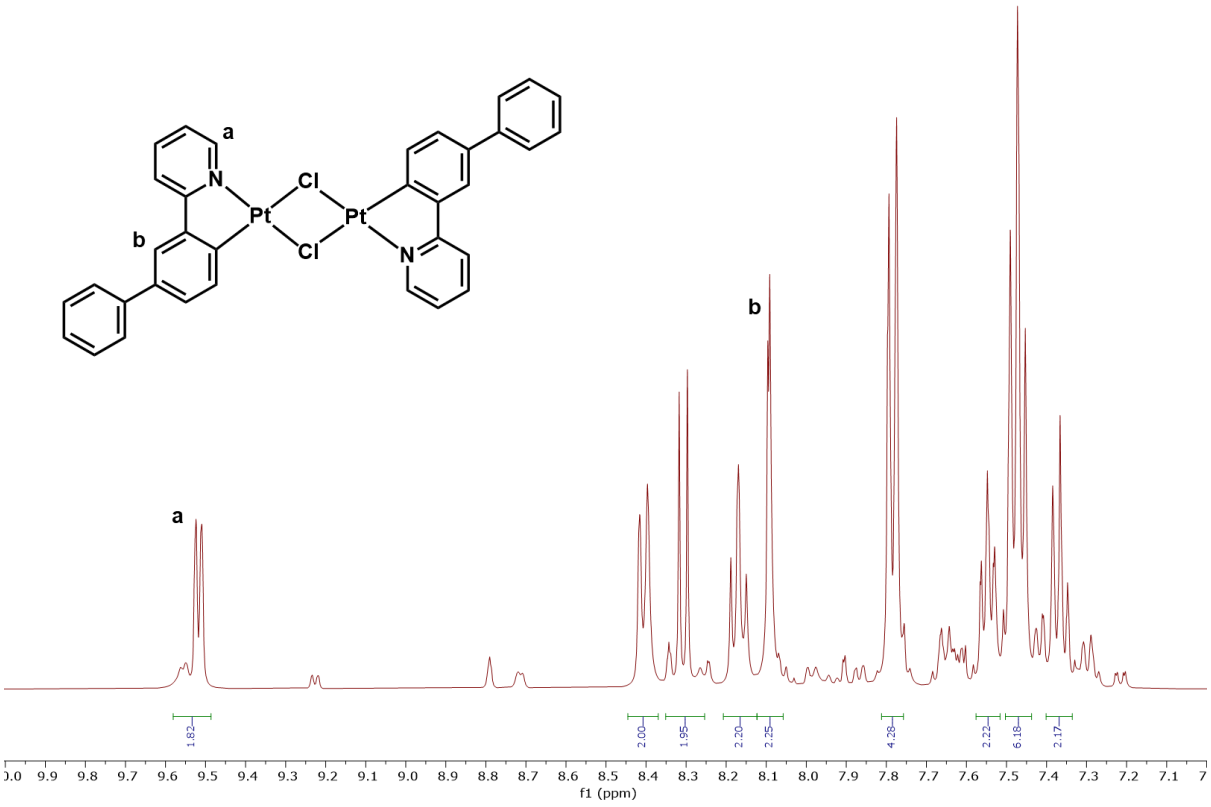

Figure 62: ^{1}H NMR spectrum of $(Pt(Hbppy)Cl)_2$.c in d_6-DMSO.

Attempted purification of this dimer encountered the same problems as the asymmetric isomer discussed above. However, several peaks assigned to the impurity were characteristic of the asymmetric isomer, such as those at 8.81 ppm and 6.23 ppm. This suggested that although the symmetric product was favoured, both isomers had been formed.

It therefore appeared likely that the asymmetric isomer forms first, before subsequently isomerising to the more thermally stable symmetric isomer. The higher stability of the symmetric isomer was likely due to steric issues stemming from the interaction of the non-cyclometallated phenyl and the bridging chlorido ligands. The preference towards the formation of the asymmetric isomer with shorter reaction times suggested that the addition of

the ligand to platinum kinetically favoured the non-cyclometallated phenyl ring in the ortho position to the cyclometallated carbon, though the reason for this was unclear.

The kinetic favourability of the asymmetric isomer suggested the coordination of the Hbppy ligand was more favourable when the non-cyclometallated phenyl ring was in the ortho position to the cyclometallated carbon. This would in turn suggest that shorter reaction times would lead to the formation of the desired $(Pt(Hbppy)Cl)_2$.a isomer. However, when the reaction time was shortened to 3 hours, the formation of $(Pt(Hbppy)Cl)_2$.b was observed, with yields drastically reduced to below 20%, with potassium tetrachloroplatinate still visible in the reaction mixture. This suggested that even if $(Pt(Hbppy)Cl)_2$.a was the kinetically favourable isomer, its rate of isomerisation to $(Pt(Hbppy)Cl)_2$.b was greater than its rate of formation. This in turn may have prevented its isolation under these conditions.

5.5 Synthesis of Pt(Hbppy)(DMSO)Cl

The procedure for the attempted synthesis of dicyclometallated C^C^N platinum(II) complex Pt(bppy)DMSO from a monocyclometallated dimer was adapted from a procedure used by Cave and co-workers[108] in 2000 to produce similar C^N^C platinum(II) complexes, and is illustrated in Figure 63. This reaction involved the splitting of the dimer by DMSO to form a mononuclear monocyclometallated intermediate species. The second cyclometallated bond was then formed by the dissociation of the chloride ligand followed by an electrophilic attack on the phenyl ring by the platinum. The driving force of this reaction was postulated by Cave and co-workers[108] to be the ionisation of hydrochloric acid. Therefore, the addition of water and/or a base to facilitate this ionisation was crucial to the second step of the cyclometallation.

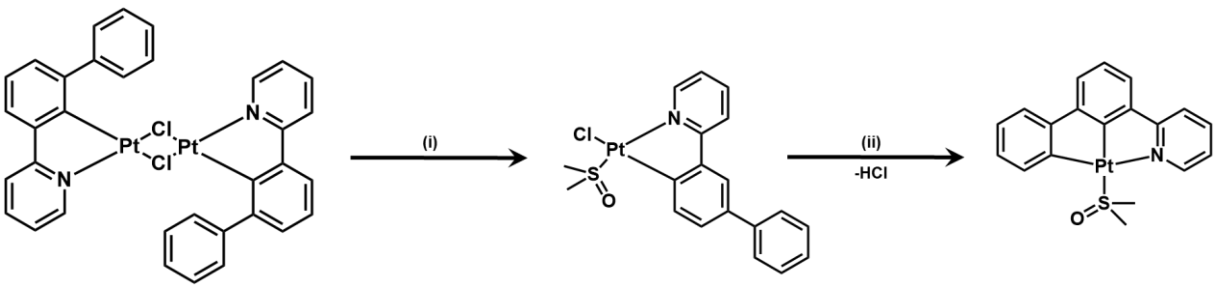

Figure 63: Proposed synthetic pathway towards Pt(bppy)DMSO from $(Pt(Hbppy)Cl)_2$.a. Conditions: (i) DMSO, 150 °C. (ii) H_2O, K_2CO_3, RT.

While $(Pt(Hbppy)Cl)_2$.a was unable to be synthesised, the $(Pt(Hbppy)Cl)_2$.b species obtained previously was theoretically able to serve as a starting material for the second cyclometallation due to the presence of one Hbppy ligand in which the non-cyclometallated phenyl ring was ortho to the cyclometallated carbon. Therefore, the second cyclometallation reaction was attempted on $(Pt(Hbppy)Cl)_2$.b using the method discussed above, illustrated in Figure 64.

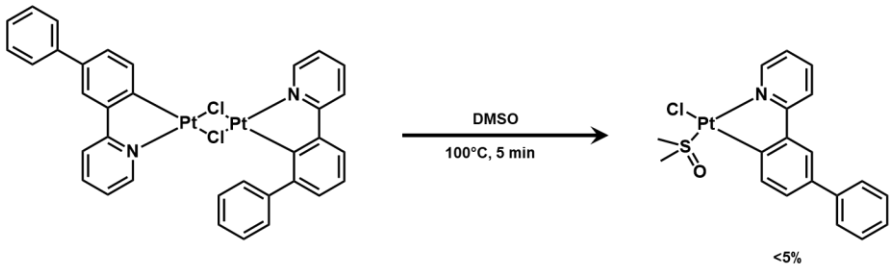

Figure 64: Synthesis of Pt(Hbppy)(DMSO)Cl from $(Pt(Hbppy)Cl)_2$.b.

The dimer was heated in DMSO at 150 °C for 5 minutes then allowed to cool before being added to water and stirred overnight. The yellow precipitate was collected by vacuum filtration and washed with water and petroleum spirits. ^{1}H NMR analysis of this yellow powder showed a complex mixture. Attempts to isolate a product via column chromatography (both neutral alumina and silica) were unsuccessful. Single crystals were obtained by the vapour diffusion of diethyl ether into a solution of chloroform containing the complex mixture. No other species could be isolated from the complex mixture.

The presence of a base such a potassium carbonate when the reaction mixture was added to water was not found to have any observable effect, with the reaction still resulting in the formation of a complex mixture, from which only one product could be isolated.

X-ray crystallographic analysis of these crystals elucidated the structure shown in Figure 65. The structure contained the Hbppy ligand coordinated to platinum through the nitrogen of the pyridine ring and cyclometallated once through the adjacent phenyl ring. The non-cyclometallated phenyl ring occupied the para position to the cyclometallated carbon. Due to significant disorder across a mirror plane, it proved difficult to resolve the exact structure of the complex. Due to this disorder, and the ancillary ligand could not be definitively resolved as DMSO and may have in fact been a methyl sulfonyl. However, the characteristic peak at 2.54 ppm in the ^{1}H NMR that integrated for 6 protons suggested that this ligand was in fact DMSO. Furthermore, the fact that DMSO was used in the reaction process, and the absence of

any powerful oxidising species suggested that it was unlikely for a methyl sulfonyl ligand to have been generated.

The fate of the other Hbppy ligand, in which the non-cyclometallated phenyl ring was ortho to the cyclometallated carbon, was unable to be ascertained as only one product was isolated. Therefore, it could not be determined whether an equivalent mononuclear species was formed, containing the ortho Hbppy ligand.

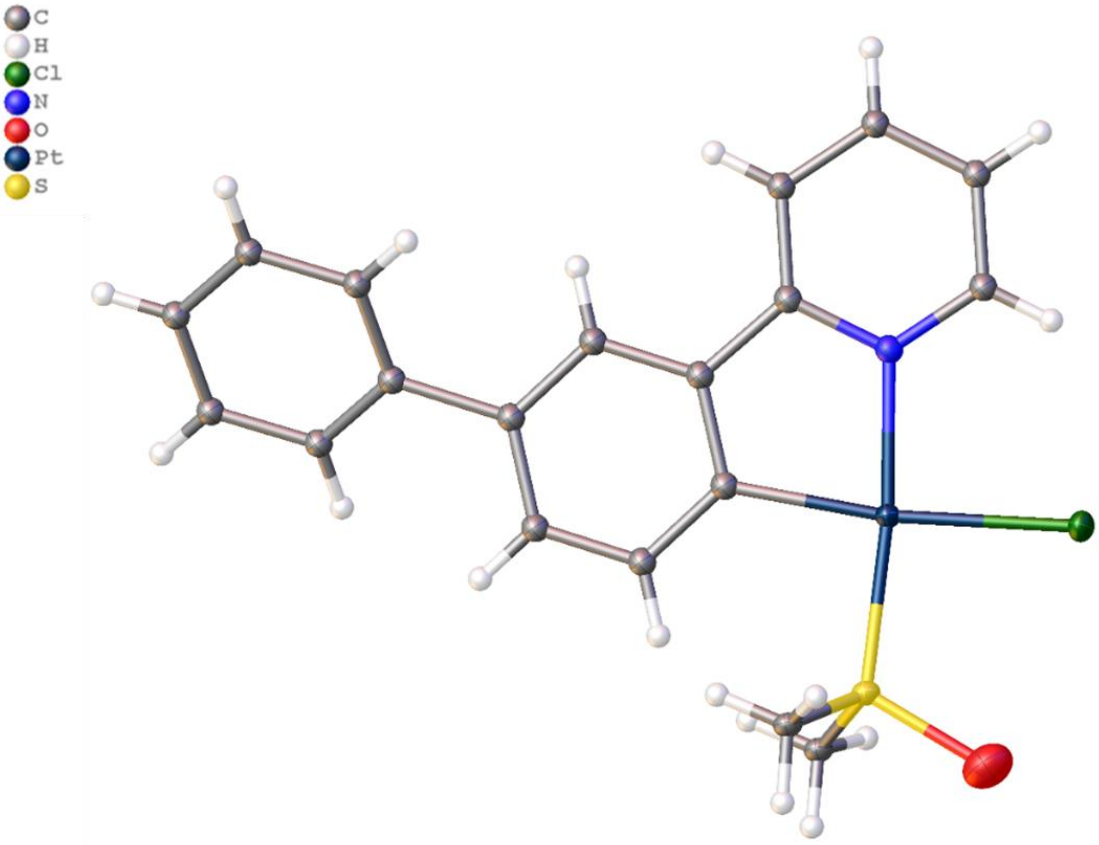

Figure 65: Solid-state structure of Pt(Hbppy)(DMSO)Cl as determined by X-ray crystallography with displacement ellipsoids drawn at 50% probability. The disorder has been removed from this structure for the sake of visual clarity.

Interestingly, the DMSO ligand occupied the trans position to the pyridine nitrogen. This was consistent with findings by Cave and co-workers,[108] in which the isomer containing the chlorido ligand cis to the pyridine nitrogen was more thermodynamically stable. This was consistent with the expected outcome due to the stronger trans effect of the cyclometallated carbon than that of the nitrogen, resulting in a more significant labilisation positions trans to carbon. Therefore, this trend was expected to continue in the case of the formation of a

theoretical mononuclear species containing the bppy ligand. This may in turn have a significant effect on the ability of such a species to undergo the second cyclometallation reaction.

In the case of the synthesis of C^N^C coordinated complexes, the second cyclometallation reaction occurs at the cis position to the nitrogen of the pyridine ring. Cave and co-workers[108] observed this reaction occurring when this position was occupied by the chlorido ligand, but were unable to observe any direct conversion to the dicyclometallated product when this position was occupied by the ancillary ligand. In the case of the synthesis of Pt(bppy)DMSO, the second cyclometallation was expected to occur at the trans position to the nitrogen. As this position was determined to be occupied by the DMSO ligand, it was therefore postulated that even if the phenyl ring were in the correct position, the reaction could not proceed due to the unfavourable position of the ancillary ligand. However, further mechanistic studies are required to definitively determine the effect of the stereochemistry on the second cyclometallation process.

In order to obtain the product with higher yields and greater purity, the reaction was repeated with the $(Pt(Hbppy)Cl)_2$.c using the same reaction conditions and workup procedure as applied to $(Pt(Hbppy)Cl)_2$.b. This reaction yielded a yellow powder. TLC analysis of the powder showed the presence of two species, though attempts to purify the product via column chromatography resulted in the degradation of the product into a complex mixture.

The formation of Pt(Hbppy)(DMSO)Cl was confirmed by ^{1}H NMR analysis (Figure 66). The aromatic region of the spectrum was virtually identical to that of the dimer starting material. However, the presence of a singlet containing 6 hydrogens at 2.55 ppm indicated the presence of free DMSO in a one to one ratio to the product. This is likely due to the labile nature of the DMSO ligand, allowing it to freely exchange with the deuterated DMSO solvent. The quintet at 2.50 ppm was assigned as the residual solvent peak of DMSO while the singlet at 3.33 ppm was ascribed to water present as an impurity in the d_6-DMSO. Furthermore, the presence of a strong, sharp band at 1111 cm^{-1} in the IR spectrum (Figure 67) was characteristic of an S=O stretch, further supporting the presence of coordinated DMSO.

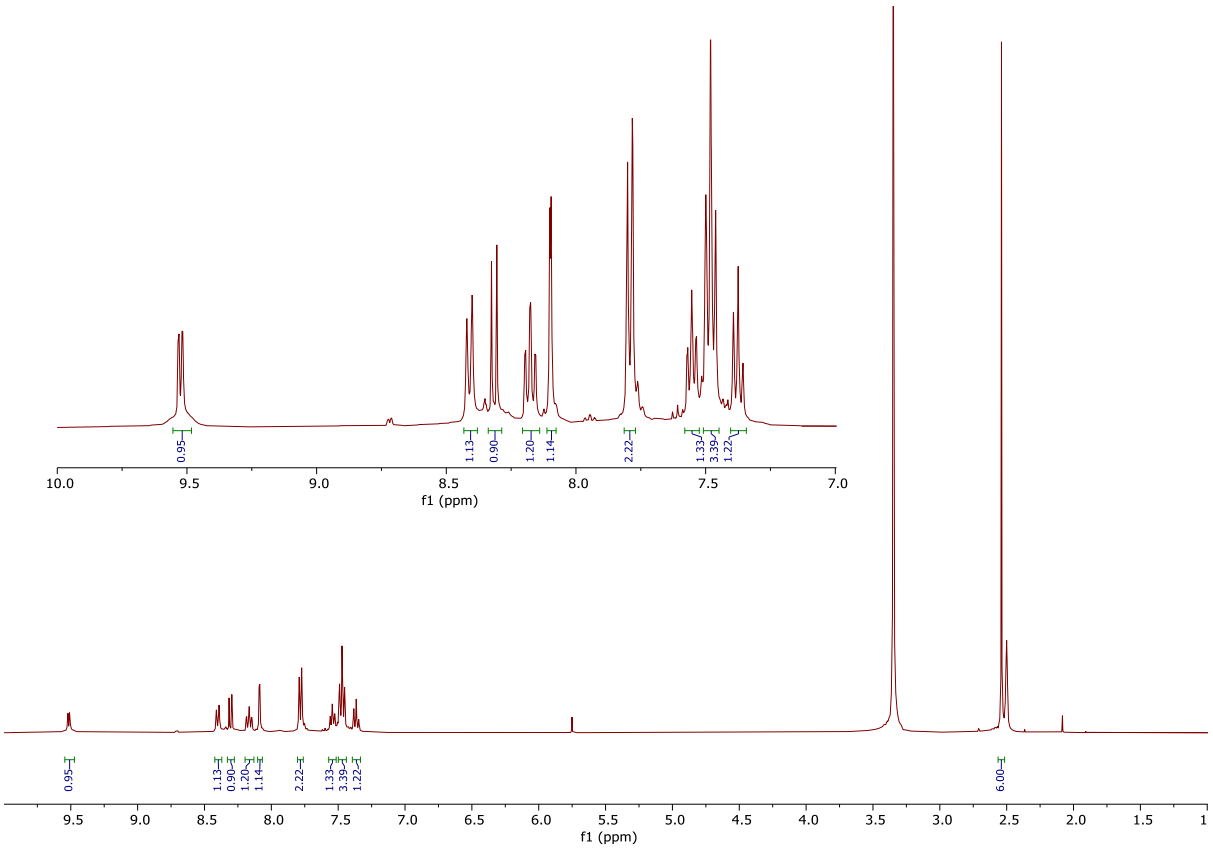

Figure 66: ^{1}H NMR spectrum of Pt(Hbppy)(DMSO)Cl in d_6-DMSO.

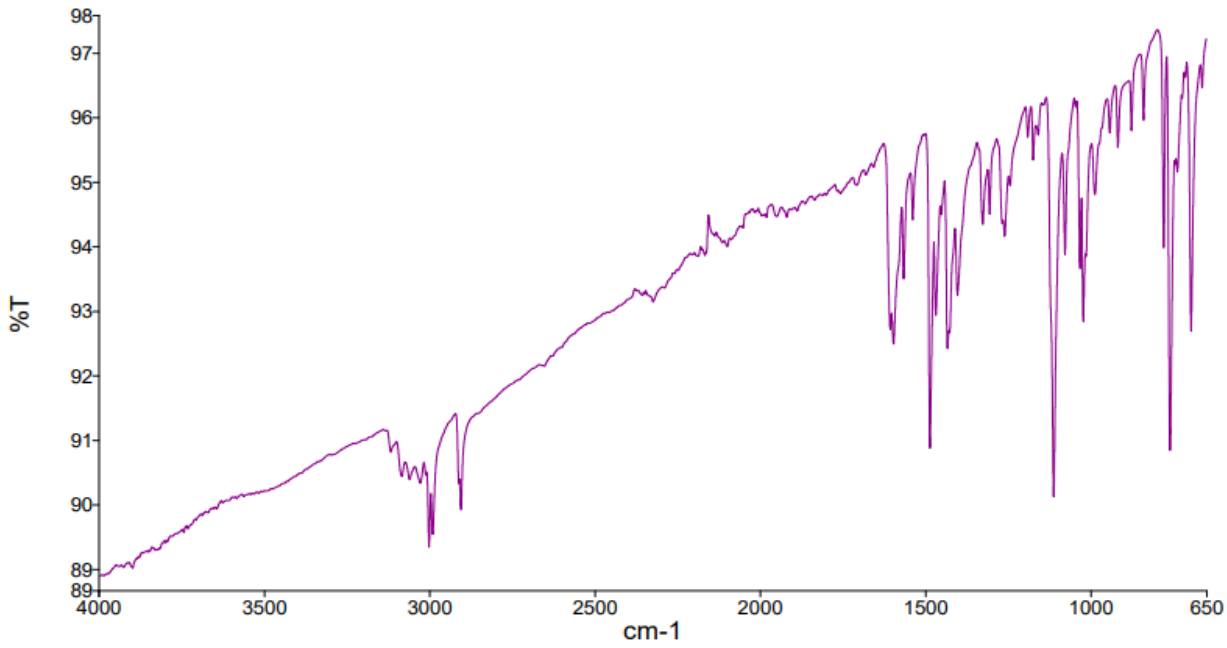

Figure 67: IR spectrum of Pt(Hbppy)(DMSO)Cl.

5.6 Preliminary Photophysical Analysis

Absorption, excitation, and emission spectra were obtained for Pt(Hbppy)(DMSO)Cl (Figure 68). However, due to the fact that the sample was unable to be completely purified, these results were entirely preliminary, as any observations may have been influenced by unknown effects of other species in solution. The complex was found to have a strong, structured absorption band at roughly 270 nm. This band was likely due to a ligand centred (LC) π- π* transitions within the biphenyl pyridine ligand. A much weaker band was also present at approximately 390 nm, which was assigned to a metal-to-ligand charge transfer. These assignments were based on previous assignments of similar bands in other platinum complexes containing similar ligands.[42, 121] The room temperature emission spectrum contained a moderately structured band at 490 to 550 nm. The lifetime of this emission was found to be 8.7 ns. It was determined that this emission originated from an excited state containing LC character due to the clear vibronic structure visible in the bands. However, the short lifetime suggested that the emission was occurring as a result of fluorescence from the free ligand present as an impurity. This in turn suggested that the complex itself was non-emissive in room temperature solutions.

a)

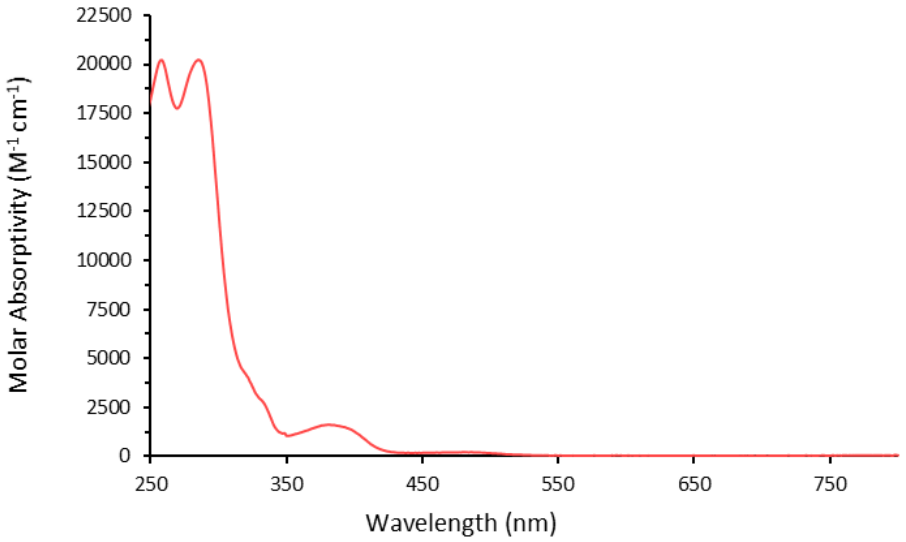

b)

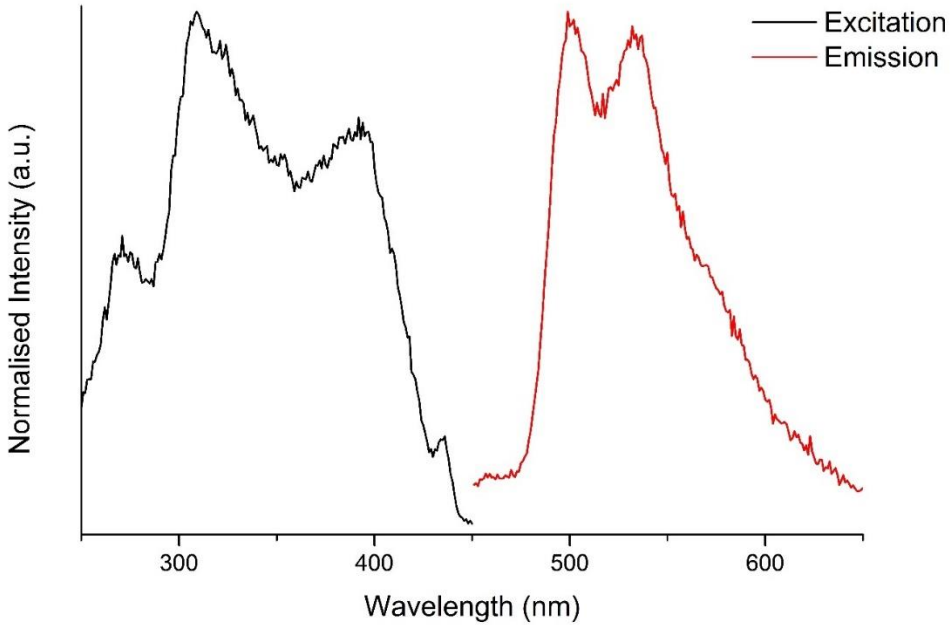

Figure 68: Absorption, excitation and emission spectra of a dilute solution of Pt(Hbppy)(DMSO)Cl in DCM (10^{-5} M). a) Absorption spectrum b) Excitation spectrum was measured at 502 nm. Emission spectrum was excited at 310 nm.

5.7 Synthesis and Investigation of an Unidentified Blue Compound

It was found that when an aqueous base was added to a solution of either $(Pt(Hbppy)Cl)_2$.b or $(Pt(Hbppy)Cl)_2$.c in DMSO at above 140 °C, the mixture immediately took on a white, turbid appearance, with the formation of a blue precipitate, as illustrated in Figure 69. This blue precipitate was collected by vacuum filtration and washed with water and diethyl ether.

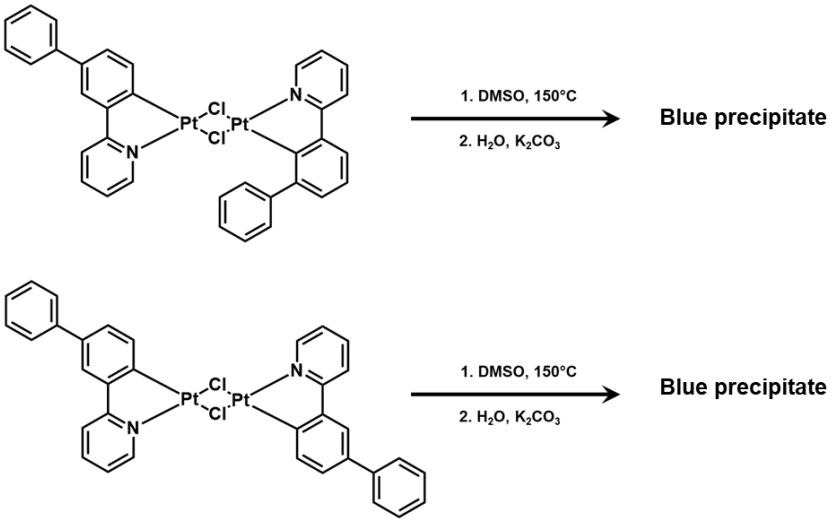

Figure 69: Reaction schemes that result in the formation of a blue precipitate.

In both cases, ^{1}H NMR and TLC analysis of the crude product showed a complex mixture. Column chromatography was able to isolate trace amounts of 2-(biphenyl-3-yl)pyridine. No other species could be isolated from either mixture by column chromatography. Recrystallisation from a system of diethyl ether into chloroform was able to yield trace amounts of Pt(Hbppy)(DMSO)Cl, but was unable to isolate any other compounds from the mixture. Recrystallisation attempts from a system of petroleum spirits into DCM were unsuccessful.

This blue precipitate displayed a deep blue-green colouration in solutions of non-coordinating solvents such as DCM and chloroform. The absorption spectrum of this compound was measured at a concentration of 10^{-2} gL^{-1} in solutions of both DCM and chloroform (Figure 70). Both solutions displayed a broad, moderately intense absorption band at 380 nm. This band was assigned to metal-to-ligand charge transfer transitions from platinum to a Hbppy ligand, based on its similarity to the MLCT absorption band observed in Pt(Hbppy)(DMSO)Cl. They also both displayed a broad, weak band at approximately 730 nm, characteristic of metal centred *d-d* transitions in the platinum atom.

However, when the blue precipitate was dissolved in solutions of coordinating solvents such as DSMO and DMF, it displayed a pale yellow colouration. The absorption spectrum of this compound was measured at a concentration of 10^{-2} gL^{-1} in solutions of both DMSO and DMF. Neither of solutions displayed the weak absorption band at 730 nm observed in solutions of non-coordinating solvents. This suggested a significant change to the inner sphere coordination. However, as the structure of the blue precipitate was unable to be identified, the nature of this change could not be accurately determined.

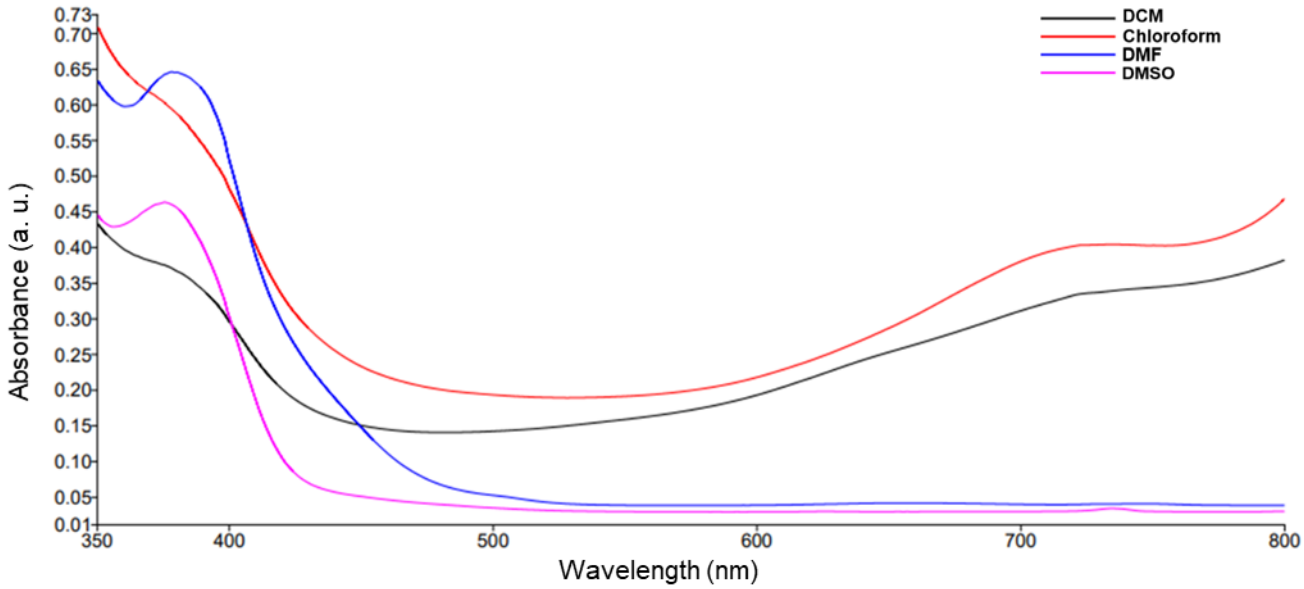

Figure 70: Absorption spectra of the blue compound in solutions of DCM, chloroform, DMF, and DMSO (5 x 10^{-2} gL^{-1}).

5.8 Microwave Reactions

The conditions used by Kumar and co-workers[72] to form C^C^N coordinated gold(III) compounds were adapted to the formation of analogous platinum(II) compounds. This method involved the formation of a non-cyclometallated complex intermediate coordinated to the ligand through the pyridine nitrogen by stirring the ligand and a platinum salt at room temperature.[72] Both cyclometallated bonds were then formed in one step by microwaving the reaction mixture at 170 °C. This procedure is detailed in Figure 71.

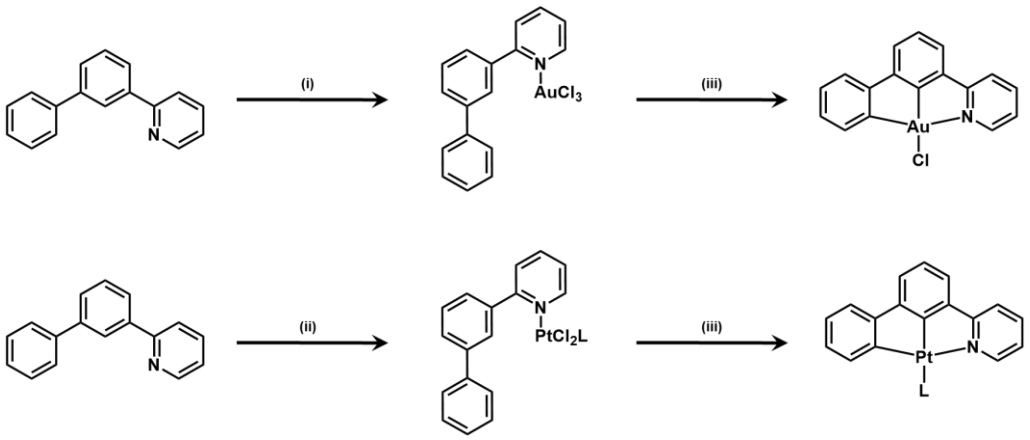

Figure 71: Top) Synthesis of Au(bppy)Cl as carried out by Kumar and co-workers[72]. Bottom) Attempted synthesis of Pt(bppy)(L), L = H_2O or MeCN. Reagents and conditions: (i) $NaAuCl_4$, MeCN, H_2O, RT. (ii) K_2PtCl_4, MeCN, H_2O, RT. (iii) 170 °C, MW, 70 min.

The H_2bppy ligand and potassium tetrachloroplatinate were added to a solution of 1:1 acetonitrile: water and mixed at room temperature for 5 minutes. The mixture was then heated to 170 °C for 70 minutes in a microwave, as illustrated in Figure 71. The workup involved a liquid-liquid extraction from DCM and brine. The organic phase was dried, filtered, and concentrated under reduced pressure to yield a yellow solid. ^{1}H NMR and TLC analysis of this solid showed a complex mixture. Attempts to isolate a product via column chromatography (neutral alumina and silica) and recrystallisation were unsuccessful.

Due to the fact that no species could be isolated from the reaction mixture, it could not be determined whether this method was successful at producing a C^C^N coordinated platinum (II) complex. The reaction may have failed for a similar reason as discussed previously when attempting to form the product through the splitting of a chlorido bridged dimer. As the platinum intermediate has a 2+ oxidation state, as opposed to a 3+ oxidation state as observed in the gold intermediate, it must possess one neutral ligand to maintain its neutrality. This neutral ligand may have hindered the second cyclometallation process, as it would likely have occupied a position trans to the pyridine due to the trans effect.

5.9 Synthesis of $PhBrPh_2$

Due to the fact that the attempted synthesis of Pt(bppy)DMSO encountered issues with the orientation of ligands in the dimer intermediates ($(Pt(Hbppy)Cl)_2$.b and $(Pt(Hbppy)Cl)_2$.c), it was determined that a new ligand could these issues. Therefore, a new ligand H_2tppy (5'-(2-pyridyl)-m-terphenyl) containing an additional phenyl ring, in the meta position to the other substituents on the central benzene ring, was identified. The presence of this additional phenyl ring would remove the possibility of differing orientations of the ligand, therefore eliminating one of the major issues encountered in the aforementioned synthesis of Pt(bppy)DMSO. This H_2tppy ligand was to be synthesised through two palladium catalysed cross-coupling reactions, the first to generate a $PhBrPh_2$ (5'-bromo-m-terphenyl) intermediate, and the second to introduce the pyridyl moiety.

The synthesis of the $PhBrPh_2$ intermediate was first attempted through the utilisation of a selective Suzuki coupling reaction of two equivalents of phenylboronic acid with 1,3,5-tribromobenzene using bis(triphenylphosphine)palladium chloride as the precatalyst, as illustrated in Figure 72. This reaction was unsuccessful when 2.2 equivalents of phenylboronic

acid were added to sparged dimethoxyethane and water and heated at 65 °C for 2 days. TLC analysis confirmed the reaction had proceeded to completion, as no starting material was present, alongside two new spots, indicating two products had been formed. These two products were isolated by column chromatography, eluted with petroleum spirits on silica. However, the major product of the reaction was found to be $PhPh_3$ (1,3,5-triphenylbenzene), with $PhBr_2Ph$ (1,3-dibromo-5-phenylbenzene) present as a minor product. No $PhBrPh_2$ was present in the reaction mixture.

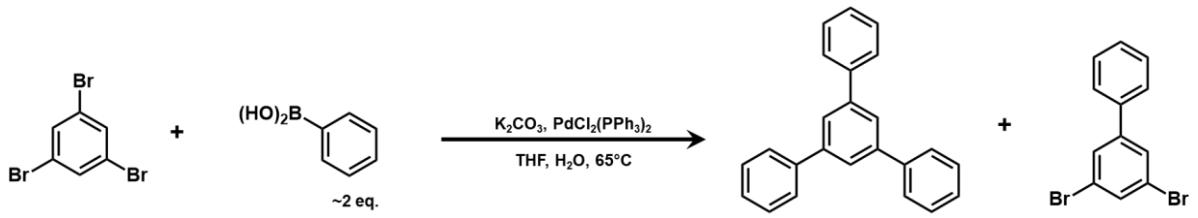

Figure 72: Unintended synthesis of $PhPh_3$ and $PhBr_2Ph$.

The structure of $PhPh_3$ was confirmed by ^1H NMR analysis (Figure 73). The peaks assigned at 7.36 to 7.42 ppm, 7.46 to 7.52 ppm, and 7.69 to 7.73 ppm displayed the splitting pattern characteristic of a singly substituted phenyl ring, and integrated to 3, 6, and 6 protons respectively. The singlet at 7.79 ppm integrated to 3, indicative of three equivalent, but otherwise isolated protons, such as in the 2, 5, and 6 positions of the central phenyl ring. The singlet at 7.26 ppm was assigned as the residual solvent peak of chloroform.

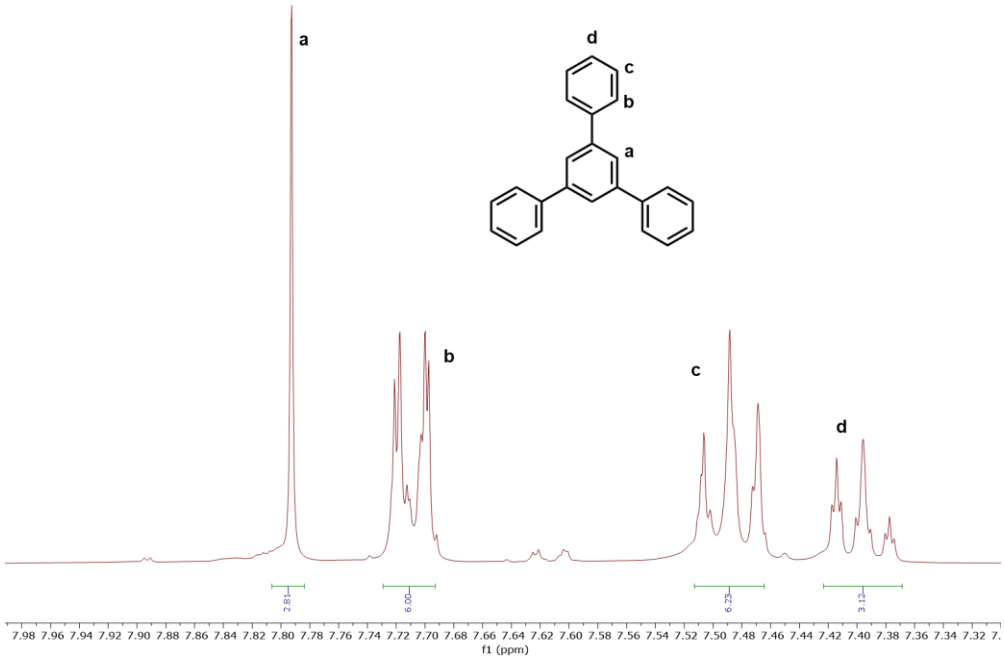

Figure 73: ^1H NMR spectra of $PhPh_3$ in $CDCl_3$.

The structure of $PhBr_2Ph$ was also confirmed by ^1H NMR analysis (Figure 74). The same peaks indicative of a singly substituted phenyl ring were present, though in this case integrating for 2, 2, and 1 respectively. The protons on the central ring were observed as two distinct peaks, appearing as a triplet at 7.63 to 7.65 ppm and a doublet at 7.65 to 7.67 ppm. These peaks integrated for one and two protons respectively, and both displayed *J* values of approximately 2 Hz. This pattern was characteristic of long distance meta coupling between the proton in the 2 position, and those in the 4 and 6 positions of a triply substituted phenyl ring. The singlet at 7.26 ppm was assigned as the residual solvent peak of chloroform.

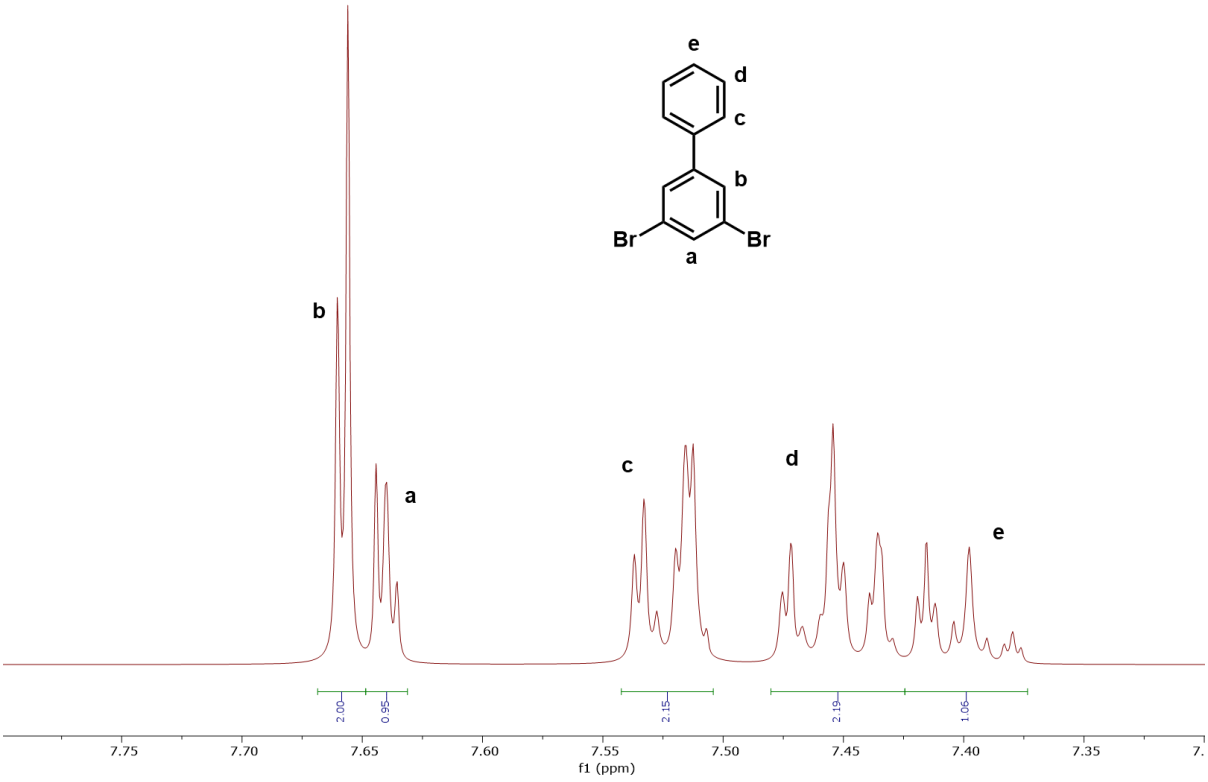

Figure 74: ^1H NMR spectra of $PhBr_2Ph$ in $CDCl_3$.

When 1.8 equivalents of phenylboronic acid were added to sparged dimethoxyethane and water and heated at 65 °C for 3 hours, the reaction still proceeded to completion, though TLC analysis suggested an increased yield of $PhBr_2Ph$, with a decreased yield of $PhPh_3$. No $PhBrPh_2$ was present in the reaction mixture.

The failure of these reaction conditions suggested that the $PhBrPh_2$ species was highly reactive towards Suzuki coupling, resulting in the phenylboronic acid preferentially reacting with this species over $PhBr_2Ph$. This seemingly contradicted the expectation that 3,5-dibromo-1,1'-biphenyl should be more reactive towards the rate determining oxidation addition step due to

the presence of a higher number of electron withdrawing bromide groups. Therefore, this cause of this behaviour was unlikely to be related to mesomeric effects, though its exact cause could not be definitively determined.

In order to slow the rate of reaction, the reaction was repeated with the dropwise addition of the boronic acid and potassium carbonate to a solution of the tribromobenzene over the course of 5 hours. This procedure is detailed in Figure 75.

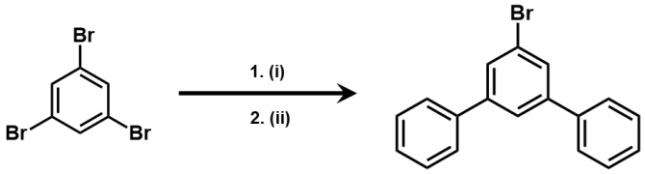

Figure 75: Synthesis of $PhBrPh_2$. Reagents and conditions: (i) DMSO, 150 °C, 5 min (ii) K_2CO_3, H_2O, 14 hrs, RT.

The reaction proceeded to completion, as evidenced by the lack of starting material detected by TLC analysis. The product was purified by column chromatography, eluted with petroleum spirits on silica, to yield $PhBrPh_2$ in 15% yield.

The presence of $PhBrPh_2$ was confirmed by ^1H NMR analysis (Figure 76). The characteristic peaks of a singly substituted phenyl ring were present, integrating to a total of 10 protons, suggesting the presence of two such rings. The signals of the protons on the central benzene ring were unable to be distinguished from one another but integrated to 3 protons. Despite this, it was determined that reaction was successful on the basis of the integration of the singly substituted phenyl rings. This determination was further supported by the successful application of the product in a Stille reaction with 2-(tributylstannyl)pyridine to form H_2tppy. The singlet at 7.26 ppm was assigned as the residual solvent peak of chloroform.

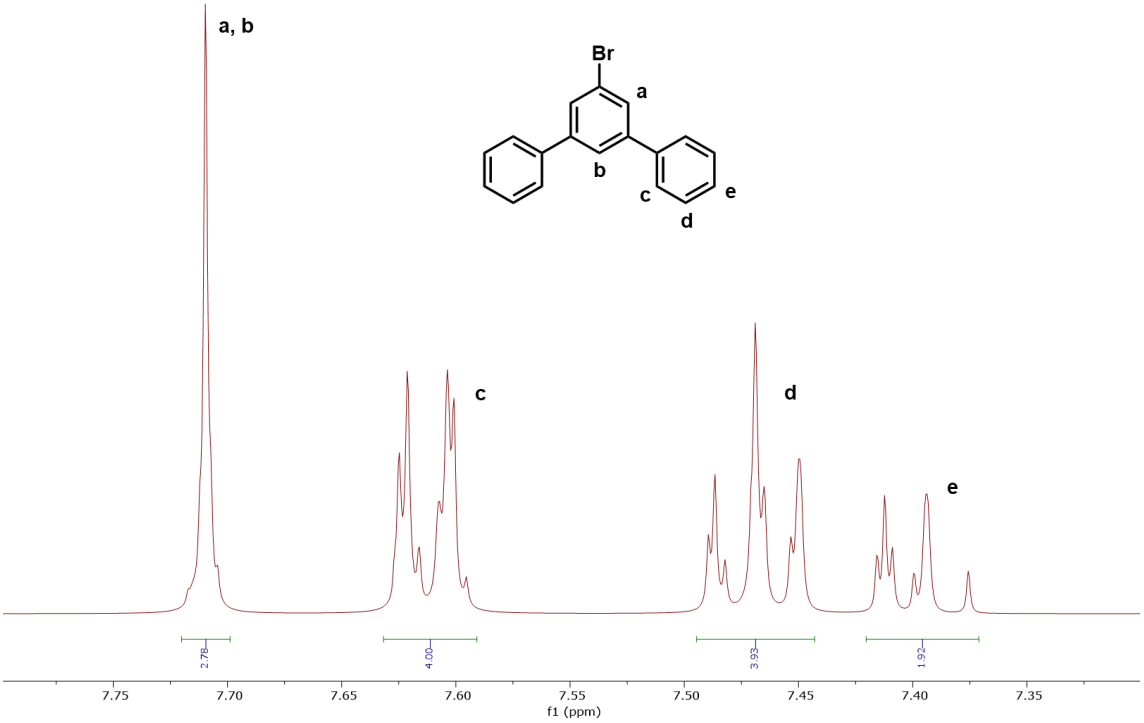

Figure 76: ^{1}H NMR spectra of $PhBrPh_2$ in $CDCl_3$.

The other major components of the mixture were determined to $PhBr_2Ph$ and $PhPh_3$. The presence of these species, alongside the low yield of the reaction, indicated that although the dropwise addition had controlled the reaction enough to allow for the isolation of the desired product, it had not entirely prevented the reaction of the desired product with phenylboronic acid to form $PhPh_3$.

5.10 Synthesis of H_2tppy

The H_2tppy ligand was synthesised through the application of another palladium catalysed cross-coupling, in this case a Stille coupling, as illustrated in Figure 77.

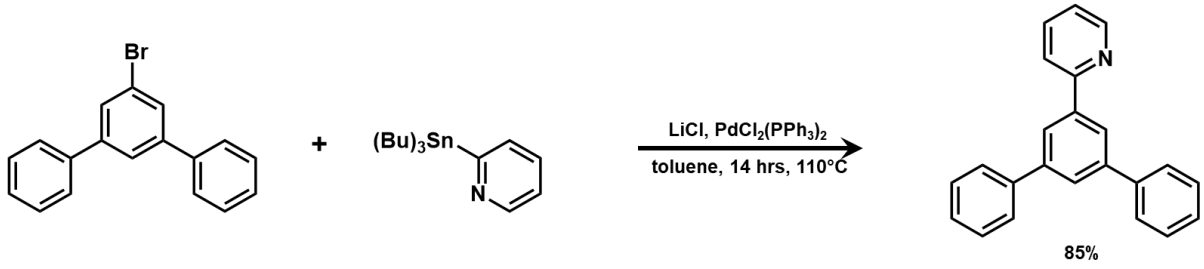

Figure 77: Synthesis of H_2tppy.

$PhBrPh_2$ and 2-(tributylstannyl) pyridine were refluxed in sparged toluene for 14 hours in the presence of lithium chloride and bis(triphenylphosphine)palladium chloride. The workup involved first washing the reaction mixture with 1 M potassium fluoride solution to convert tributyltin bromide to tributyltin fluoride, which is insoluble and was subsequently filtered off. The crude product was purified by column chromatography, eluting with a 1:19 ratio of ethyl acetate to petroleum spirits on silica.

Stille couplings, similar to Suzuki couplings, are palladium catalysed, though they involve the use of organotin reagents rather than boronic acids.[122-125] The catalytic pathway of the Stille reaction is highly complex, involving a number of competing pathways.[124] However, the general scheme of the reaction follows a very similar pathway to that of the Suzuki reaction, as illustrated in Figure 78. It begins with the oxidation addition of the organic halide to the palladium catalyst, followed by a transmetallation in which the organostannane reagent transfers an organic species to the catalyst.[124] Finally, the two organic groups coordinated to the palladium undergo an irreversible reductive elimination to yield the cross-coupled product.[124]

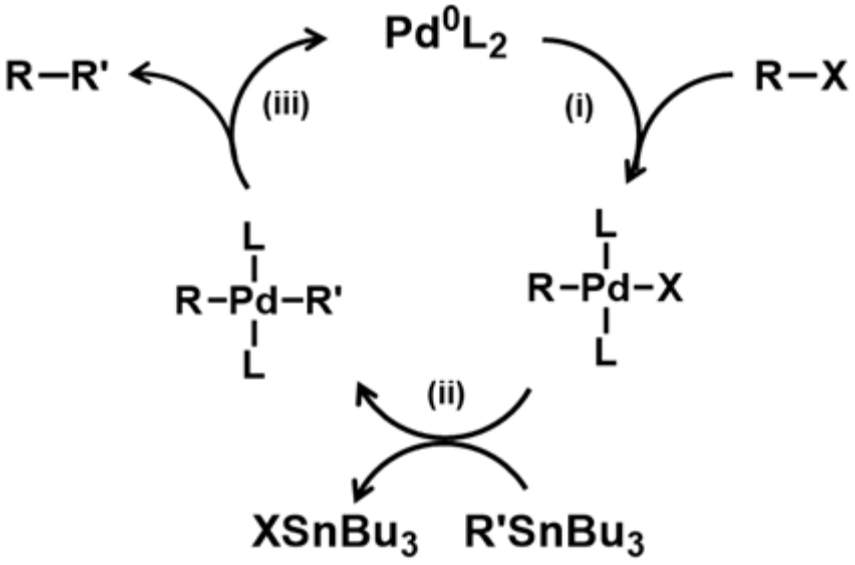

Figure 78: A simplified catalytic cycle of the Stille reaction. (i) oxidative addition (ii) transmetallation (iii) reductive elimination.

Stille reactions offer several distinct advantages to other palladium cross-coupling reactions. The organostannane reagents used are generally stable with respect to both air and moisture, and display relatively low reactivity, meaning Stille reactions can be performed in harsher conditions than most coupling reactions.[124] Furthermore, organotin reagents are widely

commercially available, and readily synthesised by relatively simple procedures. It was this commercial availability of the desired organotin reagent that was the primary factor in the decision to use a Stille reaction in the synthesis of H_2tppy.

However, the use of organostannanes presents the challenge of toxicity. Most organotin compounds are generally quite toxic to humans and are harmful to the environment.[126, 127] The toxicity of these species can be reduced by increasing the size of the organic substituents bonded to the tin atom. The increased steric hindrance of larger organic groups can have a detrimental effect on the rate of reaction. Therefore, tributyltin reagents are frequently used for Stille reactions, as they strike a balance between reduced toxicity and good reactivity.[126]

The lithium chloride additive serves to increase the rate of reaction.[124] Although the mechanism for this enhancement has not been definitively determined, it has been suggested that it increases the activity of the catalyst towards transmetallation by displacing the halide from the palladium, or towards oxidative addition by coordinating to the palladium(0) species to form anionic palladium salts.[124]

The structure of H_2tppy was confirmed by ^{1}H NMR analysis (Figure 79). The spectrum obtained from the product contained the same peaks as those in the spectrum obtained by Wang and co-workers[128] in 2015. The residual solvent peak could not be resolved due to significant overlap with the peak assigned as i.

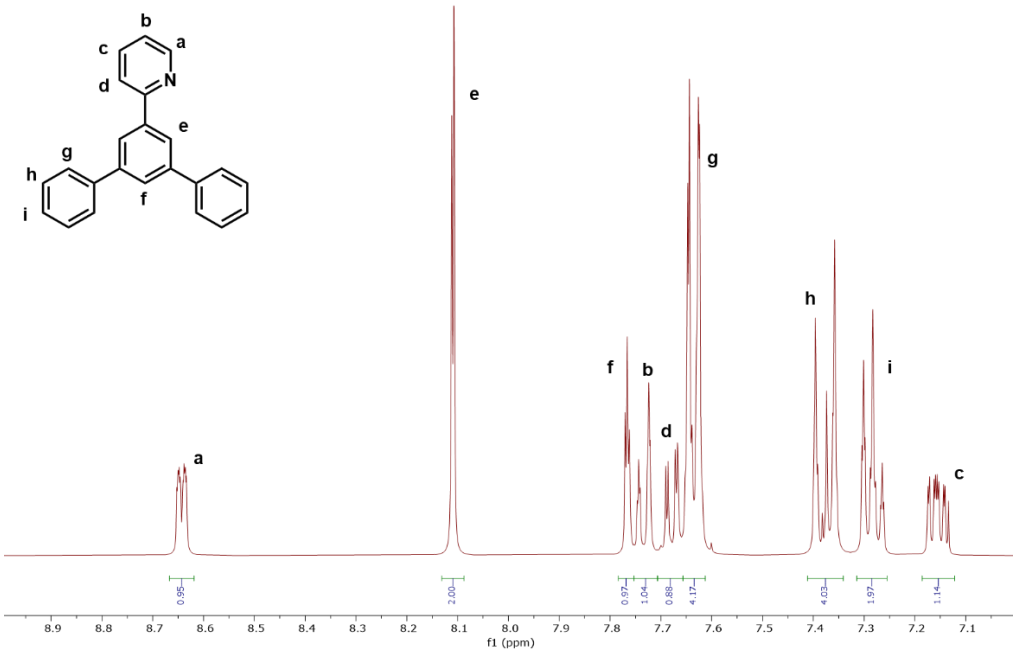

Figure 79: ^{1}H NMR spectra of H_2tppy in $CDCl_3$.

5.11 Attempted Synthesis of $(Pt(Htppy)Cl)_2$

The synthesis of $(Pt(Htppy)Cl)_2$ was attempted by application of the same conditions used to synthesise the $(Pt(Htppy)Cl)_2$.b and $(Pt(Htppy)Cl)_2$.c dimers, as illustrated in Figure 80.

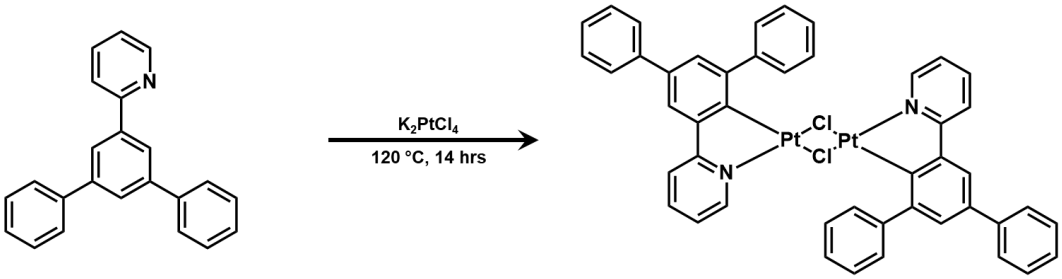

Figure 80: Attempted synthesis of $(Pt(Htppy)Cl)_2$.

The reaction yielded a yellow solid. ^1H NMR analysis of this product showed a complex mixture.

Attempts to purify the product by column chromatography using silica as a stationary phase were unsuccessful, due to the apparent decomposition of the product on silica. Using alumina as a stationary phase was similarly unsuccessful, though due to significant streaking resulting in a lack of separation between components in the mixture. Purification attempts by recrystallisation were also unsuccessful. The same yellow solid was obtained when the reaction time was increased to 3 days. No crystals suitable for x-ray crystallography could be obtained from this mixture.

Although the product could not be isolated, and therefore could not be characterised, the formation of a yellow solid suggested that a reaction had occurred. Based on this observation it was conjectured that the product may have been present in the reaction mixture, despite the lack of success of the purification attempts. Therefore, the crude reaction mixture was used in the subsequent attempted synthesis of Pt(Htppy)(DMSO)Cl.

5.12 Attempted Synthesis of Pt(tppy)DMSO

Although a pure sample of $(Pt(Htppy)Cl)_2$ was unable to be isolated from the first cyclometallation reaction, the second cyclometallation was attempted on the crude product that was obtained, as illustrated in Figure 81.

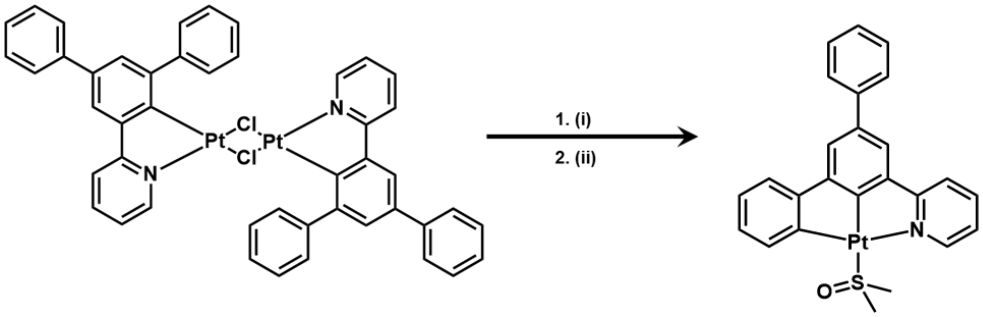

Figure 81: Attempted synthesis of Pt(tppy)DMSO. Reagents and conditions: (i) DMSO, 150 °C, 5 min (ii) K_2CO_3, H_2O, 14 hrs, RT.

The crude product was heated at 150 °C in DMSO for 5 minutes before being allowed to cool, then added to aqueous potassium carbonate and stirred at room temperature for 14 hours to yield a yellow solid. ^1H NMR analysis of the crude product indicated a complex mixture. The same chromatographic and recrystallisation techniques that were used in the attempted purification of $(Pt(Htppy)Cl)_2$ were also unsuccessful in the purification of this complex mixture. No crystals suitable for X-ray crystallography could be obtained.

The failure to isolate a product from this reaction could be ascribed to any of a number of possibilities. The first was that the initial synthesis of $(Pt(Htppy)Cl)_2$ was unsuccessful, and therefore this reaction was unsuccessful due to a lack of starting material.

The second was that, while $(Pt(Htppy)Cl)_2$ was present, the second cyclometallation itself was unsuccessful. This may have been due to the trans effect of the first cyclometallated carbon directing the DMSO ligand into the trans position to the pyridine ring. This may in turn have prevented the formation of the second cyclometallated bond, as discussed in the attempted synthesis of Pt(bppy)(DMSO).

The final possibility was that the formation of Pt(tppy)DMSO was successful, and the product was simply unable to be isolated from the reaction mixture. However, the impurity of the

starting material and this lack of any isolated species means that no definitive statements can be made regarding the source of the inability to yield Pt(tppy)DMSO from this reaction.

5.13 Conclusions and Further Work

This project made investigations towards the synthesis of C^C^N coordinated platinum(II) complexes for the purpose of photophysical analysis. Ligands containing biphenyl pyridine functionality were synthesised by palladium catalysed cross coupling reaction.

From the H_2bppy ligand, two dimeric platinum(II) species were synthesised, one of which has the potential to be used in the synthesis of a C^C^N coordinated complex. Unfortunately, the final synthesis of such a complex was unsuccessful.

A number of significant challenges to this synthetic target were identified. The first was that the desired dimeric intermediate could not be isolated. All attempts to generate it resulted in the formation of isomers that contained at least one ligand coordinated in the undesired orientation. Furthermore, attempts to bypass this issue by incorporating an additional phenyl ring in the ligand resulted in the formation of a complex mixture that could not be purified.

The second significant challenge was the stereochemistry of the reaction intermediates formed during the second cyclometallation step. When the dimer was split by an ancillary ligand such as DMSO, the trans effect dictated that that ligand occupy the position trans to that of the nitrogen of the pyridine ring. In the case of an intermediate towards the synthesis of a C^C^N coordinated complex, such a Pt(Hbppy)(DMSO)Cl, this trans position was the position in which the second cyclometallated bond was to be formed. As this cyclometallation was to be driven by the formation of HCl through the loss of the chlorido ligand, the fact that the chlorido ligand was not present in the position in which the cyclometallated bond was to be formed may have resulted in the failure of the reaction.

The third and final challenge was the difficulty of purification of platinum(II) complexes. These complexes were not stable on silica, and therefore required alumina stationary phases for column chromatography. However, the broad bands formed by platinum(II) species in alumina columns prevented this method from easily purifying them. Finally, all attempts to purify these compounds using recrystallisation were unsuccessful.

Therefore, further work should focus on solving these two major challenges. If a robust method for the purification of these cyclometallated platinum(II) complexes can be developed, then it may be possible to isolate a C^C^N coordinated complex from one of the reactions already attempted in this research. If this is not the case, then future work should focus on attempting to resolve the issue of the stereochemistry of the reaction intermediates.

Chapter 6: Conclusions and Further Work

The aim of this research was to explore a range of platinum(II) complexes for applications in biology. These platinum(II) complexes focused on three families of compounds.

The first of these families involved platinum(II) complexes containing cyclometallated N-heterocyclic carbene and pyridyl tetrazole ligands to be investigated for suitability as biological probes. While platinum complexes containing cyclometallated NHC ligands have been reported extensively in the literature, and show impressive photophysical properties, none have been explored in the context of biological imaging.[32, 34, 43, 44, 54, 86, 129] Furthermore, none of the reported platinum NHC complexes have incorporated pyridyl tetrazole functionality.

Five novel complexes bearing a phenylthiazole ligand alongside pyridyl tetrazole ligands with varying substituents were reported in this study. While their poor solubility prevented their characterisation by NMR spectroscopy, they were confirmed using HRMS techniques. These complexes display promising photophysical properties in organic solvents such as DCM and DMSO, with lifetimes in the range of 2 microseconds, and quantum yields reaching 20%. Furthermore, the substitution on the pyridyl tetrazole ligand was found to have a minimal effect on the emission wavelength of these complexes, while allowing for tuning of the quantum yield. Unfortunately, due to the fact that they were not soluble in aqueous media, they were not suitable for use in biological imaging.

Further work in this area should focus on improving the solubility of this family of complexes in aqueous environments to allow for their application in biological imaging. This could be achieved by the incorporation of charged functional groups such as triphenylphosphonium. This would also serve to introduce a biologically active group, allowing for the targeting of mitochondria in cells.[74] Another approach involves the incorporation of neutral moieties which are known to improve the solubility of organic compounds in water, such as trimethylsilyl[83] and glutaryl groups.[84] Finally, the incorporation of deprotected amino acid groups may allow for the exploitation of acid/base chemistry to generate charged species, improving water solubility.

The second family of complexes was those bearing ortho-cyclophane ligands, which were investigated for their potential antimicrobial activity. While the biological activity the platinum(II) complexes could not be determined due to synthetic difficulties, the activity of their palladium analogues was determined. The palladium complex Pd(o-cyc)Br_2 was found to

show promising activity against *Cryptococcus neoformans*, while displaying very low toxicity towards human cells. This activity was lost when the bromido ligands are replaced with a pyridyl tetrazole to generate a cationic complex. Once the results for the platinum complexes are obtained, a more detailed structure activity relationship can be established.

Further work on this family of complexes should simply focus on expanding the library of compounds sent for testing in order to generate a more detailed structure activity relationship. Once this is established, the antimicrobial properties of these complexes can be optimised. Beyond this, these compounds should undergo preclinical trials to determine their suitability as drugs for the treatment of *Cryptococcus neoformans* infections. Finally, they should also be tested against a wider range of pathogenic microbes, to determine if they are suitable for broader application than simply the treatment of *Cryptococcus neoformans*.

The third and final family of compounds that was explored was that of C^C^N coordinated terdentate platinum(II) complexes. This structural motif was chosen for the conjectured increase in sigma donating capacity of these ligands compared to C^N^C and N^C^N ligands. It was also conjectured that the cis conformation of the cyclometallated carbons would help to avoid the issues with distortion that result in the reduced luminescence of C^N^C coordinated complexes. This study aimed to establish a synthetic pathway for the generation of such C^C^N coordinated complexes, and to subsequently study their photophysical properties to determine their suitability as biological probes. Unfortunately, this synthetic goal was not achieved, though a number of important challenges in the synthesis were identified.

The first challenge was that the desired intermediate species was unable to be isolated due to the range of potential products generated by the procedure used to synthesis it. The first of these undesired species was not suitable for use in the synthesis of C^C^N coordinated complexes due to the ligand coordinating in the wrong orientation. The second was potentially viable as an intermediate. However, it contained only one ligand oriented correctly, with a second oriented incorrectly, resulting in a complex mixture that could not be purified upon attempting to generate the final product. Attempts to overcome this challenge by including an additional phenyl ring were unsuccessful, due to difficulties with purification, as discussed below.

The second was that, due to the trans effect, the lysing of the dimer resulted in the formation of a species containing a DMSO ligand in the position that the cyclometallated bond was to be formed. This cyclometallation was to be achieved through an intramolecular ligand substitution

in which the chlorido ligand is lost, and an electrophilic attack by the platinum centre on the phenyl ring forms the cyclometallated bond. Therefore, if this reaction proceeds though a concerted mechanism, then it is likely that the observed intermediate was not capable of forming this cyclometallated bond due to the chlorido ligand not being present in the correct position.

The final challenge was simply that of the purification and isolation of the platinum complexes. Both the dimeric and monomeric species obtained in this study presented significant challenges in their purification. They are not stable on silica and form wide bands on alumina that prevent their purification using chromatographic techniques. Furthermore, all attempts to purify these compounds using recrystallisation were unsuccessful, likely due to the highly similar solubilities of the compounds to be separated from one another.

Further work towards the synthesis of a C^C^N coordinated platinum(II) complex should focus on overcoming these challenges. If a reliable method for the purification of these species can be developed, then the success of the reactions can be ascertained more reliably, and therefore more conclusions regarding the required structures of the intermediates can be drawn. Additionally, future attempts at this synthesis should focus on attempting to modify the stereochemistry of the reaction intermediates in order to facilitate the final cyclometallation reaction.

References

1. E. D. Dominguez de Villota, Ruiz Carmona M. T., Rubio J. J., de Andrés S. Br J Anaesth. 1981;53(12):1325-8.
2. R. I. Weed, Reed C. F., Berg G. J Clin Invest. 1963;42:581.
3. A. Miller, Korem M., Almog R., Galboiz Y. J Neurol Sci. 2005;233(1-2):93-7.
4. R. Banerjee, Ragsdale S. W. Annu Rev Biochem. 2003;72:209-47.
5. A. Klug, Rhodes D. Cold Spring Harbor Symp Quant Biol. 1987;52:473.
6. J. Miller, McLachlan A. D., Klug A. EMBO J. 1985;4(6):1609.
7. B. Rosenberg, VanCamp L., Trosko J. E., Mansour V. H. Nature. 1969;222(5191):385.
8. I. Giacomini, Ragazzi E., Pasut G., Montopoli M. Int J Mol Sci. 2020;21(3):937.
9. K. K.-W. Lo, Choi A. W.-T., Law W. H.-T. Dalton Trans. 2012;41(20):6021-47.
10. D.-L. Ma, He H.-Z., Leung K.-H., Chan D. S.-H., Leung C.-H. Angew Chem, Int Ed. 2013;52(30):7666-82.
11. K. Mijnendonckx, Leys N., Mahillon J., Silver S., Van Houdt R. BioMetals. 2013;26(4):609-21.
12. B. M. Sutton. Gold Bull. 1986;19(1):15-6.
13. R. Alberto, Motterlini R. Dalton Trans. 2007(17):1651-60.
14. A. Arrais, Gabano E., Ravera M., Osella D. Inorg Chim Acta. 2018;470:3-10.
15. H.-Q. Liu, Cheung T.-C., Che C.-M. Chemical Communications. 1996(9):1039-40.
16. K. K.-W. Lo, Louie M.-W., Zhang K. Y. Coord Chem Rev. 2010;254(21-22):2603-22.
17. H. D. Stoeffler, Thornton N. B., Temkin S. L., Schanze K. S. Journal of the American Chemical Society. 1995;117(27):7119-28.
18. J. Ohata, Ball Z. T. Dalton Trans. 2018;47(42):14855-60.
19. J. J. Yan, Chow A. L.-F., Leung C.-H., Sun R. W.-Y., Ma D.-L., Che C.-M. Chem Commun (Cambridge, U K). 2010;46(22):3893-5.
20. Q. Zhao, Huang C., Li F. Chemical Society Reviews. 2011;40(5):2508-24.
21. G. I. Pascu, Hotze A. C. G., Sanchez-Cano C., Kariuki B. M., Hannon M. J. Angew Chem, Int Ed. 2007;46(23):4374-8.
22. C. Turro, Bossmann S. H., Jenkins Y., Barton J. K., Turro N. J. Journal of the American Chemical Society. 1995;117(35):9026-32.
23. A. I. Solomatina, Chelushkin P. S., Krupenya D. V., Podkorytov I. S., Artamonova T. O., Sizov V. V., et al. Bioconjugate Chem. 2017;28(2):426-37.
24. Y. Zhou, Jia J., Cai L., Huang Y. Dalton Trans. 2018;47(3):693-9.
25. Z.-P. Zeng, Wu Q., Sun F.-Y., Zheng K.-D., Mei W.-J. Inorg Chem. 2016;55(11):5710-8.
26. J. Li, Tian Z., Xu Z., Zhang S., Feng Y., Zhang L., et al. Dalton Trans. 2018;47(44):15772-82.
27. N. Erathodiyil, Ying J. Y. Acc Chem Res. 2011;44(10):925-35.
28. O. Kocaoglu, Carlson E. E. Nat Chem Biol. 2016;12(7):472-8.
29. B. A. D. Neto, Correa J. R., Silva R. G. RSC Adv. 2013;3(16):5291-301.
30. T. Terai, Nagano T. Curr Opin Chem Biol. 2008;12(5):515-21.
31. J. F. Callan, de Silva A. P., Magri D. C. Tetrahedron. 2005;61(36):8551-88.
32. Y. Unger, Meyer D., Molt O., Schildknecht C., Muenster I., Wagenblast G., et al. Angew Chem, Int Ed. 2010;49(52):10214.
33. S.-B. Ko, Park H.-J., Gong S., Wang X., Lu Z.-H., Wang S. Dalton Trans. 2015;44(18):8433-43.
34. T. Fleetham, Wang Z., Li J. Org Electron. 2012;13(8):1430-5.
35. K. D. M. MaGee, Wright P. J., Muzzioli S., Siedlovskas C. M., Raiteri P., Baker M. V., et al. Dalton Trans. 2013;42(12):4233-6.
36. Z. M. Hudson, Sun C., Helander M. G., Chang Y.-L., Lu Z.-H., Wang S. J Am Chem Soc. 2012;134(34):13930-3.
37. K. Li, Cheng G., Ma C., Guan X., Kwok W.-M., Chen Y., et al. Chem Sci. 2013;4(6):2630-44.

38. F. Wilkinson, Abdel-Shafi A. A. J Phys Chem A. 1997;101(30):5509-16.
39. J. R. Lakowicz. Principles of Fluorescence Spectroscopy. 3rd edit ed: Springer; 2006.
40. P. Atkins, Overton T., Rourke J., Weller M., Armstrong F. Shriver and Atkins Inorganic Chemistry. 4th ed: Oxford University Press; 2006.
41. J. A. Bailey, Miskowski V. M., Gray H. B. Inorg Chem. 1993;32(4):369.
42. J. A. G. Williams, Beeby A., Davies E. S., Weinstein J. A., Wilson C. Inorg Chem. 2003;42(26):8609-11.
43. H. Leopold, Strassner T. Dalton Trans. 2017;46(24):7800-12.
44. J. Soellner, Strassner T. Chem - Eur J. 2018;24(58):15603-12.
45. J. A. G. Williams. Photochemistry and Photophysics of Coordination Compounds: Platinum. In: Balzani V, Campagna S, editors. Photochemistry and Photophysics of Coordination Compounds II. Berlin, Heidelberg: Springer Berlin Heidelberg; 2007. p. 205-68.
46. T.-C. Cheung, Cheung K.-K., Peng S.-M., Che C.-M. J Chem Soc, Dalton Trans. 1996(8):1645.
47. V. W.-W. Yam, Tang R. P.-L., Wong K. M.-C., Lu X.-X., Cheung K.-K., Zhu N. Chem - Eur J. 2002;8(17):4066-76.
48. S. Huo, Carroll J., Vezzu D. A. K. Asian J Org Chem. 2015;4(11):1210-45.
49. H. Leopold, Tronnier A., Wagenblast G., Muenster I., Strassner T. Organometallics. 2016;35(7):959-71.
50. H. W. Wanzlick, Schoenherr H. J. Angew Chem, Int Ed Engl. 1968;7(2):141.
51. A. J. Arduengo, III, Harlow R. L., Kline M. J Am Chem Soc. 1991;113(1):361.
52. F. E. Hahn, Jahnke M. C. Angew Chem, Int Ed. 2008;47(17):3122-72.
53. M. N. Hopkinson, Richter C., Schedler M., Glorius F. Nature (London, U K). 2014;510(7506):485-96.
54. M. Tenne, Metz S., Muenster I., Wagenblast G., Strassner T. Organometallics. 2013;32(21):6257-64.
55. R. W.-Y. Sun, Chow A. L.-F., Li X.-H., Yan J. J., Chui S. S.-Y., Che C.-M. Chem Sci. 2011;2(4):728-36.
56. T. D. Ashton, Jolliffe K. A., Pfeffer F. M. Chemical Society Reviews. 2015;44(14):4547-95.
57. E. Kottelat, Zobi F. Inorganics. 2017;5(2):24/1.
58. T. Slanina, Šebej P. Photochemical & Photobiological Sciences. 2018;17(6):692-710.
59. G. T. Morgan, Burstall F. H. Journal of the Chemical Society (Resumed). 1934(0):1498-500.
60. R. J. Mureinik, Bidani M. Inorg Nucl Chem Lett. 1977;13(12):625.
61. R. J. Mureinik, Bidani M. Inorg Chim Acta. 1978;29(1):37-41.
62. R. C. Conrad, Rund J. V. Inorg Chem. 1972;11(1):129.
63. T. K. Aldridge, Stacy E. M., McMillin D. R. Inorg Chem. 1994;33(4):722.
64. F. Barigelletti, Sandrini D., Maestri M., Balzani V., Von Zelewsky A., Chassot L., et al. Inorg Chem. 1988;27(20):3644.
65. J. A. Bailey, Hill M. G., Marsh R. E., Miskowski V. M., Schaefer W. P., Gray H. B. Inorg Chem. 1995;34(18):4591.
66. E. C. Constable, Henney R. P. G., Leese T. A., Tocher D. A. J Chem Soc, Dalton Trans. 1990(2):443.
67. E. C. Constable, Henney R. P. G., Leese T. A., Tocher D. A. J Chem Soc, Chem Commun. 1990(6):513.
68. D. J. Cardenas, Echavarren A. M., Ramirez de Arellano M. C. Organometallics. 1999;18(17):3337-41.
69. C. Cornioley-Deuschel, Ward T., Von Zelewsky A. Helv Chim Acta. 1988;71(1):130.
70. A. M. Ranieri, Burt L. K., Stagni S., Zacchini S., Skelton B. W., Ogden M. I., et al. Organometallics. 2019;38(5):1108-17.
71. K. Li, Tong G. S. M., Wan Q., Cheng G., Tong W.-Y., Ang W.-H., et al. Chem Sci. 2016;7(3):1653-73.
72. R. Kumar, Linden A., Nevado C. Angew Chem, Int Ed. 2015;54(48):14287-90.

73. V. W.-W. Yam, Wong K. M.-C., Hung L.-L., Zhu N. Angew Chem, Int Ed. 2005;44(20):3107-10.
74. R. Guan, Xie L., Rees T. W., Ji L., Chao H. J Inorg Biochem. 2020;204:110985.
75. S. Daemen, van Zandvoort M. A. M. J., Parekh S. H., Hesselink M. K. C. Mol Metab. 2016;5(3):153-63.
76. V. Fiorini, Ranieri A. M., Muzzioli S., Magee K. D. M., Zacchini S., Akabar N., et al. Dalton Trans. 2015;44(47):20597-608.
77. B. Umamahesh, Karthikeyan N. S., Sathiyanarayanan K. I., Malicka J. M., Cocchi M. J Mater Chem C. 2016;4(42):10053-60.
78. P. Brulatti, Fattori V., Muzzioli S., Stagni S., Mazzeo P. P., Braga D., et al. J Mater Chem C. 2013;1(9):1823-31.
79. J. Pesch, Harms K., Bach T. Eur J Org Chem. 2004(9):2025-35.
80. C. Caporale, Ranieri A. M., Paternoster S., Bader C. A., Falasca M., Plush S. E., et al. Inorganics. 2020;8(4):23.
81. F. Himo, Demko Z. P., Noodleman L., Sharpless K. B. J Am Chem Soc. 2002;124(41):12210-6.
82. N. C. Kasuga, Sugie A., Nomiya K. Dalton Transactions. 2004(21):3732-40.
83. S.-i. Kondo, Watanabe N., Takahashi F., Takeda N., Unno M. J Inclusion Phenom Macrocyclic Chem. 2013;75(1-2):31-8.
84. R. Paradis, Page M. Anticancer Res. 1998;18(4A):2711-6.
85. R. Visbal, Gimeno M. C. Chem Soc Rev. 2014;43(10):3551-74.
86. S. Fuertes, Chueca A. J., Peralvarez M., Borja P., Torrell M., Carreras J., et al. ACS Appl Mater Interfaces. 2016;8(25):16160-9.
87. S. Rubino, Busa R., Attanzio A., Alduina R., Di Stefano V., Girasolo M. A., et al. Bioorg Med Chem. 2017;25(8):2378-86.
88. M. A. Fuertes, Castilla J., Alonso C., Perez J. M. Curr Med Chem: Anti-Cancer Agents. 2002;2(4):539-51.
89. F. M. Muggia, Bonetti A., Hoeschele J. D., Rozencweig M., Howell S. B. J Clin Oncol. 2015;33(35):4219-26.
90. M. K. Biyala, Sharma K., Swami M., Fahmi N., Singh R. V. Transition Met Chem (Dordrecht, Neth). 2008;33(3):377-81.
91. D. Kovala-Demertzi, Yadav P. N., Demertzis M. A., Coluccia M. J Inorg Biochem. 2000;78(4):347-54.
92. R. del Campo, Criado J. J., Garcia E., Hermosa M. R., Jimenez-Sanchez A., Manzano J. L., et al. J Inorg Biochem. 2002;89(1-2):74-82.
93. M. V. Baker, Bosnich M. J., Brown D. H., Byrne L. T., Hesler V. J., Skelton B. W., et al. J Org Chem. 2004;69(22):7640-52.
94. M. V. Baker, Brown D. H., Haque R. A., Skelton B. W., White A. H. Dalton Trans. 2004(21):3756-64.
95. M. V. Baker, Skelton B. W., White A. H., Williams C. C. J Chem Soc, Dalton Trans. 2001(2):111-20.
96. O. S. Koutsoni, Karampetsou K., Dotsika E. Bio-Protoc. 2019;9(21):e3410.
97. A. King, Chakrabarty S., Zhang W., Zeng X., Ohman D. E., Wood L. F., et al. Biomacromolecules. 2014;15(2):456-67.
98. O. Zaragoza, Rodrigues M. L., De Jesus M., Frases S., Dadachova E., Casadevall A. Chapter 4 The Capsule of the Fungal Pathogen Cryptococcus neoformans. Advances in Applied Microbiology. 68: Academic Press; 2009. p. 133-216.
99. K. L. Buchanan, Murphy J. W. Emerging Infect Dis. 1998;4(1):71-83.
100. I. Bose, Reese A. J., Ory J. J., Janbon G., Doering T. L. Eukaryotic Cell. 2003;2(4):655-63.
101. J. R. Perfect, Dismukes W. E., Dromer F., Goldman D. L., Graybill J. R., Hamill R. J., et al. Clin Infect Dis. 2010;50(3):291-322.
102. M. E. Klepser, Wolfe E. J., Pfaller M. A. J Antimicrob Chemother. 1998;41(3):397-401.

103. N. R. Stone, Rhodes J., Fisher M. C., Mfinanga S., Kivuyo S., Rugemalila J., et al. J Clin Invest. 2019;129(3):999-1014.
104. A. Loyse, Dromer F., Day J., Lortholary O., Harrison T. S. J Antimicrob Chemother. 2013;68(11):2435-44.
105. M. H. Nguyen, Barchiesi F., McGough D. A., Yu V. L., Rinaldi M. G. Antimicrob Agents Chemother. 1995;39(8):1691.
106. S. P. Franzot, Casadevall A. Antimicrob Agents Chemother. 1997;41(2):331-6.
107. H. Zafar, Altamirano S., Ballou E. R., Nielsen K. Curr Opin Microbiol. 2019;52:158-64.
108. G. W. V. Cave, Fanizzi F. P., Deeth R. J., Errington W., Rourke J. P. Organometallics. 2000;19(7):1355-64.
109. S. C. F. Kui, Hung F.-F., Lai S.-L., Yuen M.-Y., Kwok C.-C., Low K.-H., et al. Chem - Eur J. 2012;18(1):96.
110. N. Miyaura, Suzuki A. Chemical Reviews. 1995;95(7):2457-83.
111. A. Suzuki. Pure Appl Chem. 1991;63(3):419.
112. A. Suzuki. J Organomet Chem. 1999;576(1-2):147-68.
113. K. Matos, Soderquist J. A. J Org Chem. 1998;63(3):461-70.
114. C. Amatore, Jutand A., Le Duc G. Chem - Eur J. 2011;17(8):2492-503.
115. N. Miyaura, Yanagi T., Suzuki A. Synth Commun. 1981;11(7):513.
116. J. K. Stille, Lau K. S. Y. Acc Chem Res. 1977;10(12):434.
117. A. J. J. Lennox, Lloyd-Jones G. C. Chem Soc Rev. 2014;43(1):412-43.
118. C. Amatore, Jutand A., Le Duc G. Chem - Eur J. 2012;18(21):6616.
119. P. G. Bomben, Koivisto B. D., Berlinguette C. P. Inorg Chem. 2010;49(11):4960-71.
120. G. W. V. Cave, Alcock N. W., Rourke J. P. Organometallics. 1999;18(9):1801-3.
121. V. M. Miskowski, Houlding V. H., Che C. M., Wang Y. Inorg Chem. 1993;32(11):2518.
122. D. Milstein, Stille J. K. J Am Chem Soc. 1978;100(11):3636.
123. W. Caseri. J Organomet Chem. 2014;751:20-4.
124. C. Cordovilla, Bartolome C., Martinez-Ilarduya J. M., Espinet P. ACS Catal. 2015;5(5):3040-53.
125. T. N. Mitchell. J Organomet Chem. 1986;304(1-2):1-16.
126. Q. Luo, Zha J., Lei B., Xu Y., Wang Z. Huanjing Kexue Xuebao. 2009;29(11):2241-9.
127. S. Gomez-Ruiz, Kaluderovic G. N., Prashar S., Hey-Hawkins E., Eric A., Zizak Z., et al. J Inorg Biochem. 2008;102(12):2087-96.
128. F. Wang, Shen J., Cheng G., Cui X. RSC Adv. 2015;5(89):73180-3.
129. G. L. Petretto, Wang M., Zucca A., Rourke J. P. Dalton Trans. 2010;39(33):7822-5.
130. D. F. Eaton. Pure Appl Chem. 1988;60(7):1107.
131. K. Suzuki, Kobayashi A., Kaneko S., Takehira K., Yoshihara T., Ishida H., et al. Phys Chem Chem Phys. 2009;11(42):9850-60.

Appendix A – Experimental Methods

General Methods

Pd(o-cyc)Br_2, 1,5-cyclooctadiene platinum dichloride, and 1,2-bis(imidazole-1-ylmethyl)benzene had been previously synthesised in house and were used as acquired without further purification. All reagents were purchased from Sigma Aldrich or Alfa Aesar, and used without further purification. Column chromatography used either neutral alumina (Brockmann Grade I or Brockmann Grade II) or silica. Nuclear magnetic resonance spectra were recorded using a Bruker Avance 400 spectrometer (400.1 MHz for ^{1}H and 100.6 MHz for ^{13}C) at room temperature, and consisted of ^{1}H, ^{13}C, DEPTQ, COSY, HSQC, and HMBC measurements. Chemical shifts were calibrated to residual solvent signals ($CDCl_3$: 7.26 ppm, DMSO-d_6: 2.50 ppm, Acetone-d_6: 2.05 ppm, D_2O: 4.79 ppm for ^{1}H spectra), ($CDCl_3$: 77.2 ppm, DMSO-d_6: 39.5 ppm, Acetone-d_6: 29.8 ppm, for ^{13}C spectra). Infrared spectra were recorded using an attenuated total reflectance Perkin-Elmer Spectrum 100 FT-IR and were recorded in the solid state by mounting the sample on a diamond stage. Infrared spectra were collected with a range of 450 cm^{-1} to 4000 cm^{-1}, and the intensities of the bands are reported as strong (s), medium (m), weak (w), or broad (br).

X-Ray Crystallography

A clear light yellow plate-shaped crystal with dimensions 0.22 × 0.16 × 0.07 mm^3 was mounted. Data were collected using a Xcalibur, Ruby, Gemini ultra diffractometer operating at T = 94.3(2) K.

Data were measured using w scans using Mo Ka radiation. The diffraction pattern was indexed and the total number of runs and images was based on the strategy calculation from the program CrysAlisPro (Rigaku, V1.171.40.53, 2019). The maximum resolution that was achieved was Q = 32.736° (0.66 Å).

The diffraction pattern was indexed and the total number of runs and images was based on the strategy calculation from the program CrysAlisPro (Rigaku, V1.171.40.53, 2019). The unit cell was refined using CrysAlisPro (Rigaku, V1.171.40.53, 2019) on 21078 reflections, 49% of the observed reflections.

Data reduction, scaling and absorption corrections were performed using CrysAlisPro (Rigaku, V1.171.40.53, 2019). The final completeness is 99.70 % out to 32.736° in Q. A spherical absorption correction using equivalent radius and absorption coefficient using spherical harmonics, as implemented in SCALE3 ABSPACK scaling algorithm was used. The absorption coefficient μ of this material is 8.381 mm^{-1} at this wavelength (λ = 0.71073Å) and the minimum and maximum transmissions are 0.434 and 0.448.

The structure was solved and the space group Pbcm (# 57) determined by the ShelXT 2018/2 (Sheldrick, 2018) structure solution program and refined by full matrix least squares minimisation on F^2 using version 2018/3 of ShelXL 2018/3 (Sheldrick, 2015). All non-hydrogen atoms were refined anisotropically. Hydrogen atom positions were calculated geometrically and refined using the riding model.

Photophysical Analysis

Absorption spectra were collected using a Perkin Elmer Lambda 35 UV/Vis spectrometer operated at room temperature. Uncorrected steady state emission and excitation spectra were collected using an Edinburgh FLSP980-stm spectrometer equipped with a 450 W xenon arc lamp, double excitation and emission monochromators and a Peltier cooled Hamamatsu R928P photomultiplier (185–850 nm). Collected spectra were corrected for the intensity of the source (lamp and grating) and emission spectral response (detector and grating) by a calibration curve supplied with the spectrometer.

Absorption, emission, and excitation spectra of Pt[Ph(ThMe2)]L1-5 were measured in saturated solutions of DCM and DMSO, and in the solid state. Emission spectra were collected under excitation at 375 nm. Emission spectra were collected measuring emission at 500 nm. The excited-state decay (τ) was determined with the single photon counting technique (TCSPC) using pulsed picosecond LEDs (EPLED 375,FHWM<800ps) as the excitation source, with repetitions rates between 10kHz and 1 MHz, on the same Edinburgh FLSP980-stm spectrometer. Quantum yields were determined by comparison to a reference solution of $[Ru(bpy)_3]Cl_2$ at a concentration of 5 x 10^{-6} M, according to the equation:[130, 131]

$$\Phi = \Phi_R \times (I/I_R) \times (A_R/A) \times (n/n_R)$$

Where I is the integral of the emission spectrum, A is the absorbance at the excitation wavelength, *n* refractive index of the solvent, and a subscript R represents the value has been measured from the $[Ru(bpy)_3]Cl_2$ standard.

Absorption, emission, and excitation spectra of Pt(Hbppy)(DMSO)Cl were measured in 10^{-5} M solutions in DCM. The emission spectrum was collected under excitation at 310 nm. The excitation spectrum was collected measuring emission at 502 nm. The excited-state decay (τ) was determined with the single photon counting technique (TCSPC) using pulsed picosecond LEDs (EPLED 375,FHWM<800ps) as the excitation source, with repetitions rates between 10kHz and 1 MHz, on the same Edinburgh FLSP980-stm spectrometer.

Absorption spectra of the unknown blue compound were measured in 5 x 10^{-2} gL^{-1} solutions in DCM, chloroform, DMSO, and DMF.

HRMS Analysis

A Thermo Scientific Q-Exactive Orbitrap mass spectrometer (Thermo Fisher Scientific Corporation, Waltham, USA) was employed for high accuracy mass determination of the compounds. Stock solutions were prepared by dissolving 1 mg of compound into 1mL of MeOH or DCM. Solutions were diluted down to 10 ng/uL in MeOH containing 0.1% formic acid and infused at 3 µL/min into the mass spectrometer using a built-in syringe pump. Full calibration of the LTQ Orbitrap XL in the 70-3000 m/z range was conducted prior to each measurement with the positive and negative ion calibration solutions provided by Thermo Scientific (Australia). Optical lenses were optimised with the positive calibration solution prior each batch of samples. For increased mass accuracy on the Q-Exactive Orbitrap mass spectrometer, a plasticizer interfering peak present in the background (n-butyl benzenesulfonamide, $C_6H_5SO_2NH(CH_2)_3CH_3$, $[M+H]^+$=214.0896 m/z), was used for the lock mass function. The screening analysis was conducted operating the Q-Exactive Orbitrap mass spectrometer in full-scan mode from 70-1000 m/z with a mass resolution of 70.000 (@ 200 m/z). When necessary, samples were also analysed operating the Q-Exactive Orbitrap mass spectrometer in HRMS2 mode, where the mass spectrometer was forced to isolate the parent compound in the first quadrupole, fragment it in the HCD cell and then scan for the product ions in the Orbitrap mass analyser. A mass resolution of 17.500 (@ 200 m/z) was used for the fragmentation experiments. For substance identification the deviation of the measured mass

(i.e. parent compound and fragments) was compared against the theoretical mass (< 2ppm, relative error). To confirm elemental composition, the measured isotope pattern was also compared with that obtained from isotopic simulation. Data was processed using the Xcalibur QualBrowser software.

Biological Testing

Compounds were plated as a 2-fold dose response from 32 to 0.25 μg/mL (or 20 to 0.156 μM), with a maximum of 0.5% DMSO, final in assay concentration. Growth inhibition of all bacteria was determined measuring absorbance at 600 nm (OD600), using a Tecan M1000 Pro monochromator plate reader. The percentage of growth inhibition was calculated for each well, using the negative control (media only) and positive control (bacteria without inhibitors) on the same plate as references. Growth inhibition of C. albicans was determined measuring absorbance at 530 nm (OD530), while the growth inhibition of C. neoformans was determined measuring the difference in absorbance between 600 and 570 nm (OD600-570), after the addition of resazurin (0.001% final concentration) and incubation at 35 °C for additional 2 h. The absorbance was measured using a Biotek Synergy HTX plate reader. The percentage of growth inhibition was calculated for each well, using the negative control (media only) and positive control (bacteria without inhibitors) on the same plate as references.

Growth inhibition of HEK293 cells was determined measuring fluorescence at ex:530/10 nm and em:590/10 nm (F560/590), after the addition of resazurin (25 ug/mL final concentration) and incubation at 37 °C and 5% CO2, for additional 3 h. The fluorescence was measured using a Tecan M1000 Pro monochromator plate reader. The percentage of growth inhibition was calculated for each well, using the Negative Control (media only) and Positive Control (cell culture without inhibitors) on the same plate as references. Percentage growth inhibition of individual samples and concentration are calculated based on Negative Controls (media only; 100%) and Positive Controls (bacterial/cell media without inhibitors: 0%).

The minimum inhibitory concentration (MIC) was determined following the CLSI guidelines, identifying the lowest concentration at which full inhibition of the bacteria or fungi has been detected. Full inhibition of growth has been defined at <= 20% growth (or >80% inhibition), and concentrations have only been selected if the next highest concentration displayed full

inhibition (i.e. 80-100%) as well (eliminating 'singlet' active concentration). Please note MIC values are discrete values based on the concentration in a specific well.

CC_{50} (Concentration at 50% Cytotoxicity) were calculated by curve fitting the inhibition values vs. log(concentration) using Sigmoidal dose-response function, with variable values for bottom, top and slope. The curve fitting is implemented using Pipeline Pilot's dose-response component (giving similar results to similar tools such as GraphPad's Prism and IDBS's XlFit).

HC_{10} (Concentration at 10% Haemolytic activity) were calculated by curve fitting the inhibition values vs. log(concentration) using Sigmoidal dose-response function, with variable values for bottom, top and slope. The curve fitting is implemented using Pipeline Pilot's dose-response component (giving similar results to similar tools such as GraphPad's Prism and IDBS's XlFit). The curve fitting resulted in HC_{50} (50%) values, which are converted into HC_{10} by $HC_{10}=HC_{50}*(10/90)^{(1/Slope)}$.

All screening is performed as two replica (n=2), with both replicas on different assay plates, but from single plating and performed in a single screening experiment (microbial incubation). Each individual value is reported in the table (see ..1 and ..2). In addition, two values are used as quality controls for individual plates:

Z'-Factor=[1 -(3*(sd(NegCtrl)+sd(PosCtrl))/(average(PosCtrl)-average(NegCtrl)))]

and Standard Antibiotic controls at different concentrations (>MIC and < MIC). The plate passes the quality control if Z'-Factor >0.4 and Standards are active and inactive at highest and lowest concentrations, respectively.

Synthesis of Compounds

Synthesis of H_2bppy

Bis(triphenylphosphine)palladium chloride (14 mg, 0.02 mmol) was added to a sparged mixture of THF (20 mL) and water (20 mL) containing *B*-[1,1'-biphenyl]-3-yl-boronic acid (994 mg, 5.02 mmol), 2-bromopyridine (490 μL, 812 mg, 5.14 mmol), and potassium carbonate (2.74 g, 19.8 mmol). The mixture was heated at 65 °C for 14 hours under an inert atmosphere then allowed to cool. The product was extracted with DCM, washed with brine, then dried with magnesium sulfate. The organic phase was filtered and the solvent removed under reduced pressure to yield a yellow solid that was purified by column chromatography (silica, ethyl acetate : petroleum spirits 1:4) affording 771 mg (66.4 %) of the product as a yellow oil.

^{1}H NMR (400.1 MHz, $CDCl_3$) δ 8.75 (ddd, ^1J = 1.0 Hz ^2J = 1.7 Hz ^3J = 4.8 Hz, 1H) 8.28 (t, J = 1.8 Hz, 1H) 7.99 (ddd, ^1J = 1.2 Hz ^2J = 1.8 Hz ^3J = 7.7 Hz, 1H) 7.73-7.81 (m, 2H) 7.65-7.73 (m, 3H) 7.56 (dt, ^1J = 0.4 Hz ^2J = 7.8 Hz, 1H) 7.45-7.50 (m, 2H) 7.39 (tt, ^1J = 1.3 Hz ^2J = 6.7 Hz, 1H) 7.24-7.27 (m, 1H).

Synthesis of $(Pt(Hbppy)Cl)_2$.b

2-(biphenyl-3-yl) pyridine (298 mg, 1.29 mmol) and potassium tetrachloroplatinate (544 mg, 1.31 mmol) were added to glacial acetic acid (20 mL). The mixture was heated at reflux for 3 days then allowed to cool. The mixture was then added to water (40 mL) and the yellow precipitate collected by vacuum filtration and washed with water and diethyl ether, affording a yellow solid (851 mg, 71.0%).

^{1}H NMR (400.1 MHz, DMSO-d_6) δ 9.71 (dd, ^1J = 0.8 Hz ^2J = 5.9 Hz, 1H), 9.23 (dd, ^1J = 0.8 Hz ^2J = 5.9 Hz, 1H), 8.86 (t, J = 1.8 Hz, 1H), 8.09 (dt, ^1J = 1.6 Hz ^2J = 7.7 Hz, 1H), 7.79-7.87 (m, 4H), 7.67 (d, J = 2.1 Hz, 1H), 7.61-7.63 (m, 2H), 7.49-7.57 (m, 4H), 7.30-7.35 (m, 3H), 7.22-7.26 (m, 3H), 7.18-7.20 (m, 2H), 7.13 (dd, ^1J = 2.0 Hz ^2J = 8.0 Hz, 1H), 6.30 (d, J = 8.0 Hz, 1H)

^{13}C NMR (100.6 MHz, DMSO-d_6) δ 185.2, 160.5, 154.2, 150.1, 144.7, 140.2, 139.7, 139.4, 139.0, 138.8, 135.0, 130.9, 128.8, 128.7, 126.6, 126.1, 119.6

IR ν_{max}/cm^{-1} 3061 w, 1598 m, 1482 m, 756 s, 699 m

Synthesis of $(Pt(Hbppy)Cl)_2$.c

H_2bppy (315 mg, 1.36 mmol) and potassium tetrachloroplatinate (572 mg, 1.38 mmol) were added to glacial acetic acid (20 mL). The mixture was heated at reflux for 14 hours then allowed to cool. The mixture was then added to water (40 mL) and the yellow precipitate collected by vacuum filtration and washed with water and diethyl ether, affording a yellow solid (923 mg, 73.6%).

^{1}H NMR (400.1 MHz, DMSO-d_6) δ 9.52 (dd, ^1J = 1.5 Hz, ^2J = 6.0 2H), 8.50 (d, J = 8.0 Hz, 2H), 8.31 (d, J = 8.2 Hz, 2H), 8.17 (dt, ^1J = 1.6 Hz, ^2J = 7.8 Hz, 2H), 8.09 (d, J = 2.3 Hz, 2H), 7.78 (d, J = 7.7 Hz, 4H), 7.55 (m, 2H), 7.47 (t, J = 7.0 Hz, 6H), 7.37 (t, J = 7.4 Hz, 2H)

^{13}C NMR (100 MHz, DMSO-d_6) δ 164.9, 149.3, 145.2, 141.6, 139.7, 139.6, 136.8, 134.1, 128.8, 128.1, 127.2, 126.4, 123.0, 122.3, 120.0

IR ν_{max}/cm^{-1} 3064 w, 1595 m, 1484 m, 754 s, 693 m

Synthesis of Pt(Hbppy)(DMSO)Cl

$(Pt(Hbppy)Cl)_2$.c (210 mg, 0.228 mmol) was added to DMSO (2 mL). The mixture was heated at 150 °C for 5 minutes before being allowed to cool to room temperature and added to water (20 mL). The precipitate was collected by vacuum filtration and washed with water and diethyl ether, affording a yellow solid (114mg, 46.4 %).

^{1}H NMR (400.1 MHz, $CDCl_3$) δ 9.52 (dd, ^1J = 1.6 Hz, ^2J = 5.9 Hz 1H), 8.40 (d, J = 8.0 Hz, 1H), 8.31 (d, J = 8.2 Hz, 1H), 8.17 (dt, ^1J = 1.6 Hz, ^2J = 7.6 Hz, 1H), 8.09 (d, J = 2.2 Hz, 1H), 7.78 (d, J = 7.3 Hz, 2H), 7.54 (m, 1H), 7.47 (t, J = 7.0 Hz, 3H), 7.37 (tt, ^1J = 1.3 Hz, ^2J = 7.2 Hz, 1H), 2.54 (s, 6H)

^{13}C NMR (100 MHz, $CDCl_3$) δ 165.9, 150.2, 144.9, 140.9, 140.4, 139.3, 134.5, 129.5, 128.9, 127.2, 126.8, 122.4, 122.0, 118.7, 47.2

IR ν_{max}/cm^{-1} 3003 w, 2914 w, 1597 s, 1487 m, 1112 s, 759 s, 696 m

Synthesis of Unidentified Blue Compound

$(Pt(Hbppy)Cl)_2$.b (153 mg, 0.166 mmol) was added to DMSO (2 mL). The mixture was heated at 150 °C for 5 minutes then immediately added to an aqueous solution of potassium carbonate (5 mL, 1 M). The mixture was then allowed to cool and stirred at room temperature for 14 hours. The precipitate was collected by vacuum filtration and washed with water and diethyl ether, affording a blue solid (73 mg). No product was isolated.

Attempted Synthesis of Pt(bppy)DMSO

2-(biphenyl-3-yl) pyridine (152 mg, 0.657 mmol) and potassium tetrachloroplatinate (274 mg, 0.660 mmol) were added to a mixture of water (3 mL) and acetonitrile (9 mL). The mixture was stirred at room temperature for 5 minutes, then heated to 170 °C for 70 minutes in a microwave. The reaction mixture was added to extracted with DCM, washed with brine, then dried under magnesium sulfate. The organic phase was filtered and the solvent removed under reduced pressure to afford a yellow solid (86 mg). No product was isolated.

Synthesis of $PhBrPh_2$

A sparged mixture of water (120 mL) and methanol (60 mL) containing potassium carbonate (10.5 g, 76.0 mmol) and phenylboronic acid (3.181 g, 26.1 mmol) was added dropwise over 6 hours to sparged THF (120 mL) containing 1,3,5-tribromobenzene (4.103 g, 13.0 mmol) and bis(triphenylphosphine)palladium chloride (48 mg, 0.07 mmol) at 65 °C. The mixture was then heated at 65 °C for 14 hours before being allowed to cool. The solvents were removed under reduced pressure, and the resulting brown solid was dissolved in DCM and washed with brine. The organic phase was dried with magnesium sulfate, filtered, and evaporated under reduced pressure to yield a brown solid which was purified by column chromatography (silica, petroleum spirits) affording 615 mg (15.3%) of the product as a white solid.

^{1}H NMR (400.1 MHz, $CDCl_3$) δ 7.71 (s, 3H), 7.60-7.62 (m, 4H), 7.44-7.49 (m, 4H), 7.39 (tt, ^1J = 1.4 Hz, ^2J = 6.5 Hz, 2H)

Synthesis of H_2tppy

Bis(triphenylphosphine)palladium chloride (48 mg, 0.07 mmol) was added to sparged toluene (50 mL) containing $PhBrPh_2$ (780 mg, 2.52 mmol), 2-(tributylstannyl)pyridine (1025 μL, 1165 mg, 85%, 2.53 mmol), and lithium chloride (298 mg, 7.03 mmol). The mixture was heated at 110 °C for 14 hours, washed with aqueous potassium fluoride (1 M) and brine, dried under magnesium sulfate, and filtered. The solvent was removed under reduced pressure to yield a brown solid that was purified by column chromatography (silica, ethyl acetate : petroleum spirits 1:19) to afford 635 mg (81.5%) of the product as a white solid.

^{1}H NMR (400.1 MHz, $CDCl_3$) δ 8.76 (ddd, ^1J = 1.0 Hz ^2J = 1.9 Hz ^3J = 4.9 Hz, 1H), 8.21 (d, J = 3.2 Hz, 2H), 7.85-7.88 (m, 2H), 7.77 (apparent t, 1H), 7.73 (apparent dt, 1H), 7.62-7.69 (m, 5H), 7.36-7.40 (m, 4H), 7.29 (tt, ^1J = 1.3 Hz ^2J = 6.6 Hz, 2H), 7.16 (ddd, ^1J = 1.3 Hz, ^2J = 4.9 Hz, ^3J = 12.3 Hz, 1H)

Attempted Synthesis of $(Pt(Htppy)Cl)_2$

H_2tppy (431 mg, 1.40 mmol) and potassium tetrachloroplatinate (585 mg, 1.41 mmol) were added to glacial acetic acid (20 mL), The mixture was heated at reflux for 14 hours then allowed to cool. The mixture was then added to water (40 mL) and the yellow precipitate collected by vacuum filtration and washed with water and diethyl ether, affording a yellow solid (856 mg, 57.0 %). No product was isolated.

Attempted Synthesis of [(terphpy)Pt(DMSO)]

The yellow solid collected from the previous procedure (252 mg, 0.235 mmol) was added to DMSO (4 mL). The mixture was heated at 150 °C for 5 minutes before being allowed to cool to room temperature and added to water (40 mL). The precipitate was collected by vacuum filtration and washed with water and diethyl ether, affording a yellow solid (62 mg, 22.9 %). No product was isolated.

Synthesis of Ph(ThMe$_2$S)

Aniline (4.90 mL, 5.00 g, 53.7 mmol) and NaOH (2.18 g, 53.9 mmol) were added to DMSO (20 mL) and stirred at room temperature for 15 minutes. The reaction mixture was then cooled to 0 °C and carbon disulfide (3.25 mL, 4.09 g, 53.7 mmol) added. The reaction mixture was then stirred at room temperature for 1 hour before being cooled to 0 °C. 3-chloro-2-butanone (5.45 mL, 5.75 g, 54.00 mmol) added dropwise. The reaction mixture was then stirred at room temperature for 1 hour before being diluted with deionised water (200 mL) and stirred at room temperature for a further 1 hour. The aqueous phase was then decanted and the remaining yellow solid dissolved in a solution of hydrochloric acid (32%, 2 mL) ethanol (125 mL) and refluxed for 1 hour. The reaction mixture was allowed to cool and the solvent volume reduced to 50 mL in vacuo. The reaction mixture was then cooled to 4 °C for 16 hours, during which the product precipitated as a light brown powder. The product was collected by vacuum filtration, washed with cold ethanol (20 mL) and diethyl ether (20 mL) and dried under vacuum. (3.65 g, 30.8%)

^{1}H NMR (400.1 MHz, DMSO-d$_6$) δ 7.55-7.59 (m, 2H), 7.49-7.53 (m, 1H), 7.29-7.32 (m, 2H), 2.19 (d, *J* = 1.0 Hz, 3H), 1.81 (d, *J* = 1.0 Hz, 3H)

IR ν_{max}/cm^{-1} 2916 w, 1620 w, 1591 w, 1490 m, 1334 m, 1300 s, 1238 s, 1047 m

Synthesis of Ph(ThMe$_2$H).PF$_6$

Ph(ThMe$_2$S) (2.97 g, 13.4 mmol) was added to glacial acetic acid (30 mL). Hydrogen peroxide (30%, 4.20 mL, 41.2 mmol) was added dropwise and the reaction mixture stirred at room temperature for 30 minutes. The solvent was removed under reduced pressure and the resulting oil dissolved in deionised water (30 mL) and ethanol (60 mL). Potassium hexafluorophosphate (4.99 g, 27.2 mmol) was added and the reaction mixture stirred at room temperature for 16 hours. The reaction mixture was filtered, and the filtrate extracted with DCM (2 x 100 mL). The organic phase was dried under magnesium sulfate then evaporated under reduced pressure. The resulting oil was dissolved in DCM (10 mL) and precipitated by the slow addition of diethyl ether at 0 °C. The precipitate was collected by vacuum filtration, washed with minimal diethyl ether, and dried under vacuum to yield the product as a light brown solid (1.63 g, 36.3 %).

^{1}H NMR (400.1 MHz, DMSO-d_6) δ 10.26 (s, 1H), 7.69-7.74 (m, 5H), 2.59 (d, *J* = 0.9 Hz, 3H), 2.21 (d, *J* = 0.9 Hz, 3H)

^{19}F NMR (376.5 MHz, DMSO-d_6) δ 70.16 (d, *J* = 711 Hz)

IR ν_{max}/cm^{-1} 3124 m, 1594 w, 1493 w, 1440 w, 826 s

Synthesis of HL1

Triethylamine (1.34 mL, 970 mg, 9.60 mmol) was added to toluene (50 mL) and stirred at 0 °C for 15 minutes. Hydrochloric acid (32 %, 945 μL, 9.60 mmol) was added and the reaction stirred at 0 °C for 20 minutes. 2-cyanopyridine (1.05 g, 10.1 mmol) and sodium azide (703 mg, 11.1 mmol) were added and the reaction mixture stirred at reflux for 16 hours. The reaction mixture was cooled to room temperature and extracted with deionised water (3 x 25 mL). The combined aqueous phases were acidified to pH 2 using HCl (32 %) at 0 °C. The precipitate was collected via vacuum filtration, washed with minimal cold deionised water and diethyl ether and dried under vacuum to yield the product as pale brown needles (902 mg, 60.9 %).

^{1}H NMR (400.1 MHz, DMSO-d_6) δ 8.79-8.81 (ddd, ^{3}J = 0.9 Hz, ^{2}J = 1.8 Hz, ^{1}J = 4.7 Hz, 1H), 8.22-8.24 (apparent dt, 1H), 8.06-8.11 (apparent td, 1H), 7.62-7.65 (ddd, ^{3}J = 1.2 Hz, ^{2}J = 4.8 Hz, ^{1}J = 7.6 Hz, 1H)

^{13}C NMR (100.6 MHz, , DMSO-d_6) δ 154.8, 150.1, 143.7, 138.3, 126.1, 122.6

IR ν_{max}/cm^{-1} 2600 br

Synthesis of HL2

Triethylamine (380 μL, 276 mg, 2.73 mmol) was added to toluene (25 mL) and stirred at 0 °C for 15 minutes. Hydrochloric acid (32 %, 270 μL, 2.73 mmol) was added and the reaction stirred at 0 °C for 20 minutes. 5-bromo-2-cyanopyridine (504 g, 2.74 mmol) and sodium azide (362 mg, 5.57 mmol) were added and the reaction mixture stirred at reflux for 16 hours. The reaction mixture was cooled to room temperature and extracted with deionised water (3 x 25 mL). The combined aqueous phases were acidified to pH 2 using HCl (32 %) at 0 °C. The precipitate was collected via vacuum filtration, washed with minimal cold deionised water and diethyl ether and dried under vacuum to yield the product as a white solid (549 mg, 88.2 %).

^{1}H NMR (400.1 MHz, DMSO-d_6) δ 8.95 (s, 1H), 8.34 (d, J = 8.0 Hz, 1H), 8.16 (d, J = 8.4 Hz, 1H)

^{13}C NMR (100.6 MHz, , DMSO-d_6) δ 154.4, 151.0, 142.5, 140.9, 124.2, 122.6

IR ν_{max}/cm^{-1} 2734 br, 1555 m, 1471 s, 1356 m, 1098 m, 1024 s

Synthesis of HL3

Triethylamine (590 μL, 428 mg, 4.23 mmol) was added to toluene (25 mL) and stirred at 0 °C for 15 minutes. Hydrochloric acid (32 %, 420 μL, 4.23 mmol) was added and the reaction stirred at 0 °C for 20 minutes. 5-amino-2-cyanopyridine (498 g, 4.23 mmol) and sodium azide (549 mg, 8.26 mmol) were added and the reaction mixture stirred at reflux for 16 hours. The reaction mixture was cooled to room temperature and extracted with deionised water (3 x 25 mL). The combined aqueous phases were acidified to pH 5 using HCl (32 %) at 0 °C. The precipitate was collected via vacuum filtration, washed with minimal cold deionised water and diethyl ether and dried under vacuum to yield the product as pale brown needles (281 mg, 41.5 %).

^{1}H NMR (400.1 MHz, DMSO-d_6) δ 8.07 (dd, J^1 = 0.7 Hz, J^2 = 2.8 Hz, 1H), 7.86 (dd, J^1 = 0.7 Hz, J^2 = 8.6 Hz, 1H), 7.08 (dd, J^1 = 2.7 Hz, J^2 = 8.6 Hz, 1H), 6.06 (br s, 2H)

^{13}C NMR (100.6 MHz, , DMSO-d_6) δ 154.9, 147.1, 135.9, 130.4, 123.4, 119.8

IR ν_{max}/cm^{-1} 3332 s, 3160 s, 2498 br, 1611 m, 1569 m, 1461 m, 1412 m

Synthesis of H_2L4.Cl

A solution of sodium carbonate (339 mg, 2.44 mmol) in deionised water (2 mL) was added to HL3 (200 mg, 1.23 mmol) and stirred vigorously. 4-toluenesulfonyl chloride (235 mg, 1.27 mmol) was added and the reaction mixture stirred at 80 °C for 16 hours. The reaction mixture was allowed to cool and acidified with hydrochloric acid (32 %) until the evolution of gas stopped and a brown precipitate formed. The precipitate was collected by vacuum filtration, washed with minimal cold hydrochloric acid (3 M) and diethyl ether, and dried under vacuum to yield the product as a brown solid (165 mg, 42.4 %).

^{1}H NMR (400.1 MHz, DMSO-d_6) δ 10.98 (br s, 1H), 8.47 (d, *J* = 2.4 Hz, 1H), 8.11 (d, *J* = 8.6 Hz, 1H), 8.72-8.76 (m, 3H), 7.39 (d, *J* = 8.1 Hz, 2H), 2.34 (s, 3H)

^{13}C NMR (100.6 MHz, , DMSO-d_6) δ 144.0, 140.7, 136.5, 136.0, 130.0, 127.4, 126.8, 123.3, 21.0

IR ν_{max}/cm^{-1} 3185 m, 2514 br, 1447 s, 1160 s

Synthesis of Pt[Ph(ThMe$_2$)]L1

Dry dimethylformamide (30 mL) was added to Ph(ThMe$_2$H).PF_6 (202 mg, 0.602 mmol) and silver oxide (82 mg, 0.345 mmol) and stirred at room temperature for 2 hours under nitrogen with the exclusion of light. The reaction mixture was then stirred at 55 °C under the same conditions for 16 hours. The reaction mixture was allowed to cool and 1,5-cyclooctadiene platinum dichloride (224 mg, 0.596 mmol) added, then stirred at room temperature for 2 hours. The reaction mixture was then heated at 115 °C for 16 hours then allowed to cool. HL1 (358 mg, 2.42 mmol) and potassium carbonate (342 mg, 0.246 mmol) were added and the reaction mixture stirred at room temperature for 16 hours, then at 100 °C for 6 hours. The reaction mixture was then allowed to cool and the solvent removed under reduced pressure. The resulting brown solid was suspended in deionised water and collected via vacuum filtration, washed with diethyl ether, and dried under vacuum. The product was subjected to column chromatography (neutral Grade II alumina stationary phase, eluent gradient from DCM to 1% methanol in DCM). The fractions containing the product were combined and evaporated under reduced pressure, then washed with DCM to yield the product as a vibrant orange solid (5 mg, 1.6 %).

Synthesis of Pt[Ph(ThMe$_2$)]L2

Dry dimethylformamide (45 mL) was added to Ph(ThMe$_2$H).PF_6 (301 mg, 0.897 mmol) and silver oxide (119 mg, 0.500 mmol) and stirred at room temperature for 2 hours under nitrogen with the exclusion of light. The reaction mixture was then stirred at 55 °C under the same conditions for 16 hours. The reaction mixture was allowed to cool and 1,5-cyclooctadiene platinum dichloride (341 mg, 0.907 mmol) added, then stirred at room temperature for 2 hours. The reaction mixture was then heated at 115 °C for 16 hours then allowed to cool. HL2 (404

mg, 1.79 mmol) and potassium carbonate (253 mg, 1.87 mmol) were added and the reaction mixture stirred at room temperature for 16 hours, then at 100 °C for 6 hours. The reaction mixture was then allowed to cool and the solvent removed under reduced pressure. The resulting brown solid was suspended in deionised water and collected via vacuum filtration, washed with diethyl ether, and dried under vacuum. The product was subjected to column chromatography (neutral Grade II alumina stationary phase, eluent gradient from DCM to 10% methanol in DCM). The fractions containing the product were combined and evaporated under reduced pressure, then washed with DCM to yield the product as a deep purple solid (5 mg, 0.9 %).

Synthesis of Pt[Ph(ThMe$_2$)]L3

Dry dimethylformamide (45 mL) was added to Ph(ThMe$_2$H).PF$_6$ (307 mg, 0.915 mmol) and silver oxide (125 mg, 0.526 mmol) and stirred at room temperature for 2 hours under nitrogen with the exclusion of light. The reaction mixture was then stirred at 55 °C under the same conditions for 16 hours. The reaction mixture was allowed to cool and 1,5-cyclooctadiene platinum dichloride (340 mg, 0.905 mmol) added, then stirred at room temperature for 2 hours. The reaction mixture was then heated at 115 °C for 16 hours then allowed to cool. HL3 (587 mg, 3.62 mmol) and potassium carbonate (496 mg, 3.58 mmol) were added and the reaction mixture stirred at room temperature for 16 hours, then at 100 °C for 6 hours. The reaction mixture was then allowed to cool and the solvent removed under reduced pressure. The resulting brown solid was suspended in deionised water and collected via vacuum filtration, washed with diethyl ether, and dried under vacuum. The product was subjected to column chromatography (neutral Grade II alumina stationary phase, eluent gradient from DCM to 10% methanol in DCM). The fractions containing the product were combined and evaporated under reduced pressure, then washed with DCM to yield the product as a deep red solid (2 mg, 0.4 %).

Synthesis of Pt[Ph(ThMe$_2$)]L4

Dry dimethylformamide (45 mL) was added to Ph(ThMe$_2$H).PF$_6$ (303 mg, 0.903 mmol) and silver oxide (118 mg, 0.496 mmol) and stirred at room temperature for 2 hours under nitrogen with the exclusion of light. The reaction mixture was then stirred at 55 °C under the same

conditions for 16 hours. The reaction mixture was allowed to cool and 1,5-cyclooctadiene platinum dichloride (338 mg, 0.899 mmol) added, then stirred at room temperature for 2 hours. The reaction mixture was then heated at 115 °C for 16 hours then allowed to cool. $[H_2L4]Cl$ (620 mg, 1.96 mmol) and potassium carbonate (248 mg, 2.02 mmol) were added and the reaction mixture stirred at room temperature for 16 hours, then at 100 °C for 6 hours. The reaction mixture was then allowed to cool and the solvent removed under reduced pressure. The resulting brown solid was suspended in deionised water and collected via vacuum filtration, washed with diethyl ether, and dried under vacuum. The product was subjected to column chromatography (neutral Grade II alumina stationary phase, eluent gradient from DCM to 10% methanol in DCM). The fractions containing the product were combined and evaporated under reduced pressure, then washed with DCM to yield the product as a deep red solid (31 mg, 4.9 %).

Synthesis of Pt[Ph(ThMe$_2$)]L5

Dry dimethylformamide (45 mL) was added to $Ph(ThMe_2H).PF_6$ (303 mg, 0.903 mmol) and silver oxide (119 mg, 0.500 mmol) and stirred at room temperature for 2 hours under nitrogen with the exclusion of light. The reaction mixture was then stirred at 55 °C under the same conditions for 16 hours. The reaction mixture was allowed to cool and 1,5-cyclooctadiene platinum dichloride (314 mg, 0.835 mmol) added, then stirred at room temperature for 2 hours. The reaction mixture was then heated at 115 °C for 16 hours then allowed to cool. HL5 (556 mg, 1.74 mmol) and potassium carbonate (248 mg, 2.02 mmol) were added and the reaction mixture stirred at room temperature for 16 hours, then at 100 °C for 6 hours. The reaction mixture was then allowed to cool and the solvent removed under reduced pressure. The resulting brown solid was suspended in deionised water and collected via vacuum filtration, washed with diethyl ether, and dried under vacuum. The product was subjected to column chromatography (neutral Grade II alumina stationary phase, eluent gradient from DCM to 10% methanol in DCM). The fractions containing the product were combined and evaporated under reduced pressure, then washed with DCM to yield the product as a deep red solid (4 mg, 0.6 %).

Synthesis of [Pd(o-cyc)L1]PF_6

Pd(o-cyc)Br_2 (27 mg, 0.045 mmol) and HL1 (9 mg, 0.06 mmol) were added to dimethyl sulfoxide (2.5 mL) and heated to 100 °C. Triethylamine (50 μL, 6.4 mg, 0.063 mmol) was added and the reaction mixture slowly cooled to room temperature then stirred overnight. The volume of solvent was reduced to 0.5 mL by blowing with nitrogen. Saturated potassium hexafluorophosphate solution (5 mL) was added. The resulting precipitate was collected via vacuum filtration, washed with minimal cold water and diethyl ether, and dried under vacuum. The product was purified by recrystallisation from chloroform/acetone (4.8 mg, 14.6 %)

^{1}H NMR (400.1 MHz, acetone-d_6) δ 8.36-8.43 (m, 2H), 8.21 (apparent dt, 1H), 7.89-7.94 (m, 4H), 7.74 (s, 2H), 7.67-7.71 (m, 3H), 7.45-7.50 (m, 4H), 7.05 (d, *J* = 14.6 Hz, 2H), 6.90 (d, *J* = 14.6 Hz), 5.43 (d, *J* = 10.9 Hz, 2H), 5.39 (d, *J* = 10.9 Hz, 2H)

Synthesis of [H_2(o-cyc)]Br_2

Solutions of 1,2-bis(imidazole-1-ylmethyl)benzene (1.03 g, 4.34 mmol) in acetone (100 mL), and 1,2-bis(bromomethyl)benzene (1.13g, 4.29 mmol) in acetone (50 mL) were added dropwise to refluxing acetone (200 mL) over 6 hours. The reaction mixture was then stirred at reflux overnight before being allowed to cool to room temperature. The solvent volume was reduced to 100 mL under reduced pressure, and precipitate collected by vacuum filtration to yield the product as a white solid (1.84 g, 85.4 %)

^{1}H NMR (400.1 MHz, acetone-d_6) δ 7.73-7.80 (m, 8H), 7.05-7.35 (m, 4H), 5.29-5.56 (m, 8H)

Attempted Synthesis of [H_2(o-cyc)](OAc)$_2$

[H_2(o-cyc)]Br_2 (502 mg, 1.01 mmol) and silver acetate (168 mg, 1.01 mmol) were added to deionised water (125 mL) and stirred at room temperature for 6 hours. The reaction mixture was then filtered, and the filtrate evaporated under reduced pressure to yield a white solid (88 mg). No product was isolated.

Attempted Synthesis of $Pt(o\text{-}cyc)Cl_2$

$[H_2(o\text{-}cyc)]Br_2$ (204 mg, 0.409 mmol) and 1,5-cyclooctadiene platinum dichloride (151 mg, 0.403 mmol) were added to acetonitrile (15 mL) and heated at reflux for 4 days. The precipitate was collected by vacuum filtration and subjected to Soxhlet extraction for 3 days. No product was isolated.

Second Attempted Synthesis of $Pt(o\text{-}cyc)Cl_2$

$[H_2(o\text{-}cyc)](OAc)_2$ (88 mg, 0.129 mmol) and 1,5-cyclooctadiene platinum dichloride (48 mg, 0.129 mmol) were added to acetonitrile (12.5 mL) and heated at reflux for 4 days. The precipitate was collected by vacuum filtration and subjected to Soxhlet extraction for 3 days. No product was isolated.

Appendix B – NMR and IR Spectra

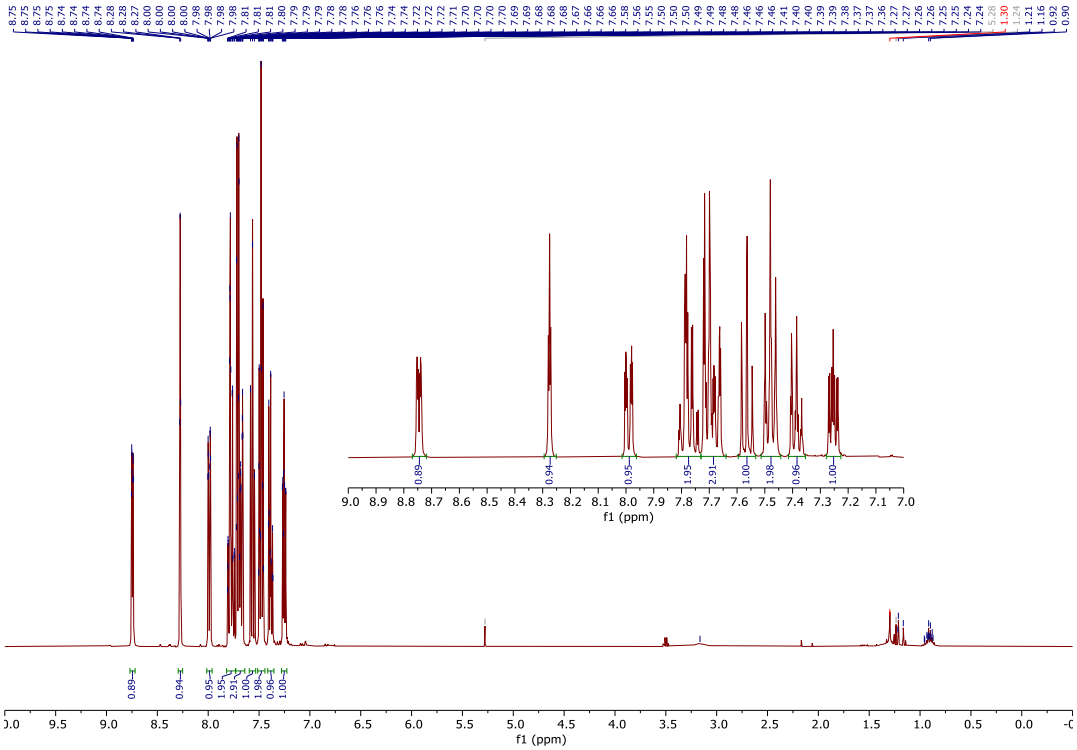

Figure 82: ^{1}H NMR spectrum ($CDCl_3$) of bppy in $CDCl_3$.

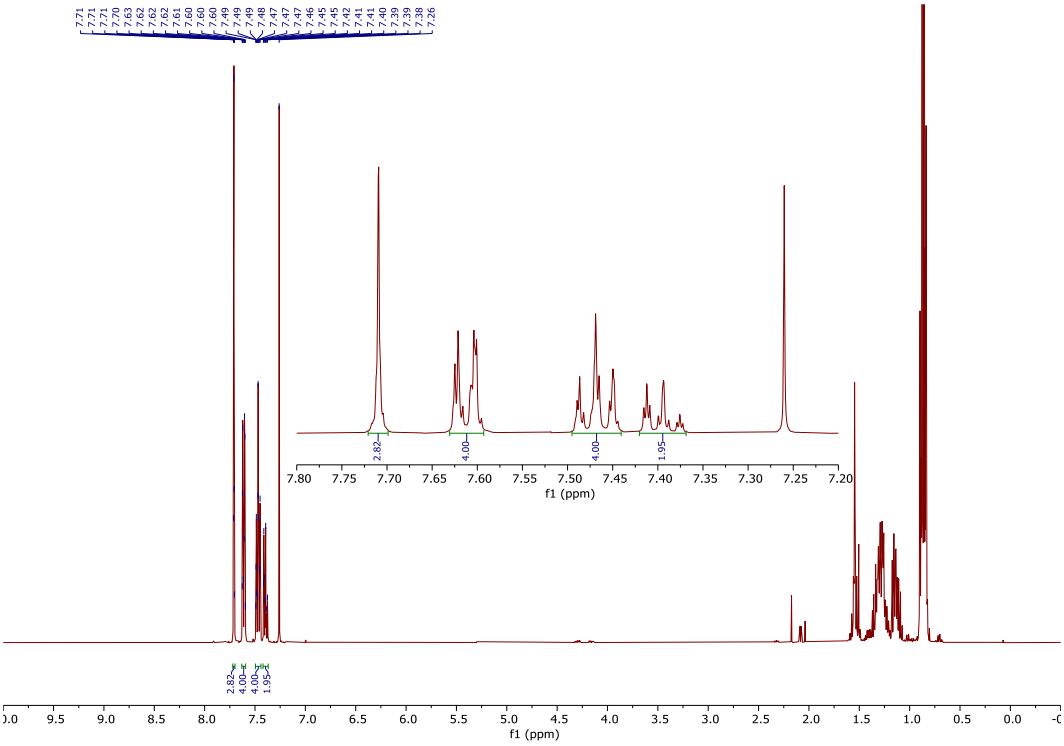

Figure 83: ^{1}H NMR spectrum ($CDCl_3$) of $PhBrPh_2$ in $CDCl_3$.

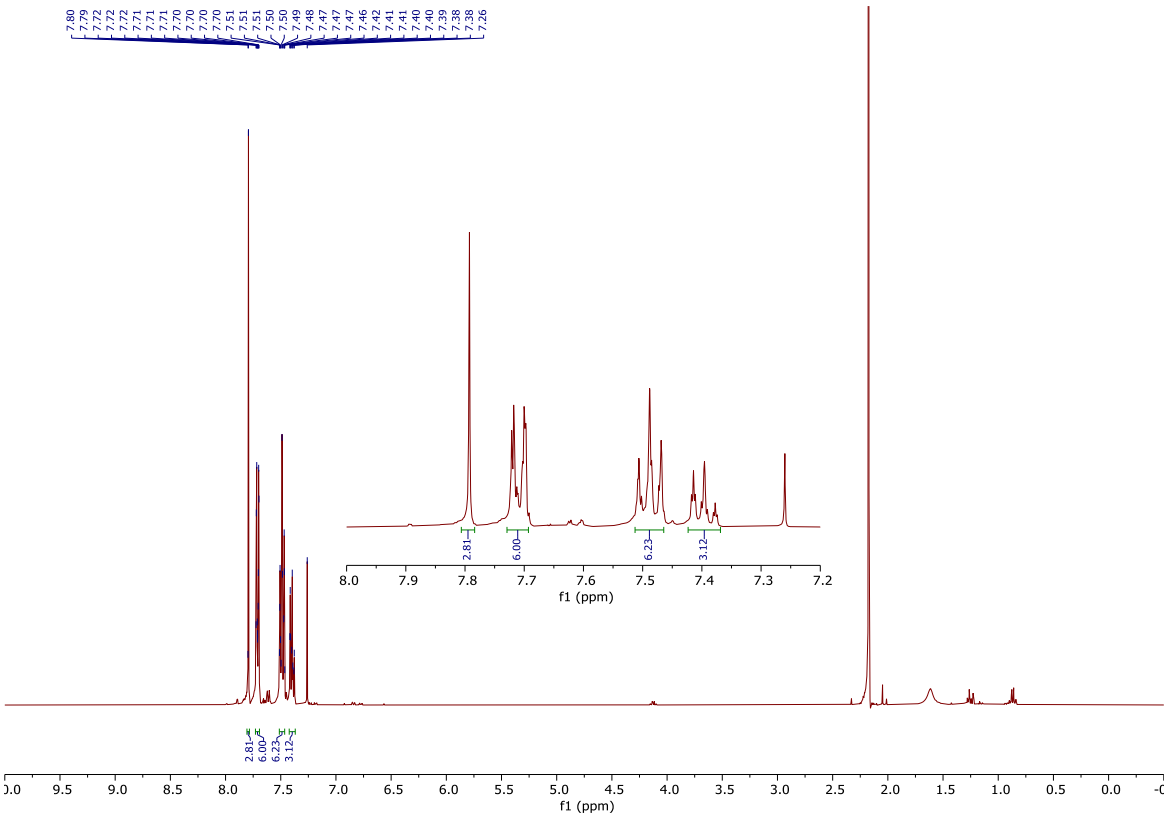

Figure 84: ^{1}H NMR spectrum ($CDCl_3$) of $PhPh_3$ in $CDCl_3$.

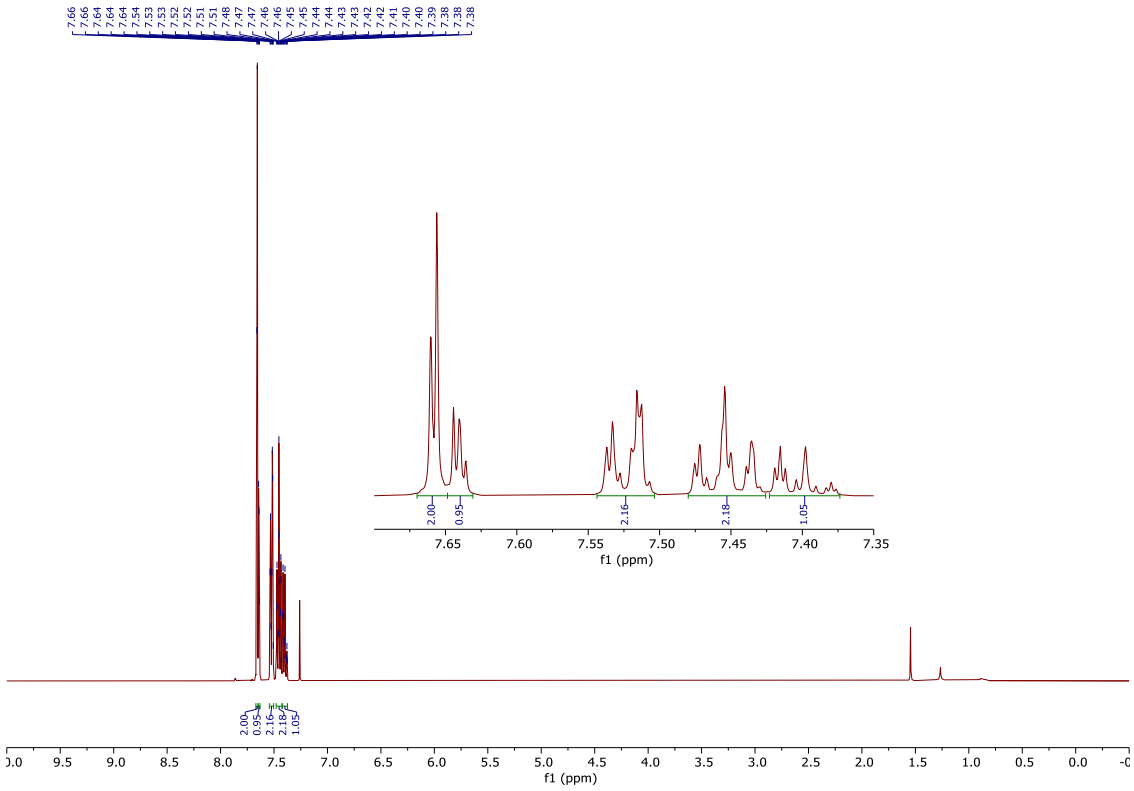

Figure 85: ^{1}H NMR spectrum ($CDCl_3$) of $PhBr_2Ph$ in $CDCl_3$.

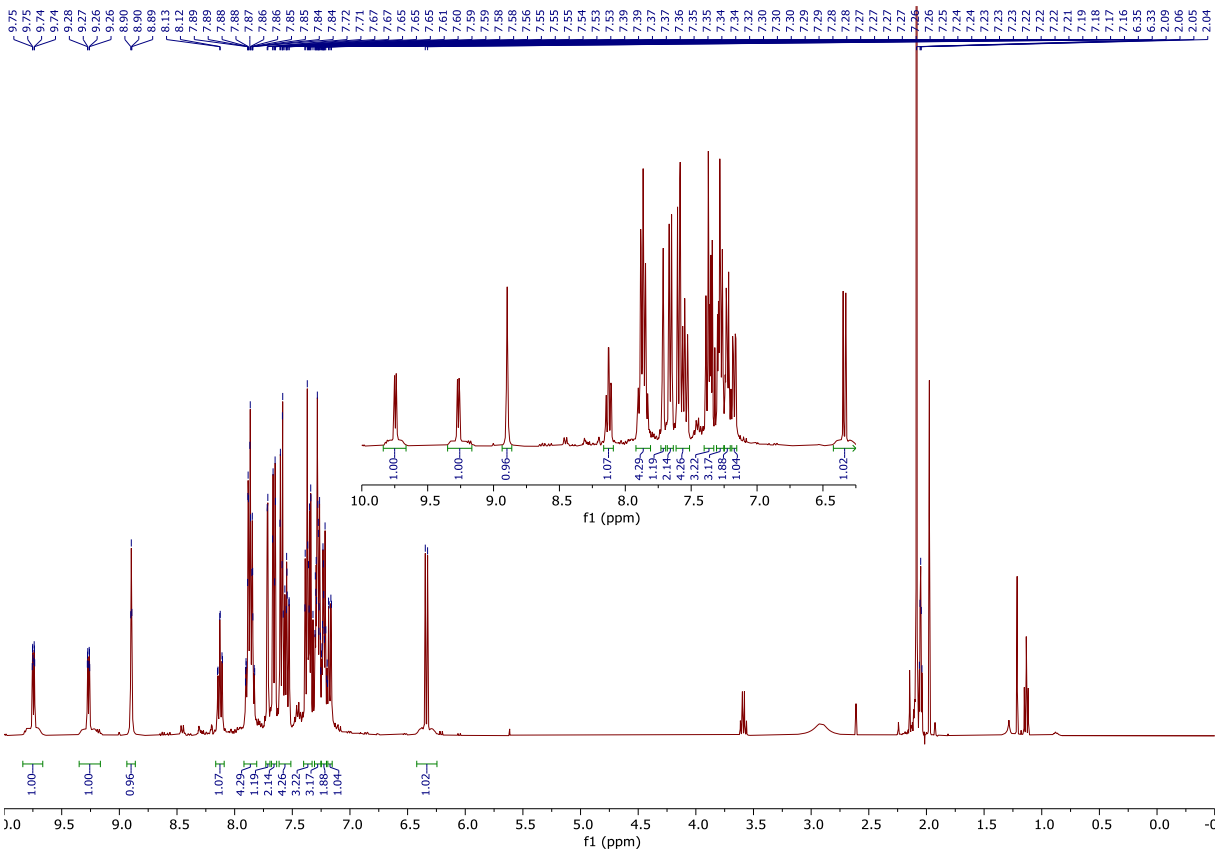

Figure 86: ^{1}H NMR spectrum of (Pt(Hbppy)Cl)2.b in d_6-DMSO.

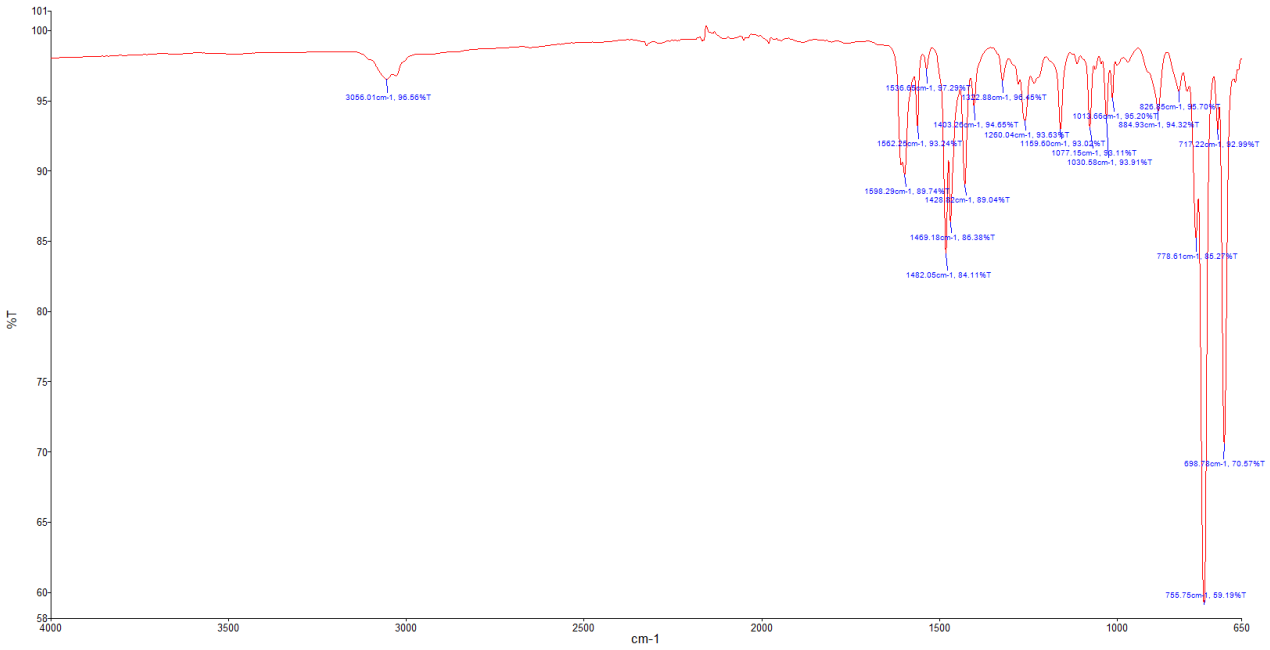

Figure 87: IR spectrum of (Pt(Hbppy)Cl)2.b.

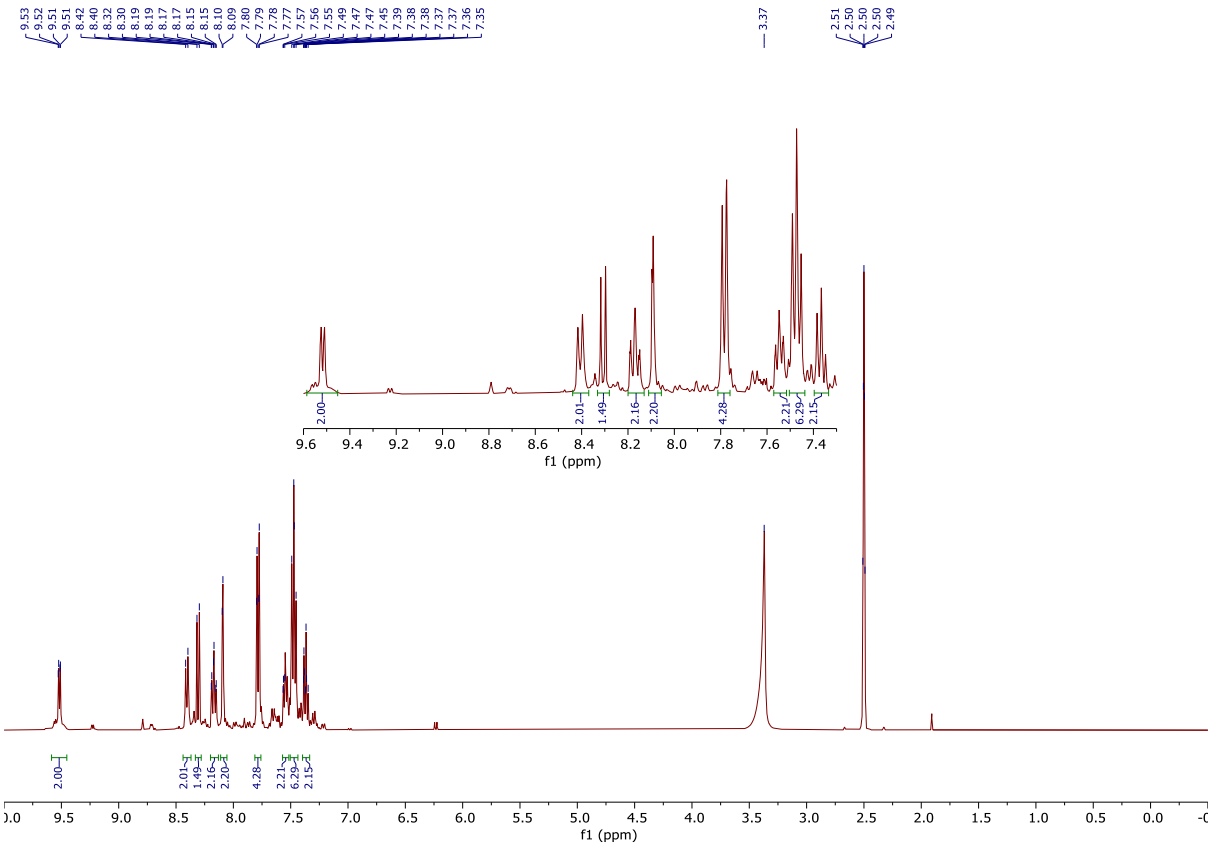

Figure 88: ^{1}H NMR spectrum of (Pt(Hbppy)Cl)2.c in d_6-DMSO.

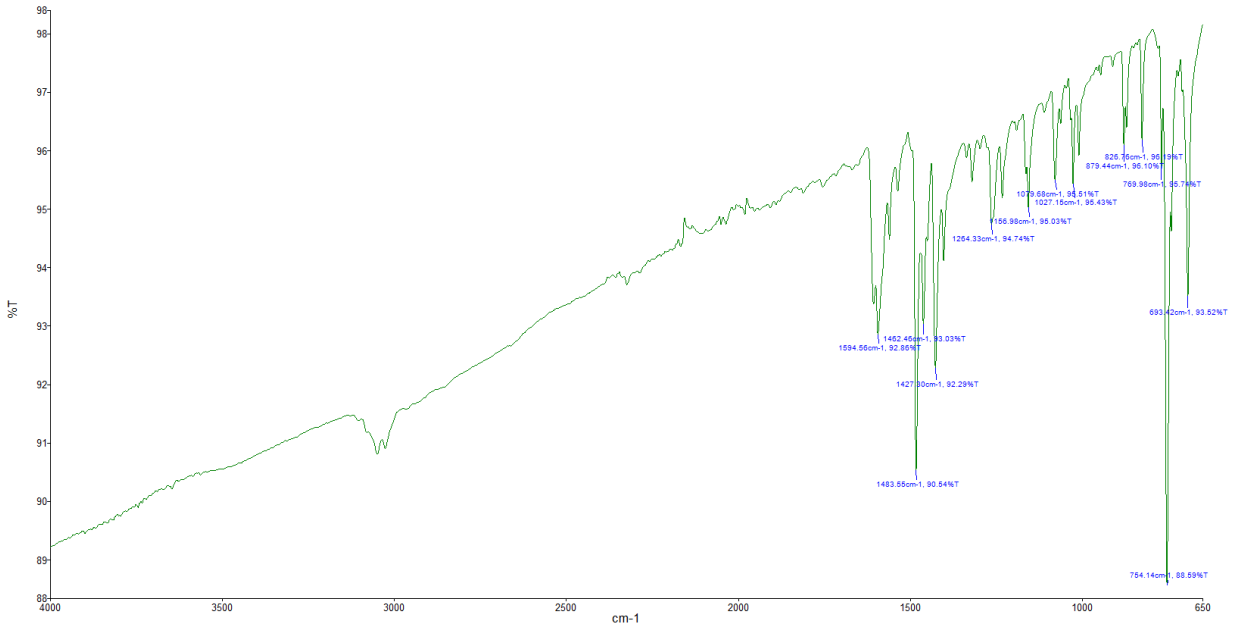

Figure 89: IR spectrum of (Pt(Hbppy)Cl)2.c.

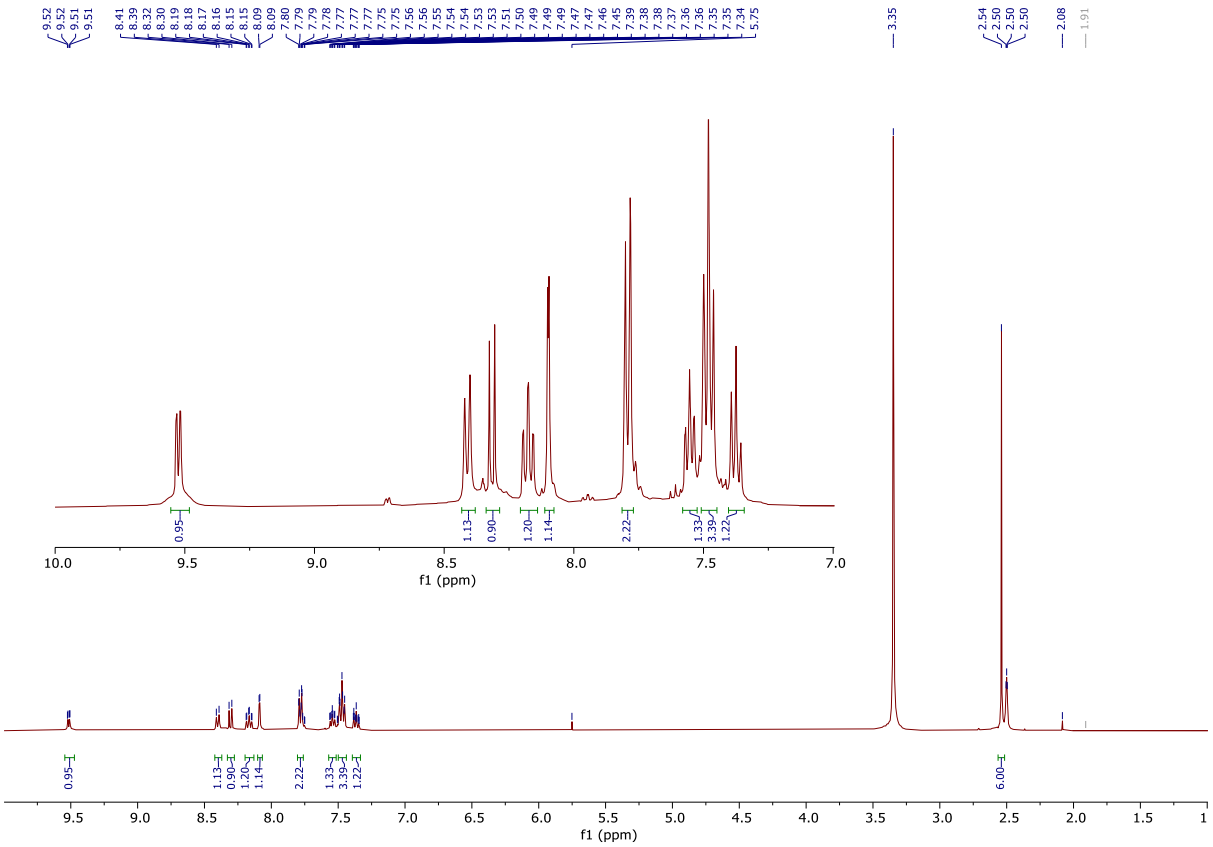

Figure 90: ^{1}H NMR spectrum of Pt(Hbppy)(DMSO)Cl in d_6-DMSO.

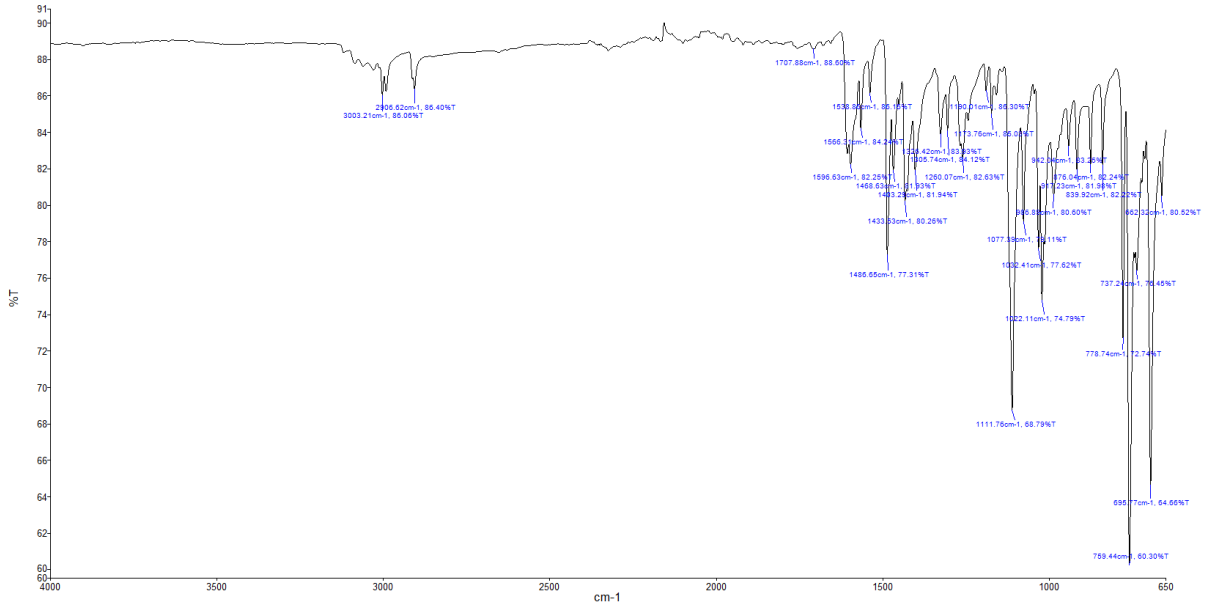

Figure 91: IR spectrum of Pt(Hbppy)(DMSO)Cl.

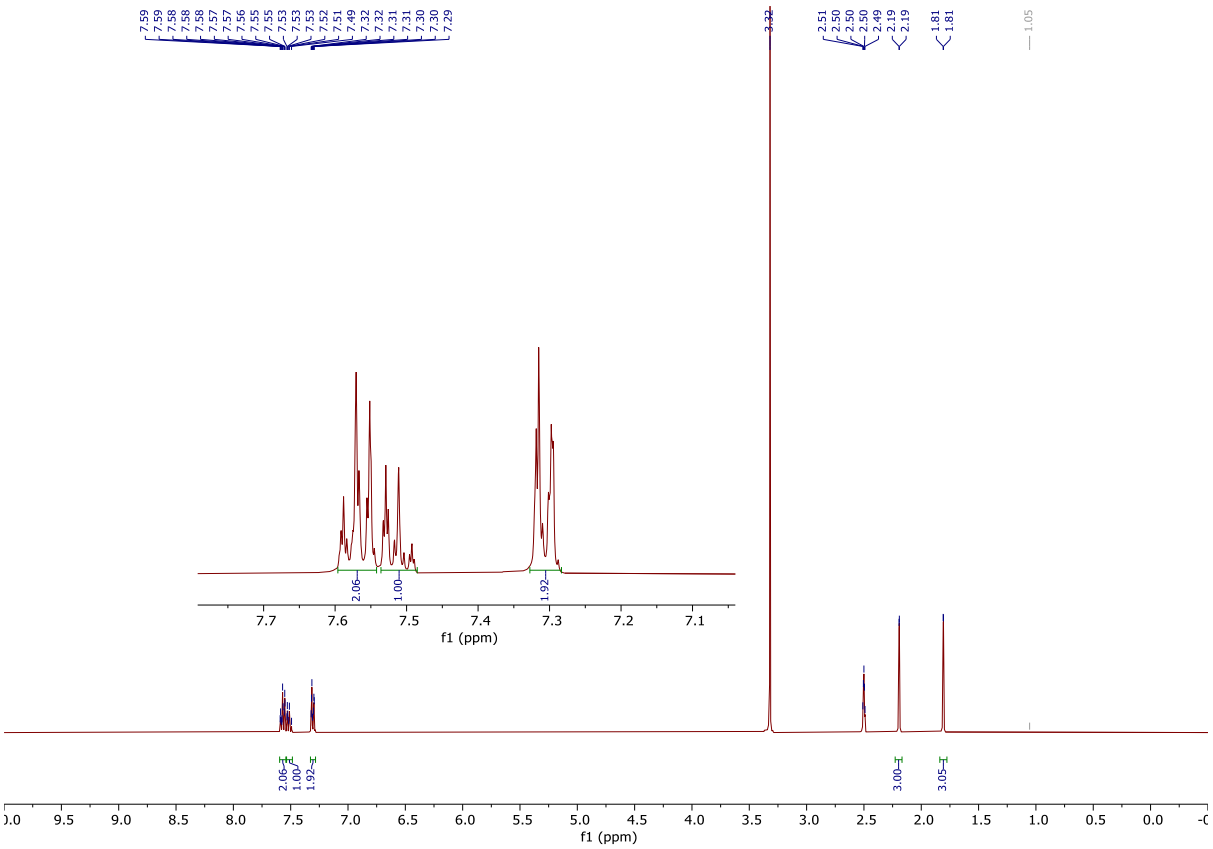

Figure 92: ^{1}H NMR spectrum of Ph(ThMe2S) in d_6-DMSO.

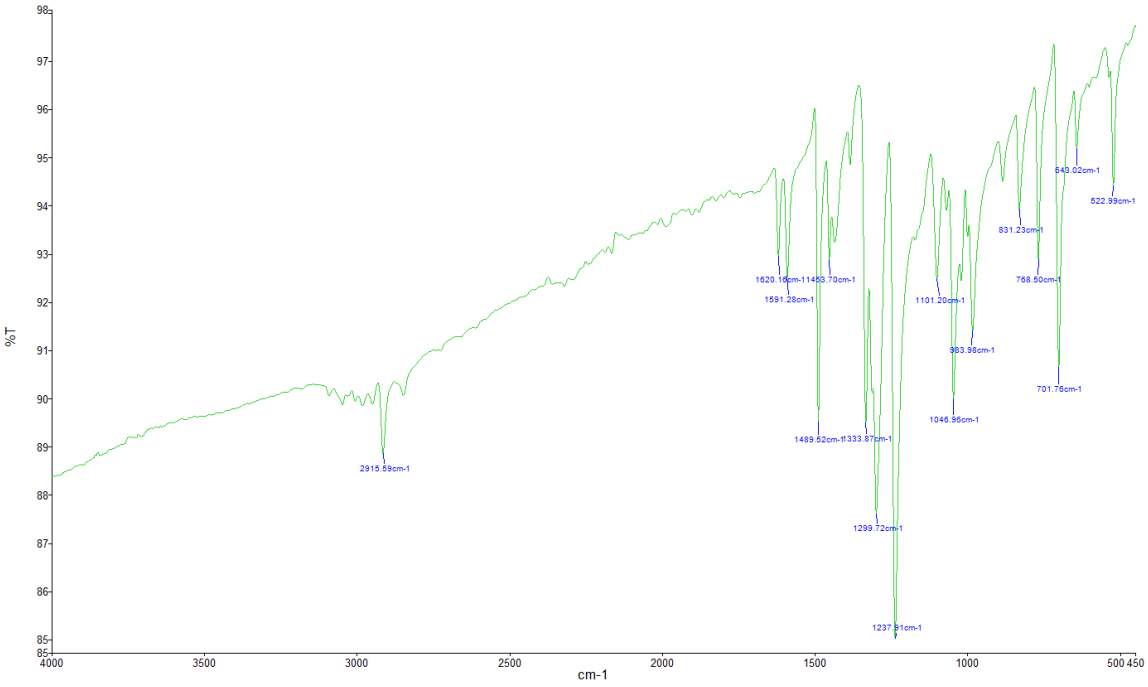

Figure 93: IR spectrum of Ph(ThMe2S).

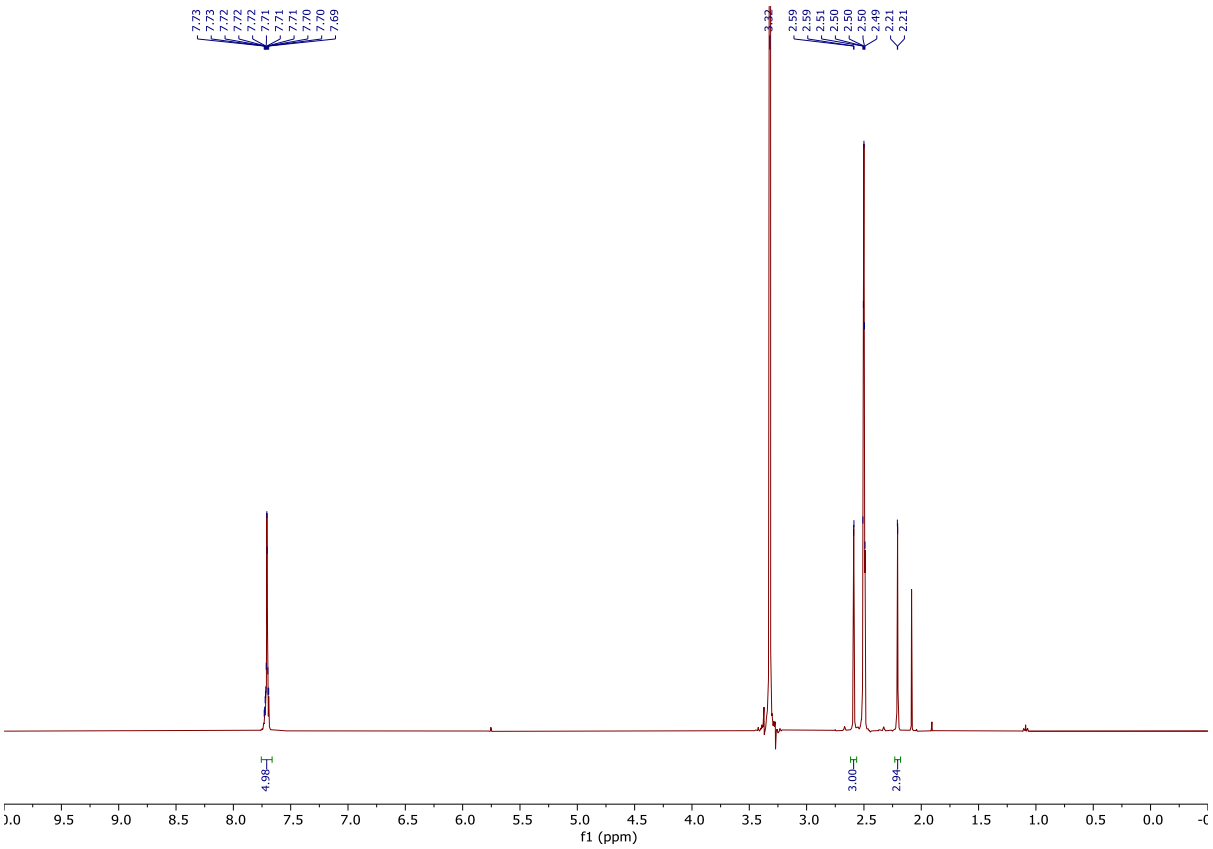

Figure 94: ^{1}H NMR spectrum of Ph(ThMe2H)PF_6 in d_6-DMSO.

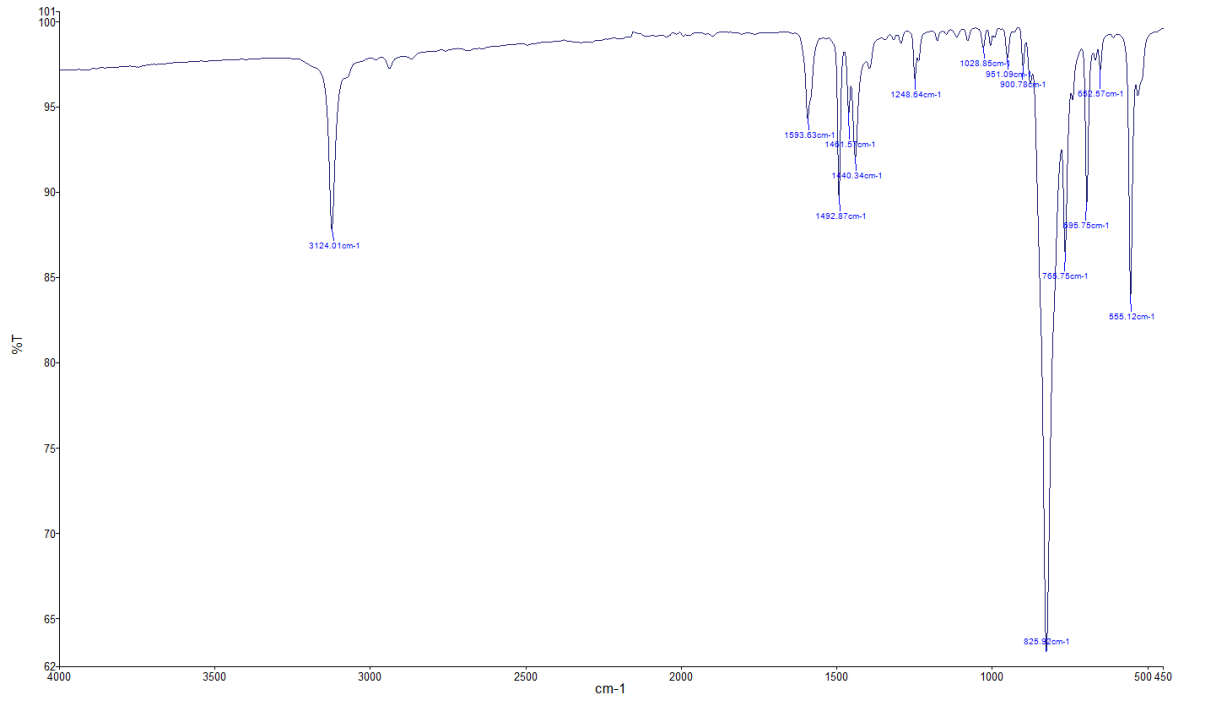

Figure 95: IR spectrum of Ph(ThMe2H)PF_6.

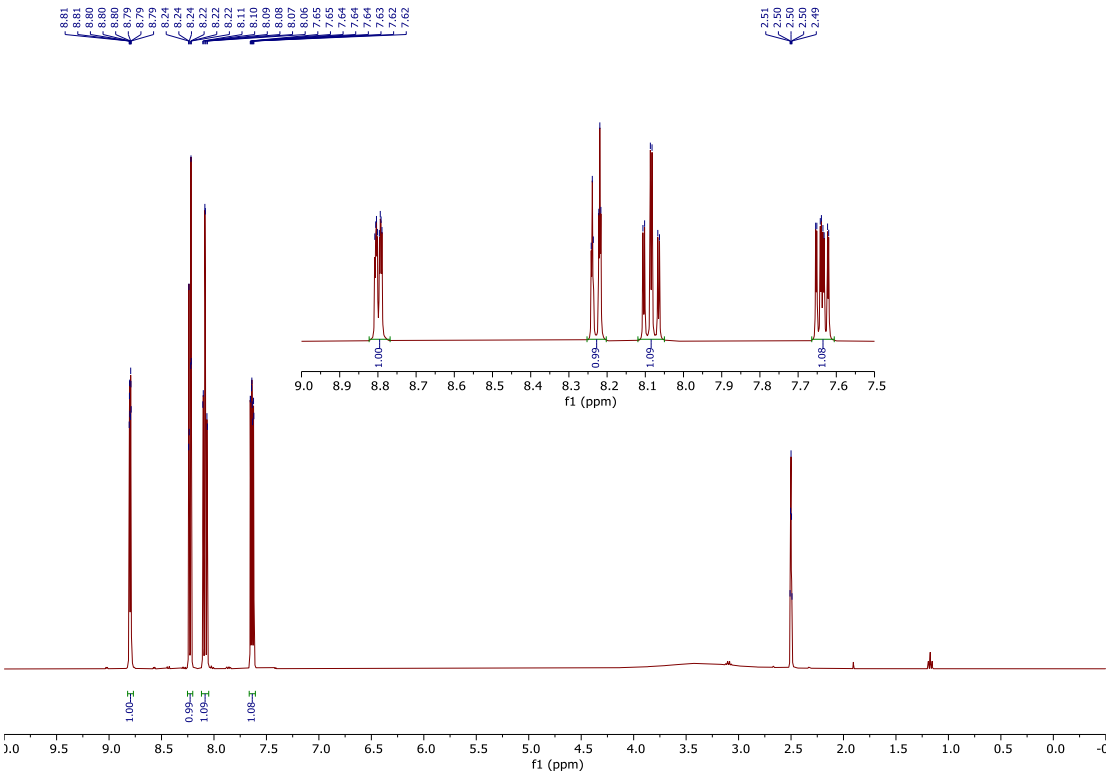

Figure 96: ^{1}H NMR spectrum of HL1 in d_6-DMSO.

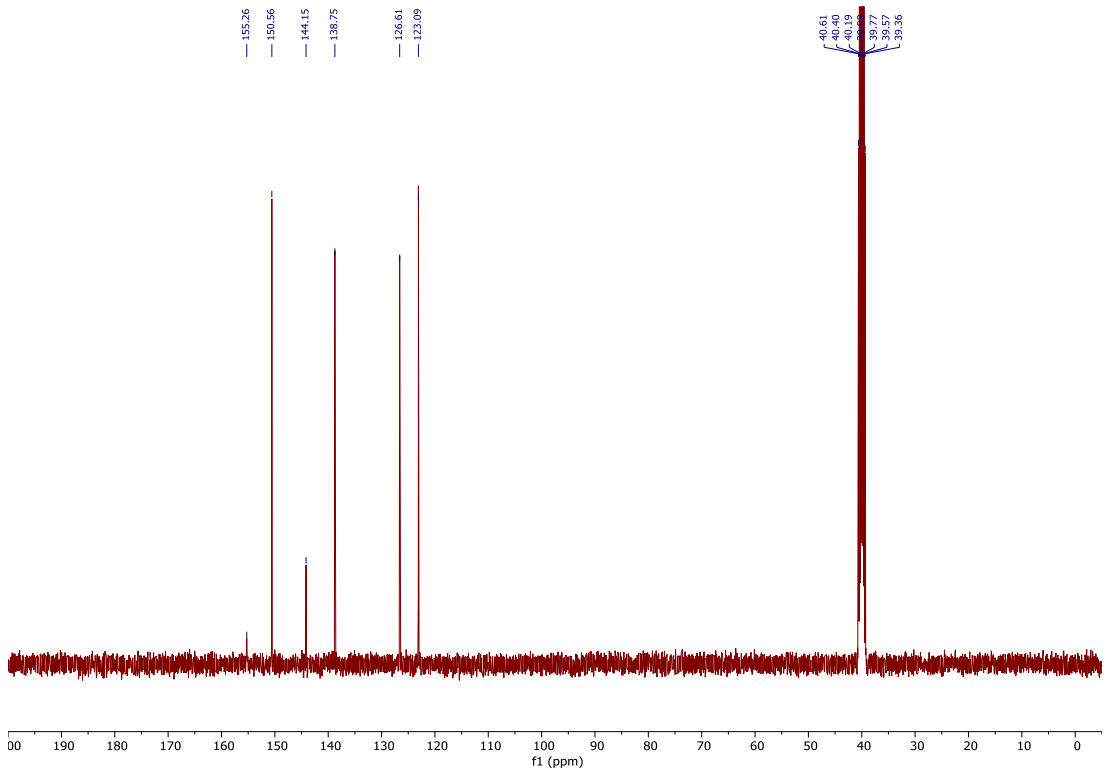

Figure 97: ^{13}C NMR spectrum of HL1 in d_6-DMSO.

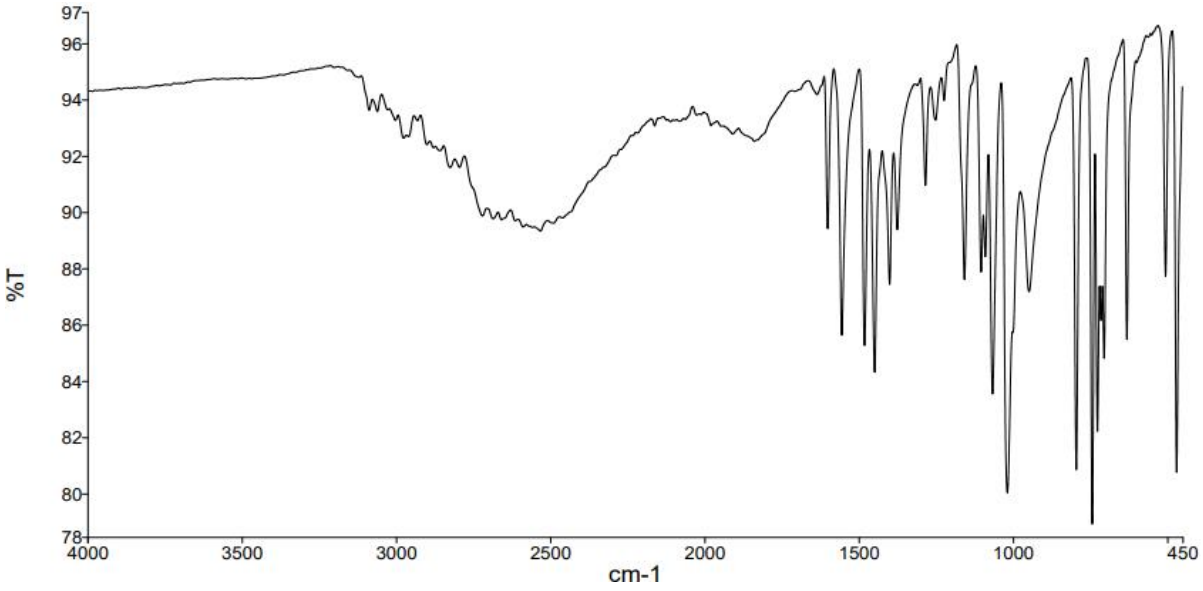

Figure 98: IR spectrum of HL1.

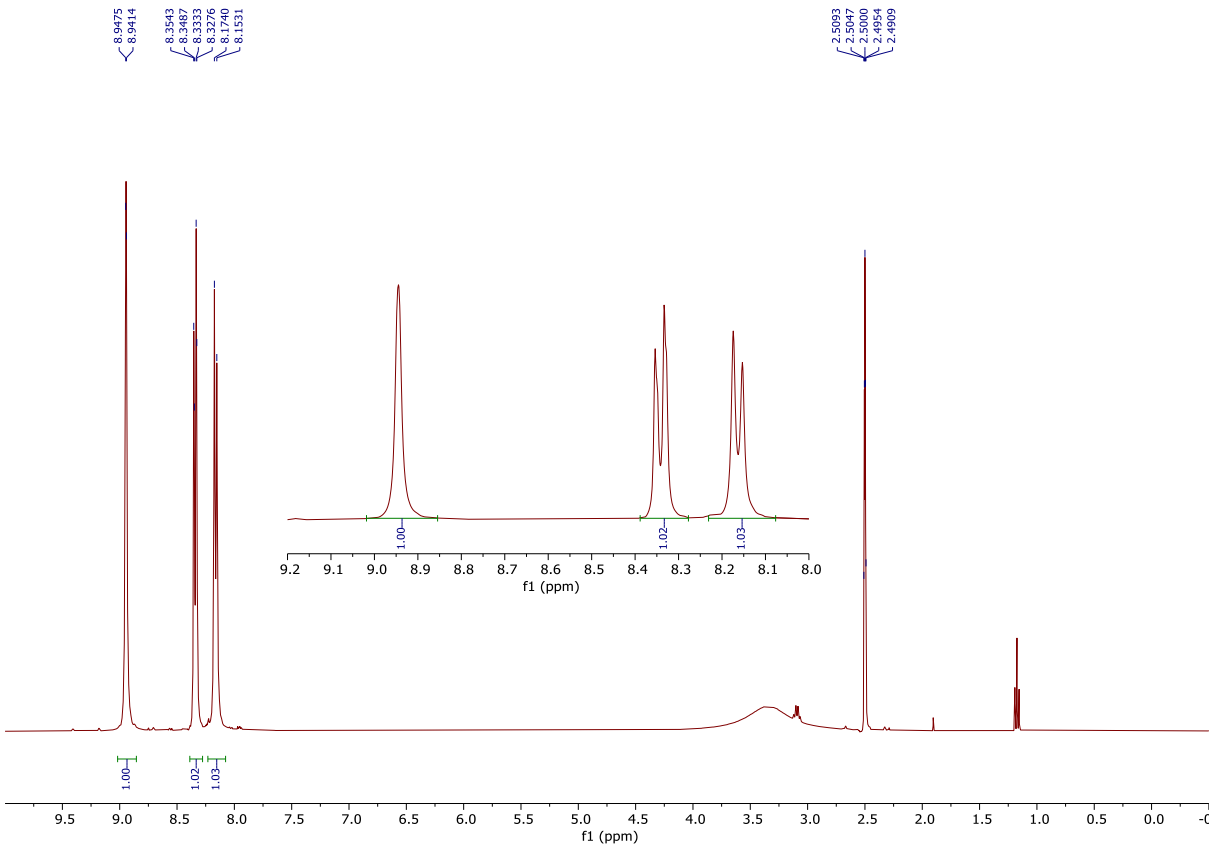

Figure 99: ^{1}H NMR spectrum of HL2 in d_6-DMSO.

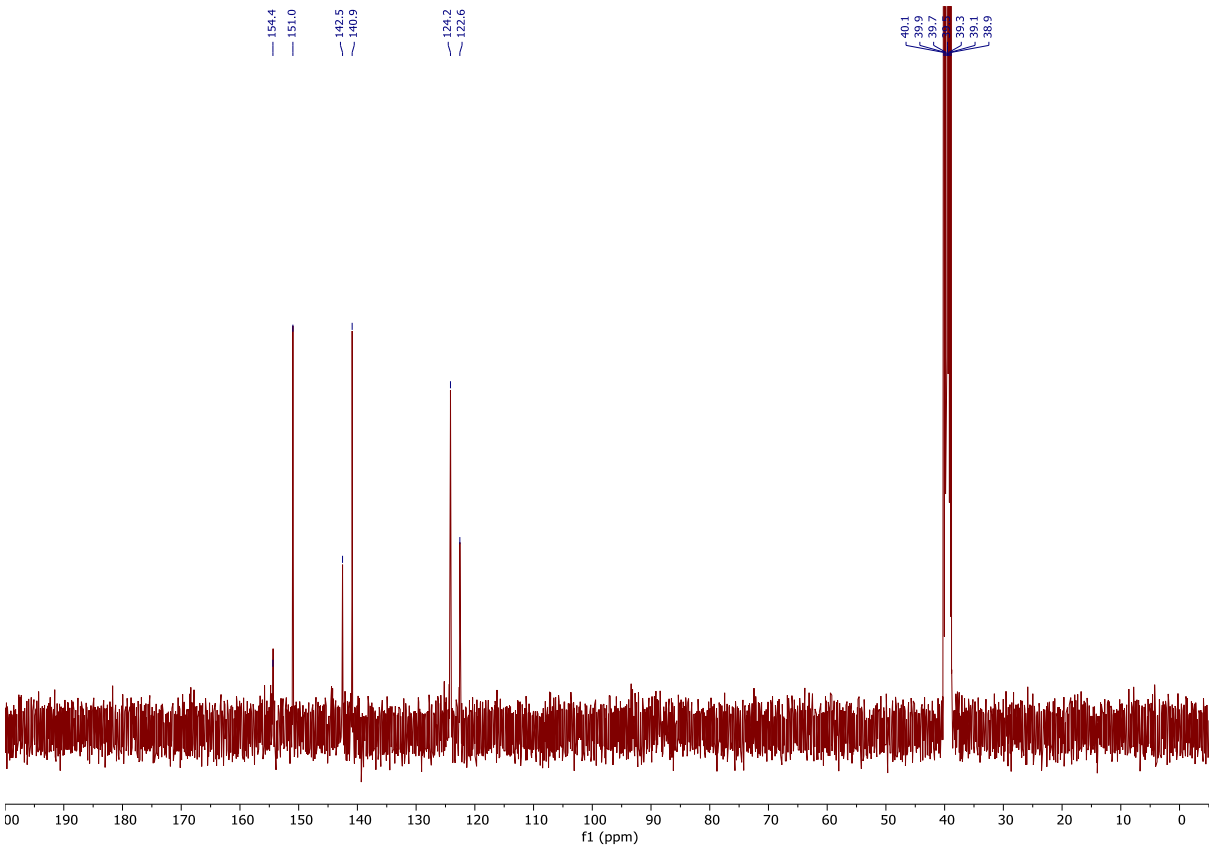

Figure 100: ^{13}C NMR spectrum of HL2 in d_6-DMSO.

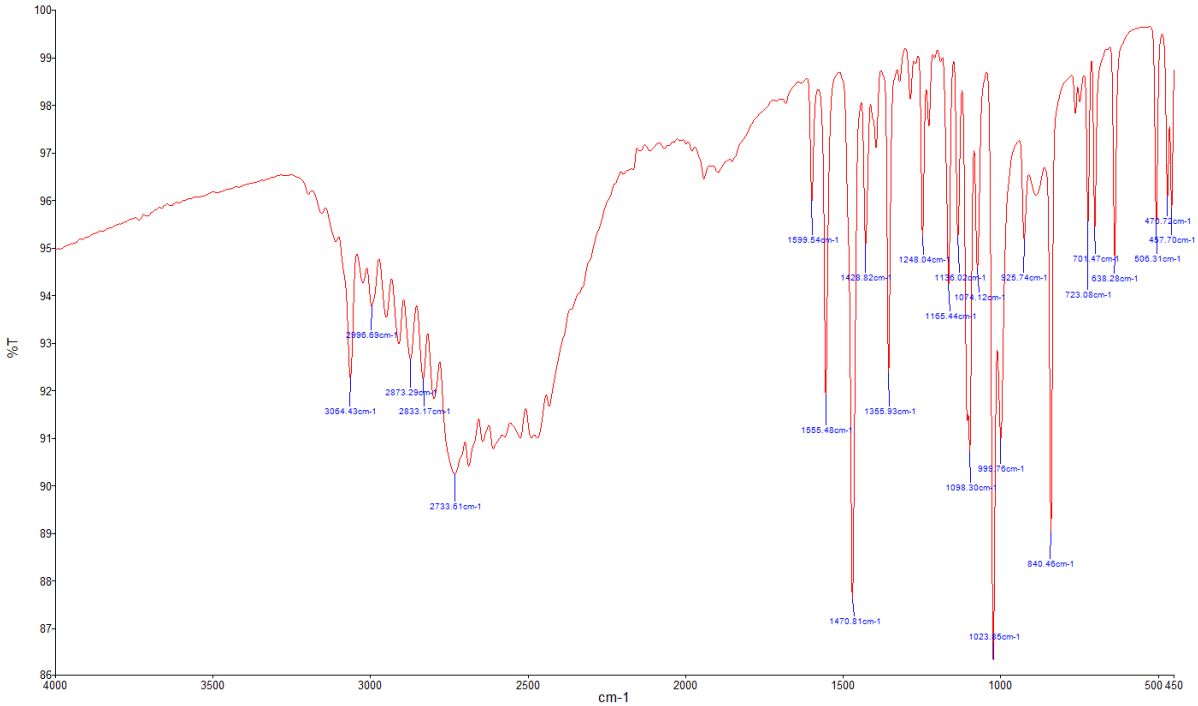

Figure 101: IR spectrum of HL2.

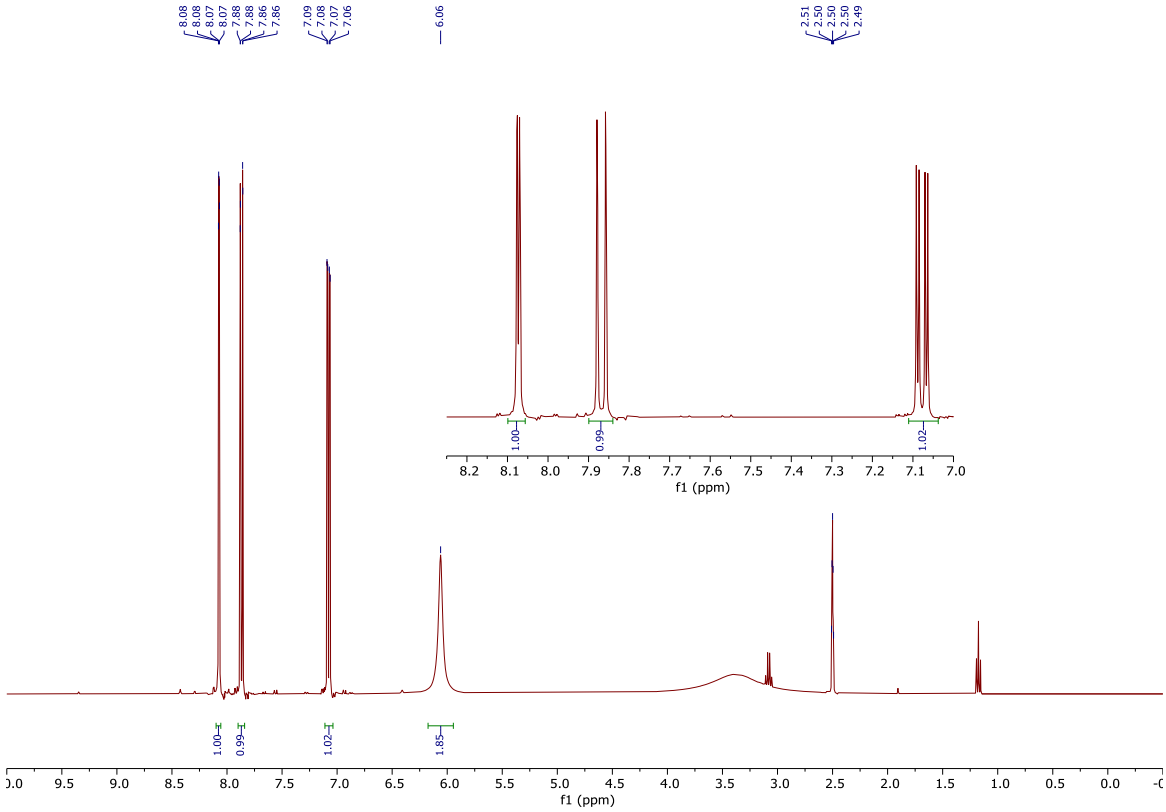

Figure 102: ^{1}H NMR spectrum of HL3 in d_6-DMSO.

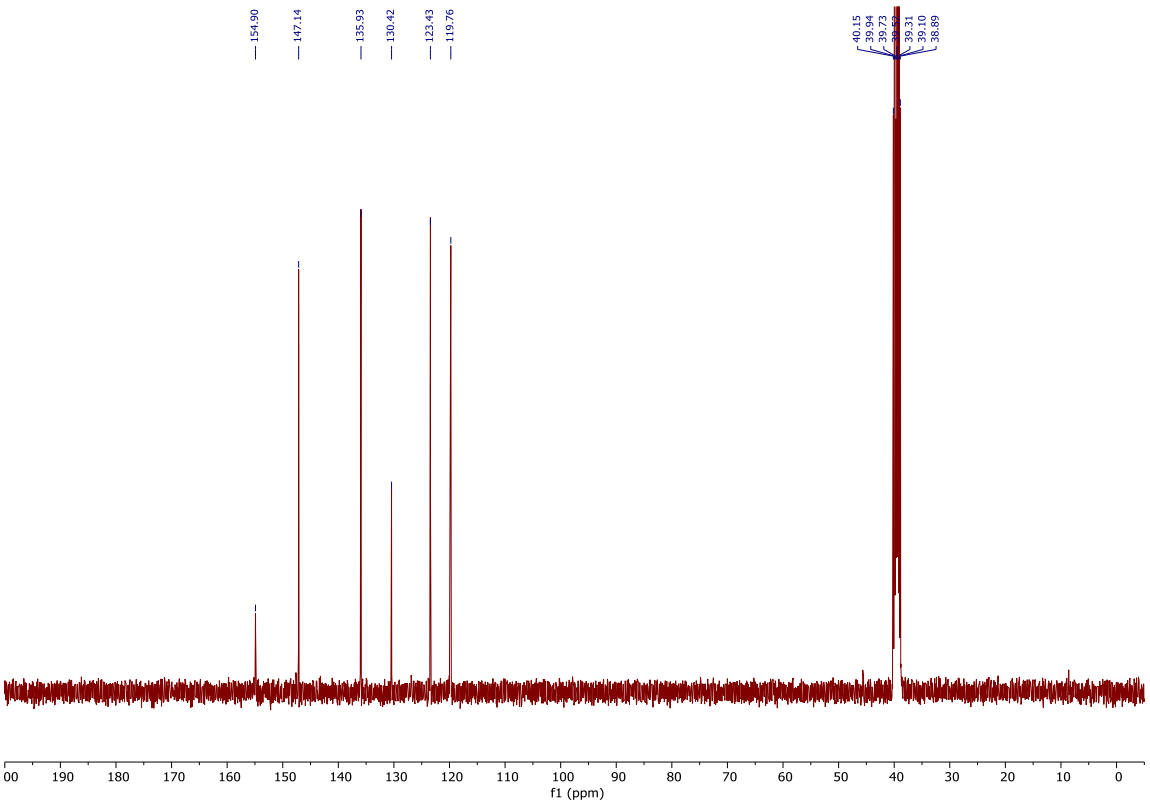

Figure 103: ^{13}C NMR spectrum of HL3 in d_6-DMSO.

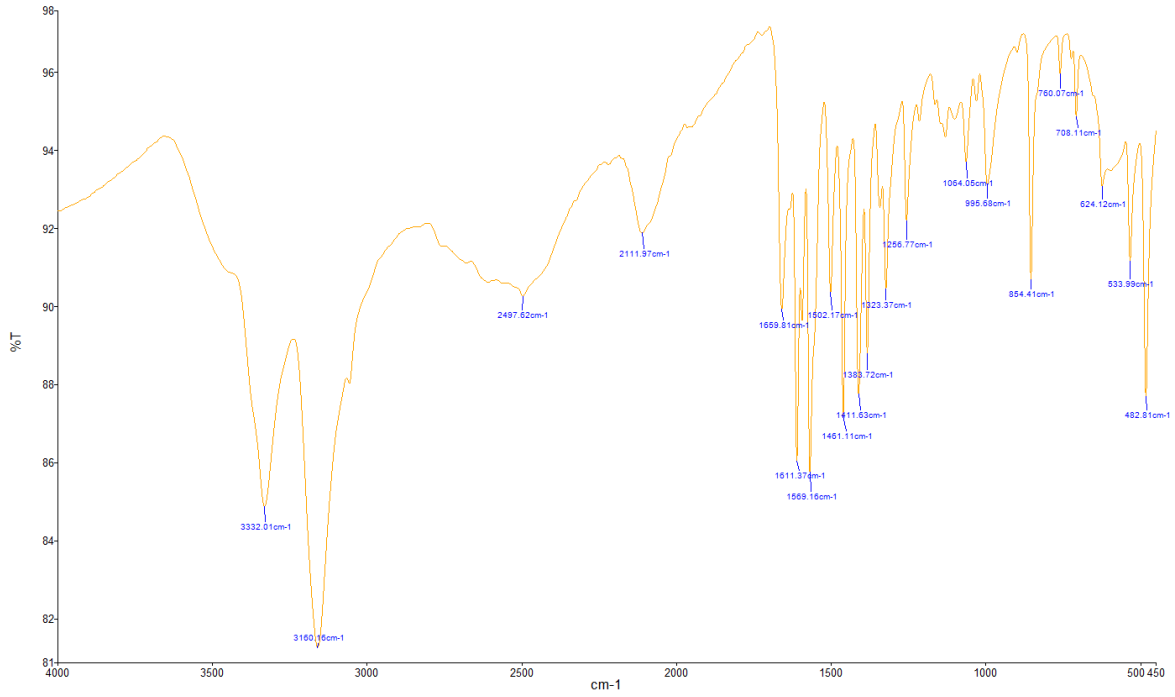

Figure 104: IR spectrum of HL3.

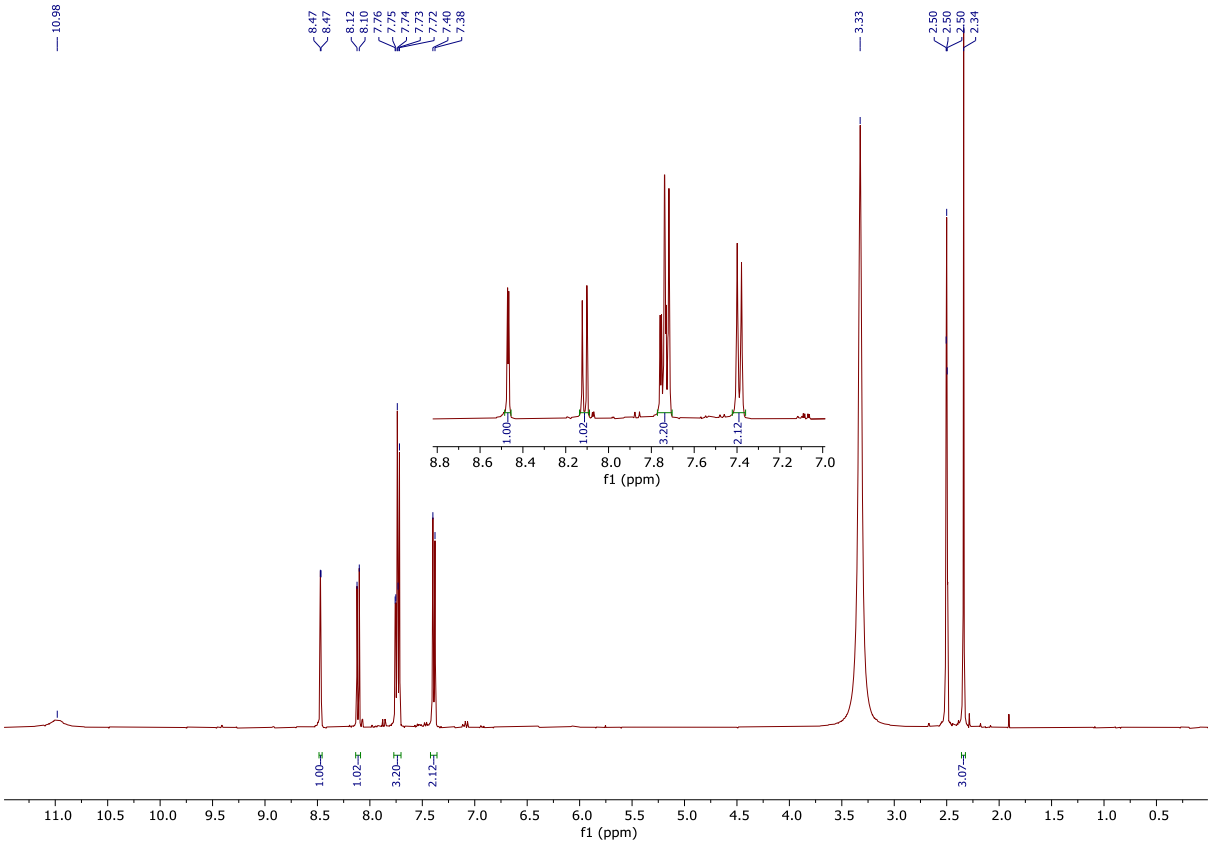

Figure 105: ^{1}H NMR spectrum of $[H_2L4]Cl$ in d_6-DMSO.

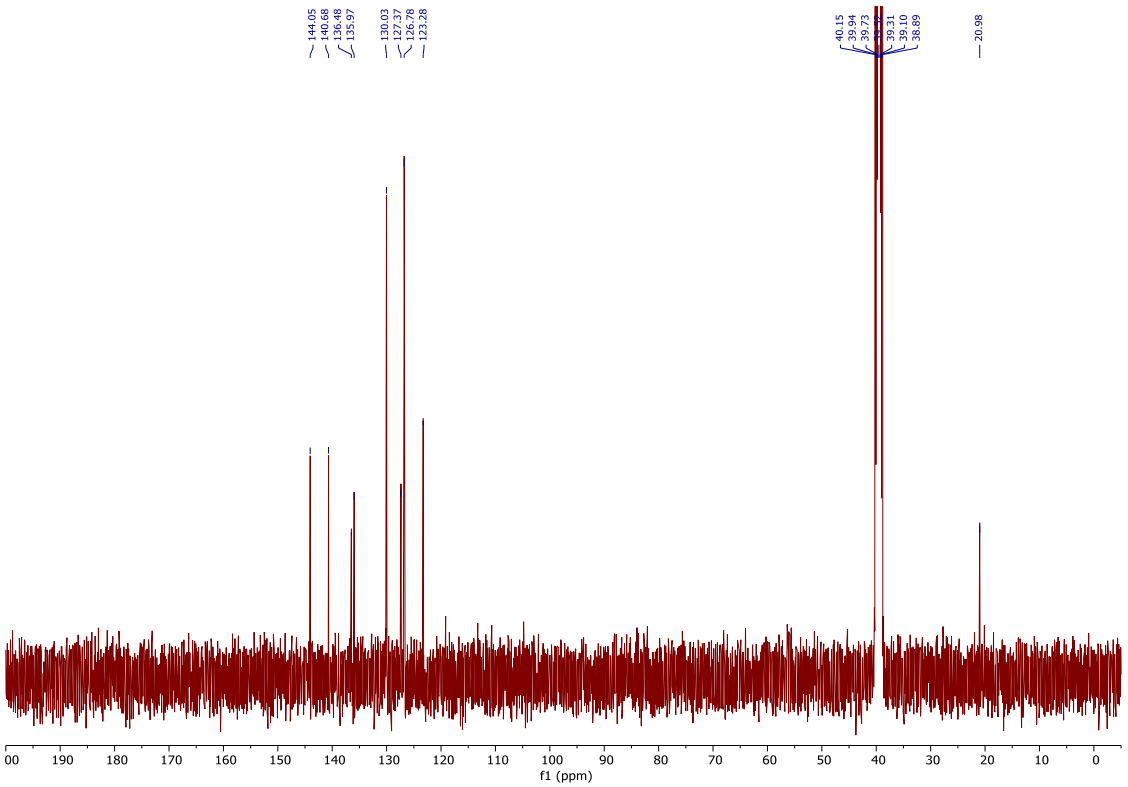

Figure 106: ^{13}C NMR spectrum of $[H_2L4]Cl$ in d_6-DMSO.

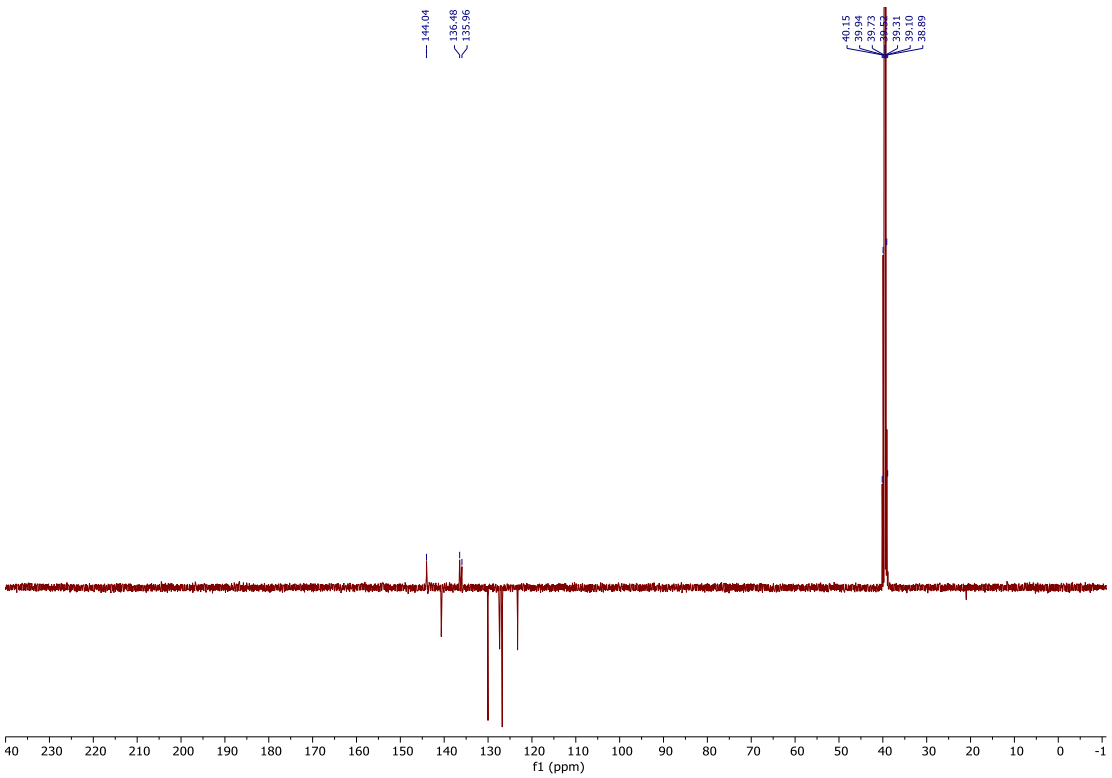

Figure 107: ^{13}C DEPTQ-135 NMR spectrum of $[H_2L4]Cl$ in d_6-DMSO.

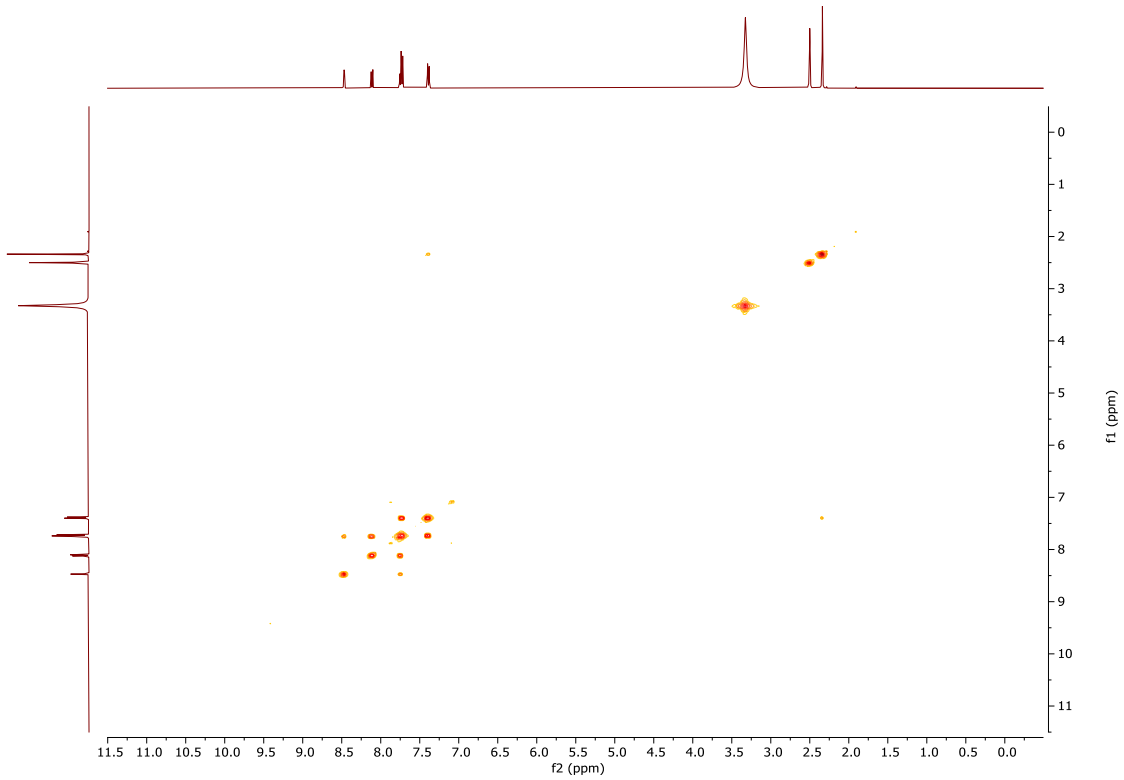

Figure 108: COSY NMR spectrum of $[H_2L4]Cl$ in d_6-DMSO.

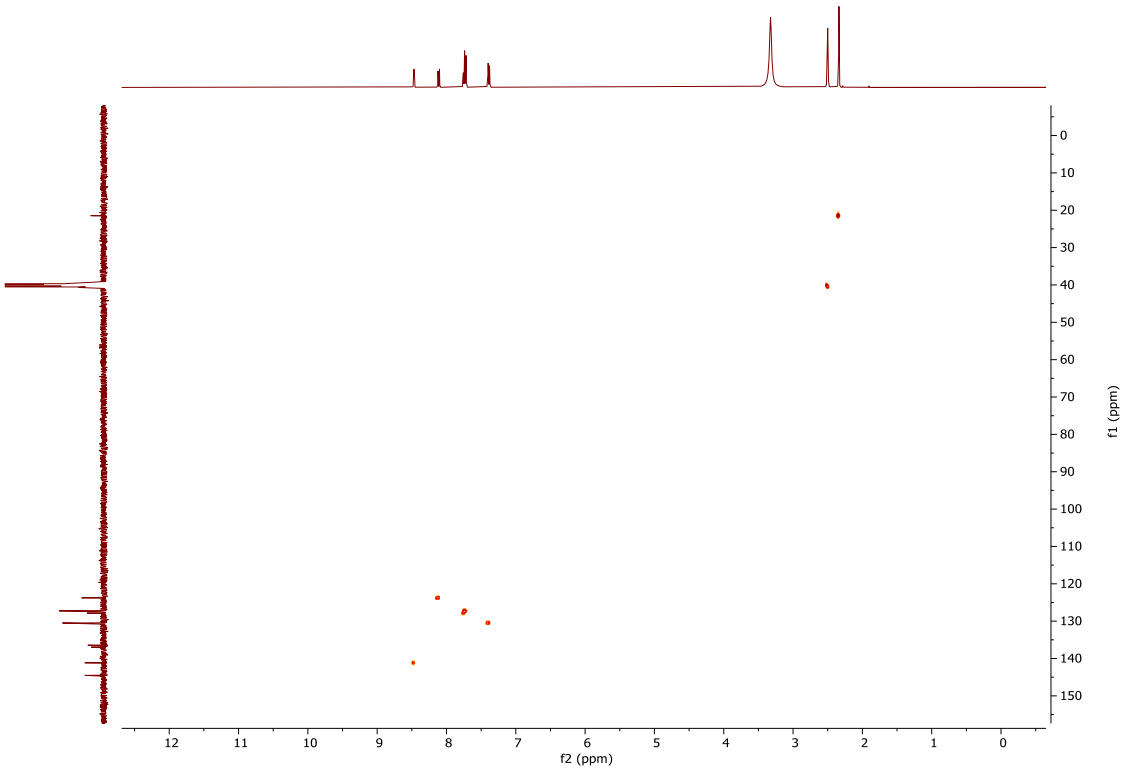

Figure 109: HSQC NMR spectrum of $[H_2L4]Cl$ in d_6-DMSO.

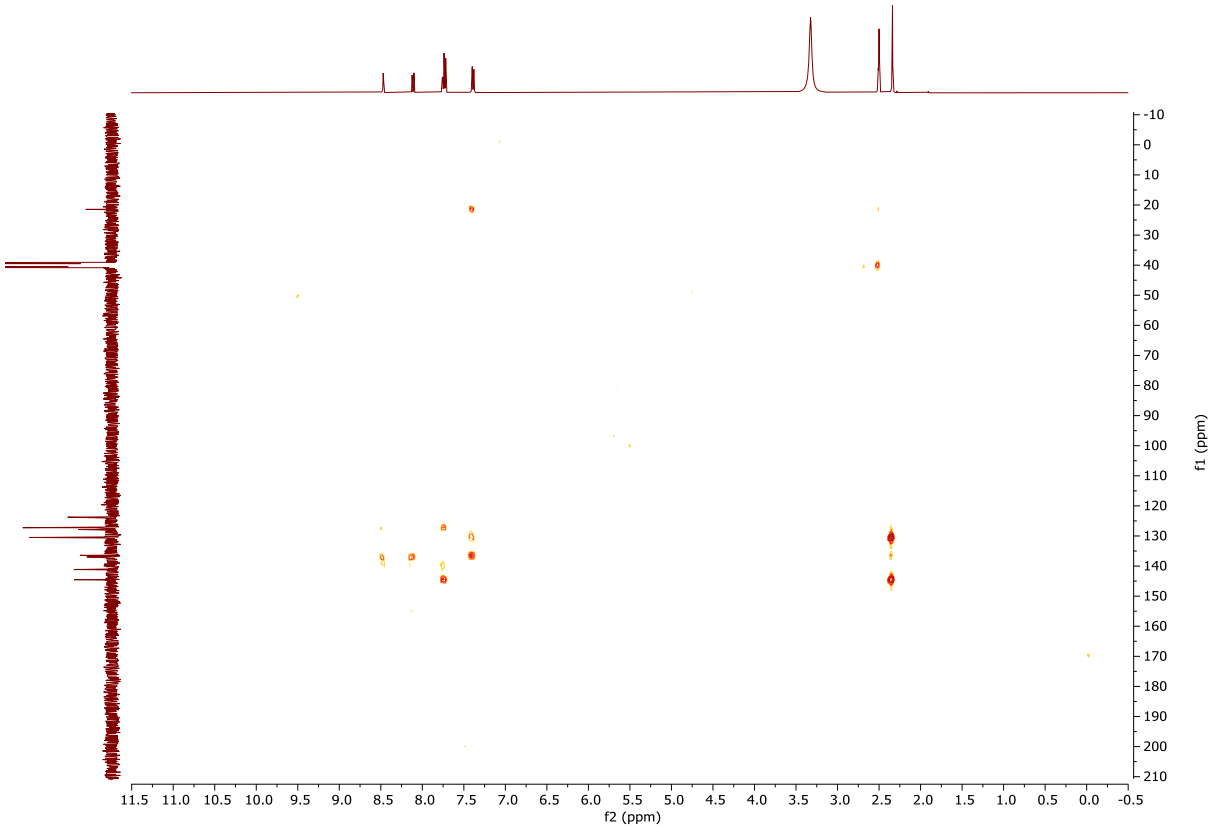

Figure 110: HMBC NMR spectrum of $[H_2L4]Cl$ in d_6-DMSO.

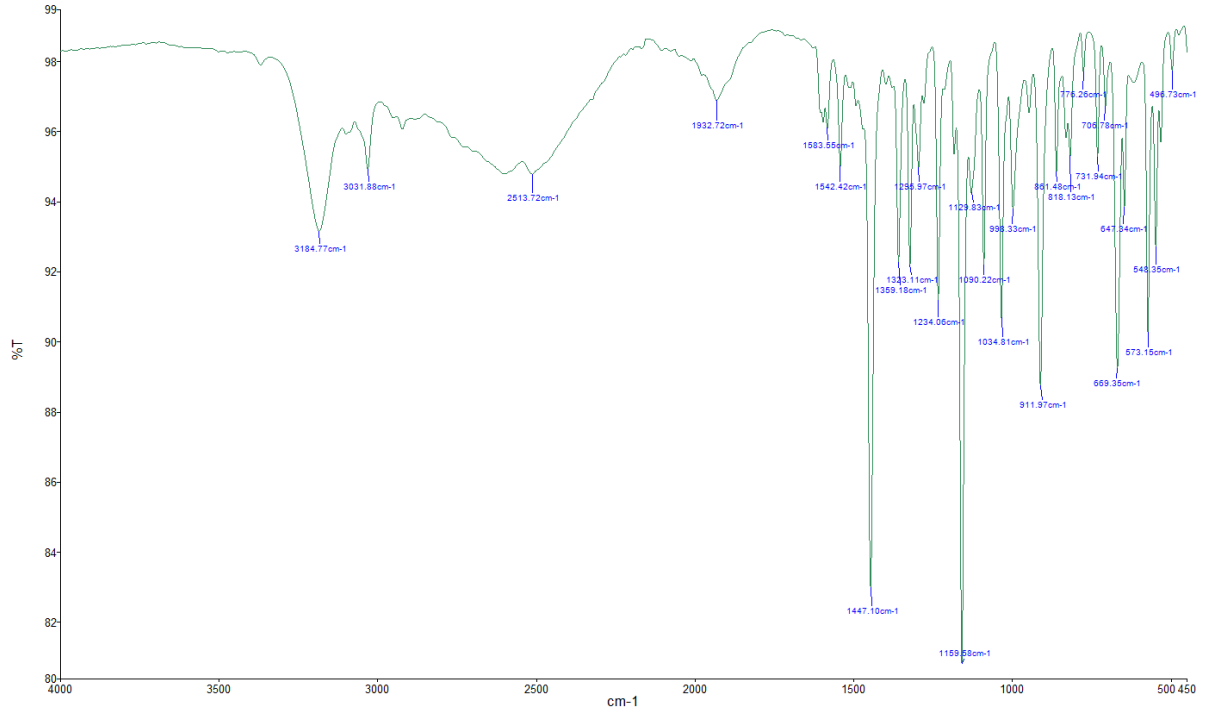

Figure 111: IR spectrum of $[H_2L4]Cl$.

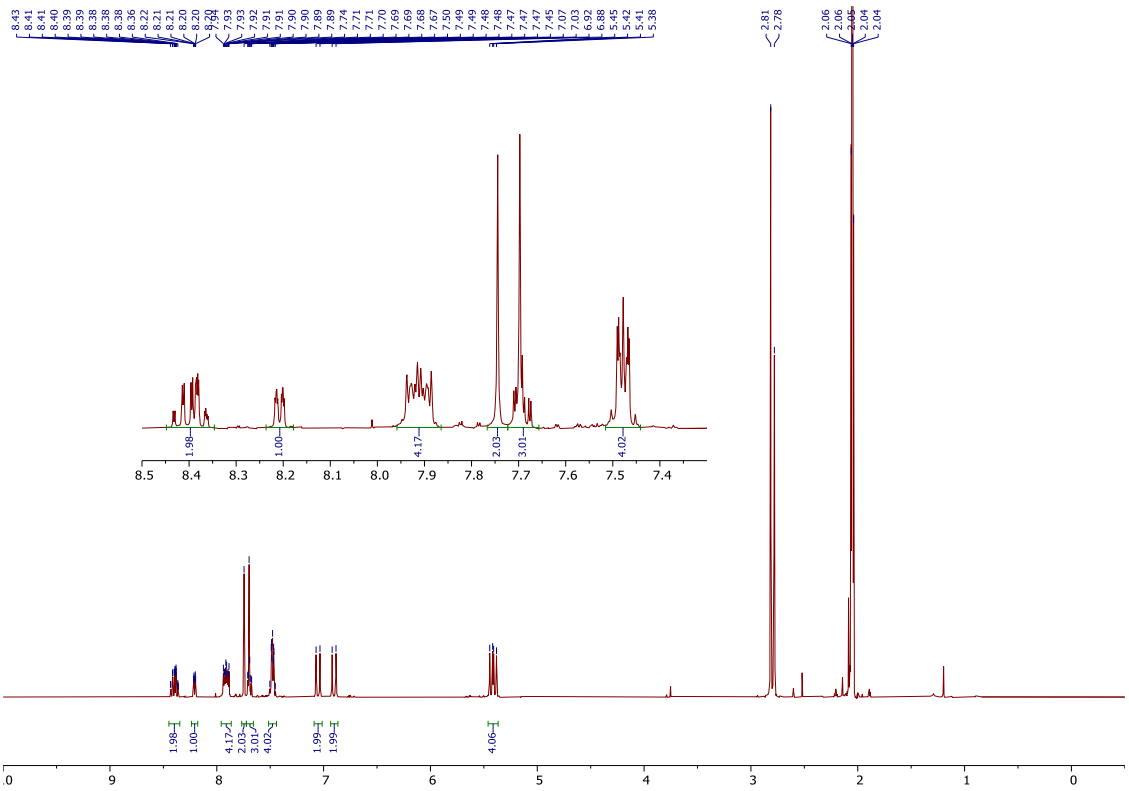

Figure 112: ^{1}H NMR spectrum of $[Pd(o\text{-}cyc)L1]PF_6$ in acetone-d_6.

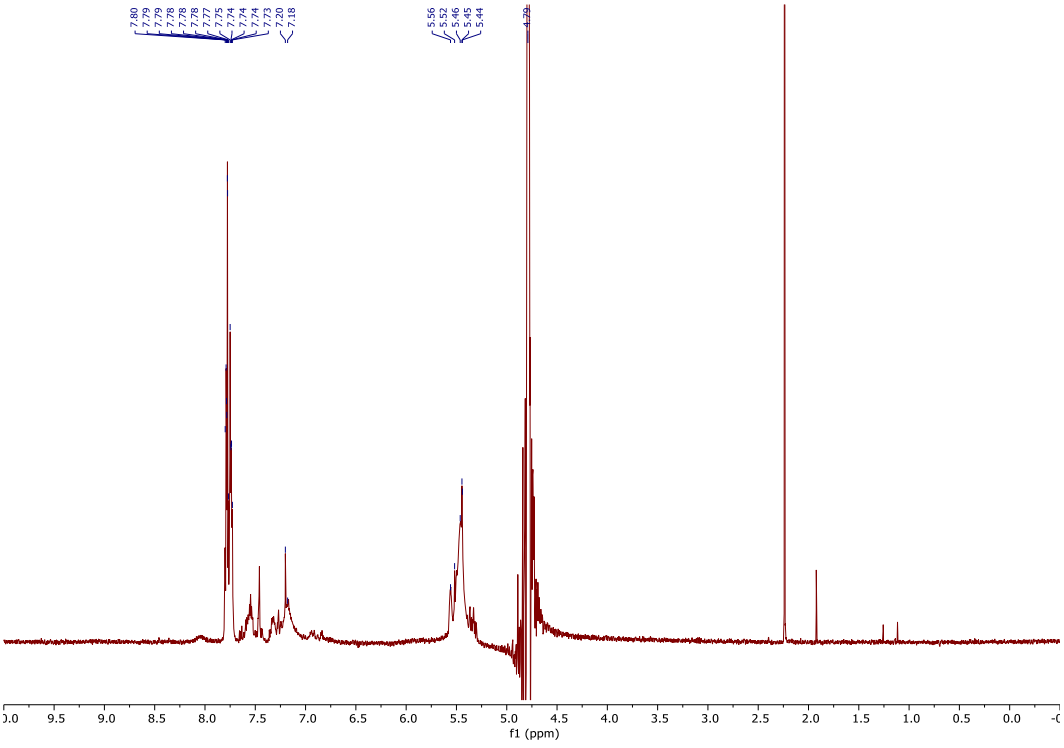

Figure 113: ^{1}H NMR spectrum of $[H_2(o\text{-}cyc)]Br_2$ in acetone-d_6.

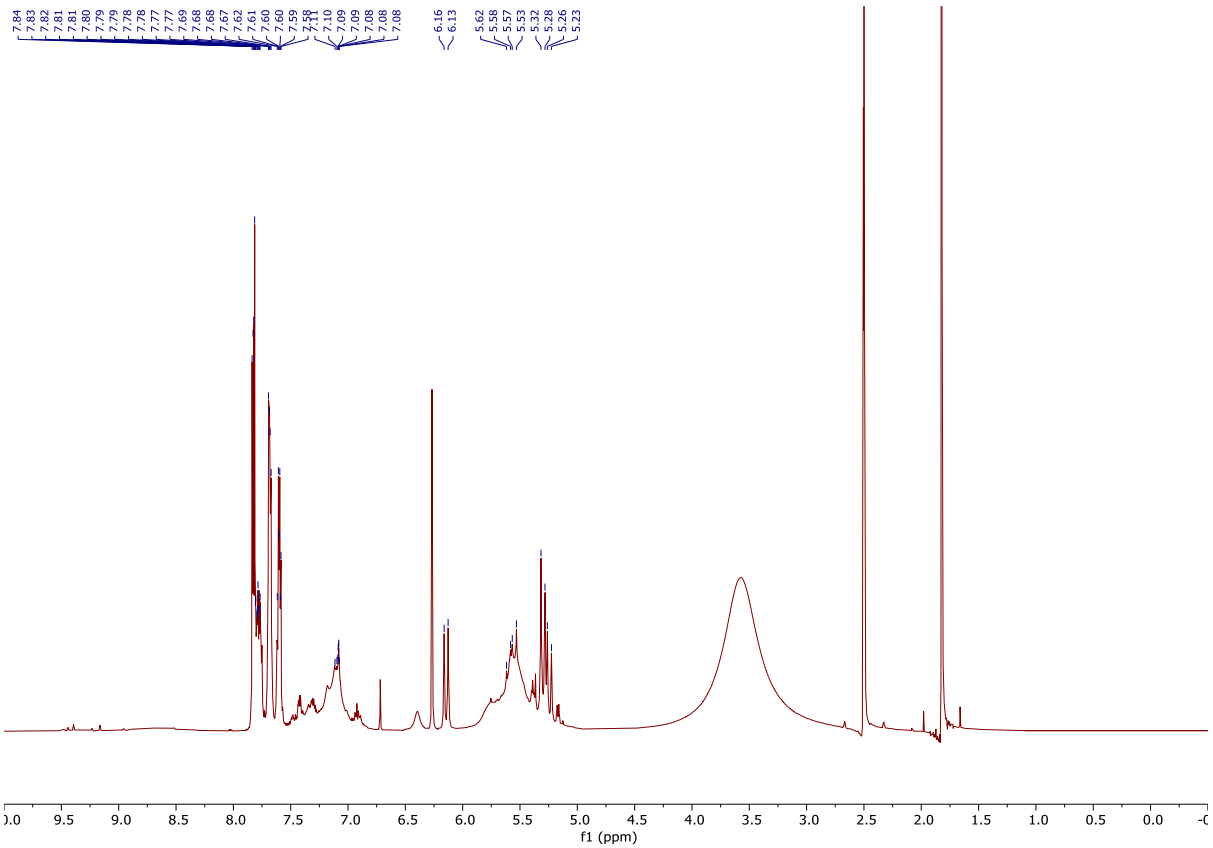

Figure 114: ^{1}H NMR spectrum of $[H_2(o\text{-}cyc)](OAc)_2$ in d_6-DMSO.

Appendix C – HRMS Data

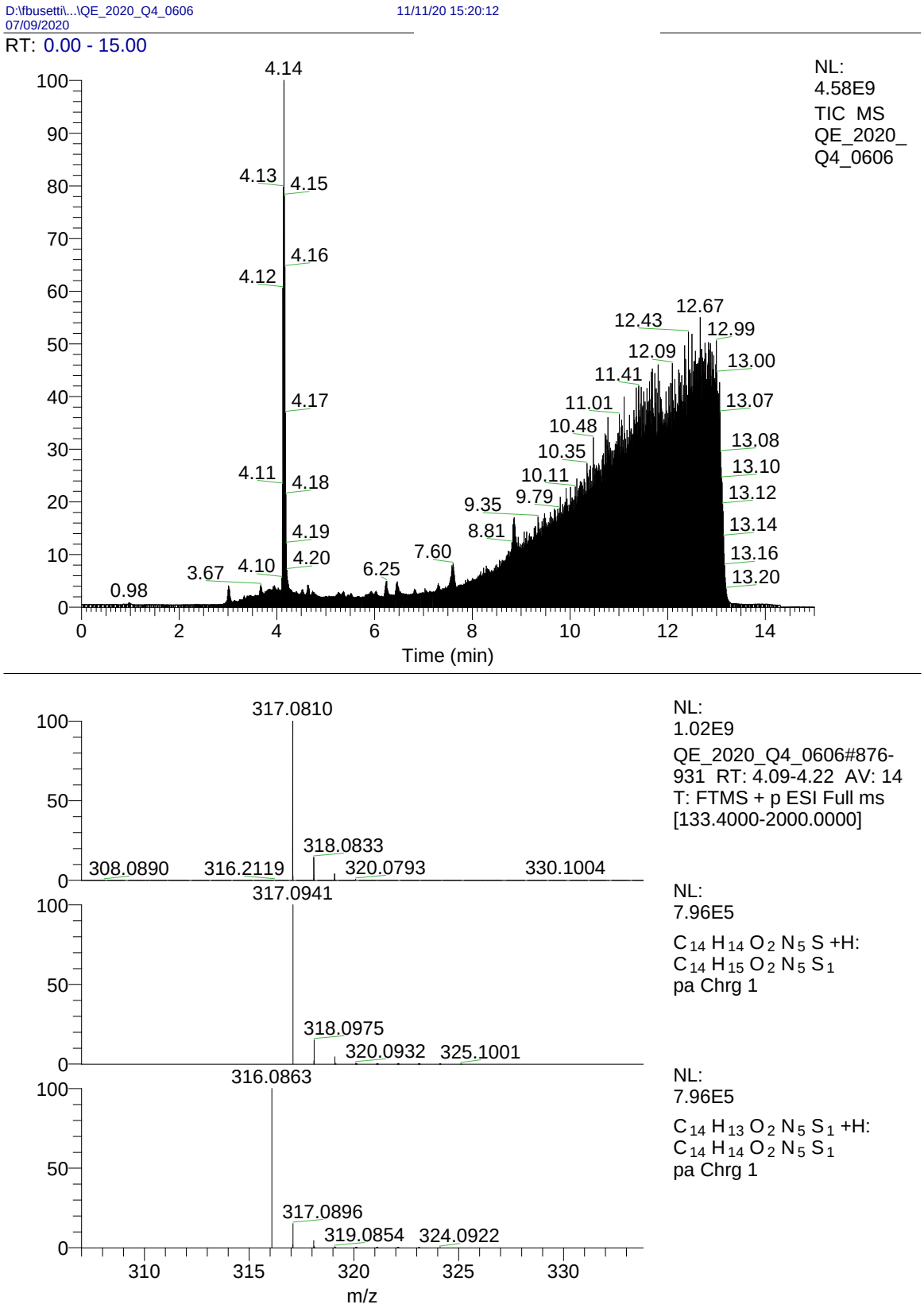

Figure 115: Chromatogram and HRM spectrum of HL4.

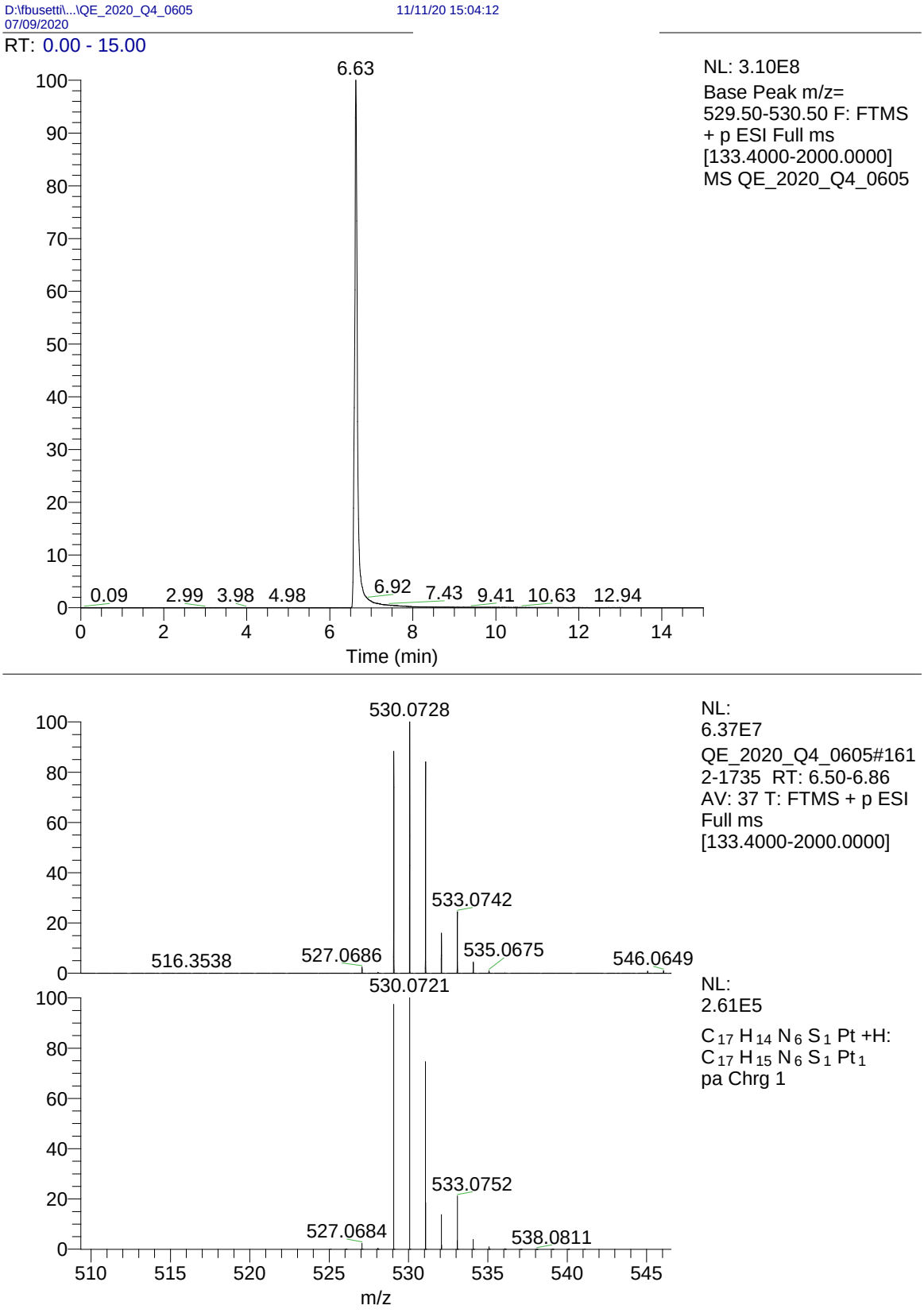

Figure 116: Chromatogram and HRM spectrum of Pt[Ph(ThMe$_2$)]L1.

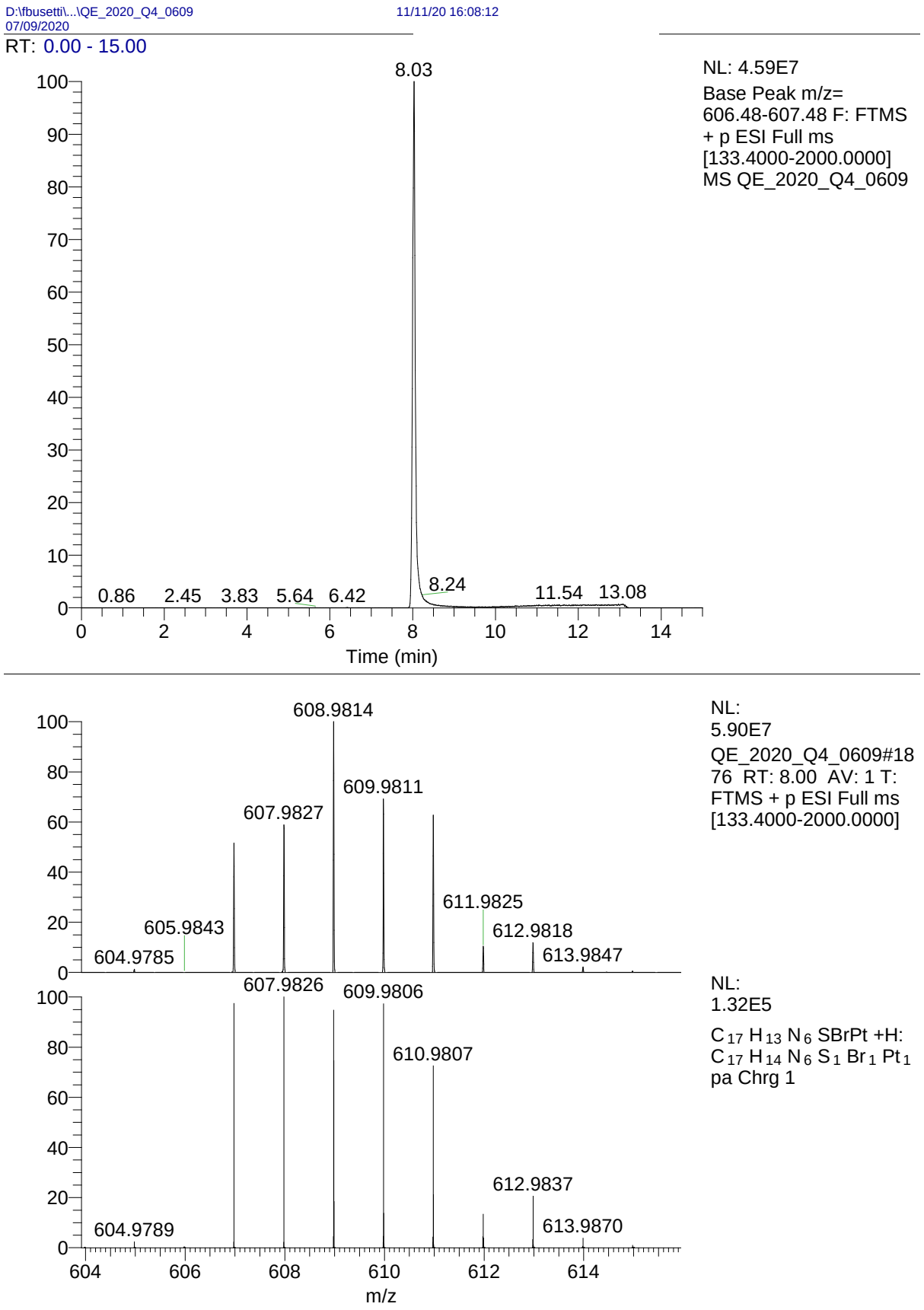

Figure 117: Chromatogram and HRM spectrum of Pt[Ph(ThMe$_2$)]L2.

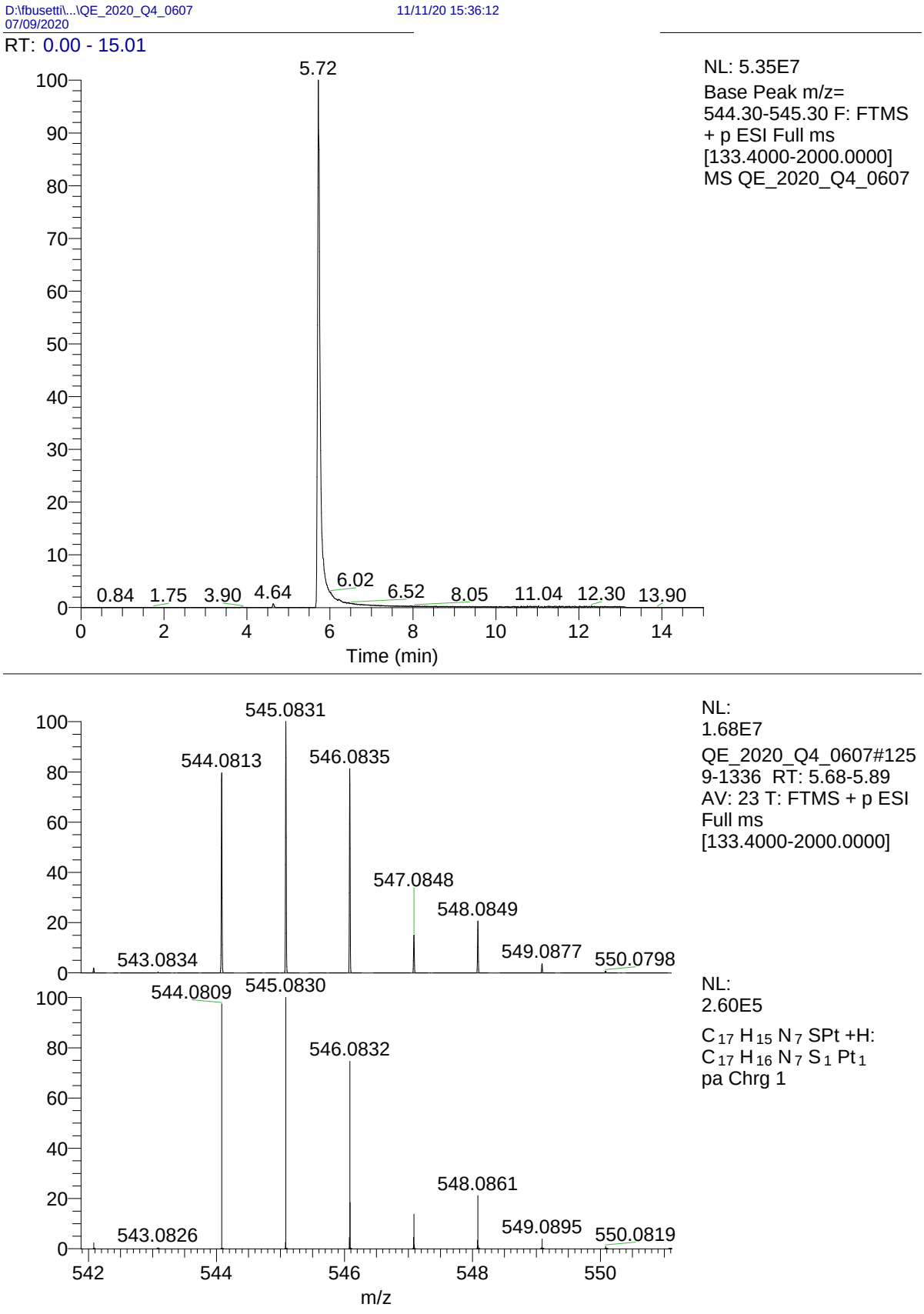

Figure 118: Chromatogram and HRM spectrum of Pt[Ph(ThMe$_2$)]L3.

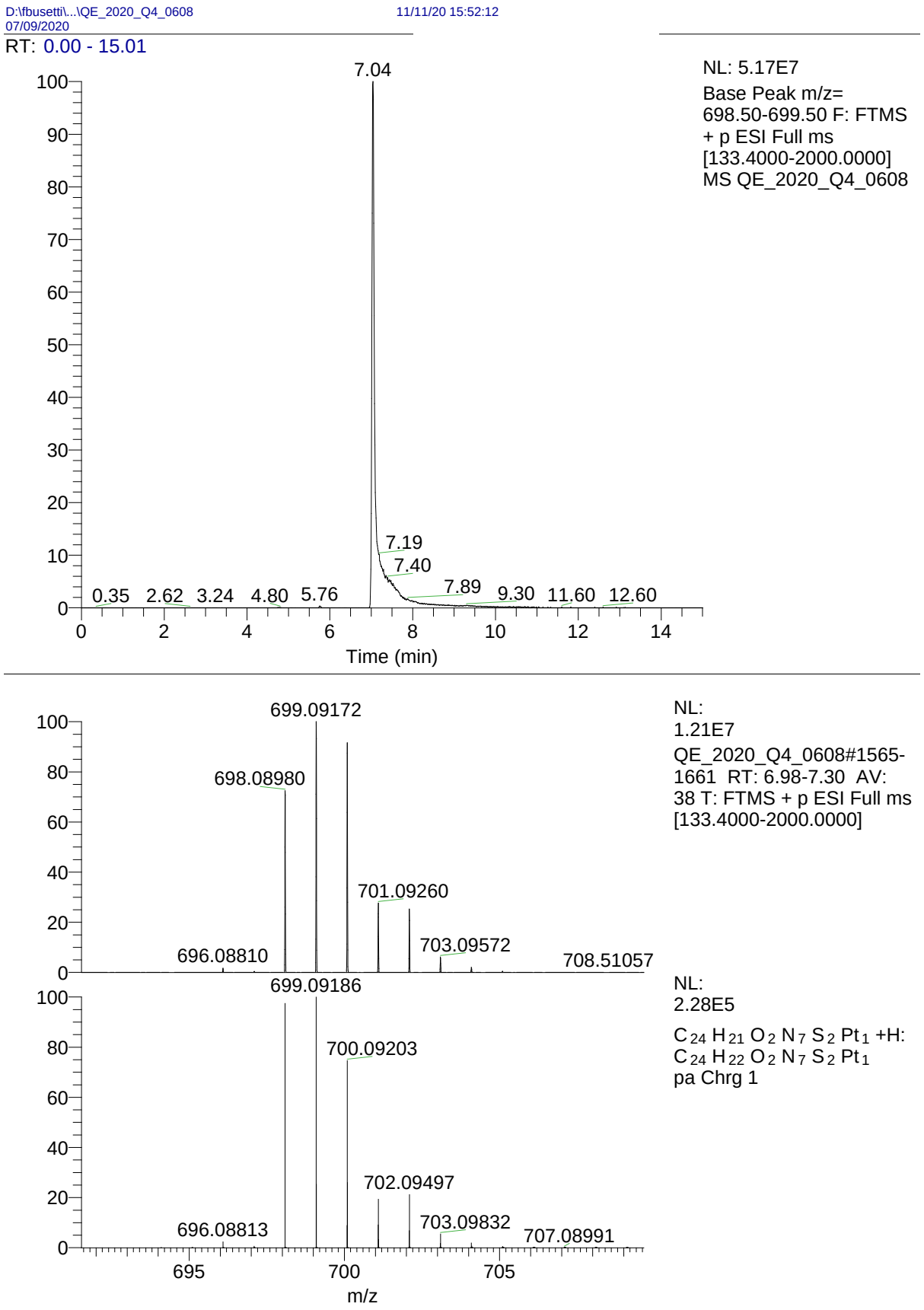

Figure 119: Chromatogram and HRM spectrum of Pt[Ph(ThMe$_2$)]L4.

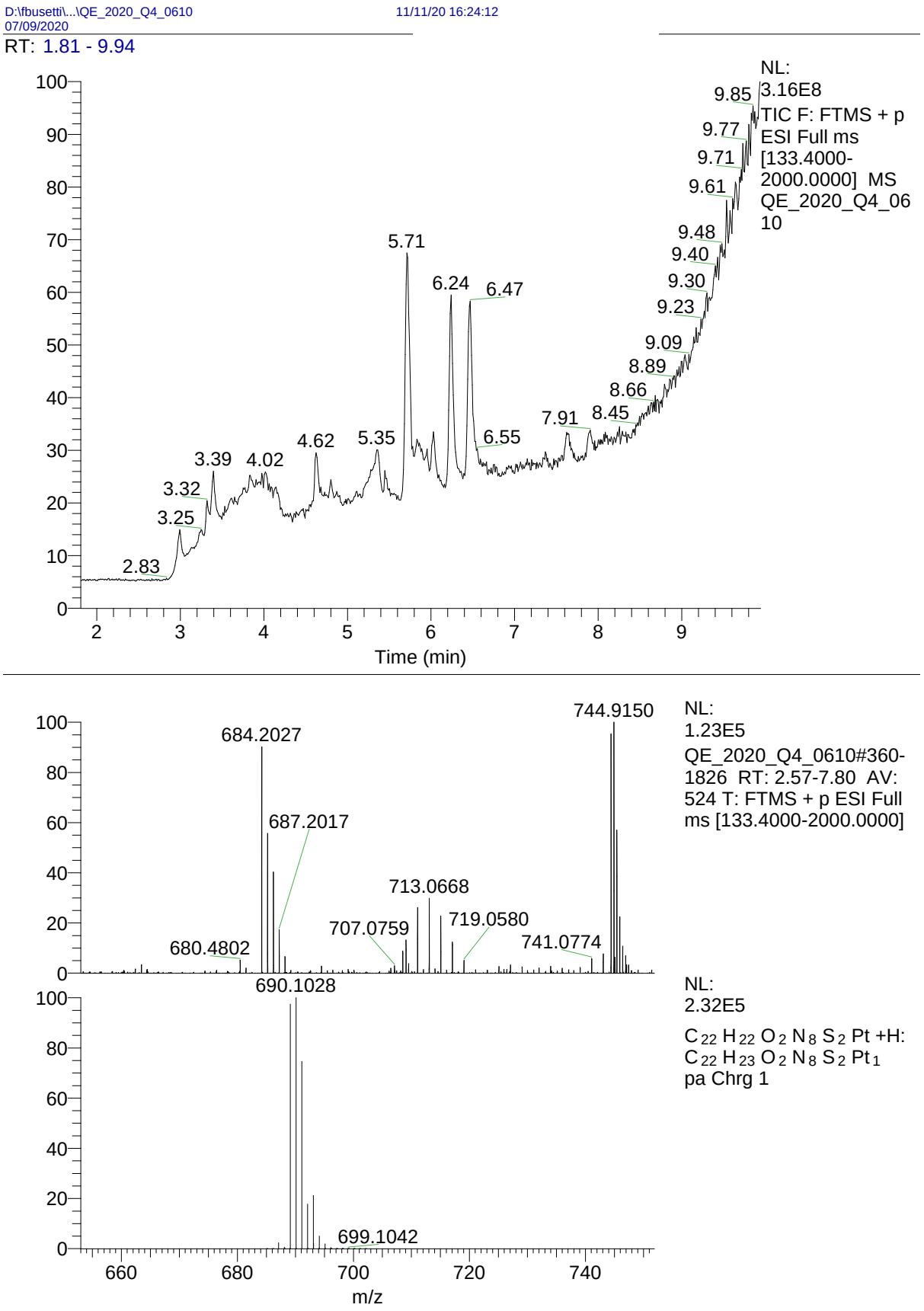

Figure 120: Chromatogram and HRM spectrum of Pt[Ph(ThMe$_2$)]L5.

Appendix D – Biological Testing Results

CompoundID	CompoundName	ProjectID	OrgID	OrgCode	Organism	Strain	PSRunID	TestPlateID	TestWellID	MIC	MIC_Unit	DMax
C0107798	TG028_B	P0844	GN_034	Ab	Acinetobacter baumannii	ATCC 19606	HCR00168	HC168-11-06	I02	>32.0	ug/mL	-2.60
C0107798	TG028_B	P0844	GN_034	Ab	Acinetobacter baumannii	ATCC 19606	HCR00168	HC168-11-05	I02	>32.0	ug/mL	15.00
C0107798	TG028_B	P0844	FG_002	Cn H99	Cryptococcus neoformans	ATCC 208821; H99	HCR00168	HC168-11-15	I02	<=0.250	ug/mL	82.00
C0107798	TG028_B	P0844	FG_002	Cn H99	Cryptococcus neoformans	ATCC 208821; H99	HCR00168	HC168-11-16	I02	0.5	ug/mL	84.80
C0107798	TG028_B	P0844	GN_049	Ec TolC	Escherichia coli	tolC; MB5747	HCR00168	HC168-11-07	I02	>32.0	ug/mL	2.20
C0107798	TG028_B	P0844	GN_042	Pa	Pseudomonas aeruginosa	ATCC 27853	HCR00168	HC168-11-22	I02	>32.0	ug/mL	15.10
C0107798	TG028_B	P0844	FG_001	Ca	Candida albicans	ATCC 90028	HCR00168	HC168-11-13	I02	>32.0	ug/mL	54.70
C0107798	TG028_B	P0844	GN_042	Pa	Pseudomonas aeruginosa	ATCC 27853	HCR00168	HC168-11-21	I02	>32.0	ug/mL	7.30
C0107798	TG028_B	P0844	GN_046	Ec LpxC	Escherichia coli	lpxC; MB4902	HCR00168	HC168-11-10	I02	>32.0	ug/mL	6.00
C0107798	TG028_B	P0844	GN_211	Pa 5mex	Pseudomonas aeruginosa	PAO397; PAO1 d(m	HCR00168	HC168-11-23	I02	>32.0	ug/mL	33.10
C0107798	TG028_B	P0844	GN_211	Pa 5mex	Pseudomonas aeruginosa	PAO397; PAO1 d(m	HCR00168	HC168-11-24	I02	>32.0	ug/mL	26.60
C0107798	TG028_B	P0844	GN_001	Ec	Escherichia coli	ATCC 25922	HCR00168	HC168-11-01	I02	>32.0	ug/mL	-0.70
C0107798	TG028_B	P0844	GP_020	Sa MRSa	Staphylococcus aureus	ATCC 43300; MRSA	HCR00168	HC168-11-12	I02	>32.0	ug/mL	6.80
C0107798	TG028_B	P0844	GN_001	Ec	Escherichia coli	ATCC 25922	HCR00168	HC168-11-02	I02	>32.0	ug/mL	-7.30
C0107798	TG028_B	P0844	GP_020	Sa MRSa	Staphylococcus aureus	ATCC 43300; MRSA	HCR00168	HC168-11-11	I02	>32.0	ug/mL	11.00
C0107798	TG028_B	P0844	GN_003	Kp MDR	Klebsiella pneumoniae	ATCC 700603; MDR	HCR00168	HC168-11-04	I02	>32.0	ug/mL	15.00
C0107798	TG028_B	P0844	GN_003	Kp MDR	Klebsiella pneumoniae	ATCC 700603; MDR	HCR00168	HC168-11-03	I02	>32.0	ug/mL	15.10
C0107798	TG028_B	P0844	FG_001	Ca	Candida albicans	ATCC 90028	HCR00168	HC168-11-14	I02	>32.0	ug/mL	-21.40
C0107798	TG028_B	P0844	GN_049	Ec TolC	Escherichia coli	tolC; MB5747	HCR00168	HC168-11-08	I02	>32.0	ug/mL	3.10
C0107798	TG028_B	P0844	GN_046	Ec LpxC	Escherichia coli	lpxC; MB4902	HCR00168	HC168-11-09	I02	>32.0	ug/mL	4.90
C0107797	TG028	P0844	GN_034	Ab	Acinetobacter baumannii	ATCC 19606	HCR00168	HC168-11-06	I21	>32.0	ug/mL	13.80
C0107797	TG028	P0844	GN_034	Ab	Acinetobacter baumannii	ATCC 19606	HCR00168	HC168-11-05	I21	>32.0	ug/mL	10.20
C0107797	TG028	P0844	FG_002	Cn H99	Cryptococcus neoformans	ATCC 208821; H99	HCR00168	HC168-11-15	I21	>32.0	ug/mL	0.20
C0107797	TG028	P0844	FG_002	Cn H99	Cryptococcus neoformans	ATCC 208821; H99	HCR00168	HC168-11-16	I21	>32.0	ug/mL	-3.00
C0107797	TG028	P0844	GN_049	Ec TolC	Escherichia coli	tolC; MB5747	HCR00168	HC168-11-07	I21	>32.0	ug/mL	4.60
C0107797	TG028	P0844	GN_042	Pa	Pseudomonas aeruginosa	ATCC 27853	HCR00168	HC168-11-22	I21	>32.0	ug/mL	18.50
C0107797	TG028	P0844	FG_001	Ca	Candida albicans	ATCC 90028	HCR00168	HC168-11-13	I21	>32.0	ug/mL	3.50
C0107797	TG028	P0844	GN_042	Pa	Pseudomonas aeruginosa	ATCC 27853	HCR00168	HC168-11-21	I21	>32.0	ug/mL	9.90
C0107797	TG028	P0844	GN_046	Ec LpxC	Escherichia coli	lpxC; MB4902	HCR00168	HC168-11-10	I21	>32.0	ug/mL	5.10
C0107797	TG028	P0844	GN_211	Pa 5mex	Pseudomonas aeruginosa	PAO397; PAO1 d(m	HCR00168	HC168-11-23	I21	>32.0	ug/mL	23.40
C0107797	TG028	P0844	GN_211	Pa 5mex	Pseudomonas aeruginosa	PAO397; PAO1 d(m	HCR00168	HC168-11-24	I21	>32.0	ug/mL	-15.60
C0107797	TG028	P0844	GN_001	Ec	Escherichia coli	ATCC 25922	HCR00168	HC168-11-01	I21	>32.0	ug/mL	-0.40
C0107797	TG028	P0844	GP_020	Sa MRSa	Staphylococcus aureus	ATCC 43300; MRSA	HCR00168	HC168-11-12	I21	>32.0	ug/mL	5.80
C0107797	TG028	P0844	GN_001	Ec	Escherichia coli	ATCC 25922	HCR00168	HC168-11-02	I21	>32.0	ug/mL	-5.90
C0107797	TG028	P0844	GP_020	Sa MRSa	Staphylococcus aureus	ATCC 43300; MRSA	HCR00168	HC168-11-11	I21	>32.0	ug/mL	16.60
C0107797	TG028	P0844	GN_003	Kp MDR	Klebsiella pneumoniae	ATCC 700603; MDR	HCR00168	HC168-11-04	I21	>32.0	ug/mL	21.80
C0107797	TG028	P0844	GN_003	Kp MDR	Klebsiella pneumoniae	ATCC 700603; MDR	HCR00168	HC168-11-03	I21	>32.0	ug/mL	12.20
C0107797	TG028	P0844	FG_001	Ca	Candida albicans	ATCC 90028	HCR00168	HC168-11-14	I21	>32.0	ug/mL	1.20
C0107797	TG028	P0844	GN_049	Ec TolC	Escherichia coli	tolC; MB5747	HCR00168	HC168-11-08	I21	>32.0	ug/mL	3.50
C0107797	TG028	P0844	GN_046	Ec LpxC	Escherichia coli	lpxC; MB4902	HCR00168	HC168-11-09	I21	>32.0	ug/mL	5.80

Figure 121: Biological acitivity testing results, where TG028_B = Pd(o-cyc)Br_2 and TG028 = [Pd(o-cyc)L1]PF_6.

CompoundID	CompoundName	ProjectID	OrgID	OrgCode	Organism	Strain	PSRunID	TestPlateID	TestWellID	CC50	CC50_Unit	DMax
C0107798	TG028_B	P0844	MA_007	Hek	Homo sapiens	HEK293; ATCC CRL1573	HCR00168	HC168-11-18	I02	>32.0	ug/mL	10.30
C0107798	TG028_B	P0844	MA_007	Hek	Homo sapiens	HEK293; ATCC CRL1573	HCR00168	HC168-11-17	I02	>32.0	ug/mL	17.70
C0107797	TG028	P0844	MA_007	Hek	Homo sapiens	HEK293; ATCC CRL1573	HCR00168	HC168-11-18	I21	>32.0	ug/mL	24.50
C0107797	TG028	P0844	MA_007	Hek	Homo sapiens	HEK293; ATCC CRL1573	HCR00168	HC168-11-17	I21	>32.0	ug/mL	19.20

Figure 122: Cytotoxicity testing results, where TG028_B = Pd(o-cyc)Br_2 and TG028 = [Pd(o-cyc)L1]PF_6.

CompoundID	CompoundName	ProjectID	OrgID	OrgCode	Organism	Strain	PSRunID	TestPlateID	TestWellID	HC10	HC50	Unit	DMax
C0107798	TG028_B	P0844	HA_150	RBC	Homo sapiens	Red blood cell	HCR00168	HC168-11-19	I02	>32.0	>32.0	ug/mL	2.30
C0107798	TG028_B	P0844	HA_150	RBC	Homo sapiens	Red blood cell	HCR00168	HC168-11-20	I02	>32.0	>32.0	ug/mL	2.40
C0107797	TG028	P0844	HA_150	RBC	Homo sapiens	Red blood cell	HCR00168	HC168-11-19	I21	>32.0	>32.0	ug/mL	8.70
C0107797	TG028	P0844	HA_150	RBC	Homo sapiens	Red blood cell	HCR00168	HC168-11-20	I21	>32.0	>32.0	ug/mL	6.00

Figure 123: Haemolysis testing results, where TG028_B = Pd(o-cyc)Br_2 and TG028 = [Pd(o-cyc)L1]PF_6.

Appendix E – Crystallographic Data

mxm456tg

Olex2
Report created with ReportPlus

R_1=3.73%

Crystal Data and Experimental

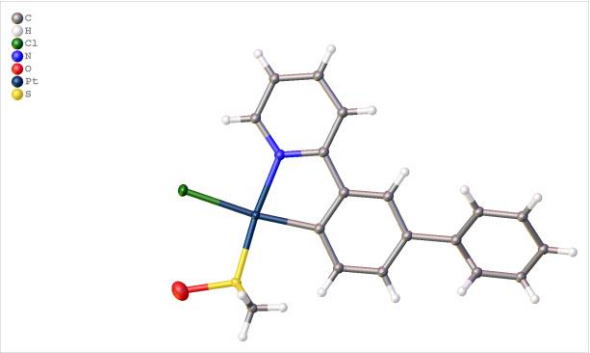

Experimental. Single clear light yellow plate crystals of **mxm456tg** were used as supplied. A suitable crystal with dimensions 0.22 × 0.16 × 0.07 mm³ was selected and mounted on a Xcalibur, Ruby, Gemini ultra diffractometer. The crystal was kept at a steady T = 94.3(2) K during data collection. The structure was solved with the ShelXT 2018/2 (Sheldrick, 2018) solution program using ? and by using Olex2 (Dolomanov et al., 2009) as the graphical interface. The model was refined with ShelXL 2018/3 (Sheldrick, 2015) using full matrix least squares minimisation on F^2.

Crystal Data. $C_{37}H_{35}Cl_2N_2O_2Pt_2S_2$, M_r = 1064.87, orthorhombic, *Pbcm* (No. 57), a = 18.3097(2) Å, b = 13.58340(10) Å, c = 6.96310(10) Å, $\alpha = \beta = \gamma = 90°$, V = 1731.78(3) Å³, T = 94.3(2) K, Z = 2, Z' = 0.25, μ(Mo K_α) = 8.381, 43221 reflections measured, 3351 unique (R_{int} = 0.0476) which were used in all calculations. The final wR_2 was 0.0916 (all data) and R_1 was 0.0373 (I≥2 σ(I)).

Compound	**mxm456tg**
Formula	$C_{37}H_{35}Cl_2N_2O_2Pt_2S_2$
$D_{calc.}$/ g cm^{-3}	2.042
μ/mm^{-1}	8.381
Formula Weight	1064.87
Colour	clear light yellow
Shape	plate
Size/mm³	0.22×0.16×0.07
T/K	94.3(2)
Crystal System	orthorhombic
Space Group	*Pbcm*
a/Å	18.3097(2)
b/Å	13.58340(10)
c/Å	6.96310(10)
α/°	90
β/°	90
γ/°	90
V/Å³	1731.78(3)
Z	2
Z'	0.25
Wavelength/Å	0.71073
Radiation type	Mo K_α
Θ_{min}/°	3.199
Θ_{max}/°	32.736
Measured Refl's.	43221
Indep't Refl's	3351
Refl's I≥2 σ(I)	3014
R_{int}	0.0476
Parameters	53
Restraints	0
Largest Peak	5.326
Deepest Hole	-3.050
GooF	1.055
wR_2 (all data)	0.0916
wR_2	0.0880
R_1 (all data)	0.0435
R_1	0.0373

Structure Quality Indicators

Reflections:	d min (Mo) 2θ=65.5° 0.66	I/σ(I) 46.4	Rint 4.76%	CAP 60.9° 98% to 65.5° 99.8
Refinement:	Shift -0.004	Max Peak 5.3	Min Peak -3.0	GooF 1.055